CANADIAN THESES

THÈSES CANADIENNES

NOTICE

The quality of this microfiche is heavily dependent upon the quality of the original thesis submitted for microfilming. Every effort has been made to ensure the highest quality of reproduction possible.

If pages are missing, contact the university which granted the degree.

Some pages may have indistinct print especially if the original pages were typed with a poor typewriter ribbon or if the university sent us an inferior photocopy.

Previously copyrighted materials (journal articles, published tests, etc.) are not filmed.

Reproduction in full or in part of this film is governed by the Canadian Copyright Act, R.S.C. 1970, c. C-30.

AVIS

La qualité de cette microfiche dépend grandement de la qualité de la thèse soumise au microfilmage. Nous avons tout fait pour assurer une qualité supérieure de reproduction.

S'il manque des pages, veuillez communiquer avec l'université qui a conféré le grade.

La qualité d'impression de certaines pages peut laisser à désirer, surtout si les pages originales ont été dactylographiées à l'aide d'un ruban usé ou si l'université nous a fait parvenir une photocopie de qualité inférieure.

Les documents qui font déjà l'objet d'un droit d'auteur (articles de revue, examens publiés, etc.) ne sont pas microfilmés.

La reproduction, même partielle, de ce microfilm est soumise à la Loi canadienne sur le droit d'auteur, SRC 1970, c. C-30.

THIS DISSERTATION HAS BEEN MICROFILMED EXACTLY AS RECEIVED

LA THÈSE A ÉTÉ MICROFILMÉE TELLE QUE NOUS L'AVONS REÇUE

Sodium Binding to Crown Ether Derivatives. Bulk Membrane Transport and Sodium-23 Nuclear Magnetic Resonance Studies

by

Harald D.H. STÖVER

A thesis
presented to the University of Ottawa
in fulfillment of the
thesis requirement for the degree of
Ph.D.
in
Chemistry

ISBN 0-315-36535-8

UNIVERSITÉ D'OTTAWA
UNIVERSITY OF OTTAWA

To see a World in a Grain of Sand

And a Heaven in a Wild Flower,

Hold Infinity in the palm of your hand

And Eternity in an hour.

"Auguries of Innocence", by William Blake

ABSTRACT

Complexation of cations by crown ethers has been studied from two angles:

A series of 15-crown-5 and 18-crown-6 derivatives were synthesized from dopamine and L-adrenaline, and provided with an aminoacid sidechain. The capacity of these crown ethers to transport sodium and potassium cations across artificial bulk membranes was studied. The amine sidechains were found to not participate directly in the cation binding. However, for the L-lysine-15-crown-5 derivative, the amine group participates in a self-regulated sodium-proton co-transport.

Following a different approach, the complexation of sodium cation by the large 'wrap-around' crown ether dibenzo-24-crown-8 was studied in detail using sodium-23 Nuclear Magnetic Resonance. Longitudinal and transverse relaxation rates together indicated molecular stacking of several planar 1:1 complexes in nitromethane. Further they revealed the existence of both the bimolecular cation interchange as well as of the classical unimolecular decomplexation mechanism. The exchange rates for both mechanisms, and the activation parameters for the bimolecular process, were determined from the line shapes, while varying composition, concentration and temperature.

In addition, the effects of four counter anions on the complexation, as well as the ion-pairing effects themselves, were determined quantitatively using sodium-23 chemical shifts and relaxation rates in conjunction.

Definitions of Symbols

d	diameter
k_a, k_b	specific exchange rates for free and complexed sodium
k_1, k_{-1}	rates of unimolecular complexation and decomplexation
k_2	bimolecular cation interchange rate

Formation constant of the:

K_c	1:1 complex
K_{c2}	2:1 complex
K	aggregate
K_p	ion-pair
K_{tr}	triple-ion

Concentration of:

[Na]	free sodium
[NaC]	1:1 sodium:DB24C8 Complex
[Na_2C]	2:1 sodium:DB24C8 Complex
[NaX]	ion-paired sodium (Na^+,X^-)s, with $X^- = PF_6^-$, SCN^- or I^-
[$NaSCN_2$]	triple-ion $Na^+(SCN^-)_2$
P_a	molar fraction of uncomplexed sodium
P_b	molar fraction of complexed sodium
ρ	[Crown]/[Sodium]

Longitudinal relaxation rate of:

$1/T_1f$	free sodium
$1/T_1c$	1:1 complexed sodium
$1/T_1c2$	2:1 complexed sodium
$1/T_1p$	ion-paired sodium
$1/T_1tr$	sodium in the triple-ion
$1/T_2obsd$	observed transverse relaxation rate
$1/T_2ex$	exchange relaxation component
$1/T_2inh$	inhomogeneity relaxation component
$1/T_2q$	quadrupolar relaxation component
τ_c	correlation time

Chemical shift of:

δ_f	free Sodium
δ_c	1:1 complexed Sodium
δ_{c2}	2:1 complexed sodium
δ_p	ion-paired sodium
δ_{tr}	sodium in the triple-ion

DB24C8	Dibenzo-24-crown-8
DB30C10	Dibenzo-30-crown-10
MB15C5	Monobenzo-15-crown-5

CONTENTS

FIGURES

TABLES

Introduction

Sodium is the sixth most abundant element on earth, and is essential for most life-forms found on it. In normal eukariotic cells the cytoplasm is kept sodium-poor and potassium-rich relative to the environment. These concentration gradients are created by enzymatic sodium-potassium pumps that are fueled by ATP. Many biochemical events, such as the progress of a nerve impulse, muscular contractions, and aminoacid transport across cell membranes depend upon these cation concentration gradients.[1][2] Higher biological life-forms require efficient chemical communication between their components, such as organelles, cells and organs. The regulated cation transport across membranes is an important link in this information chain.[2]

However, it remains difficult to study the biochemistry of the sodium cation directly. Sodium and potassium cations have a symmetrical outer s-orbital, and form predominantly electrostatic bonds in solution. In biochemical systems, coordinate bonds such as those provided by sodium cations complement the stronger covalent bonds: they mediate the first step in all chemical and biochemical reactions, that is the mutual recognition and orientation of the reaction partners.

This thesis focusses on coordination chemistry and complexation of sodium cations in non-polar solution, while capitalizing on two major points:

For one, crown ethers, pioneered by Pedersen in 1967, consist of an array of donor atoms, here oxygen, that converge onto a centrally bound cation.[3] Crown ethers share this property with natural ionophores such as valinomycin and monensin, and thus form convenient ionophore-models.

Secondly, sodium-23 nuclear magnetic resonance can be used to directly probe the coordination state of the sodium cation. Since sodium has a quadrupolar nucleus of spin I = 3/2, its spin-lattice relaxation rate and chemical shift provide information about composition and structure of the first coordination shell.[1] In addition the lineshapes can provide dynamic information about chemical exchange.

In the first chapter these two points were combined for describing the complexation of four sodium salts by the large crown ether dibenzo-24-crown-8 (DB24C8) in several solvents. The sodium:DB24C8 complex strongly resembles the potassium:valinomycin complex, in that the crown wraps itself around the cation to the exclusion of solvent and counter anions. In the low donicity solvent nitromethane, some counter anions compete with the crown for the sodium coordination sites, in accordance with their comparable nucleophilicity.

In the systems studied, the sodium-23 longitudinal relaxation rates reflect directly on the first coordination shell and on the mobility of the sodium cation. Thus they indicate coplanar aggregation of several 1:1 complexes in the presence of the large counter anion tetraphenylborate. In the case of the stronger coordinating anions hexafluorophosphate, iodide and thiocyanate, the chemical shifts and the relaxation rates reveal increasing cation-anion interactions, such as ion-pairing and stabilization of a 2:1 sodium:DB24C8 complex.

In all cases, the difference between transverse and longitudinal relaxation rates could be directly related to the rate of chemical exchange of sodium cations between solvated and complexed state. At low concentrations, this exchange proceeds via the classical unimolecular decomplexation mechanism. At concentrations above 0.001 M however, the bimolecular cation interchange mechanism is favoured, since the solvent nitromethane can stabilize the two cationic charges at the bimolecular transition state. The coordinating anion thiocyanate produces a 2:1 complex of measurable life time by further stabilizing the transient 2:1 species. This decrease of the transition state energy leads further to a fourfold increase in the exchange rates in the case of thiocyanate.

In the second chapter, to move one step from fundamental coordination chemistry to biochemical systems, the synthesis of a series of 15-crown-5 and 18-crown-6 derivatives is described. These compounds are based on the catecholamines dopamine and L-adrenaline, and bear glycyl, L-alanyl or L-lysyl sidechains. The capacities of some of these compounds regarding both simple transport of sodium and potassium picrate across a bulk artificial membrane, as well as coupled transport of sodium, protons and picrate, are described in the third chapter. For the L-lysine-15-crown-5 a sophisticated transport regulating mechanism could be shown, that is in analogy to feedback loops or reflex-arcs of biochemical regulation mechanisms.

Chapter I

COMPLEXATION OF SODIUM CATIONS BY LARGE CROWN ETHERS

Sodium-23 Nuclear Magnetic Resonance Study of Association and Exchange as a Function of Solvent and Counter-Anions.

1.1 Quadrupolar Ion NMR as Direct Probe into Ion - Ionophore Interactions

One approach to studying cation-dipole interactions is to combine several ion-dipole bonds in order to amplify the observable effects. This is the case with macrocyclic ion complexes, in which typically 4 to 10 dipole-vectors converge cooperatively onto a central cavity in which a cation (or anion) can be held very tightly. The backbone structure of the ligand and the ion-dipole attractions combine to produce this convergent geometry of the dipole vectors (Fig. 1).[4][5]

At the same time, binding of cations to large crown ethers such as DB24C8 (Fig. 1) models the role of cations in biochemical environments. It is well known that sodium cations are necessary for the activity of several enzymes, as well as fundamentally involved in neuro-chemistry and the regulation of the electrochemical and pH potential across membranes. For all of these roles, the recognition of the sodium cation by a macromolecular ligand is the crucial first step.

Of the many methods that can be used to study complexation, UV-VIS, IR, Raman, NMR, conductivity, potentiometry and calorimetry, to name just a few, only nuclear magnetic resonance of the complexed cation reflects directly upon the environment or binding site of the ion, as seen from within the ion.

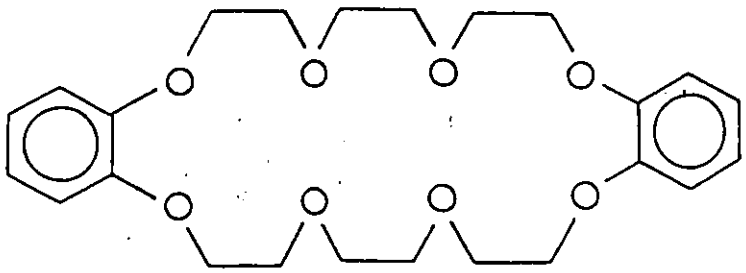

Figure 1: Dibenzo-24-Crown-8

Furthermore, NMR features three parameters: chemical shift, longitudinal relaxation rate (spin-lattice relaxation), and transverse relaxation rate (spin-spin relaxation). In favorable cases, these three NMR parameters provide complementary information about structure and dynamics of the ionic coordination shell.[1][6][7]

1.1.1 Physical Basis of the Chemical Shift in Quadrupolar NMR

The chemical shifts for sodium cations in solution span a range of about 40 ppm. They are usually given with reference to sodium chloride at infinite dilution in water. In 1971 Erlich and Popov recognized the linear relation between the chemical shift of the sodium cation in solution and the Gutmann donicity of the solvent (Fig. 2),[8] but a sound theoretical understanding of the physical causes of the chemical shift has still to be found.[1][9]

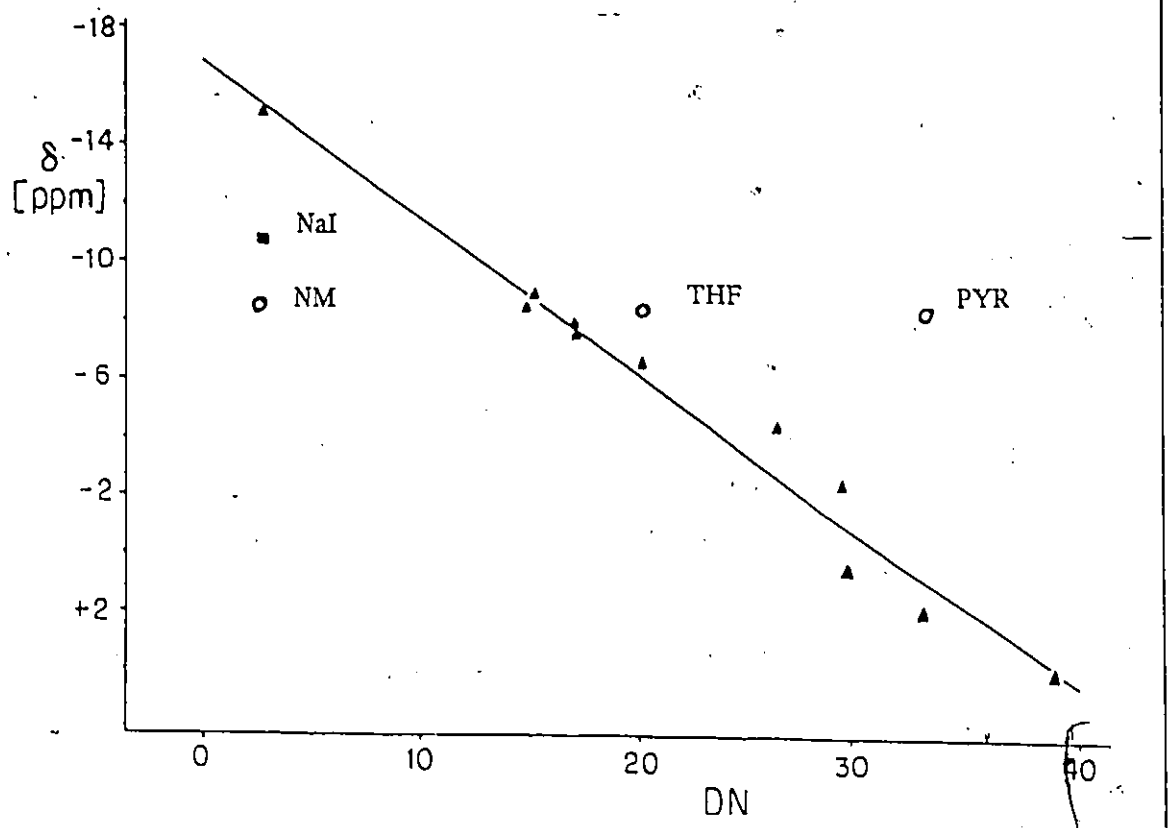

Figure 2: Na-23 Chemical Shift versus Gutmann Donor Number. for $NaBPh_4$ in a range of solvents. The Gutmann donor number (DN) of a solvent is the enthalpy of reaction between the solvent and antimony pentachloride. The triangles are experimentally measured donicities[10][11] and shifts.[18] NM, THF and PYR indicate the Na-23 NMR shifts of the sodium:DB24C8 complex in nitromethane, tetrahydrofuran and pyridine, respectively. NaI indicates the chemical shift of a 0.01 M NaI solution in nitromethane.

Originally, Na-23 chemical shifts were attributed to electronic transfer from solvent donor atoms to the empty 3p orbitals of the sodium cation. This transferred electron density would be partially unpaired, and thus enhance the effective magnetic field experienced by the sodium nuclei, causing them to resonate at a higher frequency. Recent ab initio calculations however could not confirm this partly covalent bonding between solvent molecules and cation.[12] Dipolar attractions between solvent molecules and cation alone could explain sodium solvation.

1.1.2 Nuclear Magnetic Relaxation Rates of Sodium-23 Cations

Sodium-23 has a nuclear spin number I of 3/2, and its nuclear electric charge assumes an ellipsoidal (quadrupolar) shape, with an associated nuclear electric quadrupole Q = 0.12 barn. The ligands in the sodium coordination sphere cause a residual electric field gradient q at the nucleus that can interact with the nuclear electric quadrupole Q. This interaction has the dimension Hertz, and is called the quadrupolar coupling constant χ:

$$\chi = \frac{eQeq}{\hbar} \qquad (1)$$

where $\hbar$ is Planck's constant divided by 2π. For sodium-23, quadrupolar coupling provides the most efficient pathway for energy transfer between nucleus and lattice, the spin-lattice relaxation. χ is typically between 0.1 to 1.5 MHz.[1]

The electric field gradient q arises from an asymmetric charge distribution in the first coordination sphere due to mixed solvation, ion-pairing, or asymmetric complexation, or a combination of these effects. The quadrupolar coupling is modulated by the rotation of the sodium cation or complex, τ_c being the characteristic motional correlation time.

During the NMR experiment, the equilibrium z-magnetization is flipped 90° degrees into the x-y plane by the observation pulse. It then rotates coherently in the x-y plane with its Larmor frequency ω. Stationary receivers register this rotation as an amplitude oscillation with frequency ω. This oscillation, the free induction decay (FID), is dampened by a number of effects:

- Return of the x-y magnetization into the z-direction due to the quadrupolar longitudinal relaxation, $1/T_1$. This relaxation is enthalpy driven.
- Dispersion of the Larmor frequencies among the nuclei will dephase the initially coherent x-y magnetization - the transverse or spin-spin relaxation. This too will dampen the

amplitude of the observed magnetic oscillation. Inhomogeneities of the magnetic field can cause nuclei to experience different Larmor frequencies in different regions of the sample. As well, cation exchange between two sites with different intrinsic chemical shifts (different Larmor frequencies) will dampen the transverse magnetization in each site, if exchange rate, chemical shift difference and relaxation rates are of comparable magnitude.[13] This dispersion of the initially coherent transverse magnetization is an entropy driven process.

In general, both transverse and longitudinal relaxation for a spin 3/2 nucleus like sodium are represented by two exponential rate constants.[14][15] The transverse magnetization for example decays according to:

$$M_z(t) = M_z(0)(0.6\exp(-t/T_2') + 0.4\exp(-t/T_2")) \qquad (2)$$

where $M_z(0)$ and $M_z(t)$ are the amplitudes of the FID (the transverse magnetization) immidiately after the observe pulse, and after a time t, respectively. The full expressions for the two exponential rate constants, assuming isotropic reorientation, are:[14][15]

$$1/T_2' = \frac{\pi^2}{5}\chi^2\left(\tau_c + \frac{\tau_c}{1+\omega^2\tau_c^2}\right) \qquad (3a)$$

$$1/T_2" = \frac{\pi^2}{5}\chi^2\left(\frac{\tau_c}{1+\omega^2\tau_c^2} + \frac{\tau_c}{1+4\omega^2\tau_c^2}\right) \qquad (3b)$$

where ω is the Larmor frequency of the nucleus, and τ_c is its motional correlation time. Analog expressions describe the longitudinal relaxation.

Spin-lattice relaxation, the transfer of energy between the nuclear magnetic moment and its environment, occurs by coupling of the nuclear electric quadrupole Q with the fluctuating local electric field gradient. Only fluctuations or motions at the Larmor frequency allow for quadrupolar coupling and thus magnetic relaxation. The frequencies of motions in solution are governed by the auto-correlation functions of the species involved, and range from zero for very slow motions, up to the frequency of the fastest motion possible in the solution system. The amplitude of the electric field fluctuations caused by motions of frequency ω is called the spectral density $J(\omega)$.[16]

For the 1:1 sodium:DB24C8 complex in chloroform the correlation time for the rotational reorientation has been measured as 65 (10) ps.[17] The value for nitromethane will be similar, or slightly smaller. Now if ν_{Na} = 79.35 MHz, then ω_{Na} is 250 x 10^6 s^{-1}, and the product $\omega\tau_c$ is 2.5 x 10^8 x 6 x 10^{-11} = 10^{-2} << 1. The square of this product, $\omega^2\tau_c^2$, can then safely be ignored in comparison to one (eqs. 3a and 3b). This situation is called extreme motional narrowing, and the expressions for both the transverse and longitudinal relaxation rates reduce to:

$$1/T_1 = 1/T_2 = \frac{2}{5}\pi^2\chi^2\tau_c \qquad (4)$$

The work to be described in this thesis always remains within the extreme narrowing region, since the longitudinal relaxation rates prove independent of the resonance frequency at all times (compare also eqs. 3a, 3b).

1.1.3 Chemical Shift, Longitudinal and Transverse Relaxation Rates: Three Parameters and their Information Content

How do these three parameters reflect the chemical state of the sodium cation in different solutions, that is its interactions with solvent molecules, counter anion and ligand molecules?

The sodium-23 chemical shift is empirically related to the donicity of the coordinating groups, and can thus provide information about the chemical composition of the coordination sphere (Fig. 2). For example, in a nonpolar solution containing both a crown-ether and an excess of sodium salt, the sodium cation will typically exchange between two states: solvated and complexed. In the fast exchange limit[1] only one signal will be observed, with a chemical shift representing the weighted average of both chemical states. In the slow exchange limit two independent signals will be observed.

A common theory for the origin of chemical shifts suggests that high donicity solvents inject unpaired, or paramagnetic, electron density into the sodium's electron shell. The resulting paramagnetic deshielding is about thirty times stronger than the parallel diamagnetic shielding, and thus dominates the observed shift.[1] The sodium resonance frequency would thus be higher in water than in nitromethane. For comparison, the sodium shifts of the 1:1 complex with DB24C8 in nitromethane, tetrahydrofuran and pyridine, and of 0.01 M sodium iodide and sodium thiocyanate solutions in nitromethane have been marked on Fig. 2. The complexed sodium experiences an ethereal coordination shell independent of the solvent, resulting in a chemical shift comparable to that of sodium in tetrahydrofuran solution. The chemical shifts of the two salts also show a paramagnetic shift relative to sodium tetraphenylborate in nitromethane. This clearly indicates coordination of the high donicity anions iodide and thiocyanate to the sodium cation.

[1] Fast exchange on the NMR time scale means that nuclear magnetic vectors in different states stay coherent between consecutive exchanges, and thus do not attenuate each other after the exchange.

The longitudinal relaxation rate $1/T_1$ is governed by the quadrupolar coupling constant χ as well as by the correlation time τ_c (eq. 4). This makes $1/T_1$ sensitive to the mobility of the observed cation (via τ_c), as well as to the symmetry of its coordination sphere (via χ^2).

Sodium cations in solution are usually solvated by four to six solvent molecules forming a tetragonal or hexagonal array. The effective net electric field gradient q at the nucleus is thus close to zero, the product $eqeQ/\hbar = \chi$ is small and leads to a narrow linewidth (eq. 4). If however one or more of these solvent molecules are replaced by a different solvent molecule or by a counter anion, then the resulting net electric field gradient will lead to increased quadrupolar relaxation rates. An example for this is NaSCN in nitromethane (Tab. 3; p.28).

In general, the longitudinal relaxation rate for sodium-23 complexed by macrocyclic or macromolecular ligands reflects the symmetry of the cations coordination sphere. For example, sodium in its planar 1:1 complex with MB15C5 experiences a large net electric field gradient q. In nitromethane, $1/T_1$ for sodium amounts to 750 s^{-1}.[18] The 1:1 sodium:DB24C8 complex in contrast has a spherical arrangement of its oxygen donor atoms around the sodium - and the sodium relaxation rate is accordingly only 185 s^{-1} in the same solvent.

The transverse relaxation rate $1/T_2$ is subject to the same factors as $1/T_1$, yet it can additionally be sensitive to the exchange of the nuclei between magnetically different sites.[2] For sodium-23 in solution, relaxation contributions due to dipolar, scalar, paramagnetic effects and chemical shift anisotropy are typically negligible compared to the efficient quadrupolar relaxation. The observed transverse relaxation rate can thus be given as:

$$1/T_2obsd = 1/T_2q + 1/T_2inh + 1/T_2ex \qquad (5)$$

[2] Magnetically different sites means sites with different chemical shifts or different relaxation rates. 'Exchange' between the two states may take place for instance via chemical exchange, rotation or conformational changes.

If the first three terms are known, the exchange contribution to relaxation, $1/T_2ex$, can be determined and provide access to the cation exchange rates. $1/T_2obsd$ is the observed transverse relaxation rate, obtained from the full linewidth at half height via:

$$1/T_2obsd = \nu_{1/2} \qquad (6)$$

$1/T_2q$ in the extreme narrowing region is equal to the longitudinal (spin-lattice) relaxation rate $1/T_1$. Finally $1/T_2inh$, the inhomogeneity contribution to the transverse relaxation, is just the difference between $1/T_2obsd$ and $1/T_1$ in the absence of exchange, i.e. in solutions containing only solvated or complexed sodium.

In the sodium:DB24C8 system in nitromethane, chemical exchange between solvated (a) and 1:1 complexed sodium (b) gives rise to exchange relaxation.

$$(Na^+)_a \underset{k_b}{\overset{k_a}{\rightleftharpoons}} (Na^+)_b \qquad (7)$$

Here, k_a and k_b are the rate constants for complexation and decomplexation; they are equal to the inverse life times of solvated and complexed sodium, $1/\ _a$ and $1/\ _b$, respectively. (The mechanisms of exchange will be discussed below.) The exchange relaxation will be analyzed with two methods: Near the limit of fast exchange, where only one averaged signal is seen, an equation initially developed by Woessner will be applied.[13] It relates the observed exchange relaxation $1/T_2ex$ to the sum of the specific exchange rates, $k_a + k_b$:[3][13]

$$k_a+k_b = 4\pi^2 P_a P_b (\nu_a-\nu_b)^2 T_2ex \qquad (8)$$

[3] This is an approximate expression, holding under the conditions $k_a, k_b >> 1/T_2a, 1/T_2b, |(\omega_a - \omega_b)|$; and $(\omega_a - \omega_b)^2 >> (1/T_2a - 1/T_2b)^2$.[13]

where P_a, P_b, υ_a and υ_b are the molar fractions and the chemical shifts in Hertz of the same species, as usual.

In regions of slower exchange, where two separate signals can be observed, eq. 8 does not hold and a full lineshape analysis based upon the modified Bloch equations has to be used to relate the observed lineshape to the exchange rate (see appendix 6).[19]

1.1.4 Sodium-23 Coordination Chemistry via Sodium-23 NMR

1.1.4.1 Sodium Interactions with Solvents and Counter Anions

The potential of sodium-23 NMR to provide a wealth of structural, dynamic, and kinetic information was recognized early. The first systems studied were often sodium-halide interactions in aqueous solutions. The relaxation rates[6][20][21] and chemical shifts[22][23] were often strongly dependent upon concentration and counter anion. The electrostatic relaxation model of Hertz illustrates well the different relaxation contributions due to ion-solvent and ion-ion interactions in both aqueous[21] and organic solutions.[24]

In low-donicity non-aqueous solvents, ionic interactions are usually stronger than in water. Bloor and Kidd's pioneer work[25] on the dependence of sodium-23 chemical shifts on solvent, counter anion and salt concentration stimulated much interest in the use of sodium-23 NMR to probe the non-aqueous solution chemistry of sodium.[8][26][27] The tendency of the sodium salts to form contact ion-pairs is related to solvent donicity, but not to the dielectric constant of the solvent.[27] The chemical shift in the presence of small counter anions such as iodide, thiocyanate and bromide is usually strongly concentration dependent. Bulky anions such as tetraphenylborate and perchlorate did not show concentration dependence of the sodium chemical shift.[26][28]

Ionic interactions can thus readily be observed via sodium-23 NMR, but only at low salt concentrations (=< 0.01 M) can the observed concentration dependencies safely be assumed to be due to direct ionic interaction, that is ion-pairing, alone.[6][21][29] At higher concentrations secondary effects such as change of solvent activity, long range ionic interactions and solvent structuring complicate the quantitative analysis of the shift and especially the relaxation data. The relevance and accuracy of the parameters is compromised by the large numbers required.[24]

1.1.4.2 Complexation Studies via Sodium-23 NMR

Lindman and Forsen reviewed the sodium-23 studies of sodium complexed by low molecular weight ligands such as aminoacids, organic acids, and sugars.[6] In comparison, macrocyclic compounds like crown ethers and their natural analogs, such as valinomycin[30] or monensin[31] are structurally predisposed to bind cations in their molecular cavity. Besides being of vital relevance to the cation chemistry in biological tissues, these compounds form strong and selective complexes with alkali cations. Thus one can work with two well-defined species: solvated cations and complexed cations.

Many aspects of complexation are accessible to study by cation NMR. Complex formation constants below 10^5 M^{-1}, can be obtained by fitting the chemical shifts or the relaxation rates for a number of crown/cation ratios with an expression for the complexation occurring. For higher formation constants only stoichiometric information and a lower limit for the formation constant of about 10^5 M^{-1} can be obtained.[32][4]

Bisnaire et al.[17] showed that in the case of the sodium:DB24C8 complex, both chemical shifts and relaxation rates are independent of the solvent and counter anion. This confirms the wrap-around conformation assumed by large crown rings to optimally coordinate to the bound cation.[34][35] By measuring both the quadrupolar sodium relaxation and the dipolar relaxation of

[4] Izatt et al. compiled thermodynamic and kinetic data for cation-macrocycle interactions.[33]

the crown ether carbon-13 in the tight complex,[36] Bisnaire et al. could separate the quadrupolar coupling constant χ and the reorientational correlation time τ_c.[17]

$$1/T_{2q} = \upsilon_{1/2} = \frac{2}{5}\pi^2 x^2 \tau_c \qquad (9)$$

$$1/T_1 dd = 1/T_1 obsd \frac{(nOe)_{obsd}}{1.98} = N_H \gamma_C^2 \gamma_H^2 \hbar^2 r_{C-H}^{-6} \tau_{eff} \qquad (10)$$

In eq. 10, N_H, γ_C, γ_H, and r_{C-H} denote as usual the number of protons per carbon atom, the gyromagnetic ratios of carbon and proton, and the carbon-hydrogen distance. For several organic solvents including nitromethane, the authors obtained a value for the quadrupolar coupling constant χ of 1.0 (0.2) MHz. The rotational reorientation time τ_c was 65 (11) ps in $CDCl_3$.

Another good example of sodium-23 NMR's power as a structural probe is the extensive self-association of 5'-guanosine monophosphate studied by Paris and Laszlo.[37] The increase of the sodium-23 relaxation rate with concentration reflected the degree of aggregation. Recently, other studies used alkali cation NMR to probe the solution chemistry of biological macromolecules, including proteins[38] and the channel forming antibiotic Gramicidin.[39][40]

In much of the cation NMR research into macrocyclic complexation up to date crown ether derivatives have been used as ligands. They mimic many properties of their natural analogs such as ring size, flexibility and cation-wrapping. As well, their symmetry simplifies both NMR observations and interpretations. Over 2100 macrocyclic compounds had already been synthesized by 1981, yet so far researchers have thoroughly studied only a few derivatives of 15C5 and 18C6. The complexation and decomplexation processes are of special interest, since they are the crucial steps in membrane transport. In a few cases where ligand atoms showed large chemical shifts between free and complexed state, the exchange rates could be measured using proton or carbon-13

NMR linebroadening methods.[36][41][42] However, NMR of the complexed cation is a more sensitive probe into exchange rates, since both chemical shifts and relaxation rates may be very different for the solvated and the complexed cation.

In 1971 Shchori et al. studied the sodium cation exchange with DB18C6 in dimethylformamide.[43] While there is no significant chemical shift difference between the two states in dimethylformamide, their relaxation rates are very different indeed: $1/T_2$ is 35 s^{-1} for the solvated and about 2000 s^{-1} for the complexed sodium. In the slow exchange region the authors could only observe the signal for the solvated sodium, the signal for the complex disappearing into the baseline.

In the intermediate exchange region, here between -40 and +10°C, the exchange rates are about the same as the relaxation rates for the solvated sodium. By chemical exchange the solvated state (a) transfers some x-y magnetization to the complexed state (b), where it decays rapidly. So with increasing temperature and exchange rate, the solvated sodium signal begins to broaden.

In the fast exchange region, (>10°C), each sodium cation exchanges many times between both states before its magnetization decays. The observed relaxation rate will now reflect the weighted average of both solvated and complexed state.

Now in the intermediate region, the mean life time of the two species (τ) can be derived from a quantitative analysis of the lineshape using the Bloch-McConnell equations for equivalent chemical shifts and continuous wave NMR.[43][5]

$$1/\tau = 1/\tau_a + 1/\tau_b = k_a + k_b \qquad (11)$$

Shchori et al. consider two possible routes for the chemical exchange between the two sites:[6]

[5] Woessner gave the equivalent equations for pulse NMR.[13]

[6] In this thesis the unimolecular exchange rate constants are consistently called k_1 and k_{-1}; the bimolecular constant k_2. This is in contrast to Shchori's and Popov's notations, yet makes for easier recognition.

$$(Na^+)_s + (C)_s \underset{k_{-1}}{\overset{k_1}{\rightleftharpoons}} (Na^+,C)_s \qquad (12)$$

$$(Na^+)_s + (Na^+,C)_s \overset{k_2}{\rightleftharpoons} (Na^+,C)_s + (Na^+)_s \qquad (13)$$

Since sodium cations could leave the solvated state by both pathways, the overall rate for this process is given by the sum of both pathways:[43]

$$k_a = 1/\tau_a = k_2[NaC] + k_{-1}\frac{[NaC]}{[Na]} \qquad (14)$$

To distinguish between the two pathways, Shchori et al. plotted $1/(\tau_a \times [NaC])$ versus 1/[Na]. At constant ionic strength (adjusted with LiSCN), this plot yielded a straight line with zero intercept. This indicates the bimolecular mechanism to be negligible, and gives an upper limit of 10^3 $M^{-1}s^{-1}$ for k_2.

The authors suggest that the bimolecular mechanism would force two cations into unfavorable proximity in the transition state, and that thus the unimolecular decomplexation pathway is preferred. They also find that the thiocyanate anion (d = 2.4Å) doubles the exchange rate, compared with the bulky anion tetraphenylborate (d = 5Å). The rate of unimolecular decomplexation at 25°C, $k_{-1} = 6\times10^7$ $M^{-1}s^{-1}$, is comparable to that found by Eigen et al. for the decomplexation of sodium from monactin in methanol at the same temperature:[44] $k_{-1} = 3\times10^8$ $M^{-1}s^{-1}$ The corresponding activation energy for decomplexation is 6.5 kcal/mol. Shchori et al. extended their study to the solvents methanol, dimethoxyethane and dimethylformamide; and to the ligand

DB18C6 and several of its derivatives. They found unimolecular decomplexation with similar rate constants in all systems.[45]

In 1975, Shporer and Luz[46] applied the same method to potassium complexation by DB18C6 in methanol. In 1975, and Schmidt and Popov[47] applied it to potassium complexation by 18C6 in several organic solvents. The most interesting result was the dominance of the bimolecular exchange mechanism detected by Schmidt and Popov, since all but one of the previously studied exchange systems of this type had shown purely unimolecular decomplexation.[41] The transition state is presumed to be the dicationic complex K^+ - 18C6 - K^+ ; the counter anion being the large hexafluoroarsenate.[47]

Up to now all alkali cation - crown ether complexation systems whose kinetics have been studied with cation NMR use derivatives of the near-planar 15C5 or 18C6. These ligands have little flexibility. Too small to completely cover the cation, they allow solvent molecules and counter anions access to the complexed cation from the two pole faces of the complex. They thus resemble small ionophores such as enniatin.

But many of the natural ionophores have a much larger ring structure. This allows them to form a well defined molecular cavity around the cation. Valinomycin, monensin, the actins, antamanide and others belong to this group (see also chpt. 3 - Transport).

Some crown ethers act in much the same way: DB30C10 for potassium, and DB24C8 for sodium cations. Chock studied the first potassium:DB30C10 system in methanol using temperature jump-relaxation. He found that the rate limiting step of the decomplexation involved a conformational rearrangement of the ligand backbone.[57] Other researchers have discussed similar conformational rearrangements for the decomplexation reaction of smaller crown complexes.[43][49][52]

Shamsipur and Popov[58] and Stover et al.[59] found sodium:DB30C10 complexes in nitromethane of stoichiometries 2:1 and possibly 3:2, besides the most stable 1:1 complex. No exchange broadening was detected at crown/sodium ratios smaller than one, so the lifetimes of solvated and complexed sodium cations must be shorter than 10^{-6} s at 0.05 M.[7]

Shporer et al. studied the complexation kinetics of the sodium-valinomycin system in methanol.[30] They found a unimolecular decomplexation rate of k_{-1} of 1-3 x $10^6 s^{-1}$ (E_a = 9.5 kcal/mol), in agreement with the value Funck determined earlier with temperature jump-relaxation : k_{-1} = 2 x 10^6 s^{-1}.[60] These rates are about 50 to 100 times lower than those for unimolecular decomplexation of sodium from its complexes with 18C6 derivatives in methanol.[43]

The sodium - DB24C8 system is a fascinating model for the cation complexation by large ligands: the cation fits well in the cavity formed as the ligand wraps itself around it.[17][61] The stability constant for the 1:1 complex is so high that the complexation is effectively quantitative in nonpolar solvents like nitromethane, acetonitrile, and tetrahydrofuran. The complexed sodium has a well defined ethereal coordination shell from which solvent molecules and counter anions are excluded. Furthermore, the symmetric array of the eight oxygen donor atoms results in a rather narrow linewidth for the complexed sodium. This facilitates low concentration measurements and allows observation of two separate signals in the slow exchange region. Finally, there is a large chemical shift difference between sodium solvated by nitromethane and sodium complexed by DB24C8 (540 Hz = 6.8 ppm). This makes the system very sensitive to exchange broadening near the fast exchange limit (Tab. 4).

Next to the ligand and the solvent molecules, the counter anion may also coordinate to the uncomplexed sodium cation, thereby potentially affecting it's chemical shift and it's relaxation rates, as well as the exchange rates. The cation-anion interactions themselves will be reviewed in chapter 2.2.5.. The effects of solvent and anion on the exchange rates and mechanisms are discussed below.

[7] Calculated with eq. 8.

1.1.5 Anion Effects on Complexation

What is known about the role of the solvent and the counter anion with regard to the exchange of cations between free and complexed state? In 1971 Shchori et al. used for the first time sodium-23 NMR to study complexation kinetics.[43] They noticed that the decomplexation rate of the sodium-DB18C6 complex in dimethylformamide is twice as high in the presence of thiocyanate as counter anion as with tetraphenylborate. Sodium tetraphenylborate is well known to form only solvent-separated ion pairs in solutions.

In 1981, Lin and Popov studied the cation exchange between the free and complexed site for Na:18C6 in tetrahydrofuran and 1,3-dioxolane. With tetraphenylborate as counter anion, the exchange rate was low enough to allow the observation of two signals, corresponding to free and complexed sodium. But in the presence of perchlorate, or iodide,[48] or thiocyanate,[51] these two signals coalesced due to faster exchange.

Anion effects in complexation were observed with techniques other than NMR as well: Petrucci et al. studied alkali complexation kinetics with 18C6 in dimethylformamide and ethanol using ultrasonic relaxation methods. They found that the choice of solvent may affect the number of observable complexation steps within the Eigen-Winkler model.[49][50] They further detected ionic association of sodium and potassium thiocyanate in dimethylformamide using Raman spectroscopy.[50]

The stage was now set: First, ionic interactions could not be ignored or neglected anymore, since even anions such as perchlorate, iodide and thiocyanate strongly affected the exchange kinetics. Second, development of instruments and of the understanding of the complexation processes, enabled the kinetic measurement itself to serve as a tool for studying anion and solvent effects.

Several research groups simultaneously began using NMR to study such secondary aspects of complexation.[51][52][53][54][55][56]

Popov et al. followed up their early results with a direct comparison of the rates of exchange between sodium thiocyanate and sodium tetraphenylborate and their 18C6 complex in tetrahydrofuran.[51] Sodium tetraphenylborate exchanges by the unimolecular pathway, with $k_{-1} = 53s^{-1}$, and an activation free energy $dG^{\#}$ of 64.2 kJ/mol. The activation energy (E_a = 50.6 kJ/mol) is the same as the values found by Shchori et al. for DB18C6 in methanol, dimethylformamide, and dimethoxyethane.[43][45] However, with sodium thiocyanate the exchange proceeds via the bimolecular pathway with $k_2 = 183000\ M^{-1}s^{-1}$ and $dG^{\#} = 43.7$ kJ/mol.[8] Yet Popov et al. neglect the change in ionic interaction upon the addition of crown, with the concomittant change of chemical shifts and relaxation rates of the uncomplexed sodium (and possibly also of the 1:1 complex).[51]

In a parallel work, Strasser and Popov studied the effect of solvent donicity on the sodium cation exchange in systems containing 18C6 and ether sodium tetraphenylborate or sodium thiocyanate.[51] They found dissociative unimolecular exchange in the high donicity solvents methanol, tetrahydrofuran-methanol, and 80-20% tetrahydrofuran - propylenecarbonate. Yet in neat propylenecarbonate and 40-60% tetrahydrofuran - propylenecarbonate, the bimolecular exchange mechanism prevailed.

The authors concluded that high donicity ligands, whether they are counter anions (thiocyanate, iodide, perchlorate), or solvent molecules (methanol, propylenecarbonate), promote the unimolecular decomplexation by stabilizing the transition state. Strasser and Popov in fact found a linear correlation between the free activation energy for unimolecular decomplexation and the

[8] Popov's expression for the mean lifetime $1/\tau = 2k_1[Na]_t + k_{-2}[Na]_t/[Na]$ should not contain the factor 2.[51] Instead, his equation should read: $1/\tau = k_1[Na]_t + k_{-2}[Na]_t/[Na]$, with k_1 being the bimolecular exchange rate constant, and k_{-2} the unimolecular decomplexation rate constant. Popov's values quoted in this thesis have been corrected by multiplying his bimolecular rate constant by two.

Gutmann Donor number.[52] Conversely, only the bimolecular process is possible in solvents of low donicity and high dielectric constant. The latter reduces the charge-charge repulsion between the two cations in the bimolecular transition state (see also the discussion on sodium hexafluorophosphate).

Recently, Dye et al. reported on the sodium cation complexation to 18C6 in methylamine. They described the exchange of sodium cation between the solvated ion-pair and the complexed ion-pair, with bromide[53] or sodide (Na^-) as counter anion.[54] Electron transfer (sodium cation - sodide exchange), facilitated by the crown, becomes an additional exchange pathway.[54] Dye et al. have built these studies around the assumption of quantitative ion-pairing, since they found both bromide and sodide anions to coordinate more strongly to the free and the complexed sodium cation than does the solvent methylamine.

In early cation NMR studies of exchange kinetics, the anion effects (i.e. ion-pairing) were suppressed by using high donicity solvents such as dimethylformamide, dimethoxyethane, and by using what were considered to be weakly coordinating anions, such as perchlorate, thiocyanate, tetraphenylborate, and iodide.

However it is now clear that ionic association is the rule rather than the exception, especially in non-aqueous solvents. It is clear too that the phenomena itself, and its effects on cation reactions such as complexation, warrants closer scrutiny.

As part of this study the effects of ionic association on complexation and exchange were studied in detail (chpt. 1.25, p. 85). Sodium thiocyanate and iodide were choosen since they are among the salts most widely studied in non-aqueous solutions; their strong ionic interaction is well known and generally interpreted as contact ion-pairing.[18][25][83][84][86]

Popov observed the concentration dependence of the sodium chemical shift at concentrations down to about 0.01 M in several organic solvents, and for several sodium salts.[18] However, he

did not use nitromethane as a solvent, probably because the solubilities of both salts in this solvent are too low (0.01 M) to allow for acceptable signal-to-noise ratios, using the magnetic field strengths available at this time. Thanks to the high magnetic field strength available (7T), it is now possible to easily study the complexation of sodium thiocyanate and sodium iodide with DB24C8 in nitromethane at a total sodium concentration of 0.01 M or 0.005 M. Solutions containing as little as 0.000012 M sodium could be measured within several hours at 79.349 MHz.

1.2 Complexation of Sodium Cations by DB24C8

Table 1 gives an overview of the DB24C8 - complexation systems studied in this thesis.

Table 1: Overview of DB24C8 Complexation Systems

Solvent	Counter anion PF_6^-	BPh_4^-	I^-	SCN^-
Tetrahydrofuran	–	+	–	–
Acetonitrile	–	+	–	–
Pyridine	+	–	–	–
Nitromethane	+	+	+	+

1.2.1 Experimental Methods

DB24C8, sodium tetraphenylborate and sodium hexafluorophosphate were purchased from Sigma Chemical Company; sodium iodide and sodium thiocyanate were technical grade. All salts were recrystallized from acetonitrile and cyclohexane and dried under vacuum at 60°C over phosphorous pentoxide for several hours prior to use.[9] DB24C8 was dried under vacuum at 60°C over phosphorous pentoxide for several hours prior to use.

[9] Sodium hexafluorophosphate is moisture sensitive, and forms a white smoke containing hydrofluoric acid when exposed to humid air.

Samples were prepared by weighing the appropriate amounts of solid crown ether directly into 5 ml volumetric flasks, and filling up with a stock solution of the desired sodium salt concentration. All handling was done rapidly in air.

10mm open diameter NMR tubes were then filled with about 3 ml sample, the air replaced with argon and the tubes sealed with Parafilm. Salts and DB24C8 were used within a year, freshly distilled solvents within two months, and the spectra taken within 2 days, of sample preparation.

The sodium-23 spectra were measured at 21.036 MHz (Varian FT-80), 53.92 MHz (Varian XL-200), and 79.349 MHz (Varian XL-300). An external D_2O field-frequency lock was used at 21.036 MHz, while at 53.92 and 79.349 MHz no lock was used. The field drift on the two high field instruments was less than 1 Hz per hour. The magnetic fields were shimmed on a sample containing D_2O, or on a sample containing deuterated nitromethane in acetonitrile, both methods giving a sodium-23 line width of 7 Hz at 21.036 MHz, and of 8 - 10 Hz at 79.349 MHz. These values are close to the natural line widths of dilute sodium solutions in water or nitromethane.

The chemical shifts were referenced to sodium chloride or, equivalently, to sodium tetraphenylborate at infinite dilution in water. They are corrected for the bulk susceptibility differences between the organic solvents and the aqueous reference sample. For solenoid magnets with the magnetic field lines running parallel to the long axis of the cylindrical sample tubes, the corrected shift is:

$$\text{Shift}_{true} = \text{Shift}_{obs} + (4\pi/3)(X_{ref} - X_{samp}) \qquad (53.93 \text{ and } 79.35 \text{ MHz})$$

For electromagnets where the magnetic field lines run perpendicular to the long axis of the sample tube, it is:

$$\text{Shift}_{true} = \text{Shift}_{obs} - (2\pi/3)(X_{ref} - X_{samp}) \qquad (21.04 \text{ MHz})$$

X are the volume magnetic susceptibilities of the pure solvents. (The effects of the dissolved salts on the susceptibility can be neglected.[62]) Table 2 presents the correction terms for the solvents used in this thesis:

Table 2: Magnetic Susceptibility Corrections

Solvent	X	Correction Terms[ppm] at:	
	[x 10^{-6}]	53.92 and 79.35 MHz	21.04 MHz
Nitromethane	-0.391	-1.374	+0.687
Acetonitrile	-0.534	-0.775	+0.387
Pyridine	-0.611	-0.452	+0.226
Water (H_2O)	-0.719	-	-

X are the volume magnetic susceptibilities of the pure solvents.

To measure the chemical shift at low signal to noise ratios (at low concentrations) more accurately, a line broadening of 5 to 20 Hz was applied to the FID prior to determining the chemical shift. The reported linewidths are not subject to line broadening, and are not corrected for viscosity unless indicated otherwise. The transverse relaxation rates are taken from the full linewidths at half height according to eq. 6.

1.2.2 Solvent Effects

Table 3 gives an overview of the Na-23 NMR chemical shifts and relaxation rates of solvated and complexed sodium in different solvents used in this thesis.

Table 3: Chemical Shifts of Free and Complexed Sodium in Four Solvents

Solv.	Anion	Conc.	Na-Shift free	Na-Shift comp.	$1/T_2$ free	$1/T_2$ comp.	vis.-corr.	X^a comp.
		[M]	[ppm]	[ppm]	[s^{-1}]	[s^{-1}]	[s^{-1}/cP]	[MHz]
THF	BPh_4^-	0.01	(-7.16	-8.05)[b]	66	248		
AN	BPh_4^-	0.04	-7.37	-8.20	23	132	383	0.9
PYR	PF_6^-	0.01	+0.22	-8.22	128	403	413	0.9
NM	BPh_4^-	0.037	-14.49	-8.19	25	195	314	0.8
NM	PF_6^-	0.037	-14.81	-8.20	25	195	314	0.8
NM	SCN^-	0.005	-10.84	-8.12	298	189	304	
NM	SCN^-	0.01	-10.24	-8.20	361	195	314	
NM	I^-	0.01	-10.52	-8.18	50	195	314	

The chemical shifts are relative to sodium chloride at infinite dilution in D_2O. They are corrected for the magnetic susceptibility differences between the solvents (See above). (a): Bisnaire and Detellier [17]. (b): The shifts in tetrahydrofuran are uncorrected.

1.2.2.1 Static Effects (Complexation Equilibrium)

Chemical shifts and relaxation rates of the solvated sodium vary widely for different solvents and counter anions, yet for the 1:1 complex, the viscosity corrected relaxation rates and especially the shifts are independent of both solvent and counter anion. Once again this result supports the complexation model for large crown ethers, here DB24C8, where the crown wraps itself tightly around the cation, negating any access of solvent or anion to the cation.[17][61]

Figures 3 and 4 show the sodium chemical shift and transverse relaxation rates in acetonitrile. The observed signal represents the weighted average of the solvated and complexed sodium cation. The chemical shift as well as the linewidth vary linearly with crown/sodium (P), going from the values for solvated sodium at $P = 0.0$ to the values for the 1:1 complex at $P >= 1.0$. The sharp cutoff at P where it equals 1.0 allows only a lower limit of $10^5 M^{-1}$ to be given for the complex formation constant K_c.[58][63]

In acetonitrile the sodium is solvated by 4-6 nitrogen donor atoms. Yet the chemical shift difference between solvated and DB24C8-complexed sodium is only 0.83 ppm (Tab. 3). In non-polar ether-based solvents such as tetrahydrofuran, complexation is also strong, and the chemical shift difference between solvated and complexed states is again small with 0.89 ppm. This is due to the similar coordination sphere in both states (Tab. 2).

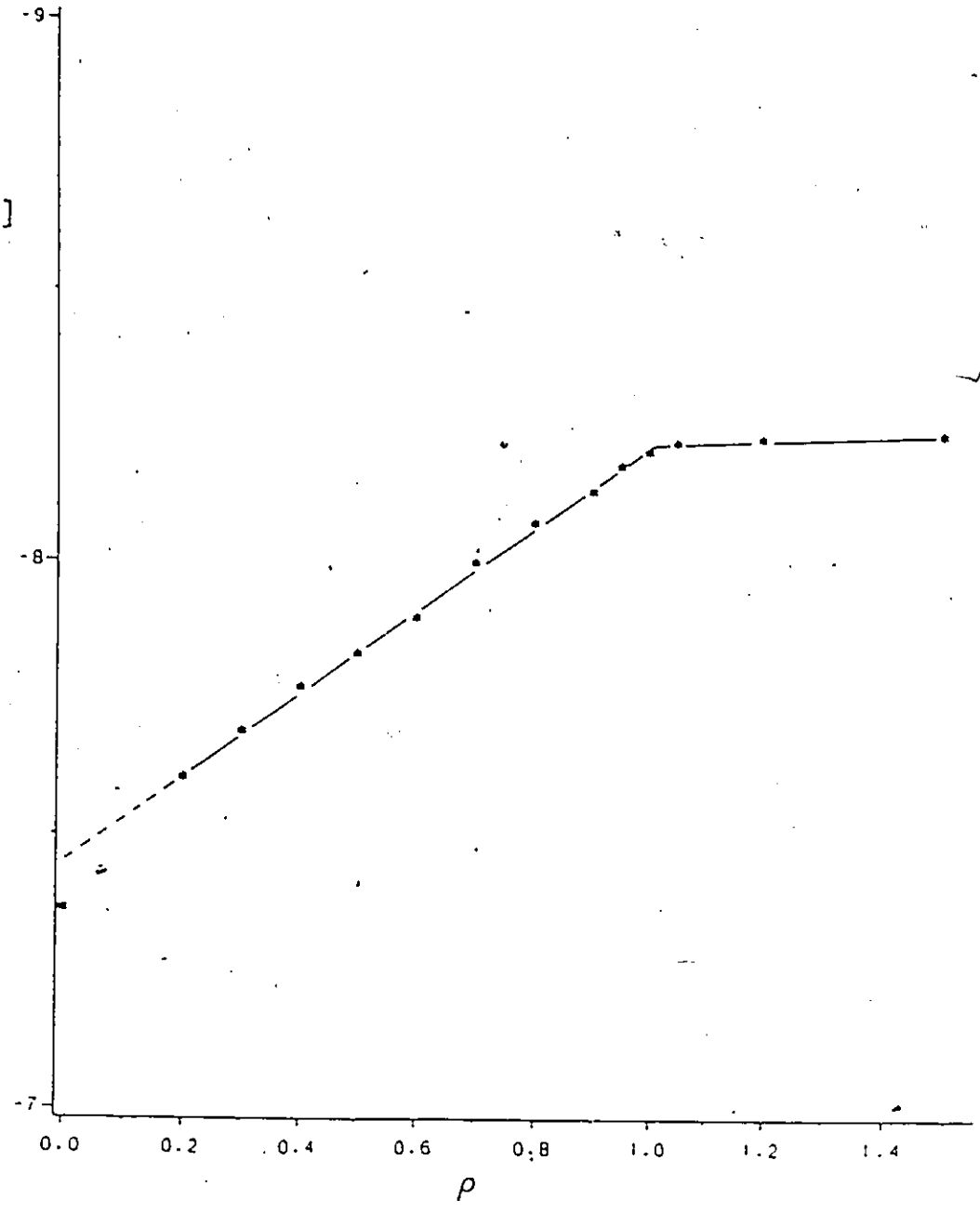

Figure 3: Sodium-23 Chemical Shift in Acetonitrile - $NaBPh_4$:DB24C8. Shift for $NaBPh_4$ (0.01 M) as function of the ratio [DB24C8]/[Sodium] at 79.35 MHz.

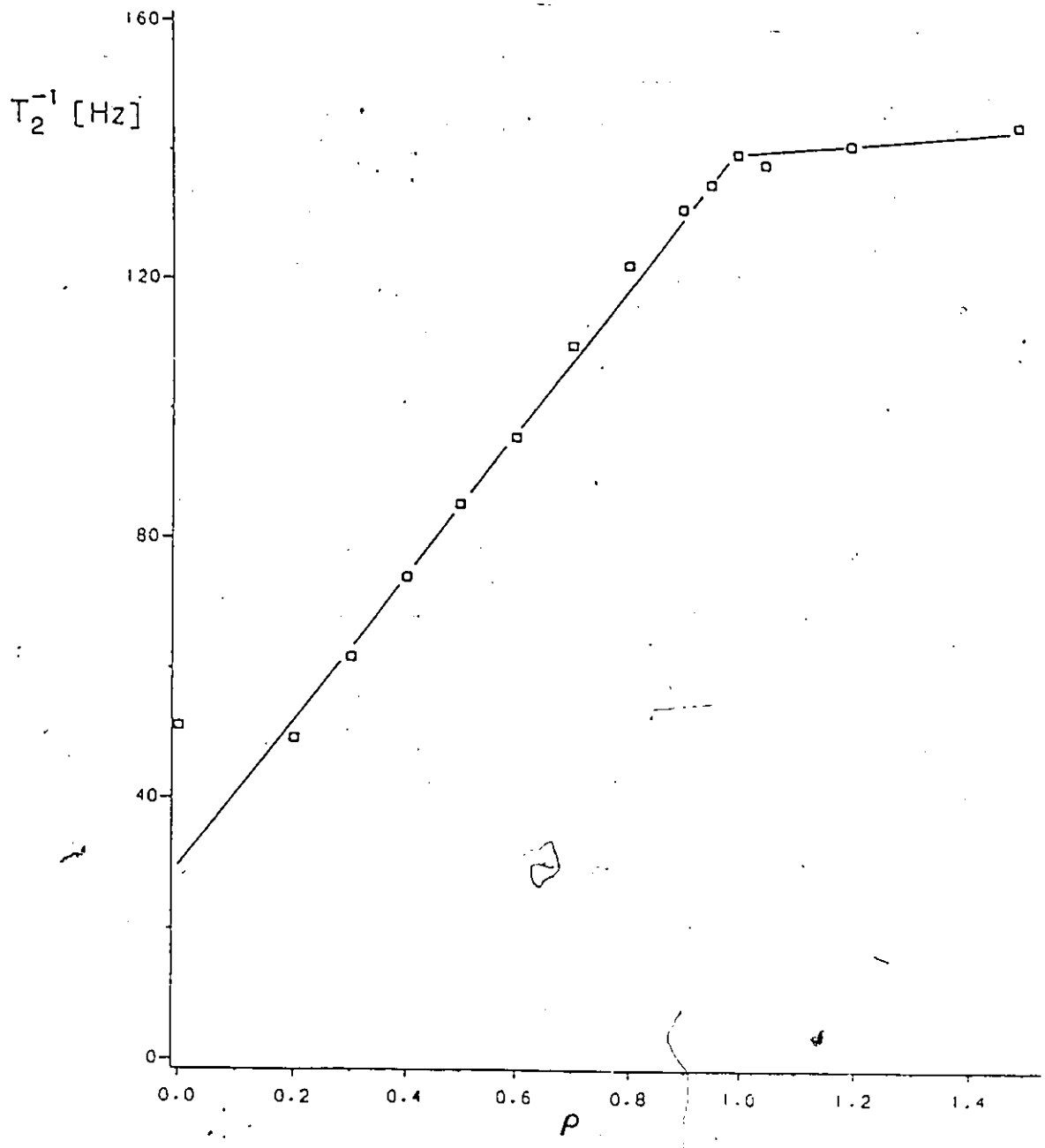

Figure 4: Sodium-23 Transverse Relaxation in Acetonitrile - $NaBPh_4$:DB24C8. Transverse relaxation rates for $NaBPh_4$ (0.01 M) as function of the ratio [DB24C8]/[$NaBPh_4$] at 79.35 MHz.

1.2.2.2 Limits of Observability of Exchange in THF, AN, PYR and NM

In the systems shown above there is only one averaged signal, and a linear change of shifts and relaxation rates with ρ. These two observations indicate that the exchange between solvated and complexed sodium is too rapid to contribute to the transverse relaxation rate at room temperature.

According to Woessner's equation the exchange contribution to transverse relaxation, $1/T_2ex$, depends upon the square of the chemical shift difference between the two exchanging states (eqs. 15 and 16 are identical to eq. 8, p.15):[13]

$$1/T_2ex = 4\pi^2 P_a P_b (\nu_a - \nu_b)^2 / (k_a + k_b) \qquad (15)$$

or

$$k_a + k_b = 4\pi^2 P_a P_b (\nu_a - \nu_b)^2 T_2ex \qquad (16)$$

If the lowest detectable exchange relaxation $1/T_2ex$ is taken to be 31 s^{-1} (or 10 Hz in line width), then the limiting rates can be calculated, below which exchange becomes noticable in the four solvents studied: Table 4 illustrates how the large chemical shift difference between solvated sodium and its DB24C8 complex should allow the observation of faster exchange in nitromethane and pyridine, than in tetrahydrofuran and acetonitrile.

Yet in pyridine chemical shifts and relaxation rates vary nonlinearly with the ratio crown/sodium (ρ) (Fig. 5), indicating a relatively small complexation constant K_c.

The equilibrium model below was fit to the experimental points in Figs. 5 and 6, using a least squares fitting routine inside a SIMPLEX minimization program.[74]

Table 4: Lowest Exchange Rates Observable at 0.037 M

	AN	THF	PYR	NM
$(\nu_a-\nu_b)^2$ [Hz]	4360	4990	448 000	275 000
$(k_a+k_b)'$ [s^{-1}]	1300	1500	130 000	90 000

$(\nu_a-\nu_b)^2$ is the square of the chemical shift difference in Hz between solvated and DB24C8 complexed sodium. $(k_a+k_b)'$ gives the exchange rates that will cause an exchange relaxation $1/T_{2ex}$ of 31 s^{-1} (10Hz in the line width), for sodium : DB24C8 in four solvents. (k_a+k_b) is the sum of the exchange rates, or the sum of the inverse life times, $1/\tau_a$ and $1/\tau_b$; its dimension is s^{-1} for unimolecular and $M^{-1}s^{-1}$ for bimolecular exchange mechanism.

$$(Na^+)_s + (C)_s \underset{}{\overset{K_c}{\rightleftharpoons}} (Na^+,C)_s \qquad (17)$$

$$Y_{obsd} = P_f Y_f + P_c Y_c \qquad (18)$$

Here P_f and P_c are the molar fractions of free and complexed sodium; Y_{obsd}, Y_f and Y_c are either shifts or relaxation rates observed, of free and of complexed sodium. $[Na]_t$ is the total sodium concentration. K_c is the complex formation constant. (See Appendix 1 for [Na] as a function of K_c and $[Na]_t$.) Table 5 gives the iterated values for shift and relaxation rates of free and complexed sodium, as well as the complexation constant.

The chemical shifts and the relaxation rates of $NaPF_6$:DB24C8 in pyridine show a similarly variation with ρ, and give comparable complex formation constants. This indicates the absence of exchange broadening in the transverse relaxation rates, so the exchange rate under these conditions

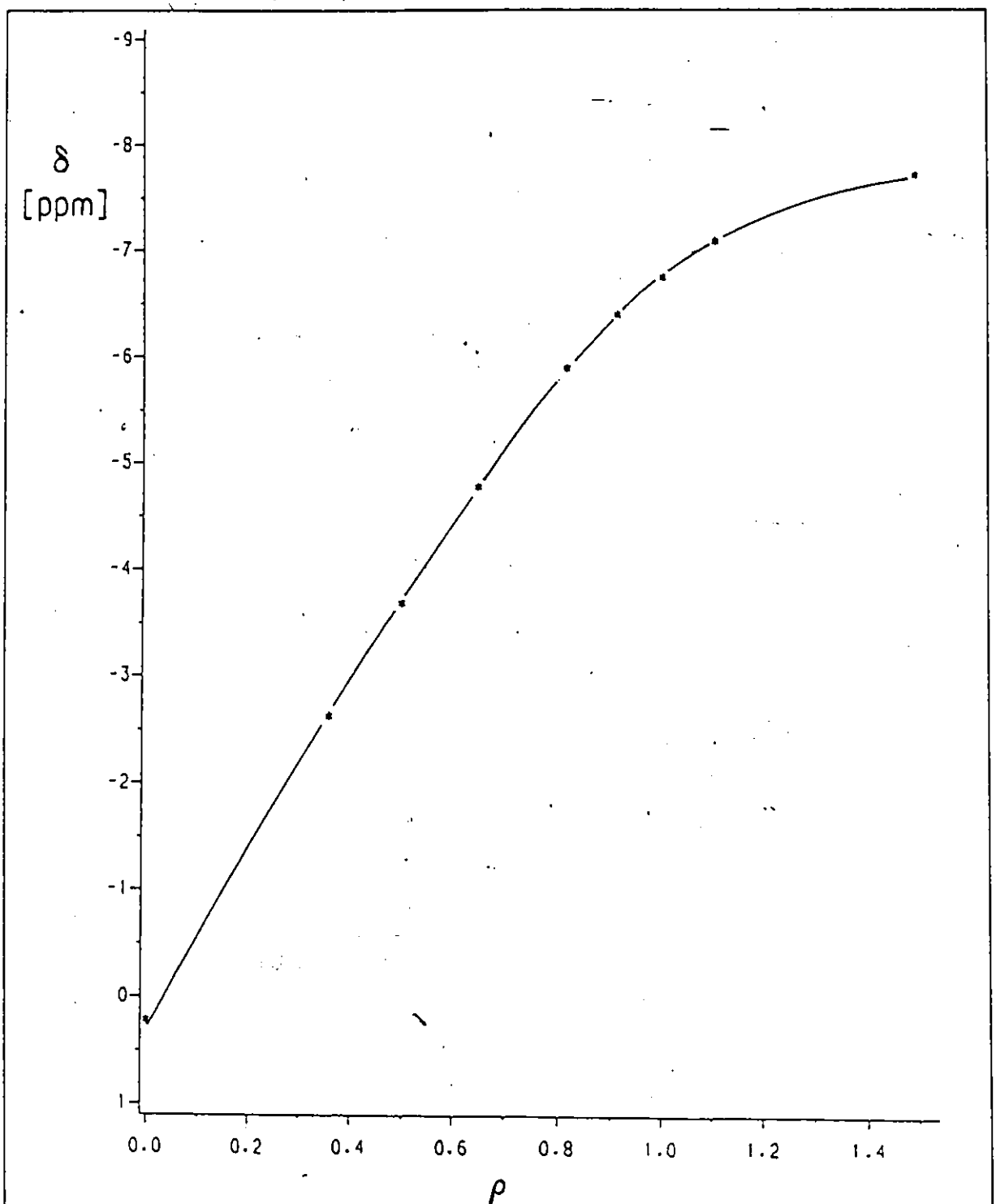

Figure 5: Sodium-23 Chemical Shifts in Pyridine - $NaPF_6$:DB24C8. Shifts as function of [DB24C8]/[$NaPF_6$] with [$NaPF_6$] = 0.01 M. The points are experimental. The solid curves are calculated from eq. 18 and the complexation parameters (Tab. 5).

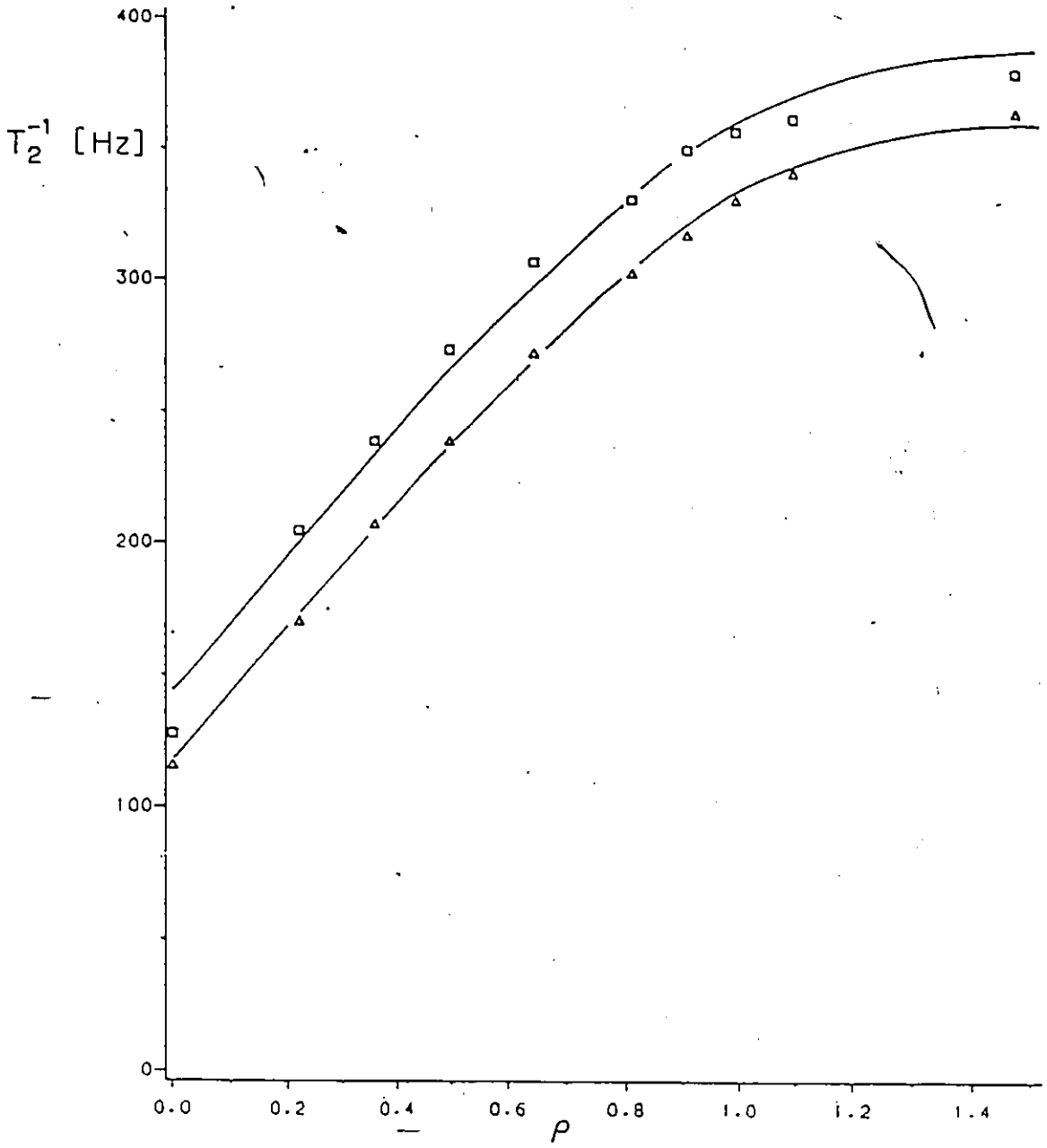

Figure 6: Sodium-23 Relaxation Rates in Pyridine - $NaPF_6$:DB24C8. Transverse (□) and longitudinal (△) relaxation rates for $NaPF_6$ (0.01 M) in pyridine as function of [DB24C8]/[Sodium]. The points are experimental, the solid curve is calculated from eq. 18 and the complexation parameters (Tab. 5).

Table 5: Complexation Parameters in Pyridine - $NaPF_6$:DB24C8

K_c [M^{-1}]	δ_f [ppm]	δ_c [ppm]	$1/T_1f$ [s^{-1}]	$1/T_1c$ [s^{-1}]	$1/T_2f$ [s^{-1}]	$1/T_2c$ [s^{-1}]
3020 (50)	+0.28 (0.1)	-8.22 (0.1)				
3040 (100)			117 (5)	376 (10)		
2600 (300)					144 (10)	403 (20)

δ_f, δ_c are iterated shifts; $1/T_1f$, $1/T_1c$ and $1/T_2f$, $1/T_2c$ are the iterated longitudinal and transverse relaxation rates for free and complexed sodium. K_c are the complexation constants from the three data sets.

has to be larger than 10^5 s^{-1} (Tab. 4). As seen from the relatively low complexation constant (Tab. 5), pyridine is an efficient competitor for the sodium cation. Its high donicity (Fig. 2) causes fast exchange.

The following chapters focus on the complexation of sodium salts by DB24C8 in nitromethane.

1.2.3 Complexation Mechanisms and Dynamics in Nitromethane - Sodium Hexafluorophosphate

1.2.3.1 Introduction and Methods

Nitromethane stands out as a solvent of extremely low donicity (D.N = 2.7; Fig. 2), but it has a comparatively high dielectric constant (ε = 35.9). The low donicity results in a high complexation constant and a large chemical shift difference between the solvated and the 1:1 complexed sodium (Tab. 2). Furthermore, anions have easier access to the coordination sphere of the free sodium. These properties make nitromethane a most useful solvent for studying exchange kinetics and weak anion effects. Table 6 gives, for each sodium salt, an overview of the observed complexation phenomena.

Table 6: Overview of Observed Phenomena

Salt	Exchange Broadening	Aggregation	Ionic Interaction	2:1-Complex
$NaPF_6$	+		+	
$NaBPh_4$	+	+		
NaI	+		+	
NaSCN	+		+	+

For sodium hexafluorophosphate and tetraphenylborate both the classical unimolecular decomplexation and the bimolecular cation interchange mechanism (see page 17) are active. As well, tetraphenylborate, as the most bulky anion, allows for the sodium induced aggregation of several crown molecules. Sodium thiocyanate and sodium iodide also showed bimolecular exchange. The rate of sodium thiocyanate exchange was about three times higher than those of the other salts.

All salts except sodium tetraphenylborate showed strong ionic interactions. These were quantitatively taken into account during the analysis of complexation and exchange. Sodium thiocyanate furthermore forms a 2:1 complex with DB24C8.

1.2.3.2 Two-Site Exchange - Results and Interpretation

Figure 7 shows the chemical shift of sodium hexafluorophosphate as a function of [DB24C8]/[sodium] in nitromethane. Only one signal was observed, representing the weighted average of complexed and solvated sodium. The linear slope and the sharp cutoff where equals 1.0 are again characteristic of a large complexation constant, and only a lower limit of about 10^6 M^{-1} could be estimated for K_c.

Judging from this chemical shift curve, one might expect a similar variation of the transverse and longitudinal relaxation rates with P (Fig. 8). Yet while the longitudinal relaxation rate is in fact analogous to the shift curve, the transverse relaxation rate shows a field dependent maximum at P about 0.6.

This maximum in the transverse relaxation rate could in principle be due to the formation of a 2:1 sodium : crown complex with a high quadrupolar coupling constant. Shamsipur and Popov,[58] and Stover et al.[59] have observed the analogous 2:1 sodium:DB30C10 complex in nitromethane. Yet in that case the longitudinal relaxation rate should also show this maximum, since in the extreme narrowing region longitudinal and transverse relaxation rates are equal (eq. 4).[10]

[10] Two facts combined verify the extreme narrowing situation. The first is the linear variation of both chemical shift and longitudinal elaxation rates with P. The second is the field independence of the transverse relaxation rate at P equal to 0.0 and 1.0.

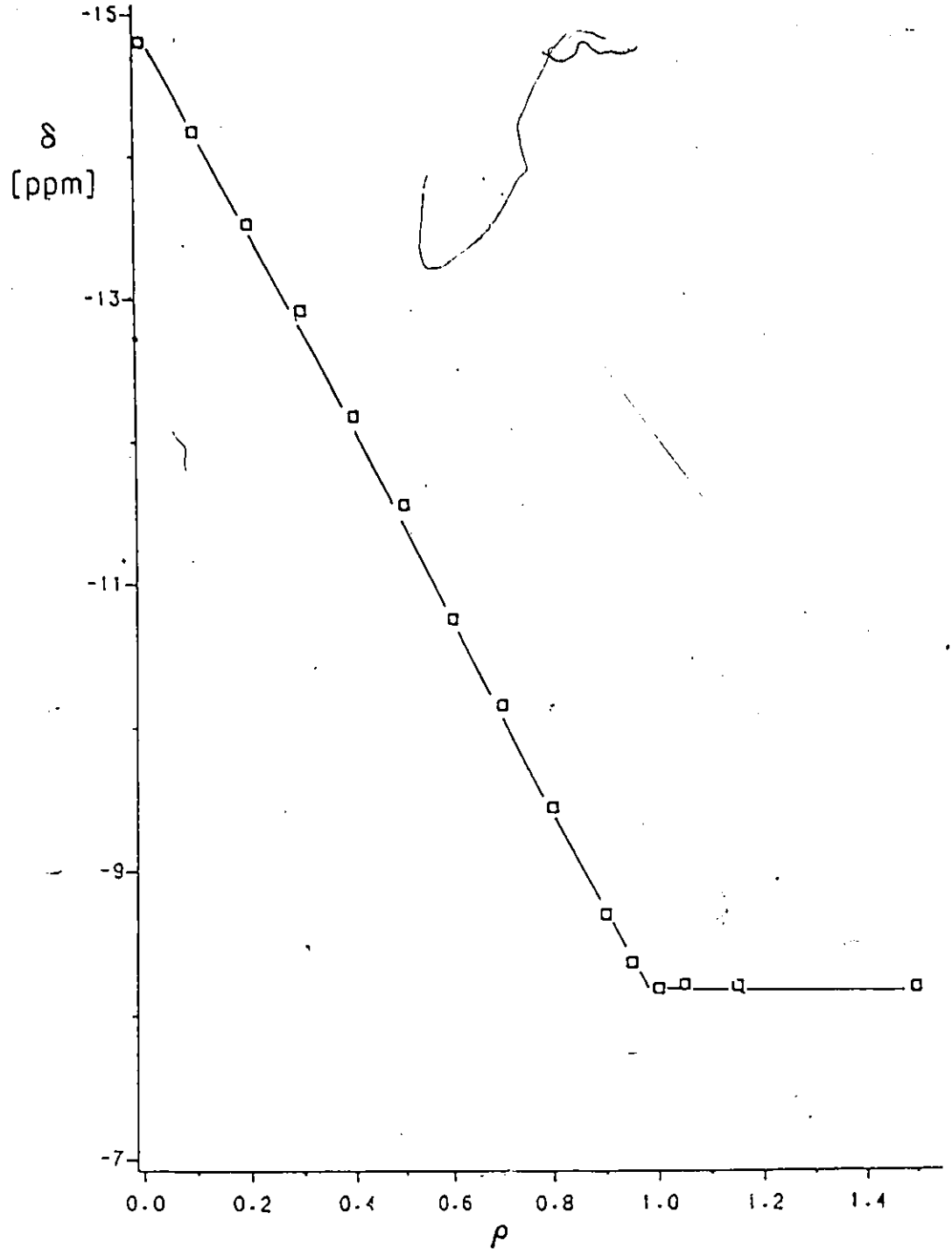

Figure 7: Sodium-23 Chemical Shifts in Nitromethane - $NaPF_6$:DB24C8. Shifts as function of the ratio [DB24C8]/[$NaPF_6$] at 79.35 MHz. [$NaPF_6$] is constant at 0.037 M.

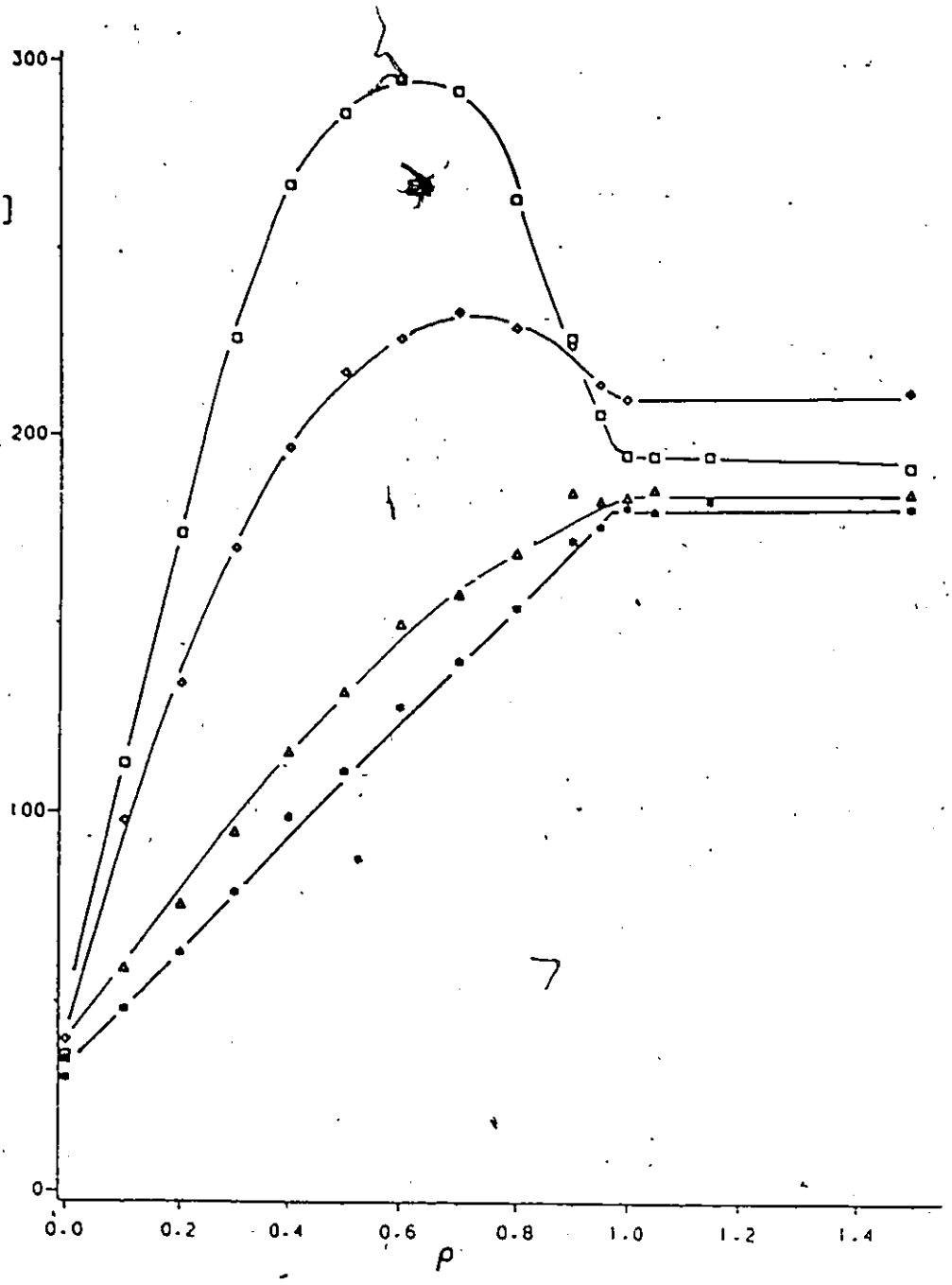

Figure 8: Relaxation Rates in Nitromethane - $NaPF_6$:DB24C8. Na-23 transverse relaxation rates at 79.35 MHz (□), 52.92 MHz (◇), and 21.04 MHz (△); and Na-23 longitudinal relaxation rates at 52.92 MHz (✳); as functions of [DB24C8]/[$NaPF_6$] (ρ) in nitromethane. The temperatures of measurement were 294 K (79.35 MHz and 52.92 MHz) and 297 K (21.04 MHz). All line shapes were Lorentzian.

This leaves only one possible explanation: exchange relaxation. As stated in the introduction, chemical exchange of sodium between two states (solvated and complexed) with unequal resonance frequency can lead to a mutual dampening of the x-y magnetization in both states, that is, to exchange relaxation ($1/T_2ex$):

$$1/T_2ex = 1/T_2obsd - 1/T_1 - 1/T_2inh \qquad (19)$$

The observed transverse relaxation rate $1/T_2obsd$ is π times the linewidth at half height (eq. 6). $1/T_1$ was measured at 53.92 MHz; since it has to be field independent in the extreme narrowing limit, the values measured at 53.92 MHz are valid at 21.04 MHz and 79.35 MHz as well. The inhomogeneity broadening $1/T_2inh$ was estimated at each field by taking the difference of $1/T_2obsd$ and $1/T_1$ for values of equal to 0.0, and larger than 1.0. At these values of P the exchange contribution to the observed relaxation rate, $1/T_2ex$, is zero.

In this way the exchange contribution $1/T_2ex$ to the transverse relaxation rate $1/T_2obsd$ can be isolated. Figure 9 shows the plot of $1/T_2ex$ against for all three resonance frequencies. According to Woessner,[13] the exchange contribution $1/T_2ex$ near the fast exchange limit can be approximated as (eqs. 20 and 21 are identical to eq. 8, p.15):

$$1/T_2ex = 4\pi^2 P_a P_b (\nu_a - \nu_b)^2 \; / \; (k_a + k_b) \qquad (20)$$

or

$$k_a + k_b = 4\pi^2 P_a P_b (\nu_a - \nu_b)^2 T_2ex \qquad (21)$$

where the symbols have their usual meaning (see page 15). Comparing Fig. 9 with eq. 20, we can make two observations:

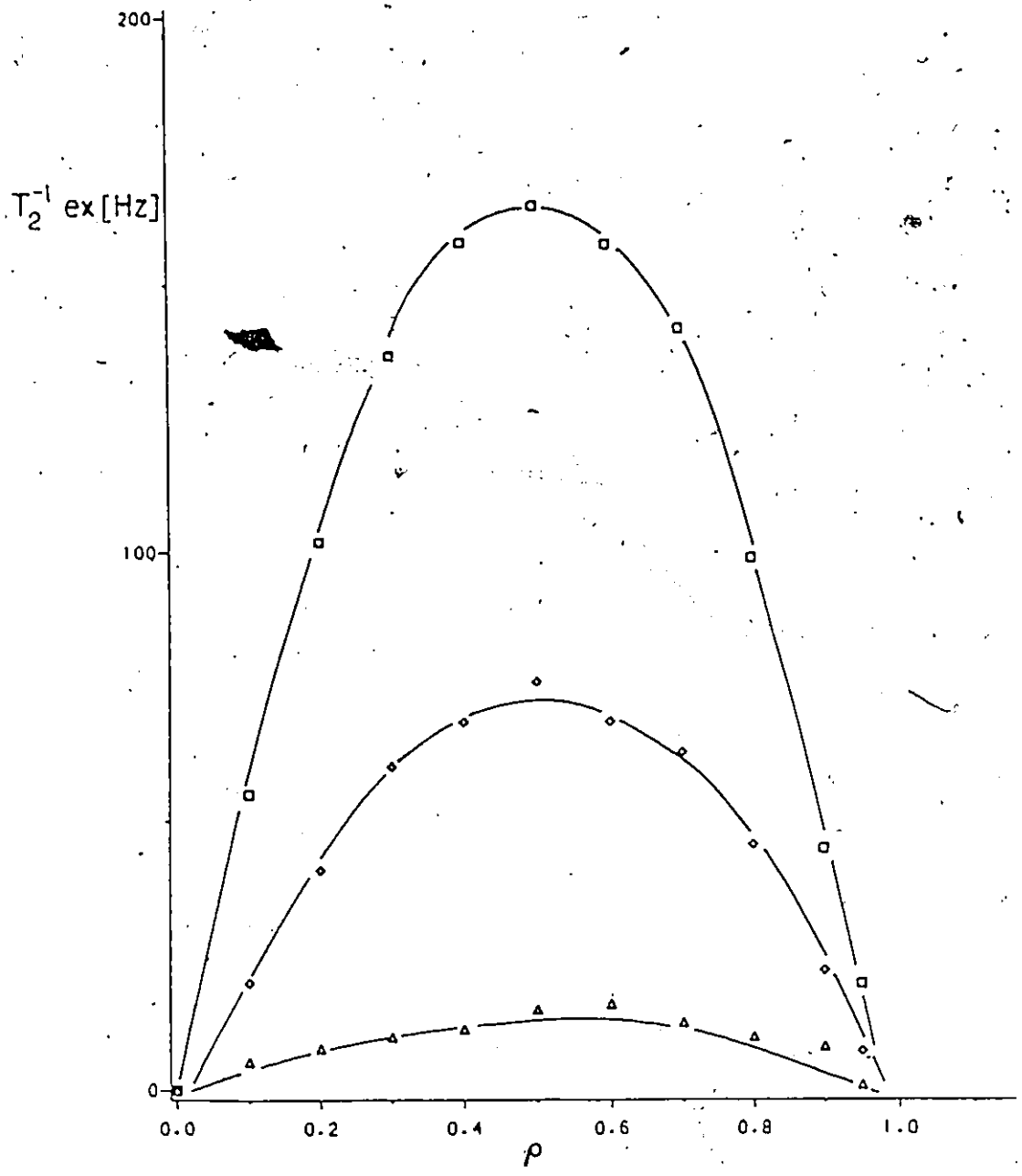

Figure 9: Exchange Relaxation $1/T_2ex$ in Nitromethane - $NaPF_6$:DB24C8. $1/T_2ex$ as a function of [DB24C8]/[$NaPF_6$] (ρ) at 79.35 MHz (□); 52.92 MHz (◇) and 21.04 MHz (△). [$NaPF_6$] = 0.037 M. $1/T_2inh$ is 10 s^{-1}, 30 s^{-1}, and =< 1 s^{-1} at 79.35 MHz, 52.92 MHz, and 21.04 MHz, respectively.

- At all three resonance frequencies $1/T_2ex$ is parabolic with the maximum at ρ equal to 0.5. This demonstrates the strict dependence of $1/T_2ex$ on the product P_aP_b in eq. 20: Since K_c is large ($> 10^5\ M^{-1}$), P_aP_b is approximately equal to $\rho(1-\rho)$, which has its maximum at ρ equal to 0.5.

- Eq. 20 further predicts a linear dependence of $1/T_2ex$ on the square of the chemical shift difference between the two exchanging states. Or, what comes out to the same, on the square of the magnetic field strength. Figure 10 demonstrates the close agreement between the predicted and the observed field dependencies of $1/T_2ex$ for ρ equal to 0.5.

The two points above each prove the adequacy of eqs. 20 and 21 to describe the $NaPF_6$: DB24C8 exchange kinetics.

The sodium-23 NMR data for sodium hexafluorophosphate : DB24C8 are listed in appendix 5.

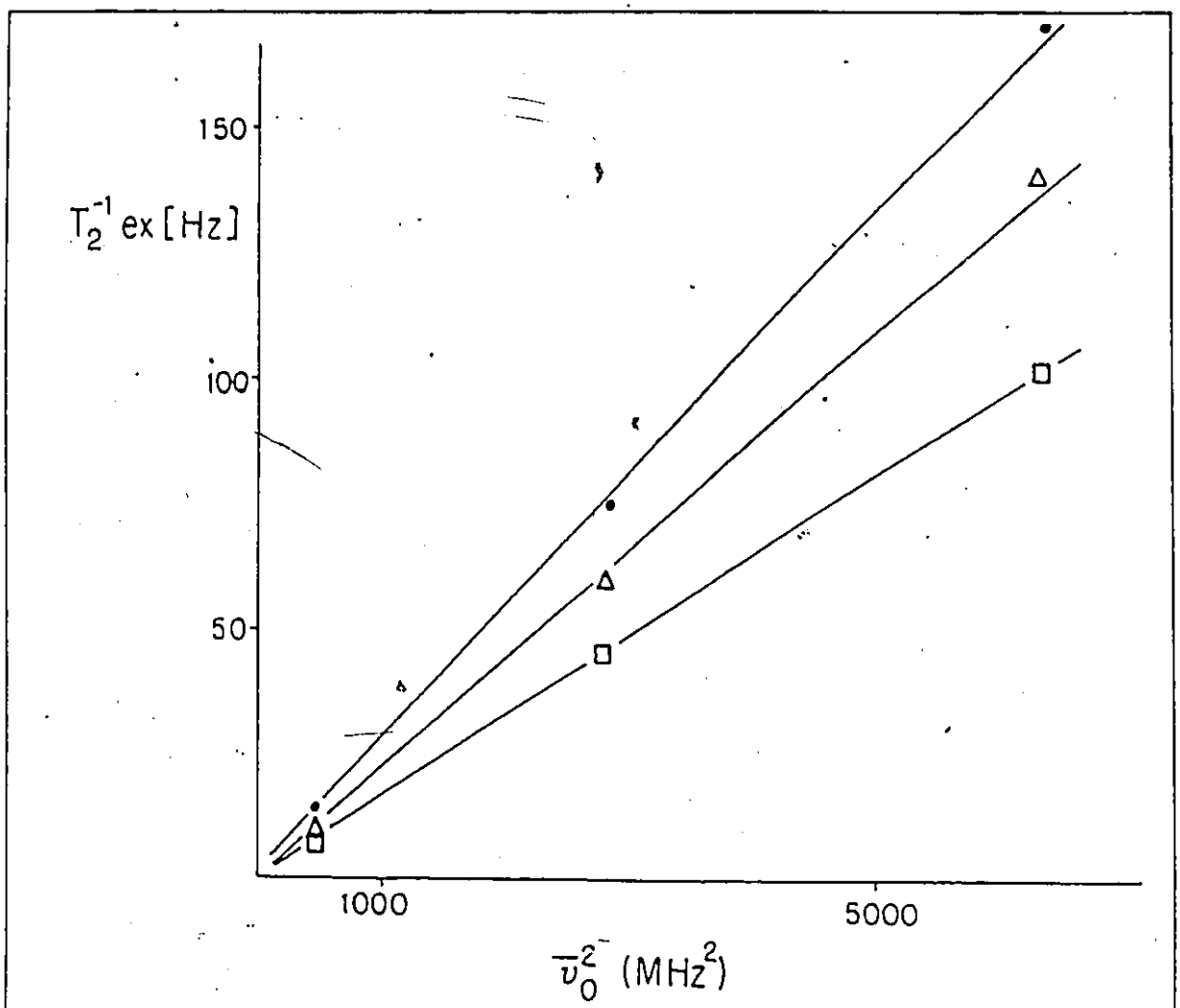

Figure 10: Exchange Relaxation $1/T_2$ex versus Field - $NaPF_6$:DB24C8. $1/T_2$ex for [DB24C8]/[$NaPF_6$] (ρ) equal 0.50 (•), 0.80 (□), and 0.30 (Δ) as a function of $\bar{\upsilon}_0^2$, the square of the observation frequency. [$NaPF_6$] = 0.037 M.

1.2.3.3 Exchange Mechanisms and Methods

Sodium-23 NMR has now provided a chemical exchange rate, (k_a+k_b). It is the sum of complexation and decomplexation rates:

$$(Na^+)_a \underset{k_b}{\overset{k_a}{\rightleftharpoons}} (Na^+)_b \qquad (22)$$

where $(Na^+)_a$ and $(Na^+)_b$ stand for free and complexed sodium.[43][45] The chemical exchange of sodium between solvated and DB24C8 complexed state can in principle proceed via two mechanisms, in analogy to Shchori's sodium : DB18C6 systems:

$$(Na^+)_s + (C)_s \underset{k_{-1}}{\overset{k_1}{\rightleftharpoons}} (Na^+,C)_s \qquad (23)$$

unimolecular decomplexation

$$('Na^+)_s + (Na^+,C)_s \overset{k_2}{\rightleftharpoons} ('Na^+,C)_s + (Na^+)_s \qquad (24)$$

bimolecular cation interchange

The rates of disappearance of the solvated and complexed sodium from their respective states can be expressed as:

$$-\frac{d[Na]}{dt} = \frac{[Na]}{\tau_a} = [Na]k_a = k_1[Na][C] + k_2[Na][NaC] \qquad (25)$$

$$-\frac{d[NaC]}{dt} = \frac{[NaC]}{\tau_b} = [Na]k_b = k_{-1}[NaC] + k_2[Na][NaC] \qquad (26)$$

where τ_a and τ_b are the average residence times of a sodium cation in the solvated and complexed states, respectively. Then:

$$1/\tau_a = k_a = k_1[C] + k_2[NaC] \qquad (27)$$

$$1/\tau_b = k_b = k_{-1} + k_2[Na] \qquad (28)$$

where $1/\tau_a$ and $1/\tau_b$ or k_a and k_b are the inverse lifetimes, that is the probabilities for the solvated and complexed sodium cations to leave their respective states.

Finally, the desired sum of the inverse lifetimes, (k_a+k_b) is :

$$k_a+k_b = k_1[C] + k_{-1} + k_2([Na]+[NaC]) \quad (29)$$

$$k_a+k_b = k_1[C] + k_{-1} + k_2[Na]_t \quad (30)$$

The last equation permits a separation of the unimolecular from the bimolecular exchange mechanisms by their different concentration dependencies:

If unimolecular exchange would dominate:

$$(k_a+k_b) = k_1[C] + k_{-1} \quad (31)$$

then the observed exchange rates (k_a+k_b) should vary with the concentration of free crown [C], and thus with crown/sodium. Yet the symmetric curve of $1/T_2ex$ versus P (Fig. 9) clearly shows that k_a+k_b is constant with P, the curvature arising from the term P_aP_b in eq. 8, p.15. To be consistent with unimolecular exchange, this constancy with crown/sodium would require $k_1[C]$ to be negligible compared to k_{-1} in eq. 31. But under the assumption of quantitative complexation:

$$K_c = \frac{k_1}{k_{-1}} = \frac{[NaC]}{[Na][C]} = \frac{\rho}{(1-\rho)[C]} \qquad (32)$$

and

$$\frac{k_1[C]}{k_{-1}} = \frac{\rho}{1-\rho} \qquad (33)$$

So if $k_1[C]$ would be negligible compared to k_{-1}, then the left term in eq. 31 would become very small. This however would contradict the term on the right side, for instance at ρ equal to 0.5. Thus unimolecular exchange cannot be the major exchange mechanism at this concentration.

There is a direct test for the mechanism: This is to study the dependence of the exchange rate on the total sodium concentration $[Na]_t$, while keeping ρ constant. With purely unimolecular exchange, (k_a+k_b) should be constant with $[Na]_t$, the Y-intercept being k_{-1}.
With purely bimolecular exchange, (k_a+k_b) should vary linearly with $[Na]_t$; the slope being k_2, and any residual Y-intercept being k_{-1}.

The spectra from the concentration study are shown in Fig. 11. In all samples, ρ was 0.5, while the concentration of total sodium hexafluorophosphate was reduced from 0.05 M to 0.00002M. One can see a slowing-down of the exchange with decreasing concentration, leading to separate signals for complexed and solvated cations. This concentration coalescence already shows that the bimolecular exchange mechanism is active at higher concentrations.

Before the line shapes can be analyzed for the exchange rates, another experimental result has to be considered: the chemical shift of sodium hexafluorophosphate in nitromethane in the absence of crown proved to be concentration dependent (Fig. 12). With increasing concentration

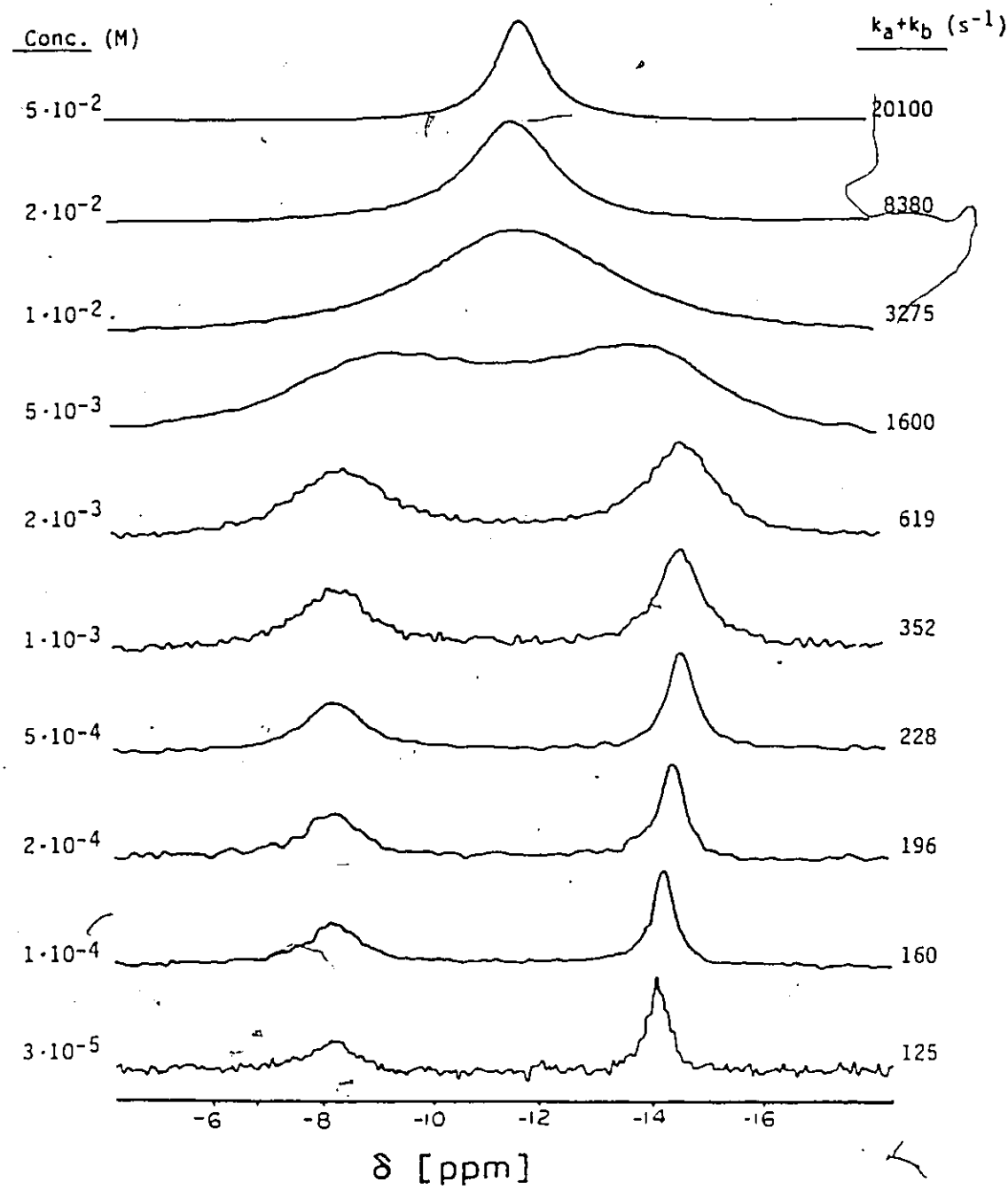

Figure 11: Concentration Coalescence for $NaPF_6$:DB24C8 in Nitromethane. Na-23 NMR spectra at 79.35 MHz of $NaPF_6$ (0.037 M) in nitromethane in the presence of DB24C8 ([DB24C8]/[$NaPF_6$] = 0.50) at different concentrations (295 K).

the sodium-23 resonance shifts diamagnetically (to lower frequency), and forms a plateau at sodium concentrations above 0.001 M.

Ionic interaction in non-polar solutions is common enough for sodium salts with coordinating anions, such as sodium iodide or thiocyanate,[8][18][24][51][64] but this is the first time that a large variation of a sodium-23 NMR parameter with concentration has been observed for the sodium salt of a bulky anion such as hexafluorophosphate.[8][18]

In analyzing this concentration dependence a bimolecular association has been assumed, of either solvated ions to the solvent separated ion-pair, or of two solvent separated ion-pairs to the proper dimer. At the low concentrations used in this study, secondary concentration effects such as changes of solvent or ion activity, of solvent-solvent or of solvent-ion interaction, can be neglected.[24][64][11]

Based on the simple ion-pairing model:

$$(Na^+)_s + (PF_6^-)_s \underset{}{\overset{K_p}{\rightleftharpoons}} (Na^+, PF_6^-)_s \qquad (34)$$

where K_p is the ion-pairing constant, The observed chemical shift can be expressed as the sum of the contributions of free and ion-paired sodium:

$$\delta_{obsd} = P_f \delta_f + P_p \delta_p \qquad (35)$$

[11] Later the ionic interactions of sodium iodide and sodium thiocyanate in nitromethane will be analyzed in much the same way. Throughout the thesis this ionic interaction is somewhat simplistically called 'ion-pairing'. It is probably more a dimerization of solvent-separated ion-pairs for sodium hexafluorophosphate, contact ion-pairing for sodium thiocyanate, and ionic clouding for sodium iodide.

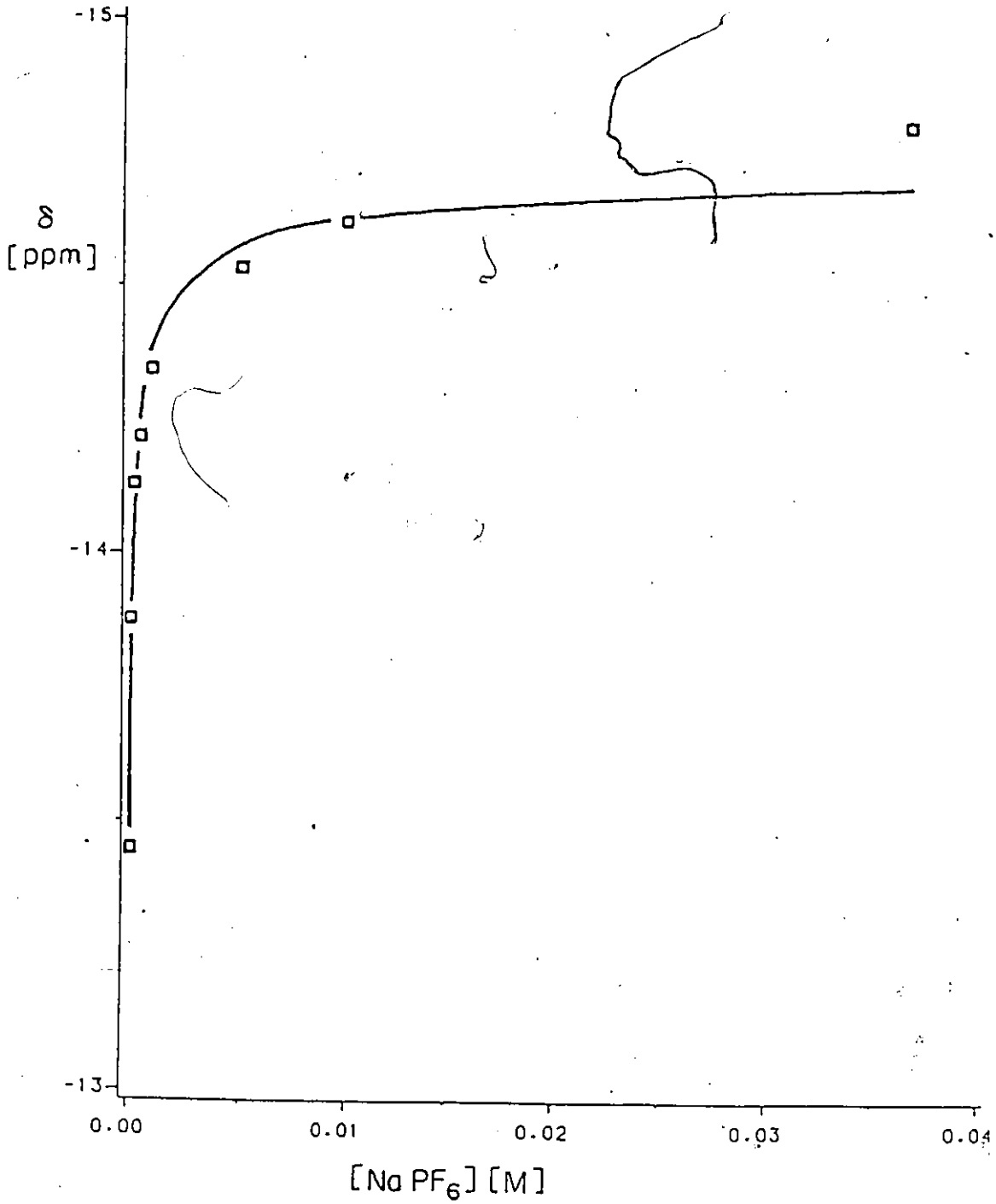

Figure 12: Concentration Dependence of $NaPF_6$ Shift in Nitromethane. The data points are experimental, the solid line comes from fitting with the ion-pairing model described in the text.

P_f and P_p are the molar fractions of free and ion-paired sodium cations, they are functions of K_p and $[Na]_t$ (the exact expressions are shown in Appendix 2.) Then the three unknown parameters K_p, δ_f, and δ_p were obtained by fitting eq. 35 to the observed shift versus concentration curve (Fig. 12), using a non-linear least-squares regression routine. The obtained parameter values are shown in Tab. 7, and the curve calculated with these values is shown as the solid line in Fig. 12.

The ion-pairing constant K_p is surprisingly strong for a counter anion as bulky as PF_6^-. Above all the diamagnetic shift (to lower frequencies) upon ion-pairing is unexpected. Strongly coordinating ligands or counter anions (SCN^-, I^-) usually cause a shift to higher resonance frequencies (paramagnetic shift; see Tab. 2 and Fig. 2).

Table 7: Ion-Pairing Parameters for $NaPF_6$ in Nitromethane

K_p is the ion-pairing constant, δ_f and δ_p are the iterated shifts for free and ion-paired sodium. The values in brackets are uncertainties.

K_p [M^{-1}]	δ_f [ppm]	δ_p [ppm]
25000 (5000)	-12.7 (0.5)	-14.8 (0.1)

The chemical shift difference between free and ion-paired sodium is however quite small (about -1 ppm, compared to +6 ppm for NaSCN and +12 ppm for NaI). Furthermore both longitudinal and transverse relaxation rates are independent of the ionic interaction. These findings suggest that the formed aggregates are solvent-separated ion-pairs or dimers of ion-pairs. However, we were most interested in the cation exchange process, and will consider this ionic interaction only as far

as it affects the exchange.[12]

Eqs. 36 and 37 describe the equilibrium in the presence of crown:

$$(Na^+)_s + (X^-)_s \underset{}{\overset{K_p}{\rightleftharpoons}} (Na^+,X^-)_s \qquad (36)$$

$$(Na^+)_s + (C)_s \underset{}{\overset{K_c}{\rightleftharpoons}} (Na^+,C)_s \qquad (37)$$

K_p is again the ion-pairing constant, and K_c the complex formation constant (K_c is fixed to 10^6 M^{-1}). The observed shift can now be described as the sum of the contributions from solvated, ion-paired and complexed sodium:

$$\delta_{obsd} = P_f\delta_f + P_p\delta_p + P_c\delta_c \qquad (38)$$

where δ_f, δ_p, and δ_c are the chemical shifts of free, ion-paired and crown-complexed sodium. (See appendix 3 for derivation.)

The solvated and the ion-paired sodium are in diffusion controlled equilibrium. Together they form the 'free sodium pool' (Fpool), in contrast to the complexed sodium. The chemical shift of Fpool corresponds to the weighted average of the shifts of free and ion-paired sodium, and thus depends directly upon the degree of ion-pairing. Now this ratio of ion-paired over solvated sodium is dependent upon the presence of crown as well as the concentration of the sodium salt, since DB24C8, by complexation, effectively removes cations from the ion-pairing equilibrium (eq. 37). Left behind are their 'naked' counter anions. They are denied access to the complexed sodium cations, and thus will shift the ion-pairing equilibrium further to the right.

12 This analysis will become more important for the strongly coordinating anions iodide and thiocyanate.

At concentrations above 0.001 M, the sodium shift has reached a pseudo-plateau, where all sodium cations are ion-paired (Fig. 12). Addition of crown could not lead to more ion-pairing, and thus could not affect the chemical shift of the uncomplexed sodium pool. So the chemical shift difference between both sites and thus the measured exchange rate should be independent of P at sodium concentrations greater than 0.001 M.

However, at concentrations below 0.001 M ion-pairing is incomplete in the absence of crown. Addition of crown would markedly shift the ion-pairing equilibrium and so the chemical shift of the uncomplexed sodium pool. Accordingly, the chemical shift of Fpool has been calculated for equal to 0.5 using eq. 39 (see also appendix 3), and the ion-pairing parameters from Tab. 7:[13]

$$\delta_{Fpool} = (P_f\delta_f + P_p\delta_p)\frac{[Na]_t}{[Na]_t-[NaC]} \qquad (39)$$

Knowing the exact chemical shift difference between the two sites (see Tab. 8), the full lineshape expression based upon the modified Bloch equations was then fitted to the observed spectra to obtain the exchange rates (Tab. 8).[19] In addition, the spectra at concentrations above 0.01 M were analyzed using eq. (21). This gave identical values for (k_a+k_b).[14]

13 We can clearly see the effect of ion-pairing in the low concentration region (Fig. 11): with increasing concentration the narrow signal corresponding to the free sodium pool (naked and paired sodium) first shifts to lower frequency (to the right) due to increasing ion-pairing. Then the onset of coalescence moves it back to the left. The shift of the 1:1 complex is constant at all times.

14 Near the slow exchange limit, the exchange rate becomes a function of only the linewidths of both signals, not of their chemical shift separation as above. In the line shape fitting program initially used, the chemical shifts still had to be known exactly to achieve a good fit. The shift values for the sodium pool calculated from the ion-pairing model resulted in excellent fits of the line shape expression to the experimental curves. Later, the fittings could be checked with a program that allowed the shift of the sodium pool to vary freely. These exchange rates were identical with those obtained earlier. This supports the validity of the ion-pairing model to account for the chemical shift variations with salt concentration and P.

Fig. 13 shows the variation of (k_a+k_b) with the total sodium concentration $[Na]_t$. At concentrations above 0.001 M k_a+k_b varies linearly with $[Na]_t$ as predicted for the bimolecular exchange mechanism. The slope is $k_2 = 3.6 \times 10^5\ s^{-1}$, corresponding to an activation free energy $dG^{\#}$ of 42 kJ/mol.

Towards the low concentration limit the bimolecular exchange mechanism becomes less and less efficient, and the exchange rates eventually become independent of the total sodium concentration (Fig. 13). So the residual exchange at the low concentration limit proceeds by unimolecular decomplexation, with $(k_a+k_b) = k^{-1} = 60\ s^{-1}M^{-1}$. This corresponds to an activation free energy $dG^{\#}$ of about 63 kJ/mol for the unimolecular decomplexation. Table 8 gives the exchange rates.

The temperature dependence of the bimolecular exchange rate at $[Na]_t = 0.037$ M has been studied to obtain the activation enthalpy and entropy for the bimolecular exchange. Figure 22 shows the variation of $\ln(k_2h / kT)$ with the inverse of the temperature for P equal to 0.5. Slope and intercept of the graph give the enthalpy and entropy of activation for the bimolecular cation interchange; they are shown in Tab. 9.

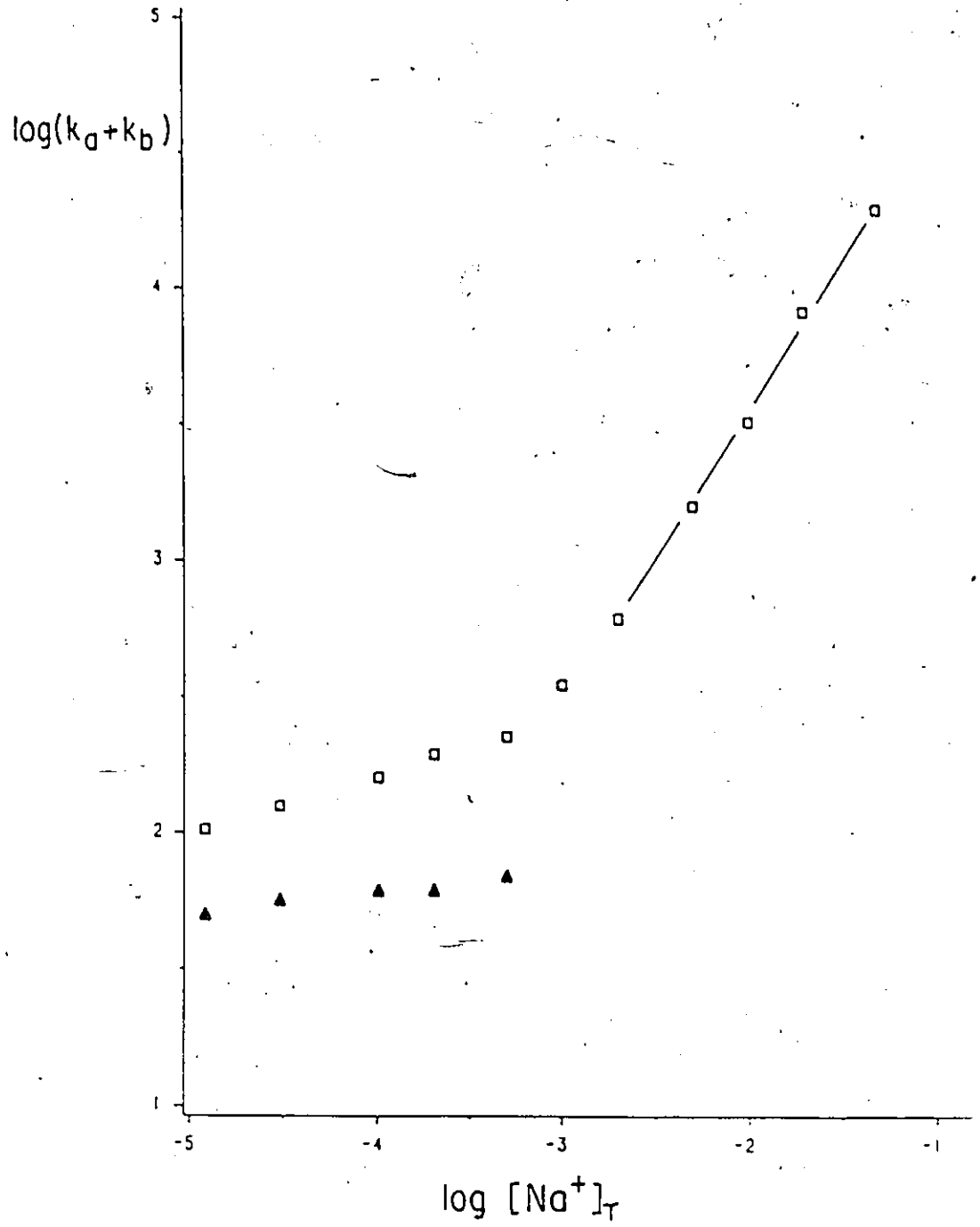

Figure 13: (k_a+k_b) against $[Na]_t$ for $NaPF_6$:DB24C8 in Nitromethane. The squares are calculated by lineshape analysis, the values for $[Na]_t > 0.001$ M were additionally checked using eq. 21. The triangles are the residual unimolecular exchange rates obtained by substracting the extrapolated bimolecular exchange rate from the observed rates.

Table 8: Exchange Rates for $NaPF_6$:DB24C8 in Nitromethane

$[Na]_t$ [M]	$(\nu_a-\nu_b)_{Fpool}$ [Hz]	k_a+k_b [s^{-1}]	RMS	$k_a+k_b/[Na]_t$ [$x10^5 s^{-1}M^{-1}$]	k_1 [s^{-1}]
0.05	522	20100(60)	0.3	4.02	-
0.02	522	8380(60)	0.2	4.19	-
0.01	520	3275(60)	0.5	3.28	-
0.005	518	1600(30)	0.6	3.20	-
0.002	511	619(9)	0.6	3.10	-
0.001	503	352(4)	0.4	3.52	-
0.0004	491	228(2)	0.4	-	72
0.0002	471	196(2)	0.5	-	62
0.0001	455	160(2)	0.6	-	62
0.00003	432	125(4)	0.8	-	57
0.000012	423	103(3)	0.9	-	50

$(\upsilon a-\upsilon b)$Fpool is the chemical shift difference between Fpool and the complexed sodium, calculated with eq. 39. (k_a+k_b) are the observed exchange rate. $(k_a+k_b)/[Na]_t$ is equal to the bimolecular exchange rate k_2 at high concentrations ($[Na]_t$ > 0.001 M). k_{-1} is the unimolecular exchange rate constant, derived by deducing the extrapolated bimolecular contribution from (k_a+k_b) in the low concentration region ($[Na]_t$ < 0.001 M).

Table 9: Activation Parameters for Bimolecular Exchange - $NaPF_6$

$dH^{\#}$ [kJ/mol]	$dS^{\#}$ [J/molxK]	$dG^{\#}$ [kJ/mol]
29.5 (2)	-36.9 (10)	40.4 (2)

1.2.3.4 Discussion - Sodium Hexafluorophosphate Two-Site Exchange

The most interesting aspect of this system is that it allowed the observation of both the unimolecular and the bimolecular exchange mechanisms within the same complexation system. Both mechanisms could then be separated, using their different concentration dependencies (eq. 30).

But how do these two mechanisms proceed? Let us first consider the structure of the sodium complexes with the large crown ethers DB24C8 and DB30C10. The uncomplexed DB24C8 in solution probably assumes an elongated centrosymmetric conformation like its larger analog DB30C10.[34][65] In its 1:1 complex with sodium in solution, DB24C8 wraps itself around the cation, excluding solvent and counter anions from the cation's coordination sphere. The 1:1 complex is the predominant sodium : DB24C8 complex species in solution.[17][35][58] Sodium : DB30C10, on the other hand, forms 2:1 complexes (and possibly 3:2 complexes) in nitromethane solutions.[58][59] For both DB24C8 and DB30C10 in the solid state 2:1 sodium : crown complexes are the rule rather then the exception. For example DB30C10 needs anhydrous conditions as well as the bulky counter anion tetraphenylborate to form a 1:1 complex with sodium. In the presence of small counter anions or water, the 2:1 sodium : DB30C10 complex prevails.[66][67]

With DB24C8, both potassium thiocyanate[68] and sodium o-nitro-phenolate[69] form 2:1 complexes in the solid state. The potassium cations each bind to five oxygens of the nearly co-planar crown ring. One thiocyanate anion is above and one below the ligand plane; each bridges the two cations through nitrogen.[68] To accommodate the smaller sodium cations, the DB24C8 folds into a propeller shape. In each of its blades, one sodium coordinates to three ether oxygens, leaving two oxygens free. In addition both cations are coordinated to one nitro-oxygen, and are bridged by the phenolate-oxygens of both anions.[69] It is thus clear that high donicity anions such as thiocyanate and o-nitro-phenolate stabilize the 2:1 complexes by saturating the cations coordination shell, and by reducing the inter-cationic repulsion.

How can this structural information be correlated with the kinetic results? Regardless of mechanism, the first decomplexation step must include the conformational opening of the tight 1:1 complex. It must open to a roughly planar conformer, in which solvent and anions may coordinate to the sodium. According to Truter[70] four trans-to-gauche dihedral changes in the uncomplexed DB30C10 interconvert the closed into the open conformer. The activation free energy for this process is about 50 kJ/mol. If one adds to this the activation energy needed to disrupt two or three oxygen-sodium bonds during the opening, then the observed activation free energy for the unimolecular decomplexation, 65 kJ/mol, is reasonable. Neither nitromethane nor hexafluorophosphate are strong enough donors to stabilize the transition state of the unimolecular decomplexation.

With higher concentrations the probability of encounter between solvated and complexed sodium increases, and the bimolecular pathway becomes dominant ($[Na]_t > 0.001$ M). This mechanism also starts with the opening of the tight 1:1 complex, but now this opening is assisted by the solvated sodium cations. The intermediate species present at the transition state of the bimolecular exchange is assumed to resemble the 2:1 complexes of the solid state: Two sodium cations residing on opposite faces of the crown ring, with their uncomplexed sides coordinated to solvent

or counter anions or to both. Thus the second sodium cation can be said to stabilize the decomplexation transition state of the first, complexed, cation.

The presence in solution of an intermediate 2:1 complex is not noticeable from either chemical shift or longitudinal relaxation rate curves (Fig. 7 and 8). Since chemical shifts are additive, its shift would be expected between those for solvated and complexed sodium. On the other hand, the coordination shell of sodium in the 2:1 complex resembles that of the 1:1 sodium:12C4 complexes. The longitudinal relaxation rate is a sensitive measure for the presence of even small amounts of such an asymmetric species. In the presence of such species $1/T_1$ would show a positive curvature centered around P equal to 0.5.

Whereas the kinetic analysis shows the necessary presence of a 2:1 intermediate, its concentration and lifetime are very small as seen from the perfectly linear variation of $1/T_1$ with P (Fig. 8). This validates the implicit assumption that the system can be treated as consisting of two sites, with no relaxation taking place during the exchange itself.

Many factors influence the relative importance of both exchange mechanisms for a given complexation system. Besides the properties of cation and ligand, the solvent and the counter anion play major roles.

Shchori et al., studying the sodium exchange with 18C6 derivatives in methanol and dimethylformamide, found the unimolecular decomplexation mechanism to be dominant.[43][45] Dye et al. found the same for sodium bromide binding to 15C5 or 18C6 in methylamine.[53] These crowns were initially considered too small to bind the two cations required for the intermediate species in the bimolecular mechanism. However Schmidt and Popov found the bimolecular exchange mechanism to dominate in the potassium : 18C6 in 1,3-dioxolane system.[47] Subsequently, Popov et al. did a comprehensive study of the effects of counter anions and solvent on

the exchange mechanism for the system sodium : 18C6. They found that in tetrahydrofuran, sodium tetraphenylborate exchanges slowly by unimolecular decomplexation, whereas sodium thiocyanate exchanges much faster, and by the bimolecular process.[48][51] As in the solid state, coordinating anions clearly stabilize 2:1 sodium : crown stoichiometries in solution.

Concerning the solvent, Strasser and Popov found that solvents or solvent mixtures of high dielectric constant but low donicity such as propylenecarbonate (DN = 15, ε = 65) stabilize the bimolecular transition state. Yet solvents of high donicity, regardless of their dielectric constant, strongly promote the unimolecular decomplexation (methanol, tetrahydrofuran).[52]

In the system of sodium hexafluorophosphate : DB24C8, the high dielectric constant of the solvent nitromethane (ε = 35.9) reduces the charge-charge repulsion at the bimolecular transition state, and thus promotes the bimolecular exchange. Meanwhile its donicity (DN=2.7)[10] is too low to speed up the rate of unimolecular decomplexation.

A lower limit for the complexation rate can be estimated from the unimolecular decomplexation rate (k_{-1} = 60 s^{-1} M^{-1}), and the lower limit of the complexation constant (K_c >= 10^6 M^{-1}):

$$K_c \geq 10^6 M^{-1} = k_1/k_{-1}$$

and thus

$$k_1 \geq 10^8 s^{-1}$$

Eigen et al. reported a similar complexation rate for sodium : monensin in methanol (k_1 = 3 x $10^8 M^{-1} s^{-1}$).[44]

Let us recall from Tab. 2 that both the chemical shift and the relaxation rates of the 1:1 complexed sodium are independent of solvent and counter anion. This indicates that, in the competition of solvent molecules and counter anions with the crown for the sodium cation, the equi-

librium lies far on the side of the wrapped 1:1 complex. Even a solvent with a high donicity such as pyridine, or a coordinating anion such as thiocyanate, cannot gain enough residence time in the sodium chelation shell to have an effect on chemical shift or quadrupolar coupling.[17] So the study of the 1:1 sodium:DB24C8 complex itself would not reveal any information about the role of the solvent or counter anion in the complexation and decomplexation processes. In contrast, the unimolecular exchange process directly measures the competition between the crown on one side, and the solvent and counter anion on the other side, for the cation. Even small increases in the donicity of the solvent or anion should lead to a related increase in the rate of unimolecular decomplexation. On the bimolecular cation interchange the influences of anions and solvent are more complex, since a second sodium cation takes part in the exchange. This will be described in on chpt. 1.2.5 for the case of sodium thiocyanate.

In the following chapter, the substitution of sodium tetraphenylborate for sodium hexafluorophosphate results in association of several 1:1 complexes to larger species.

1.2.4 Aggregation and Exchange - Sodium Tetraphenylborate

Tetraphenylborate is well known as a non-coordinating counter anion that promotes the formation of sandwich crown complexes.[27][65] Strasser and Popov found the exchange rate of sodium tetraphenylborate with 18C6 in tetrahydrofuran solution to be slow at room temperature (k_{-1} = 53 (6) s^{-1}). The exchange rates were fast for NaSCN (k_2 = 92000 $M^{-1}s^{-1}$) and $NaClO_4$.[51] So in the sodium:DB24C8 complexation system, tetraphenylborate could provide a 'zero-anion-effect standard', against which to gauge the effects of the stronger coordinating anions PF_6^-, SCN^- and I^-.

Figure 14 shows the variation of the Na-23 chemical shift with P for sodium tetraphenylborate in nitromethane solution. The curve is similar to the one observed with sodium hexafluorophosphate (Fig. 7). Again free and complexed sodium are the two dominant species, undergoing rapid exchange. More striking however are the variations of the transverse relaxation rates with P at three different field strengths (Fig. 15). They are similar to the relaxation rate curves for the hexafluorophosphate (Fig. 8), except that the maximum now shifts to higher P values with decreasing field strength. To test for the quadrupolar contribution to relaxation, the longitudinal relaxation rates were measured at 79.35 and 52.93 MHz (Fig. 16).

Three main features can be noted:

- $1/T_1$ shows a maximum at P equal to 0.95. Going left from the plateau region (P larger than 1.0), $1/T_1$ increases dramatically as soon as a slight excess of sodium over crown is present;
- $1/T_1$ is independent of the external magnetic field;
- $1/T_1$ is the same as for the hexafluorophosphate case at P equal to 0.0 or larger than 1.0 (Fig. 8).

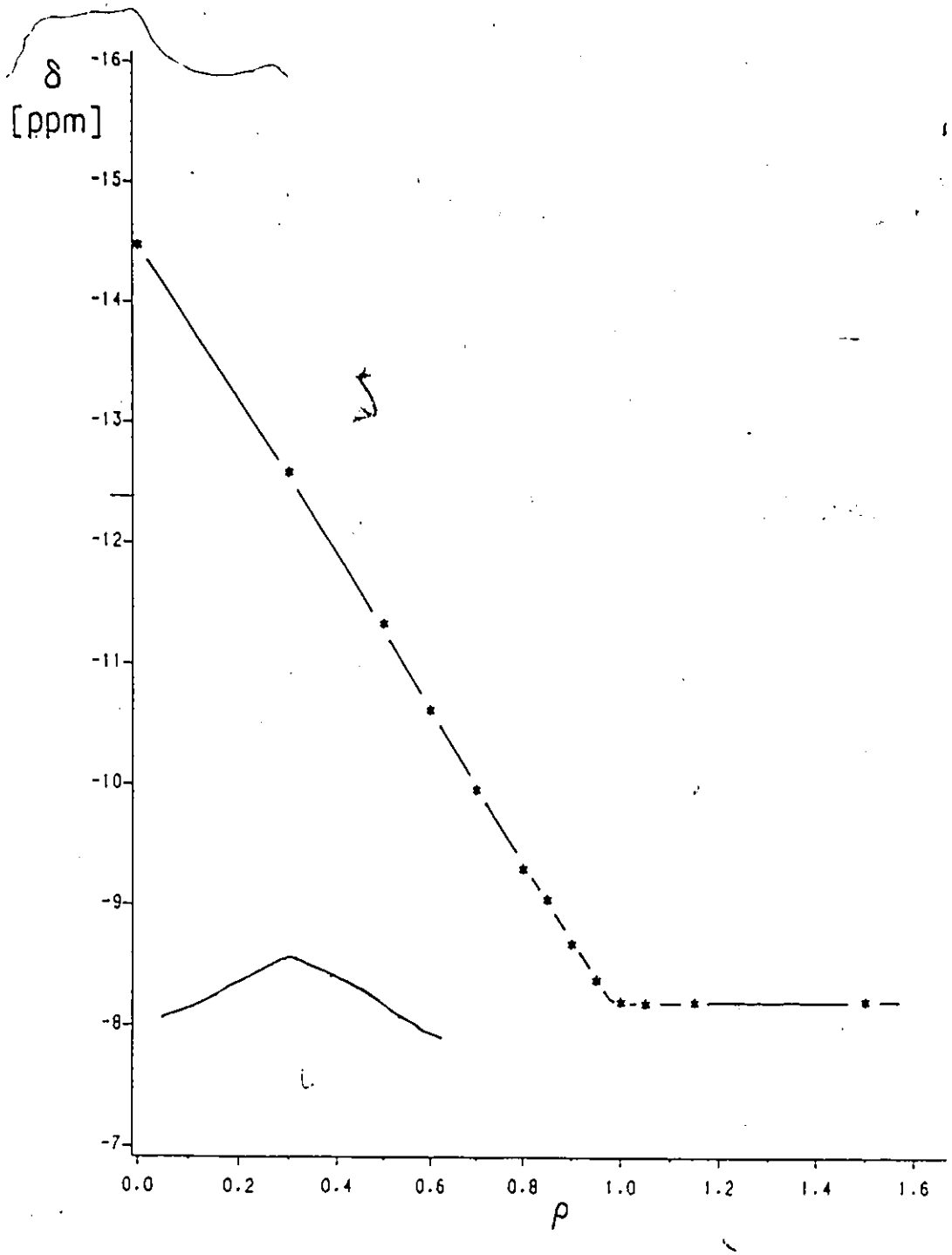

Figure 14: Chemical Shifts for $NaBPh_4$:DB24C8 in Nitromethane. Shifts as function of [DB24C8]/[$NaBPh_4$] (ρ) at 79.35 MHz in nitromethane. [$NaBPh_4$] is 0.037 M.

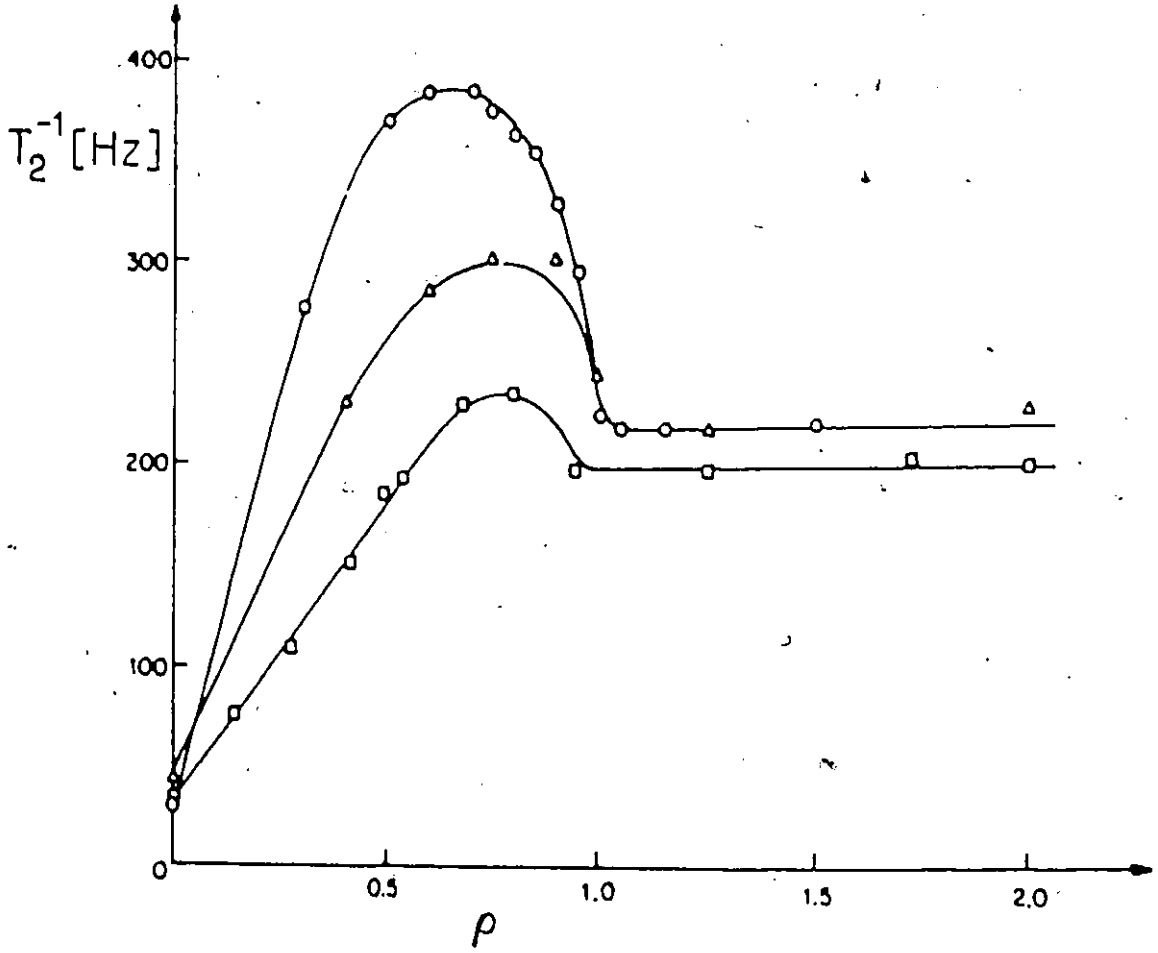

Figure 15: Transverse Relaxation rates - $NaBPh_4$:DB24C8. $1/T_2$ as function of [DB24C8]/[$NaBPh_4$] (ρ) in nitromethane at 79.35 MHz (o), 52.92 MHz (Δ), and 21.04 MHz (□). [$NaBPh_4$] is 0.037 M. Temperatures of measurements are 294 K (79.35 MHz and 52.92 MHz) and 297 K (21.04 MHz). All line shapes are Lorentzian.

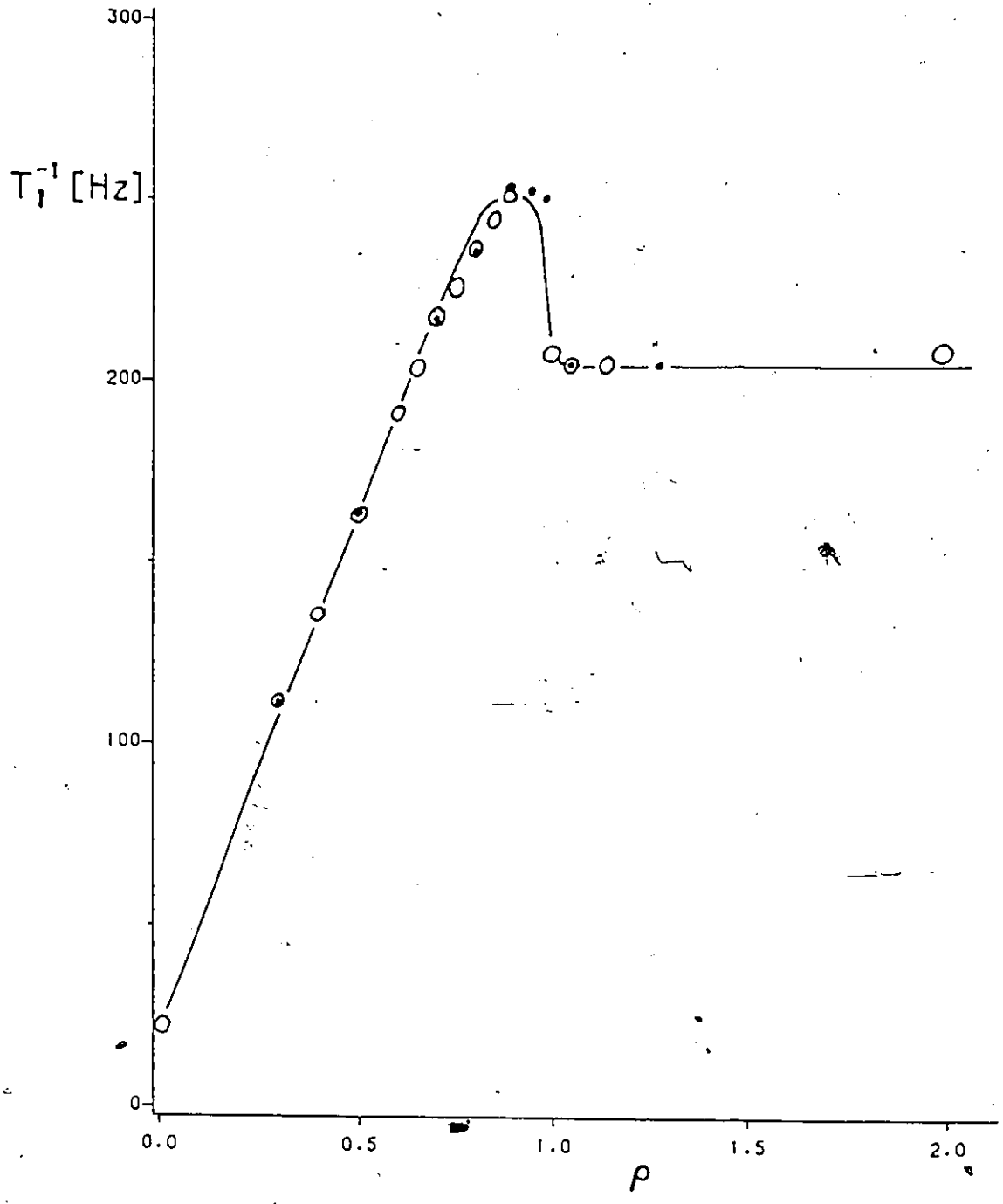

Figure 16: Longitudinal Relaxation Rates - $NaBPh_4$/DB24C8. $1/T_1$ as function of ρ at 79.35 MHz (O) and at 52.92 MHz (•). The experimental conditions are the same as in Figs. 14 and 15. The points are experimental, and the curve is fitted with the aggregation model described by eqs. 41 - 43 and 48.

The field independence of $1/T_1$ confirms that the system is within the extreme narrowing region. As well, the exchange rates cannot influence the longitudinal relaxation rate, since the exchange rate [$(k_a+k_b)=3000s^{-1}$] is much higher than the highest relaxation rate in the two-site system [$1/T_2c = 200s^{-1}$].[13] So the maximum of $1/T_1$ at P equal to 0.95 must result from species other than the solvated and the 1:1 complexed sodium. These species must have a sodium relaxation rate higher than the 1:1 complex. Meanwhile, the field dependence of the transverse relaxation can again only be due to exchange broadening as in the case of hexafluorophosphate.

In this situation the longitudinal relaxation reflects only the structural aspects of complexation, in particular the product $\chi^2\tau_c$; whereas the transverse relaxation contains information about both structure and exchange. By separating these two relaxation contributions insight into both aspects of the $NaBPh_4$:DB24C8 complexation system could be gained.

As mentioned above, the maximum of $1/T_1$ shows the presence of additional species besides the solvated and the 1:1 complex. 2:1 and 3:2 stoichiometries are already known for $NaBPh_4$:DB30C10 complexes in nitromethane.[58][59] In the solid state, 2:1 complexes between sodium isothiocyanate and DB30C10,[67] between sodium o-nitro-phenolate and DB24C8,[69] and between potassium isothiocyanate and DB24C8[68][71] are also well known. So the model used to account for the maximum in $1/T_1$ (or for the additional species this observation implies) is based on initial formation of the 2:1 sodium : crown complex. Yet if this were the only other species formed, the maximum of $1/T_1$ would appear around P equal to 0.5. Thus the position of the maximum indicates that species of a higher stoichiometry are present, since the $1/T_1$ maximum appeared around crown/sodium equal to 0.9.

1.2.4.1 Aggregation Model

The first step in creating a model is to try to visualize the aggregate species. At the transition state of the bimolecular exchange of sodium hexafluorophosphate two cations are bound to the DB24C8 in a roughly planar 2:1 transient species. The two cations are held on opposite sides of the crown by about four oxygen donors (see p. 75).

The next higher analog to this 2:1 species would be the 3:2 species: two co-planar crown molecules sandwiched between three sodium cations. Larger aggregates would be similar (Fig. 17).

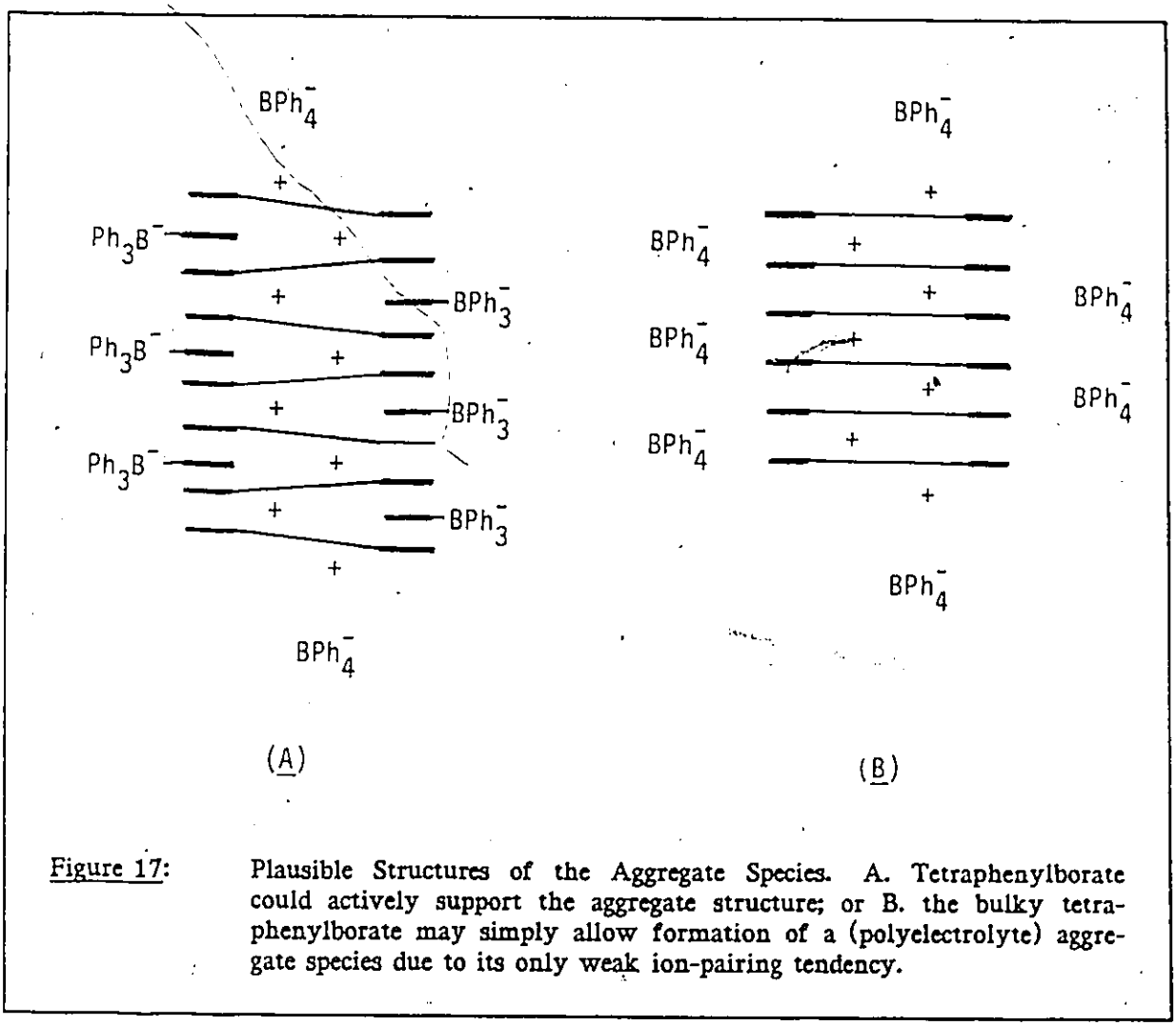

Figure 17: Plausible Structures of the Aggregate Species. A. Tetraphenylborate could actively support the aggregate structure; or B. the bulky tetraphenylborate may simply allow formation of a (polyelectrolyte) aggregate species due to its only weak ion-pairing tendency.

The simplest complexation model that could account for the formation of such species has a 2:1 complexation step and then many aggregation steps after the initial 1:1 complexation:

$$(Na^+)_s + (C)_s \xrightleftharpoons{K_c} (Na^+,C)_s \qquad (40)$$

$$(Na^+,C)_s + (Na^+)_s \xrightleftharpoons{K_{c2}} (Na^+_2,C)_s \qquad (41)$$

$$(Na^+_{i},C_{i-1})_s + (Na^+,C)_s \xrightleftharpoons{K} (Na^+_{i+1},C_i)_s \qquad (42)$$

In the first aggregation step, the 1:1 complex NaC adds a second sodium cation to form the transient complex Na_2C (eq. 41). In the second step, this 2:1 complex acts as a nucleating species by further adding 1:1 complexes on both sides: in turn this forms higher aggregates of stoichiometry (i+1):i sodium : crown (eq. 42).

To fit this model to the experimental data, the observed $1/T_1$ had to be expressed as the sum of the contributions of all species described by eqs. 40 - 42. The unknown parameters are the formation constants K_c, K_{c2}; the aggregation constant K; and the relaxation rates for all species $Na_{i+1}C_i$. The full derivation is given in Appendix 4, here only the main arguments and key expressions. Either structure in Fig. 17 allows for some simplifying assumptions to be made:

- There are two sodium-environments in each aggregate: in the 'internal' sites the sodium cation is complexed by a half-crown on each side. So it has a spherical ethereal coordination sphere like in the 1:1 sodium:DB24C8 complex. In the two 'outside' sites of each aggregate the cations coordinate to four oxygen donors on one side and to the solvent and anions on the other.

To reduce the number of parameters, the longitudinal relaxation rates of these two sites was fixed at values found for similar complexes. The internal site was attributed $1/T_1$in = $205s^{-1}$, corresponding to the 1:1 sodium:DB24C8 complex. The less symmetric external site, where the cation is bound to only 4 oxygen donors, was considered analogous to the 2:1 sodium:DB30C10 complex in nitromethane.[59] Thus it was assigned a $1/T_1$out of $1600s^{-1}$.

- Furthermore, the complexation constant K_c was taken as 10^6M^{-1}. This is the lower limit obtained from the chemical shift variation with P.

This model provides expression 43 for the relaxation contribution of one aggregate species $Na_{i+1}C_i$:

$$1/T_1i = i[2/T_1out + (i-1)/T_1in] \qquad (43)$$

where $1/T_1$out and $1/T_1$in are the relaxation rates of 'outside' and 'inside' sodium for a fictitious aggregate complex containing only one crown molecule. The factor 'i' represents the number of crown molecules in the aggregate species. This reflects the assumption that the correlation times of sodium in the aggregates are linearly related to the size of the aggregates.

The observed longitudinal relaxation rate is then given by the sum of the contributions of all sodium species:

$$1/T_1 = \frac{P_f}{T_1f} + \frac{P_c}{T_1c} + [Na_{i+1}.C_i](T_1i)^{-1}/[Na]_t \qquad (44)$$

where P_f and P_c are the fractions of solvated and complexed sodium, and $1/T_1f$, $1/T_1c$ and $1/T_1i$ are the relaxation rates of free and complexed sodium and of the aggregate. $1/T_1i$ for each aggregate species is given by eq. 43 above, so that eq. 44 can be reduced to:

$$1/T_1 = \qquad (45)$$

$$= \frac{P_f}{T_1 f} + \frac{P_c}{T_1 c} + \frac{2P_f K_{c2} X}{K(1-X)^2}\left[\frac{1}{T_1 out} - \frac{1}{T_1 in} + \frac{1}{(1-X)T_1 in}\right]$$

Using power series,[72] expressions can be derived for the total sodium and crown concentrations:

$$[Na]_t = [Na] + \frac{X}{K} + \frac{K_{c2}}{K}[Na]\left(\frac{1}{(1-X)^2} - 1\right) \qquad (46)$$

$$[C]_t = [C] + \frac{X}{K} + \frac{K_{c2}}{K}[Na]\left(\frac{X}{(1-X)^2}\right) \qquad (47)$$

X stands for $K_c K[Na][C]$, and $[Na]_t$ and $[C]_t$ are the total concentrations of sodium and crown, respectively. Eqs. 46 and 47 were solved for the concentrations of free sodium and crown using a simultaneous Newton-Gauss procedure.

This leaves only two variable parameters: the formation constant for the 2:1 complex K_{c2}, and the aggregation constant K. Expression 45 was fitted to the observed $1/T_1$ data (Fig. 16) with a SIMPLEX optimization routine,[73] and double-checked with a Newton-Gauss procedure.[74] The fit is excellent, and the results are presented in Tabs. 10 and 11.

The average size of the aggregates is:

$$\langle SI \rangle = \frac{i[Na_{i+1}, C_i]}{[Na_{i+1}, C_i]} = \frac{1}{1-X} \qquad (48)$$

where <SI> gives the average number of crown molecules per aggregate.

Table 10: Results of $1/T_1$ Fitting - $NaBPh_4$:DB24C8

$1/T_1f$ [Hz]	$1/T_1c$ [Hz]	$1/T_1out$ [Hz]	$1/T_1int$ [Hz]	K_c [M^{-1}]	K_{c2} [M^{-1}]	K [M^{-1}]
22 (1)	205 (5)	1600	205	10^6	0.66 (0:06)	20.3 (0.5)

$1/T_1f$ and $1/T_1c$ are observed values. $1/T_1out$ is the lower estimate of the Na-23 relaxation rate of the 2:1 sodium:DB30C10 complex.[59] $1/T_1int$ is assumed equal to $1/T_1c$ (see discussion). K_c is larger than 10^5. Any values higher than this limit give similar results in the fitting. K_{c2} and K are obtained by a Newton-Gauss fitting procedure of the 79.35 MHz data (rms = 5.5 Hz for 13 datapoints).

Figure 16 shows the observed $1/T_1$ values (79.35 and 52.92 MHz) and the fitted curve. <SI> varies from 1 to 3.2, which corresponds to aggregate sizes well within the extreme narrowing region (Tab. 11). Figure 18 shows the populations of the different species in solution, as calculated with eqs. 40 - 42. The major species are the solvated and 1:1 complexed sodium. The sodium bound in the aggregates amounts to about two percent of the total sodium.

Table 11: $1/T_1$ Observed and Calculated - $NaBPh_4$:DB24C8

ρ	$1/T_1$obsd $[s^{-1}]$	$1/T_1$calc $[s^{-1}]$	‹SI›
0.00	22(1)	-	-
0.30	111(3)	103	1.3
0.40	135(4)	131	1.4
0.50	163(4)	160	1.6
0.60	191(5)	190	1.8
0.65	204(5)	204	1.9
0.70	217(10)	218	2:0
0.75	226(3)	231	2.2
0.80	236(6)	247	2.4
0.85	243(5)	250	2.6
0.90	253(7)	251	2.9
0.95	253(5)	241	3.2
1.00	208(5)	211	-
1.05	205(5)	205	-
1.15	205(4)	205	-
2.00	209(5)	205	-

The error is given as three σ, σ being the standard deviation given by the nonlinear regression analysis. The calculated values are obtained from the fitting procedure described in the text. <SI> gives the average number of crown molecules in the aggregates.

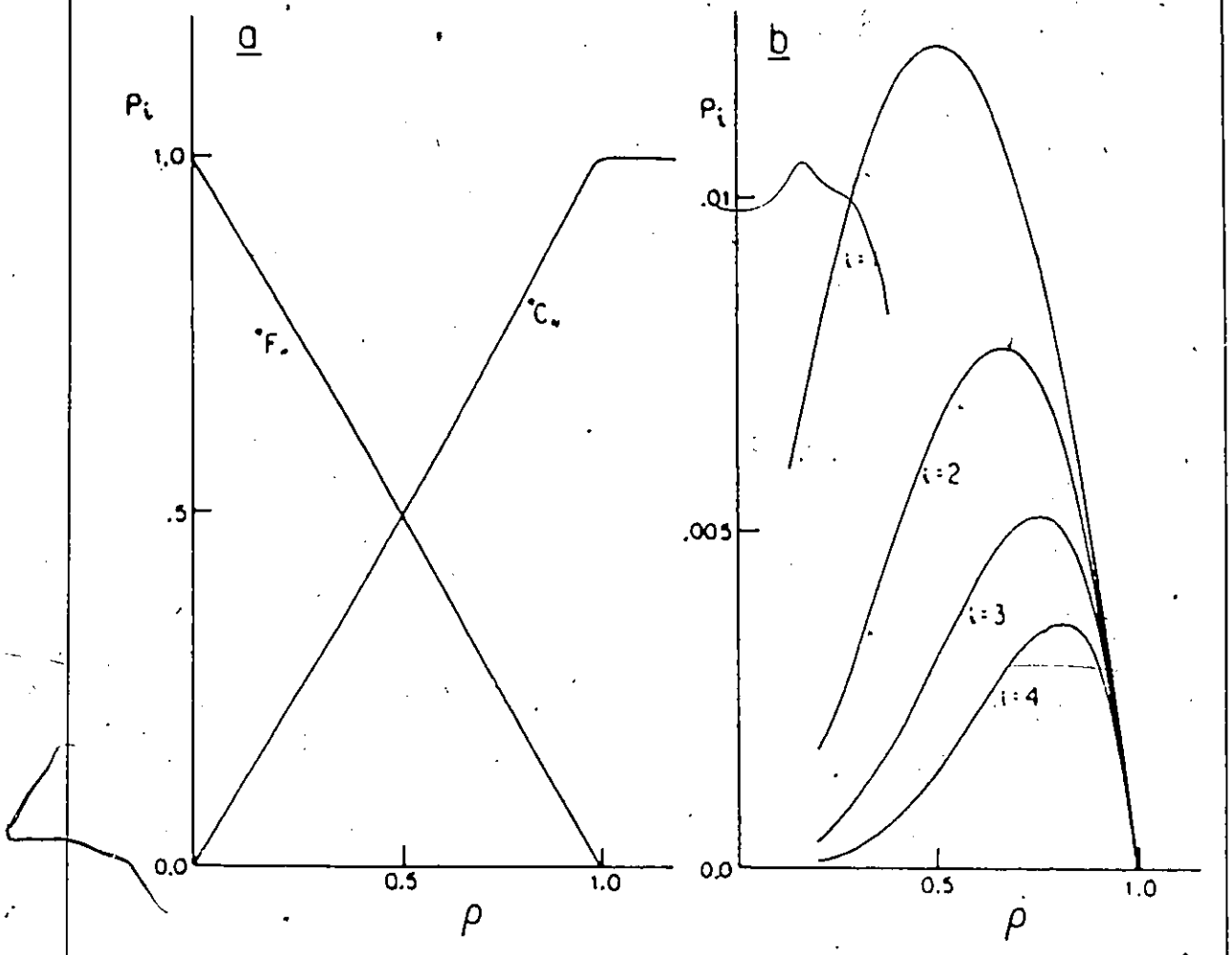

Figure 18: Populations of Aggregate Species in Nitromethane.
(a) Populations of free (F) and 1:1 complexed sodium (C); (b) Populations of the aggregate species $Na_{i+1}C_i$ for i = 1-4, calculated with the model described by eqs. 40 - 42, as a function of [DB24C8]/[$NaBPh_4$].

1.2.4.2 Discussion of Aggregation Model

Comparison of the chemical shifts (Fig. 14), the transverse relaxation rates (Fig. 15) and the longitudinal relaxation rates (Fig. 16) shows that the sodium - DB24C8 aggregates can be detected unambiguously only by their contribution to the longitudinal relaxation rate. The aggregate con-

centrations are too small to have an effect on the chemical shift curve. Moreover, the chemical shifts of the aggregated sodium should be intermediate between the shifts for solvated sodium and 1:1 complexed sodium.

Under extreme narrowing conditions, the spin 3/2 quadrupolar relaxation is given by:

$$1/T_1 = 1/T_{2q} = (2/5)\pi^2 x^2 \tau_c \qquad (49)$$

where X is the quadrupolar coupling constant and τ_c the correlation time for the quadrupolar relaxation. As discussed earlier, 1/Tq is sensitive to the symmetry of the charge distribution around the nucleus through X; and to the cations' mobility through the reorientational correlation time τ_c. The linear increase of $1/T_1 i$ with τ_c, and thus with aggregate size, amplifies the relaxation contribution of even small amounts of aggregate species present. The quadrupolar component of the transverse relaxation rate is identical to $1/T_1$ in the extreme narrowing region. However, in this system it is masked by the larger exchange contribution $1/T_2 ex$, especially so at higher resonance frequencies.

In order to be within the extreme narrowing region, $(\omega^2 \tau_c^2)$ has to be negligible compared to one (see eqs. 3a,b). In nitromethane, τ_c is be about 50 ps for the 1:1 sodium:DB24C8 complex (see p. 18), and i x 50 ps for an aggregate species containing i crown molecules. The Larmor frequency ω corresponding to the 79.35 MHz observation frequency is $2\pi\ 79.35\ 10^6\ s^{-1}$, so that the product $(\omega^2 \tau_c^2)$ for an aggregate comprising 10 crown molecules is:

$$(2\pi\ 79.35\ 10^6)^2 \times (500\ 10^{-12})^2 = 0.062 \ll 1$$

Thus the aggregate species are still within the extreme narrowing region, as also seen by the field independence of the longitudinal relaxation rates (Fig. 16).

The key feature of the aggregation model is the cooperation of a less favorable initial step (formation of the 2:1 complex, K_{c2} = 0.66) with a more favorable second step (aggregation, K = 20). This so-called 'semi-isodesmic', indefinite aggregation model, also known as Type III SEK or cooperative indefinite self association model, is well known in the field of nucleotide self association. The first (often dimerization) aggregation constant is a magnitude lower than that for the higher aggregation steps. Stilbs and Rymden find values of 0.4 M^{-1} for the dimerization constant (in our model = K_{c2}) and 6 M^{-1} for the aggregation constant (= K) for the self association of mono-nucleotides such as adenosine monophosphate (AMP) and guanosine monophosphate (GMP) in D_2O.[75][76]

1.2.4.3 Discussion of Assumptions

The model of $Na_{i+1}C_i$ aggregates, as described by eqs. 40 - 42, is based upon the following assumptions:

1. From Fig. 16 it is clear that the stoichiometry of the aggregate must be (i+x):i sodium:crown. For this model, x is assumed to be one, in agreement with the proposed structures (Fig. 17).

2. K_c is taken equal to $10^6 M^{-1}$. The chemical shift curve gives a lower limit for K_c of $10^6 M^{-1}$. In the fitting of eq. 45 to the experimental $1/T_1$ data, the results were independent of K_c if K_c was equal to 10^6 M^{-1} or larger.

3. Eq. 42 describes the addition of a 1:1 complex to an aggregate species $Na_{i+1}C_i$. The aggregation constant K is independent of the size of the initial aggregate, for i >= 1. In this model, both terminal or 'outside' sodium cations of an aggregate species are considered active, nucleating sites.

4. According to the proposed structures (Fig. 17), the aggregates contain two types of bound sodium: (i-1) sandwiched 'inside' sodium cations and two semi-solvated 'outside' sodium cations. To reduce the number of unknown parameters, $1/T_1$ values of similar complexes have been assigned to these binding sites. Modest variations of these parameter values do not significantly alter the results of the fitting procedure.

5. The reorientational correlation time of sodium bound in the aggregates is assumed to be equal to the rigid reorientation time of the whole aggregate. This in turn is assumed to be proportional to the number of crown molecules per aggregate.

These assumptions are justified, since:

a) the sodium:DB24C8 1:1 complex reorients rigidly as a whole[17]; so that there the correlation time of the sodium is the same as that of the complex; and

b) the correlation time τ_c of a rigid aggregate is proportional to the volume of the aggregate according to the Debye-Stokes-Einstein relationship:[77]

$$\tau_c = (4/3)\pi a^3(\eta/kT)f_r \qquad (50)$$

where (a) is the radius of a spherical species, (η) the viscosity of the medium, and (fr) the coefficient of microviscosity.[78] If the aggregates have the assumed rod-like shape, then τ_c is linearly related to the length of the aggregate.[15]

15 Changes of the microviscosity as well as the spherical-to-ellipsoid shape transition with increasing aggregate size are neglected because of the relatively small aggregate sizes found (Tab. 10).

1.2.4.4 Exchange Phenomena - $NaBPh_4$

The kinetic analysis was done similar to that for hexafluorophosphate. Subtracting the quadrupolar (= longitudinal) and the inhomogeneity contribution from the observed transverse relaxation provides again the exchange relaxation $1/T_2ex$ (Fig. 19):

$$1/T_2ex = 1/T_2obsd - 1/T_1 - 1/T_2inh \qquad (51)$$

Figure 20 shows the linear dependence of the exchange contribution $1/T_2ex$ on the square of the resonance frequencies, for P values 0.3, 0.5 and 0.8, as predicted by Woessner's expression for two-site exchange (eq. 52 is identical to eq. 8, p.15):

$$k_a + k_b = 4\pi^2 P_a P_b (\upsilon_a - \upsilon_b)^2 T_2ex \qquad (52)$$

Again we can extract the exchange rates. $(\upsilon_a - \upsilon_b)$ is 525 Hz in this case, and k_a, k_b, P_a and P_b have their usual meaning. Table 12 shows the exchange rates (k_a+k_b) values obtained with eq. 52:

The invariance of (k_a+k_b) with P confirms that Woessner's equation can be applied again. Moreover it shows that the measured exchange rates are not affected by the aggregation, so that the exchange process can be described with a two-site model.

To again distinguish between the unimolecular and the bimolecular process, the variation of (k_a+k_b) with the total sodium concentration was measured in the range of $[Na]_t$ from 2×10^{-5} to 5×10^{-2}M (Fig. 21).

The general shape of the curve is identical to that for the case of hexafluorophosphate (Fig. 13). At low concentration the (k_a+k_b) is contentration independent, indicating unimolecular decomplexation to be the dominant exchange pathway. At high concentrations, the linear variation of (k_a+k_b) with $[Na]_t$ shows the effectiveness of the bimolecular cation interchange mechanism (Tab. 13).

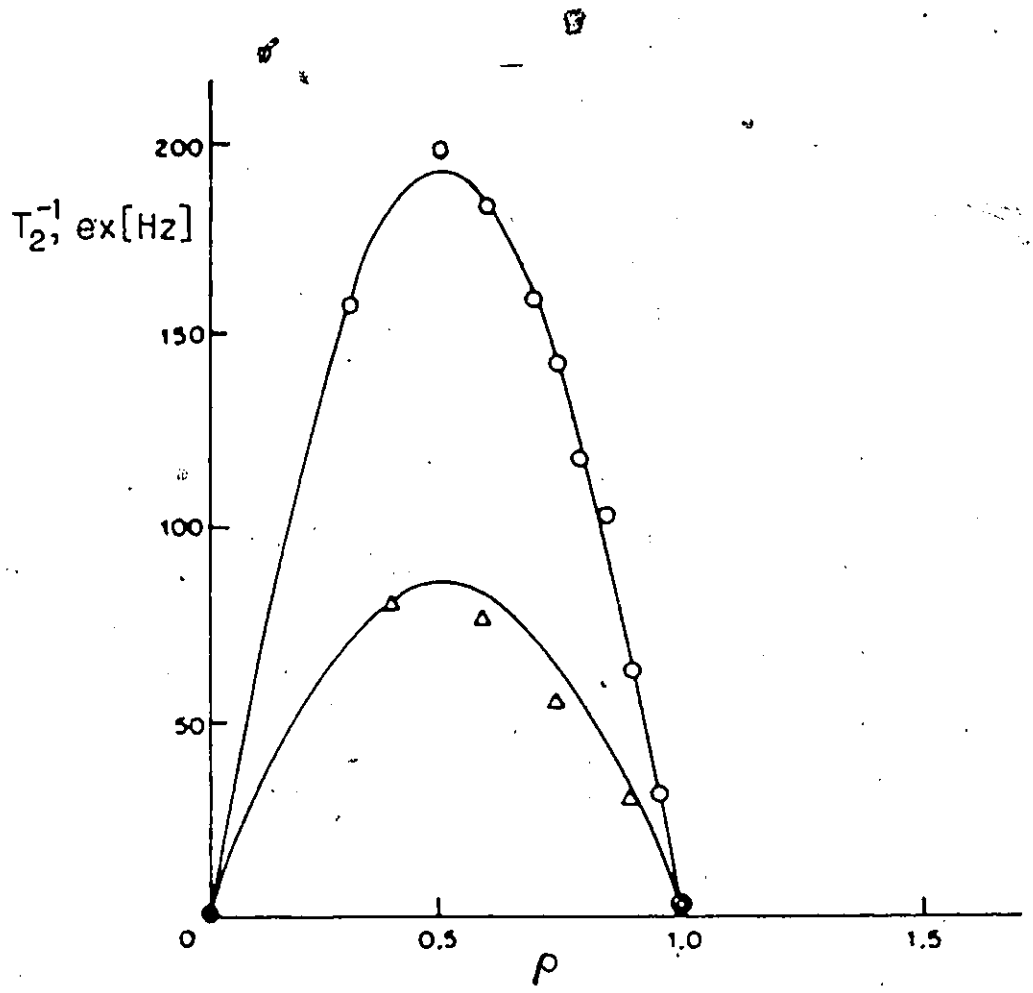

Figure 19: Exchange Relaxation $1/T_2ex$ - $NaBPh_4$:DB24C8. $1/T_2ex$ in nitromethane as a function of [DB24C8]/[$NaBPh_4$] (ρ) at 79.35 MHz (O) and 52.92 MHz (Δ). [$NaBPh_4$] is 0.037 M. Temperature of measurement is 294 K.

The temperature variation of k_2 was measured for sodium tetraphenylborate : DB24C8 at crown/sodium equal 0.5 (Fig. 22). The slope and intercept give the enthalpie and entropie of activation shown in Tab. 14. From the activation energies the bimolecular exchange mechanisms appear to be similar for both anions.

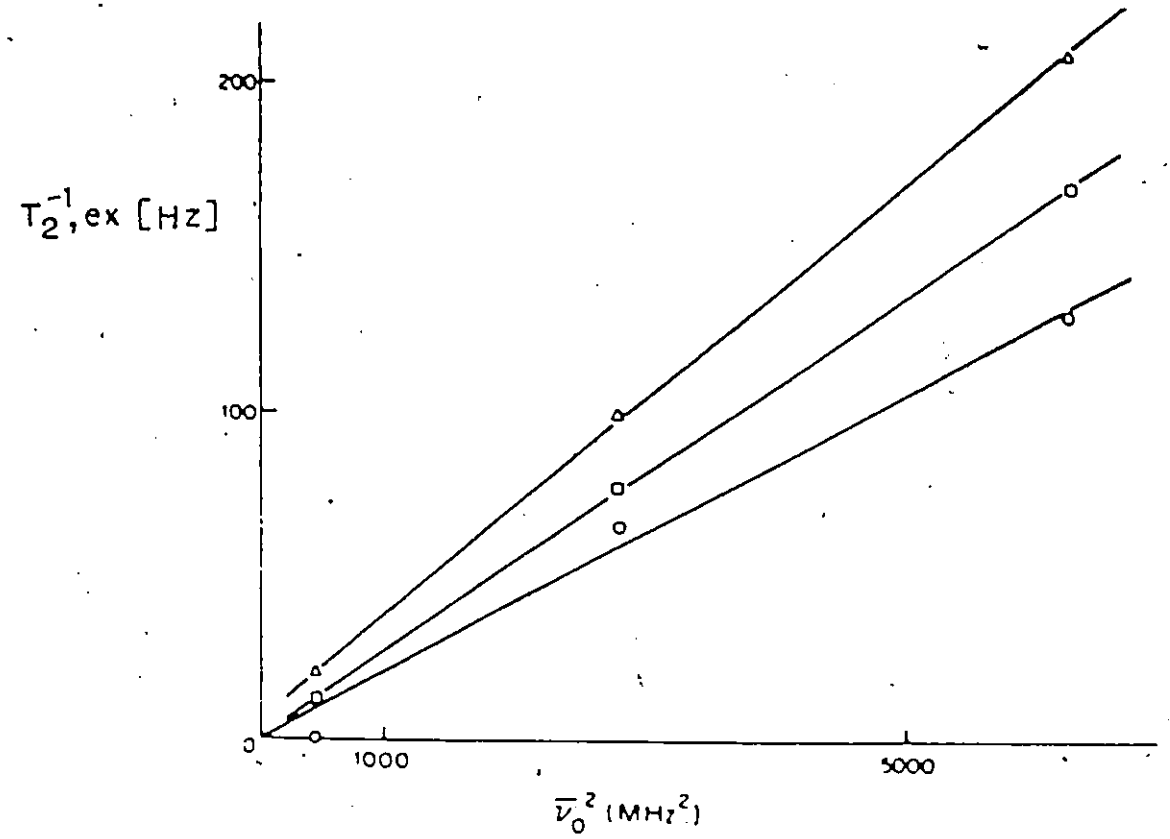

Figure 20: Exchange Rates versus Field Strength - $NaBPh_4$:DB24C8. $1/T_2ex$ for $NaBPh_4$ (0.037 M) in the presence of DB24C8 (ρ = 0.50 (△), 0.80 (○), and 0.30 (□)) as a function of $\overline{\nu}_0^2$, the square of the observation frequency.

Table 12: (k_a+k_b) as function of DB24C8/$NaBPh_4$

P	$1/T_1$ [s^{-1}]	$1/T_2$ [s^{-1}]	$1/T_2ex$ [s^{-1}]	k_a+k_b [$x10^4$Hz]
0.0	22(1)	30(3)	-	-
0.30	110(3)	278(6)	157(9)	1.3(0.1)
0.50	162(4)	370(7)	197(11)	1.3(0.1)
0.60	191(5)	385(7)	183(12)	1.3(0.1)
0.70	217(10)	386(7)	158(17)	1.3(0.1)
0.75	225(3)	377(7)	141(10)	1.3(0.1)
0.80	236(6)	365(7)	118(13)	1.3(0.1)
0.85	243(5)	356(7)	103(12)	1.2(0.1)
0.90	253(7)	327(6)	63(13)	1.4(0.3)
0.95	253(5)	296(6)	32(11)	1.5(0.5)
1.00	208(5)	222(5)	-	-
1.15	205(4)	218(5)	-	-

P is the ratio DB24C8/sodium for a constant sodium concentration of 0.037 M. $1/T_1$ is the observed lonitudinal relaxation rate. Its error is given as three σ, σ being the standard deviation given by the nonlinear regression analysis. $1/T_2$ is the observed transverse relaxation rate, and $1/T_2ex$ is the exchange contribution to $1/T_2$ ($1/T_2ex = 1/T_2 - 1/T_1 - 1/T_2inh$). (k_a+k_b) is the sum of the pseudo-first-order rate constants for the two-sites exchange at 295K.

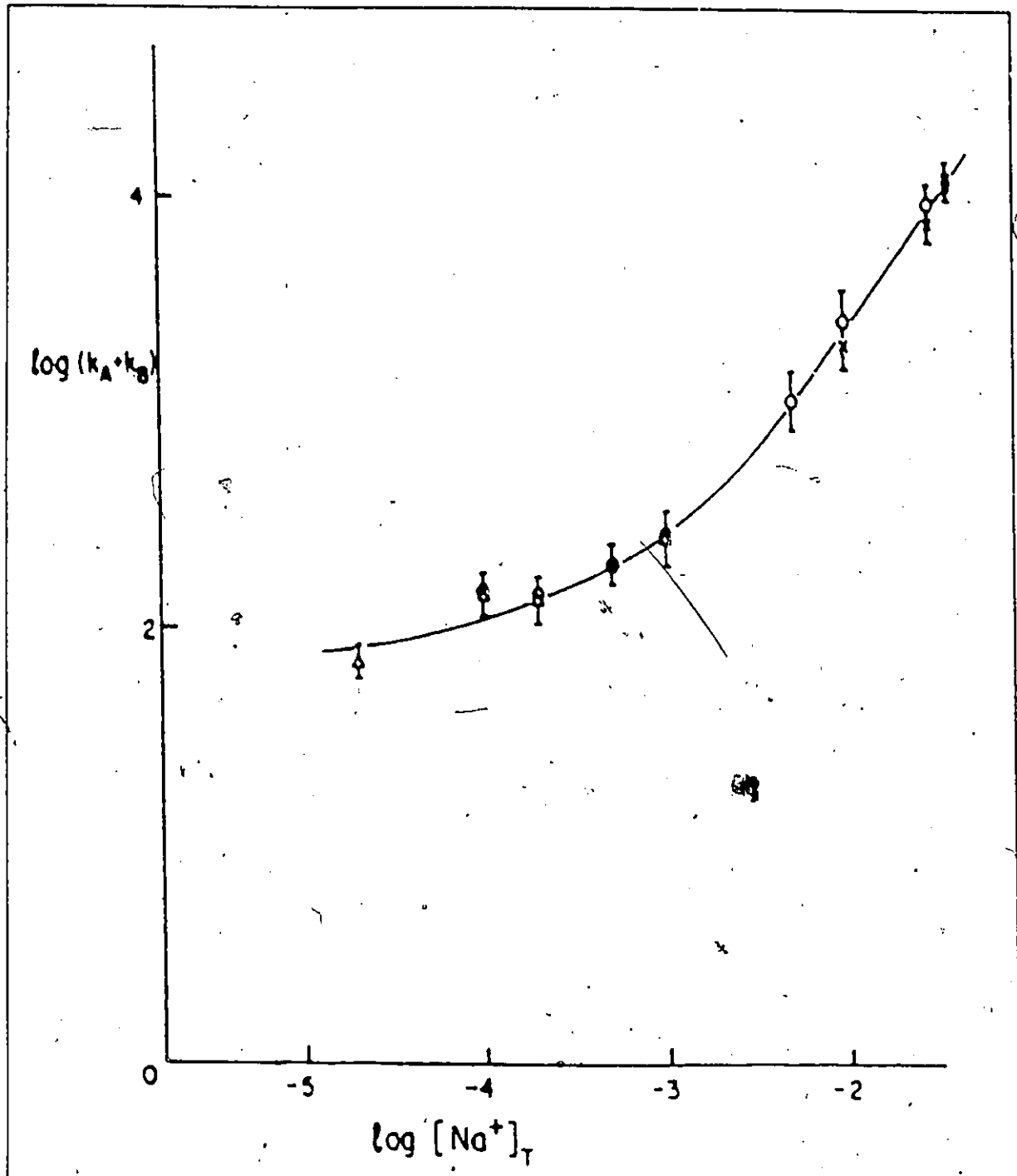

Figure 21: (k_a+k_b) against $[Na]_t$ - $NaBPh_4$:DB24C8. (k_a+k_b) is calculated using eq. 52 (x), a complete line shape analysis (o), or a line-shape analysis on the exchange broadened resonance of the solvated sodium (X).

Table 13: Exchange Kinetics in Nitromethane – $NaPF_6$ and $NaBPh_4$

Salt	k_{-1} [s^{-1}]	dG^* [kJ/mol]	k_2 [$s^{-1}M^{-1}$]	dG^* (kJ/mol)
$NaPF_6$	60	63 (3)	$3.6\ 10^5$	42 (2)
$NaBPh_4$	50	64 (3)	$2.8\ 10^5$	41 (2)

k_{-1} and k_2 are the rate constants for unimolecular and bimolecular cation exchange, dG^* are their free activation energies.

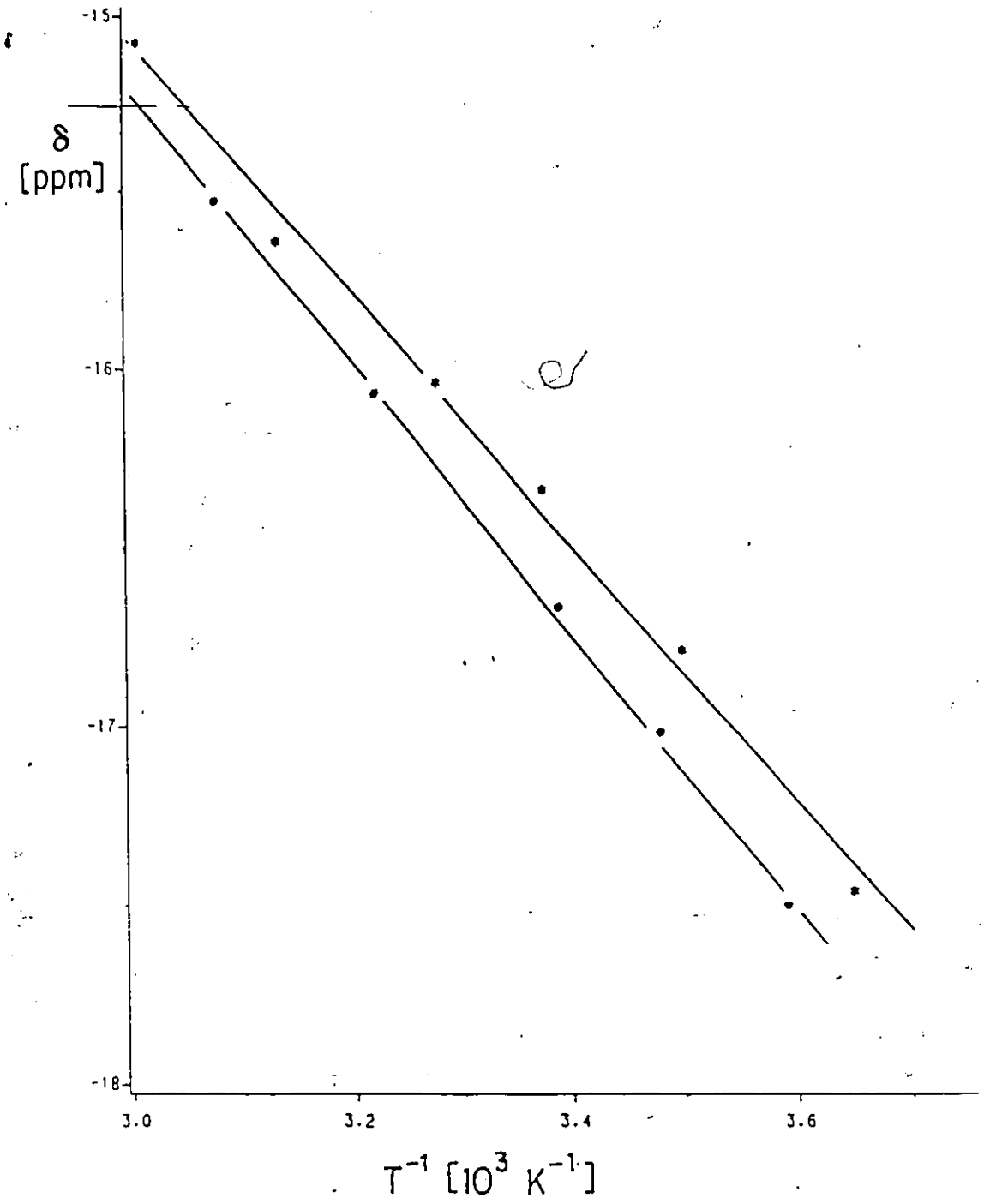

Figure 22: Temperature Variation of k_2 - $NaPF_6$ and $NaBPh_4$. [NaX] is 0.037 M in nitromethane in both cases, [DB24C8]/[sodium] is 0.50. Under these conditions the exchange is purely bimolecular, and $k_2 = (k_a+k_b)/[Na]_t$. (k_a+k_b) values are calculated with eq. 52.

Table 14: Activation Parameters for Bimolecular Exchange - $NaBPh_4$

Salt	$dH^{\#}$ [kJ/mol]	$dS^{\#}$ [J/molxK]	$dG^{\#}$ [kJ/mol]
$NaBPh_4$	31 (3)	-32 (10)	41 (3)
$NaPF_6$	29.5 (2)	-36.9 (10)	40 (2)

1.2.4.5 Anion Effects on Aggregation

The aggregation model as described by eq. 40 - 42 for sodium tetraphenylborate and DB24C8 in nitromethane can be seen as an extension to the exchange model for sodium hexafluorophosphate (see p. 69): The initial opening of the wrapped 1:1 complex and the addition of a second sodium cation lead to an intermediate 2:1 species in both cases. With sodium hexafluorophosphate its lifetime is too short to let it contribute to the observed shifts and longitudinal relaxation rates. But with sodium tetraphenylborate, this 2:1 intermediate has a formation constant of 0.66 M^{-1}. Furthermore it serves as a nucleating 'seed' by adding 1:1 complexes to form the aggregate species (Fig. 17).

The aggregation model suggests a plausible description, but it does not inform about the driving forces behind the aggregation. Intercalation of a tetraphenylborate-phenyl-ring between two adjacent DB24C8 aromatic rings could lead to favourable aromatic stacking. This implies an active role for the tetraphenylborate (Fig. 17, A). Alternatively, the tetraphenylborate anion, due to its weak interaction with the sodium cation, may simply allow for the stacking of coplanar complexes (Fig. 17, B). The planar conformation is preferred by large crown ethers in the uncom-

plexed state.[65] Given equal coordination to the sodium cation, partial release of backbone conformational strain (gauche to trans) upon forming the planar aggregate structure may help to compensate for the lower translational entropy of the aggregate.

Other evidence supporting aggregation are the low donicity of the solvent nitromethane (DN=2.7), and the known tendency of tetraphenylborate to form solvent separated ion pairs even in nonpolar solutions, as well as sandwich complexes.[27][65]

The aggregates formed in the presence of tetraphenylborate resemble polyelectrolytes, with the counter anions restricted to atmospheric charge compensation.[1] These aggregates are analogous to some ternary 'super-complexes',[79] or to some covalently designed channel ligands.[80] They are probably rigid (on the reorientational time scale) stacks of planar 1:1 complexes. Their noncovalent structure is controlled by cation-dipole attractions, backbone conformation strain and possibly aromatic stacking (Fig. 17).[81]

The boron-11 chemical shift of the tetraphenylborate counter anion was independent of ρ, indicating again the presence of solvent separated $NaBPh_4$ ion pairs. The sodium-23 NMR chemical shift of sodium hexafluorophosphate and sodium tetraphenylborate in nitromethane differ by 0.32 ppm in the absence of crown (Tab. 4). This points to a difference in the ionic interaction of sodium with the two anions, possibly already large enough to inhibit aggregation in the presence of hexafluorophosphate. Alternatively the chemical shift difference may be due to a diamagnetic shift on the sodium cation induced by the tetraphenylborate.

1.2.5 Ionic Interaction in Complexation Systems

Sodium cations in solution relax magnetically via coupling of their nuclear electric quadrupole with the electric field gradient created by the cation's chelation shell. For simple salt:ligand systems this shell has three components: solvent molecules, ligand molecules and counter anions. They all compete for coordination sites on the sodium cation.

In the systems studies here, DB24C8 clearly dominates the sodium coordination sphere, compared with the solvents nitromethane, acetonitrile and even pyridine (Figs. 7, 3 and 5). Nitromethane in turn dominates over the bulky anions hexafluorophosphate and tetraphenylborate. Tetraphenylborate shows no competition while hexafluorophosphate only forms solvent-separated ion-pairs and interferes with the aggregation of sodium:DB24C8 complexes. The decomplexation rates are quite similar for these two counter anions. However, stronger coordinating anions such as iodide and thiocyanate are known to significantly affect both exchange rates and mechanisms (see pp. 19-22) as well as the coordination state of the cation. This second aspect will be discussed below.

1.2.5.1 Introduction to Ionic interaction in Solutions

Cation NMR studies of ionic interactions in salt solutions have elicited much interest since the 1960s. Some good reviews cover this field.[6][1][7] Much of the early work on ionic interactions was done on aqueous alkaline halide solutions, at concentration ranges from 0.5 M to 10 M.[20][21] In all studies both relaxation and chemical shifts varied non-linearly with the concentration. These concentration dependencies were attributed to direct and indirect ionic interactions, but often too many effects had to be considered to allow for their clear separation.

Hertz et al. were the first to propose a theoretical analysis that successfully accounts for the observed quadrupolar relaxation of alkali halides in aqueous solutions:

$$1/T_1 = 1/T_2 = \pi^2[(2I+3)/I^2(2I-1)][eQ(1+\gamma_\infty)/h]^2(A+B+C+D) \quad (53)$$

In this schematic representation, A accounts for the relaxation contribution of the (randomly distributed) solvent molecules in the first solvation shell (Fully Random Distribution, FRD). C is the purely inter-ionic contribution, determined by the relative translational motion of two ions and their distance of closest approach. Hertz found higher ion-ion correlation, also called ion-clouding, to quench this ionic contribution to the electric field gradient at higher concentrations. This is an intriguing new aspect of alkali cation relaxation in solution.[21][82] B considers the effect of other ions on the orientation of solvent molecules in the first coordination shell of the relaxing ion. Finally D takes into account ion-water cross correlation effects. Usually B and D can be neglected at low concentrations.

In 1968, Bloor and Kidd reported strong solvent and concentration dependencies for the sodium-23 chemical shift of sodium iodide. Furthermore, the shifts were linearly related to the pK_a values of the solvents.[25]

Erlich and Popov confirmed Bloor and Kidd's findings with a more detailed study. In particular, they found the shift of sodium tetraphenylborate and sodium perchlorate to be constant at concentrations between 0.01 M to 0.5 M, whereas the chemical shifts of sodium iodide, bromide and thiocyanate depended strongly on the concentrations in acetonitrile, acetone, dimethylformamide, dimethylsulfoxide and other organic solvents.[8] Towards the low concentration limit, the chemical shifts of different sodium salts in any solvent converged towards one value. This shift was taken as characteristic for the solvated sodium cation in this particular solvent. These concentration dependencies were generally attributed to contact ion-pairing.[26]

In 1974, Buxton and Caruso studied the ion solvation of the same group of sodium salts in four derivatives of 2-oxazolidone. These are solvents of low donicity but with large dielectric constants ranging from 56 to 77.[83] Again these researchers found concentration independent shifts for sodium perchlorate and tetraphenylborate, and strong concentration dependencies for solutions of sodium iodide and sodium thiocyanate. These concentration dependencies were linearly related to the dielectric constant of the particular 2-oxazolidone.[16] Detellier and Gertmans demonstrated ionic association of sodium iodide in amine solution, using both Na-23 chemical shift and relaxation rates.[84] Chabanel et al. detected contact ion-pairs of sodium thiocyanate in tetrahydrofuran solutions, using Raman and Infrared spectroscopy.[86]

Melendres and Hertz expanded their electrostatic treatment of quadrupolar relaxation to non-aqueous solvents. They had to add a relaxation term to account for thermodynamically stable ion-pairs. Their concepts describe well the complexity of ionic interactions in solution at higher concentrations. Yet the large number of different relaxation contributions at the high concentrations used makes it difficult to separate them reliably.[24]

Chemical shifts have proved to be less problematic. They do not depend on the geometry of the chelation shell, rather they depend on the cumulative donicity of the direct ligands. Anion dependent electrostriction may cause varying internal pressure at the ion, but this should not falsify the extracted association constants. The problem of interpreting the chemical shift variation with concentration has been given a sound theoretical basis by the work of Richards et al. on Cesium-133 NMR in aqueous solution.[29][85] The authors assume that the concentration dependence of the chemical shift at low concentration is only determined by dynamic cation-anion interactions. They relate it to the probability of encounters between cation and anion, or direct bimolecular interaction. For higher concentrations Richards et al. had to account for the influence of the ionic atmosphere on the encounter-probability, using a Debye-Huckel type treatment.

16 The solution far-infrared spectra of the sodium cation's vibration inside its coordination sphere was independent of the anion. Thus the cation-anion interaction must have a duration that is short on the far-infrared time scale, that is less than 10^{-7} s.[83]

Recently, Hertz et al. took implicit advantage of the fact that at low concentrations direct bimolecular interactions should dominate the concentration dependent effects.[64] In fact, the authors find that in aqueous solutions, as well as in one of the organic solutions, the longitudinal relaxation rates of some alkaline salts tend, at concentrations around 0.01 M and 0.001 M, to vary linearly with the square root of the salt concentration. Again this points to a bimolecular cation-anion interaction. However, at the higher end of the concentration ranges studied by Hertz there are again strong relaxation contributions arising from secondary ionic interactions.

In brief, the chemical shifts and quadrupolar relaxation rates of alkaline salts in aqueous and non-aqueous solutions often show significant concentration dependencies. This could provide a wealth of information about the structure of the first chelation shell around the ion. Yet at higher concentrations, the indirect contributions to shift, and especially to relaxation rates, are difficult to account for.[21][82] In fact, other necessary parameters, such as Hertz's polarisability factor, only take away from the concept's neatness.

The availability of high magnetic field magnets offers a way out: towards the low concentration limit, only the direct cation-anion interactions will be concentration dependant.[17] The studies described here, with salt concentrations between 0.01 M and 0.00004 M, fall into this category. As will be shown below, the generally most promising approach is to consider both the sodium chemical shift and the sodium relaxation rates jointly.[84] Figures 23 - 26 present the variations with P of chemical shift and relaxation rates for both sodium iodide and sodium thiocyanate.

17 This is not to say that indirect or secondary ionic interactions will not occur, but only that their contribution to both chemical shift and relaxation rates will be independant of the concentration in this region.

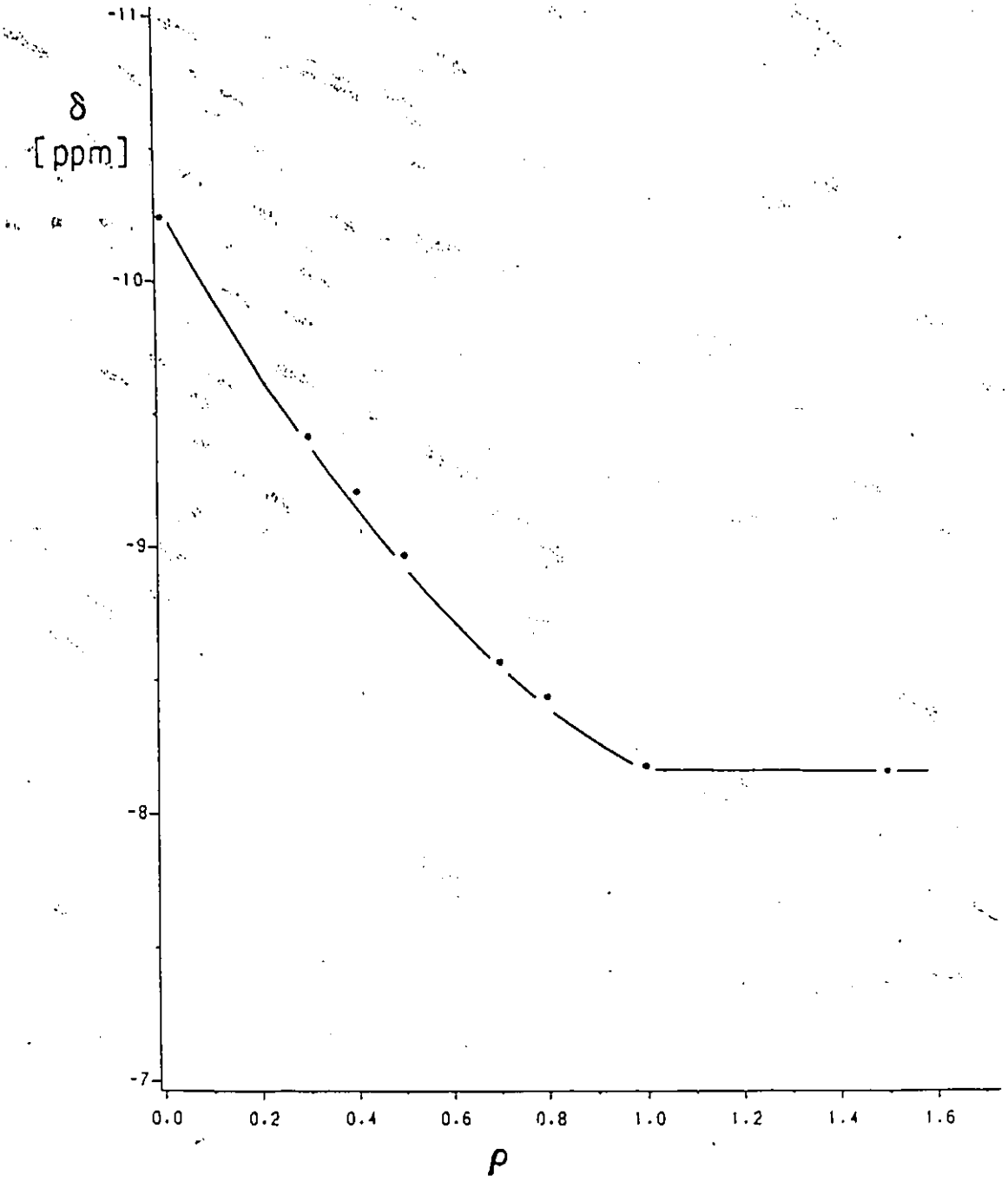

Figure 23: Sodium-23 Shifts of NaI versus DB24C8/Sodium. The points are experimental for NaI (0.01 M) in nitromethane at 79.35 MHz as a function of $[DB24C8]/[NaI]_t$ (ρ). The solid curve is fitted with the ion-pairing model, in a simultaneous regression of complexation and concentration data.

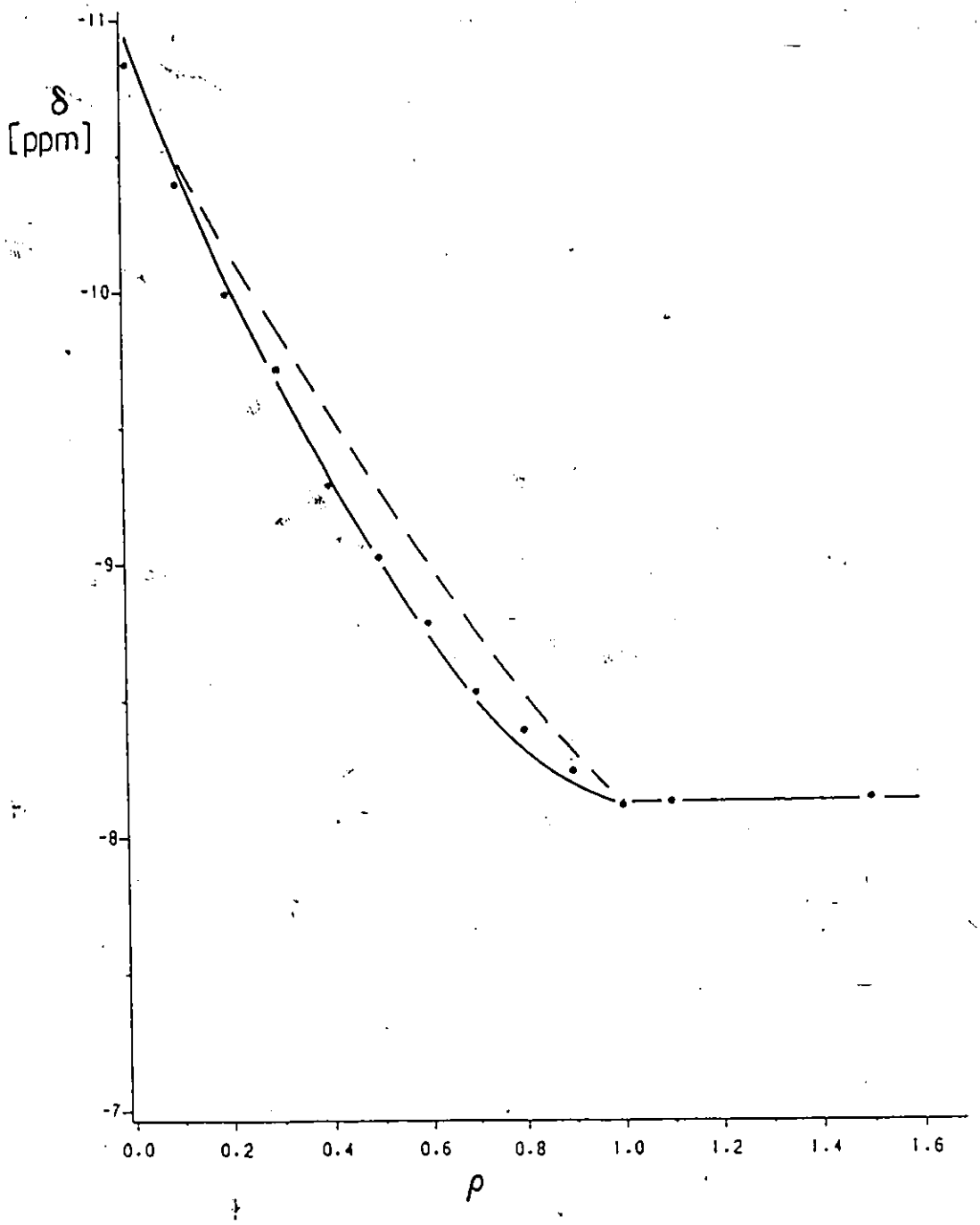

Figure 24: Sodium-23 Shifts of NaSCN versus DB24C8/Sodium. The points are experimental for NaSCN (0.005 M) in nitromethane at 79.35 MHz as a function of [DB24C8]/[NaSCN]$_t$ (ρ). The solid curve is fitted with the (ion-pairing + 2:1) model; the broken line is fitted with only the ion-pairing model; using simultaneous regression of complexation and concentration data for both models.

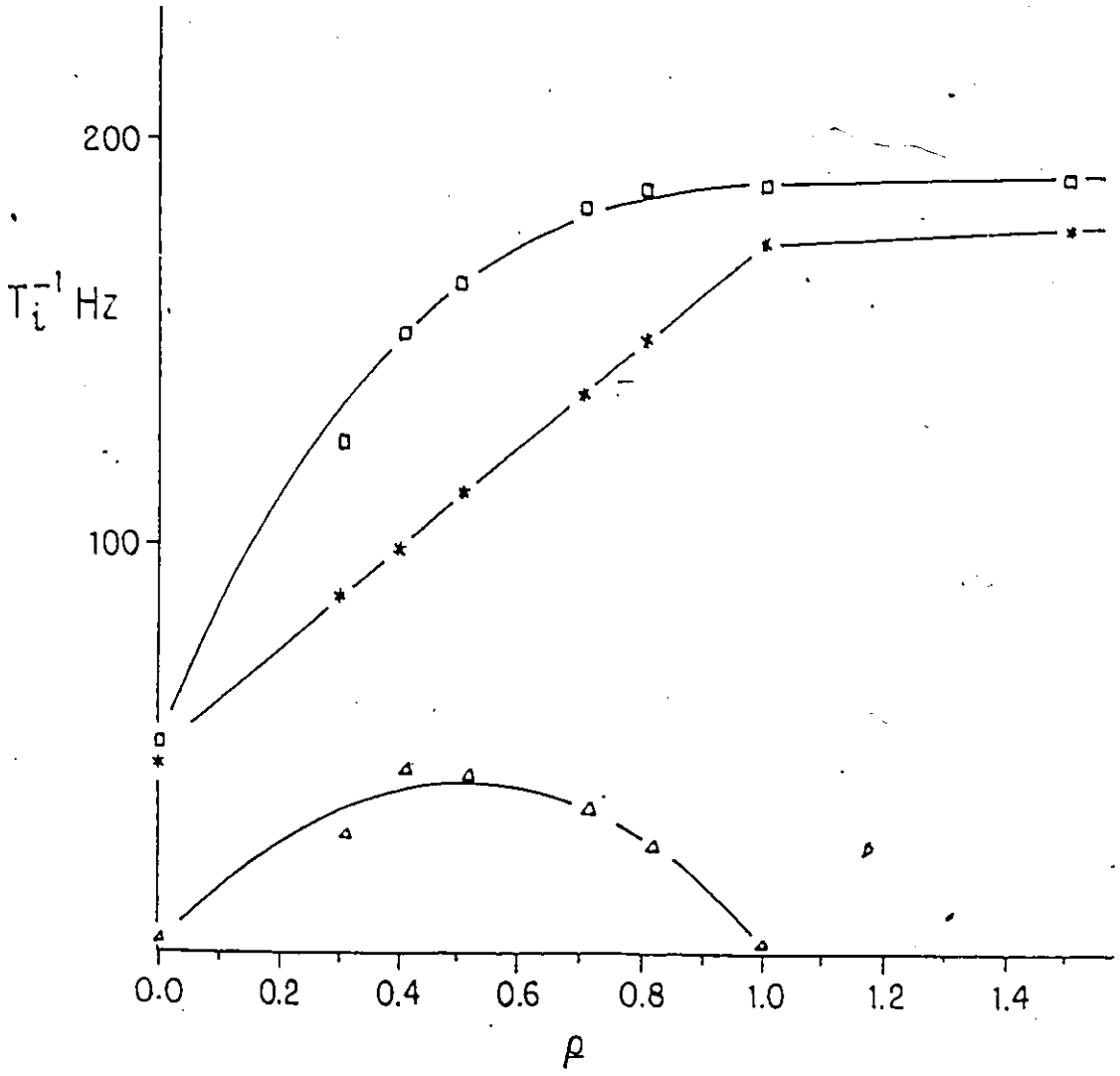

Figure 25: Relaxation Rates of NaI versus DB24C8/Sodium. Na-23 transverse (□) and longitudinal (✱) relaxation rates for sodium iodide (0.01 M) in nitromethane at 79.35 MHz as a function of [DB24C8]/[NaI] (ρ). As well, the exchange contribution to the transverse relaxation, $1/T_2ex = 1/T_2obsd - 1/T_1 - 1/T_2inh$, is shown (Δ). Temperature of measurement is 295 K.

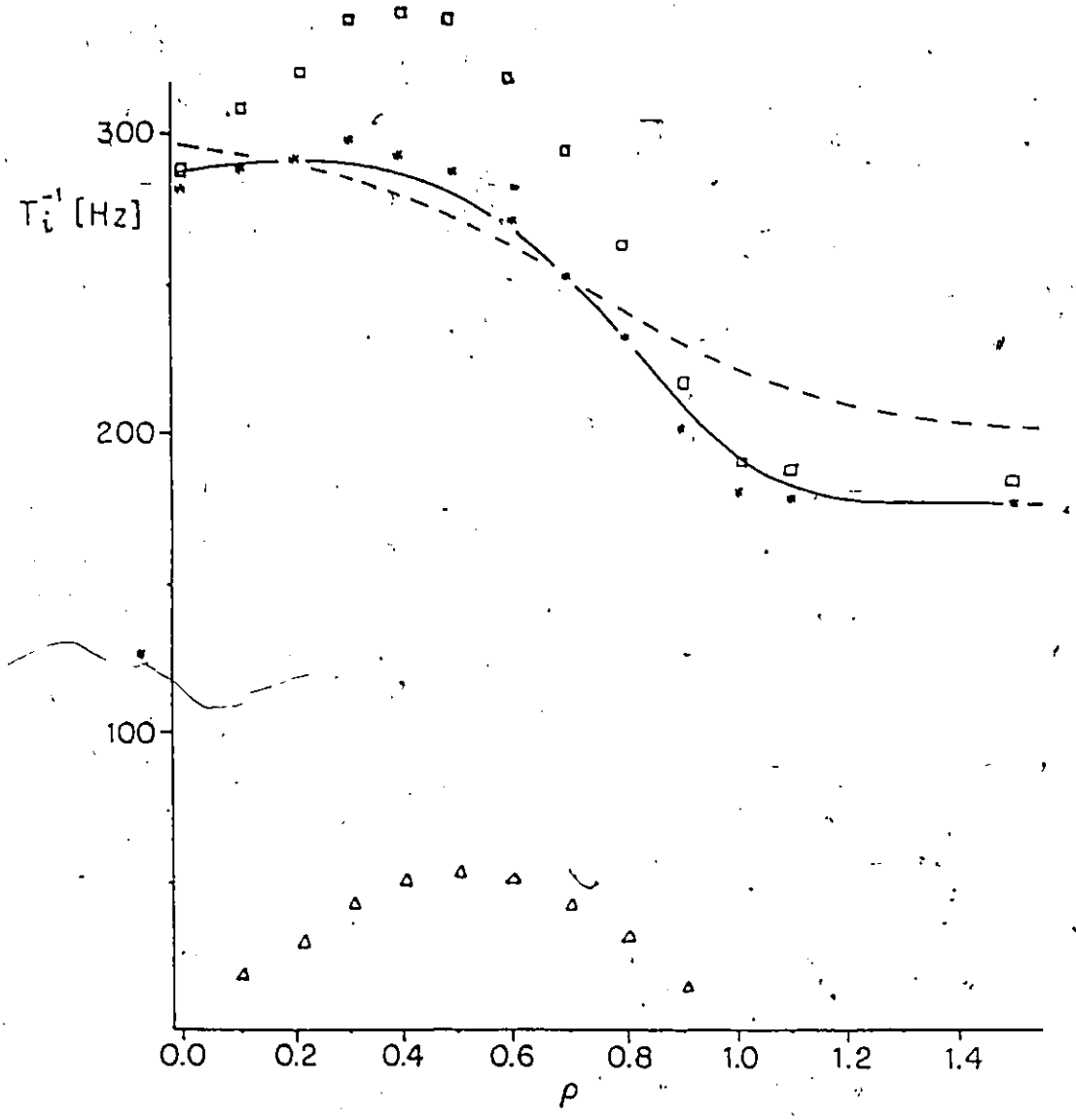

Figure 26: Relaxation Rates of NaSCN versus DB24C8/Sodium. Na-23 transverse (□) and longitudinal (✱) relaxation rates for sodium thiocyanate (0.005 M) in nitromethane at 79.35 MHz as a function of [DB24C8]/[NaSCN] (ρ). The points are experimental, the broken line is fitted using the ion-pairing model (eqs. 60), the solid line is fitted using the ion-pairing + 2:1 complex model (eqs. 65b). In both cases, the concentration data were simultaneously fitted with the ion-pairing model. The exchange contribution to the transverse relaxation, $1/T_2ex = 1/T_2obsd - 1/T_1 - 1/T_2inh$, is also shown (Δ). Temperature of measurement is 295 K.

the sodium thiocyanate indicate strong participation of the anions in the solvation sphere of the cation, that is contact ion-pairing.[8]

In order to separate the sodium - anion from the sodium - crown interactions, the concentration dependence of the sodium shifts and relaxation rates were studied for sodium thiocyanate and sodium iodide in nitromethane. The concentrations ranged from 0.01 M down to 0.00004 M for sodium thiocyanate, and from 0.01 M down to 0.0001 M for sodium iodide. The results are presented in Figs. 27 and 28:

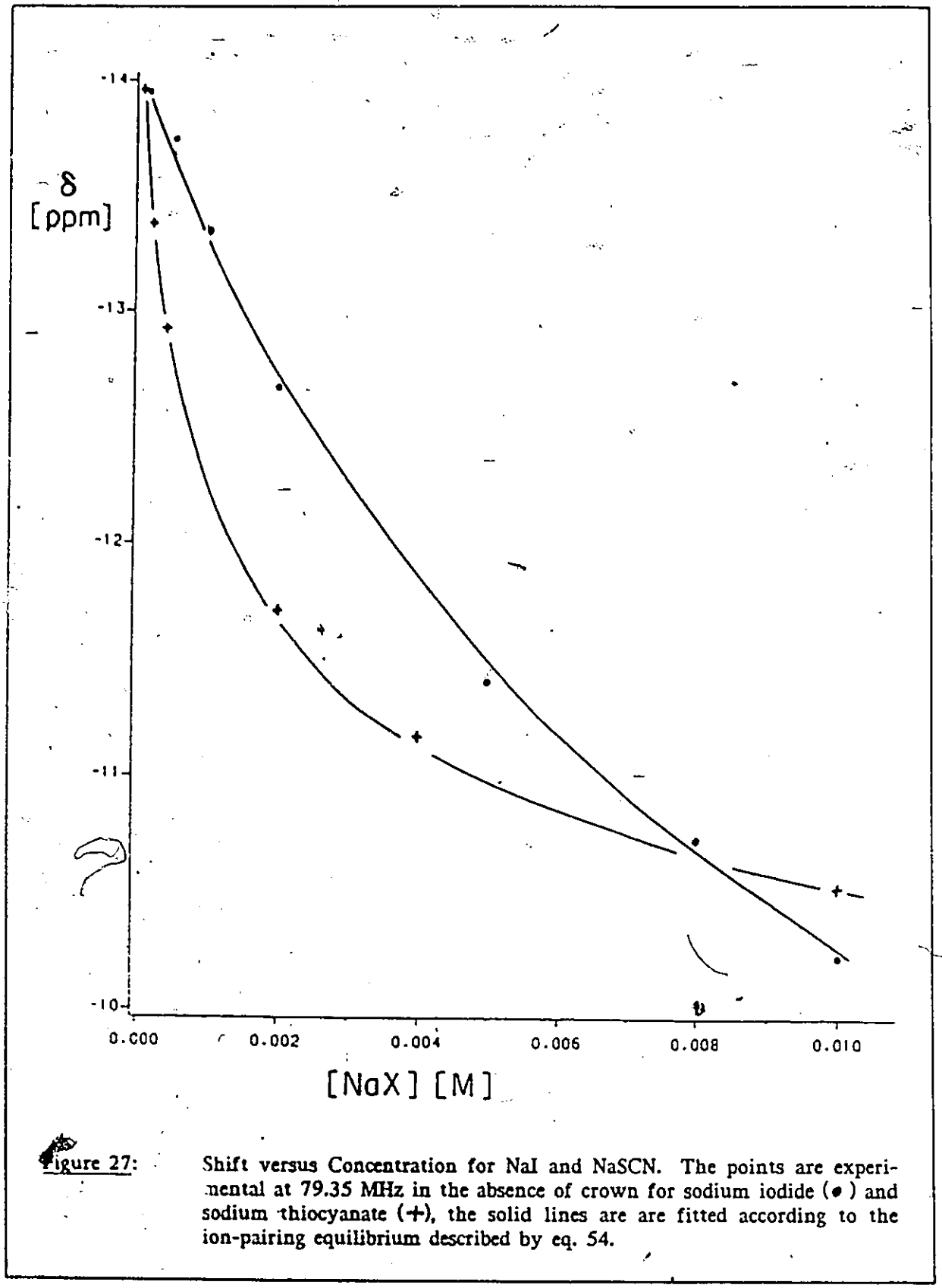

Figure 27: Shift versus Concentration for NaI and NaSCN. The points are experimental at 79.35 MHz in the absence of crown for sodium iodide (•) and sodium thiocyanate (+), the solid lines are are fitted according to the ion-pairing equilibrium described by eq. 54.

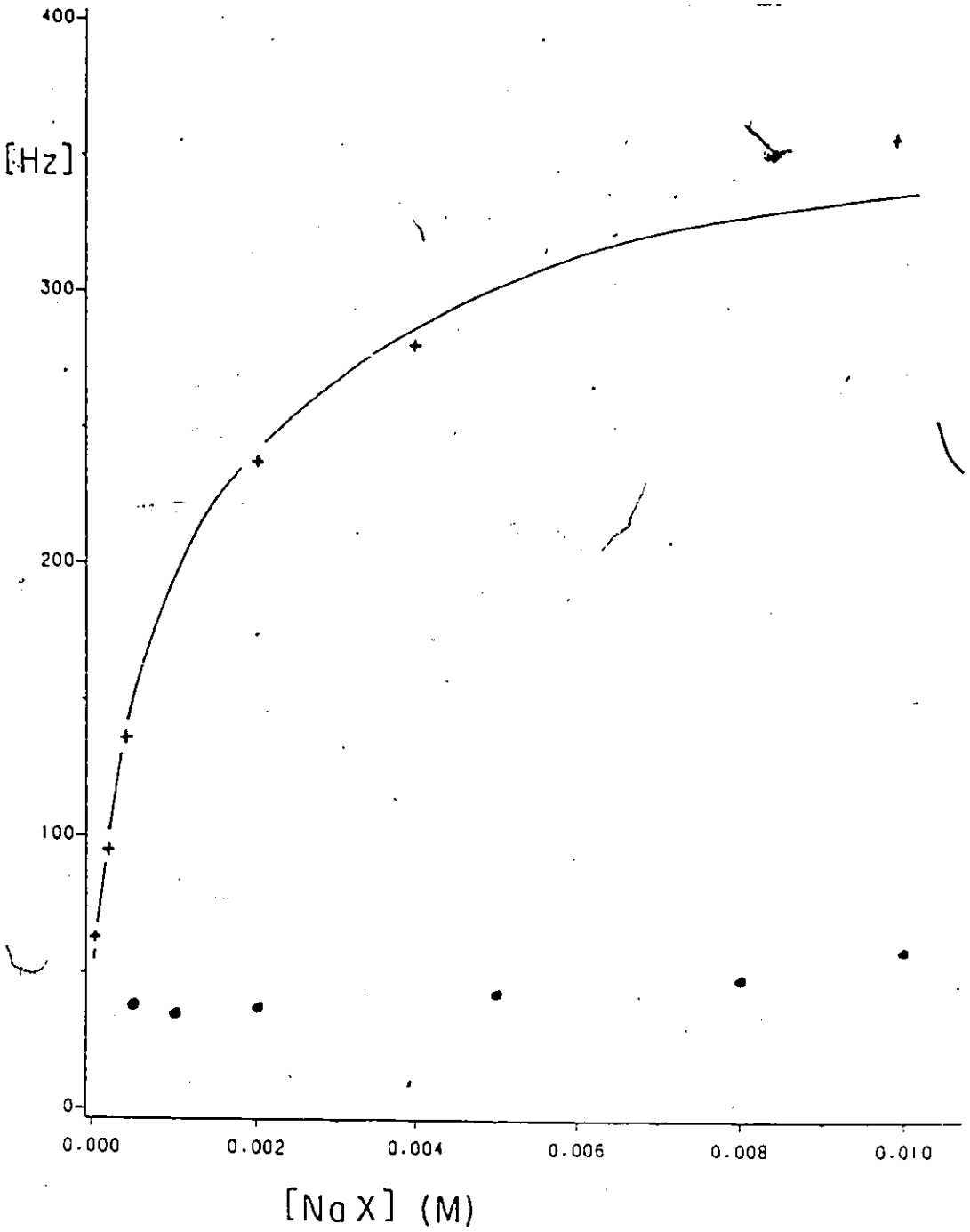

Figure 28: Relaxation versus Concentration for NaI and NaSCN. The points are experimental at 79.35 MHz in the absence of crown for sodium iodide (●) and sodium thiocyanate (+), the solid line is fitted according to the ion-pairing equilibrium described by eq. 55. Temperature is 296 K.

Asymptotic curves are observed for the shifts of both salts and for the transverse relaxation rate of sodium thiocyanate. This clearly indicates ionic association, but of what nature?

As discussed earlier, one can, for alkaline salts in solution, divide the concentration dependent contributions to the chemical shifts and relaxation rates into those due to direct, and those due to indirect, interionic effects. The direct effects include thermodynamically stable contact ion-pairs; as well as collisional contact between cation and anion.[8][18][51] The indirect effects include changes of the orientation of chelating solvent molecules due to the proximity of other ions, as well as contributions from other ions in the vicinity.[24]

Many studies on ionic interactions were done at salt concentrations between 0.1 M to 5 M. At such high concentrations the theoretical models of both Richards and Hertz have to cope with quantifying the contributions of the indirect interactions: they become larger and more complex with increasing concentrations.[64][24][29][85]

At the very low concentrations used in this work the indirect interactions become negligible, or at least concentration independent. So the observed concentration dependence can be attributed to direct bimolecular cation-anion interactions alone, of a lifetime of less than 10^{-7}s.[83] In the following, this interaction is referred to as 'ion-pairing', even though it is not possible to distinguish between diffusion controlled penetration of the solvation shell (Debye-Hückel contact, collisions), or thermodynamically stable ion-pairs (Bjerrum ion-pairs). Thus the ionic interaction is described as bimolecular formation of ion-pairs from the solvated ions (see eq. 34).[18]

18 Two factors combined to show that the ionic interactions are fast on the NMR time scale: first, the chemical shift and relaxation rate curves for sodium thiocyanate are parallel; and the ion-pairing constants K_p calculated from shift and relaxation data are similar.
Second, $1/T_1$ and $(1/T_2obsd - 1/T_2inh)$ are equal at the low and high concentration limits. If we assume a thermodynamically stable ion-pair and a chemical shift difference between free and paired sodium of 390 Hz, then, using Woessner's expression (eq. 52), the lifetime of the sodium thiocyanate ion-pair has to be shorter than about 10^{-6} s. This agrees with the upper life-time limit of 10^{-7} s calculated by Buxton and Caruso for 2-oxazolidones as solvents.[83]

As in the case of sodium hexafluorophosphate, the observed chemical shifts (and relaxation rates) can then be expressed as the sum of the contributions from free and ion-paired sodium. Again the final expressions are (eq. 54 is identical to eq. 35, p.49):

$$\delta_{obsd} = P_f \delta_f + P_p \delta_p \qquad (54)$$

and

$$1/T_2 obsd = P_f/T_2 f + P_p/T_2 p \qquad (55)$$

where δ_{obsd}, δ_f and δ_p are the observed shifts, the shift of free and of ion-paired sodium; while $1/T_2$obsd, $1/T_2$f and $1/T_2$p are the corresponding transverse relaxation rates. P_f and P_p are functions of $[Na]_t$ and K_p (see Appendix 2).

A three parameter nonlinear least squares optimization routine was used to fit eqs. 54, 55 to the data sets (Figs. 27 and 28). Here the variable parameters were the chemical shifts (or relaxation rates) of free and ion-paired sodium, and the ion-pairing constant K_p. The calculated shift and relaxation rates for sodium thiocyanate, and the calculated shift for sodium iodide, are shown as solid lines in Figs. 27 and 28. Table 15 gives the obtained ion-pairing constants, shifts and relaxation rates.

The excellent fit of the ion-pairing model (eqs. 54, 55) to the experimental data (Figs. 27, 28) supports the initial assumption that the ionic interactions can be represented by one formation constant alone. So the nature of the interaction appears indeed to be concentration independent.[19] For sodium thiocyanate, the similar concentration dependence of shift and relaxation rate is in good agreement with stoichiometric 1:1 ion-pairing.

19 Strictly speaking, this only means that all ionic interactions present have the same concentration dependency. It does not necessarily mean that only one effect, the bimolecular ion-pairing, is active.

Table 15: Ion-Pairing Parameters for NaSCN in nitromethane

PARAMETER	SALT		
	NaSCN	NaSCN	NaI
$K_p[M^{-1}]$	1010(50)	980(50)	85(5)
δ_f[ppm]	-14.1(0.1)		-14.1(0.1)
δ_p[ppm]	-9.3(0.1)		-2.8(0.7)
$1/T_1f[s^{-1}]$		37 (2)	
$1/T_1p[s^{-1}]$		452 (35)	
(RMS)	(2.8)	(5.5)	(6.5)

δ_f and δ_p are the chemical shift of free and ion-paired sodium; $1/T_1f$ and $1/T_1p$ are the relaxation rates of free and ion-paired sodium; K_p is the ion-pairing constant.

For sodium iodide (Fig. 27) the shift curve shows an asymptotic variation with concentration similar to that of sodium thiocyanate, and again the ion-pairing equilibrium (eq. 54) was used to extract the ion-pairing constant and the shifts of free and ion-paired sodium (see Tab. 15).

However, the variations of the sodium iodide longitudinal and transverse relaxation rates with concentration are different (Fig. 28). First, the relaxation rates do not show the asymptotic behavior seen in the shift curve. And second, the absolute increase of relaxation rates with concentration is much lower for iodide than for thiocyanate for equivalent increases in the chemical shifts. Plotting the transverse relaxation rate against the chemical shift does give linear relationships for both salts, but the two lines have very different slopes (Fig. 29).

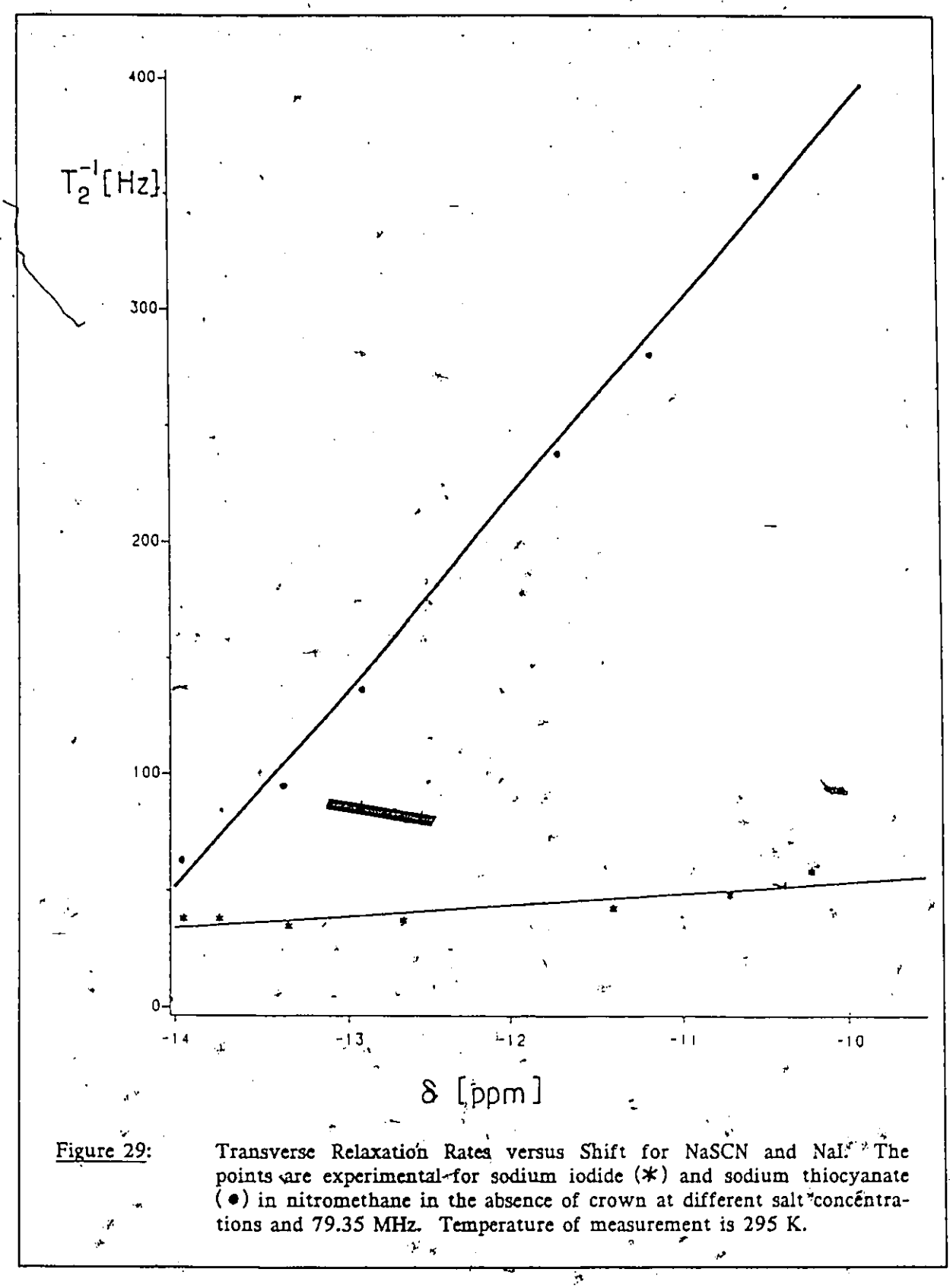

Figure 29: Transverse Relaxation Rates versus Shift for NaSCN and NaI. The points are experimental for sodium iodide (*) and sodium thiocyanate (•) in nitromethane in the absence of crown at different salt concentrations and 79.35 MHz. Temperature of measurement is 295 K.

In other words, for sodium thiocyanate both chemical shifts and relaxation rates are equally sensitive to the ionic interaction, whereas for sodium iodide only the shift is significantly affected. Clearly, the nature of the ionic interaction must be different for the two salts. The joint interpretation of chemical shifts and relaxation rates could shed some light on the situation:

There are two major theories concerning the mechanism of quadrupolar relaxation of alkali salts in solution: In the 'electronic theory' developed by Deverell,[87][88] both the quadrupolar relaxation and the paramagnetic shift term are attributed to distortions of the cations' electron shell during collisions with solvent and anion molecules. These induced electric field gradients couple with the nuclear electric quadrupol to cause magnetic relaxation. Furthermore, they are held responsible for the dominating paramagnetic chemical term. Thus this theory predicts a linear relation between chemical shift and quadrupolar relaxation rates. This is often found to be the case. Hertz's 'electrostatic theory' attributes the electric field gradient solely to the point dipoles and point charges of solvent and counter anions residing in the chelation shell of the cation.[21] As yet, no direct connection between the chemical shift and the relaxation rate has been found.

A stoichiometric ion-pair could explain the parallel concentration dependence of chemical shifts and relaxation rates for sodium thiocyanate, within the framework of either Deverell's electronic theory or Hertz's electrostatic theory.

With sodium iodide in nitromethane, we also observed a paramagnetic shift to higher resonance frequency with increasing concentration (Fig. 27). This again indicates the presence of strong donors such as the iodide anion in the chelation shell of the sodium cation. But we only observed a small increase of the quadrupolar relaxation rates (Fig. 28), indicating that the ionic interaction could not induce an asymmetric electric charge distribution around the sodium cation. Apparently, sodium iodide does not form 1:1 contact ion-pairs, with their high electric field gradient at the sodium. Instead, sodium iodide must form an ionic lattice or ionic cluster in solution,

or possibly dimers and higher aggregates of ion-pairs. This model accounts for the observed shift variation with concentration, assuming paramagnetic polarization of the sodium electron shell due to its interaction with the anion. At the same time, the symmetric arrangement of the anions around the cation results in only a small net ionic contribution to the electric field gradient. Thus the ionic interaction does not affect the quadrupolar relaxation. The following considerations support this interpretation:

- Hertz and coworkers detected the formation of similar 'ion clouds' or 'ion clusters' at high concentrations, where the individual interionic contributions to the electric field gradient quench each other.
- At a concentration of 0.01 M, both sodium thiocyanate and iodide are near their solubility limits in nitromethane. In this situation, one may well expect the formation of such 'crystal lattices'.

In fact, the ions in these clusters may well be solvent separated most of the time. It remains open whether the paramagnetic shift contribution is due to short term contact interaction, or the long term solvent separated interaction. This is true for sodium thiocyanate as well.

In conclusion, the results for sodium thiocyanate fit both Deverell's and Hertz's theory well. With sodium iodide on the other hand, the discrepancy between the concentration dependence of the chemical shift and the concentration independence of the relaxation rates contradicts the electronic distortion model. However it can be well explained on the basis of electrostatic interactions, if these include ion clouding.

In the next chapter, the system will be complicated by addition of DB24C8 to the equilibrium.

1.2.6 Effect of Ionic Association on Complexation to DB24C8

This chapter describes the effects of ion-pairing on structural and dynamic aspects of the complexation of sodium thiocyanate and sodium iodide with DB24C8.

The longitudinal relaxation rate for sodium iodide in the presence of DB24C8 varies linearly with P, suggesting once again quantitative formation of the 1:1 complex in fast exchange with the solvated sodium (Fig. 25). The transverse relaxation rate varies nonlinearly with P, such that the difference

$$1/T_2ex = 1/T_2obsd - 1/T_1 - 1/T_2inh \qquad (56)$$

forms a symmetric curve around P equal to 0.5. As with sodium hexafluorophosphate and tetraphenylborate, bimolecular exchange between solvated and complexed sodium causes this excess transverse relaxation (Fig. 25). But unlike with the two bulky anions hexafluorophosphate and tetraphenylborate, the chemical shift for sodium iodide shows a clear curvature towards higher frequency that is centered around P equal to 0.5 (Fig. 23). This deviation of the chemical shift curve from the classical linear variation with P is the most interesting feature of the sodium iodide case. Figure 25 shows again that sodium-iodide interaction in nitromethane does not affect the quadrupolar relaxation rates, but that it only affects the chemical shifts. This result is in line with the exclusive concentration dependence of the sodium iodide shift noted in the concentration study (Figs. 27, 28). In both cases, ion-cloud formation accounts for this distinction.

But can the chemical shift variation of sodium iodide with P be explained using only the ion-pairing model, as was possible in the case of sodium hexafluorophosphate?

Again the sum of solvated and ion-paired sodium were considered as a 'free sodium-pool' (Fpool), exchanging with the 1:1 complexed sodium. Solvated and ion-paired sodium are in

diffusion-controlled equilibrium. This is seen by the parallel variation with of the chemical shift and the relaxation rate for sodium thiocyanate; and by the identity of $1/T_1$ and $1/T_2$ at both the low and the high limiting concentrations for both sodium iodide and sodium thiocyanate (Figs. 27 and 28).

The addition of DB24C8 to the ion-pairing equilibrium again effectively removes free sodium cations by complexation (eqs. 57 - 59 are identical to eqs. 36 - 38, p. 50):

$$(Na^+)_s + (X^-)_s \underset{}{\overset{K_p}{\rightleftharpoons}} (Na^+,X^-)_s \qquad (57)$$

$$(Na^+)_s + (C)_s \underset{}{\overset{K_c}{\rightleftharpoons}} (Na^+,C)_s \qquad (58)$$

$$\delta_{obsd} = P_f\delta_f + P_p\delta_p + P_c\delta_c \qquad (59)$$

And as before, the chemical shift (δ_{obsd}) can be expressed as the sum of the three sodium species' contributions (Eq. 59, see also appendix 3). Removal of free sodium by complexation increases the ratio of ion-paired over free sodium cations in the sodium pool. Table 16 shows the results of simulating how adding DB24C8 affects the observed chemical shift of sodium iodide.[20]

The excellent agreement between simulated and observed values supports the adequacy of the ion-pairing model. In order to test the ion-pairing model on the complexation data, a nonlinear least squares optimization routine was used to fit eq. 59 to the experimental data of Fig. 23. A good fit could be obtained, but the iterated ion-pairing constant K_p and the iterated shifts for free (δ_f) and ion-paired sodium (δ_p) differed substantially from those obtained from the concentration

20 The equilibrium chemical shift was calculated according to eqs. 57 - 59 (see appendix 3), using K_p, δ_f and δ_p from the concentration study (Tab. 15), and $K_c = 10^6\ M^{-1}$.

Table 16: Ion-pairing Effects on Chemical Shift for NaI : DB24C8

ρ	CHEMICAL SHIFT [ppm]		
	simulated	observed	iterated
0.0	-10.30	-10.24	-10.30
0.3	-9.43	-9.42	-9.41
0.4	-9.18	-9.21	-9.17
0.5	-8.94	-8.97	-8.94
0.7	-8.55	-8.57	-8.55
0.8	-8.39	-8.44	-8.39
1.0	-	-8.18	-8.15
1.5	-	-8.16	-8.14

ρ is [DB24C8]/[NaI], with [NaI] = 0.01 M. The simulated values are obtained under the assumption of quantitative complexation. The iterated values are obtained by fitting the ion-pairing model (eq. 59) to the observed chemical shifts (Fig. 23).

dependence of the sodium iodide chemical shift (Tab. 17). This might just have been the result of linear covariance between these two parameters, but it could also indicate that the stoichiometric ion-pairing model is inadequate for explaining the complexation behavior. So to use all the relevant data available, a simultaneous fitting of the ion-pairing equilibrium (eq. 54) to the concentration curve (Fig. 27); and of eq. 59 to the complexation data (Fig. 23) was done. The parameter values so obtained are in close accord with those of the concentration data (Tab. 17).

The solid lines in Figs. 24 and 27 were calculated using the parameters from the simultaneous regression (Tab. 17). The close fit to the observed values clearly sanctions expressing the ionic

Table 17: NaI Complexation - Simultaneous Parameter Fitting

	From Data Set: concentration data (Fig. 27)	complexation data (Fig. 24)	simultaneous analysis (both)
$K_p[M^{-1}]$	85(10)	62(10)	82(10)
δ_f[ppm]	-14.1(1.5)	-13.7(0.1)	-14.1(0.1)
δ_p[ppm]	-2.8(0.2)	-2.3(0.2)	-3.1(0.2)
(RMS)	(6.46)	(2.58)	(6.58+4.77=11.4)

Simultaneous fitting of ion-pairing constant (K_p), and shifts of free (δ_f) and ion-paired (δ_p) sodium to the shift versus ρ (Fig. 25) and the shift versus concentration data (Fig. 27).

interaction as a simple bimolecular process. Again the linear variation of $1/T_1$ with ρ shows that the sodium - iodide interaction is symmetric about the cation, and thus does not affect the quadrupolar relaxation.

Can an ion-pairing model also account for shift and relaxation rates in the case of the more strongly coordinating sodium thiocyanate?

1.2.6.1 Sodium Thiocyanate - 2:1 Complex

The curvature of both sodium thiocyanate shifts (Fig. 24) and longitudinal relaxation rates (Fig. 26) with crown/sodium is striking. As before there is an excess of transverse over longitudinal relaxation rates (Fig. 26). Their difference, minus $1/T_2$inh, is plotted as $1/T_2$ex versus ρ in Fig.

26, and was attributed again to bimolecular exchange relaxation. Assuming the same equilibrium system as for sodium iodide (eqs. 57, 58, p.103), both the chemical shift (eq. 59) and the relaxation rate (eq. 60) can be expressed as the sum of the contributions from solvated, ion-paired, and 1:1 complexed sodium (see appendix 3):

$$1/T_1 obsd = P_f/T_1 f + P_p/T_1 p + P_c/T_1 c \qquad (60)$$

However, for sodium thiocyanate the ion-pairing model alone proves insufficient to explain the strong curvatures observed in both shift (Fig. 24) and longitudinal relaxation (Fig. 26). In Figs. 24 and 26, the broken lines represent the shift and $1/T_1$ values obtained by simultaneously fitting the ion-pairing model (eqs. 59, 60) to complexation and concentration data. Clearly, enhanced ion-pairing due to addition of the crown can not account for all of the observed curvature, as it does in the case of sodium iodide. Another effect must be present in the sodium thiocyanate complexation.[21] For both chemical shift (Fig. 24) and relaxation rate (Fig. 26), the residual curvature not accounted for by the ion-pairing model is symmetric around ρ equal to 0.5. This clearly shows the presence of an additional sodium species in solution, with a maximum concentration at ρ equal to 0.5.

[21] The case of sodium thiocyanate demonstrates the importance of fitting parameters simultaneously to the independent concentration and complexation data sets. It was possible to fit the complexation data alone with the ion-pairing model (Fig. 24), but the obtained ion-pairing constant and chemical shifts for solvated and ion-paired sodium were completely incompatible with the concentration data (Fig. 27 and 28). The simultaneous fitting of both data sets strongly reduced the covariance between different parameters.

1.2.6.2 2:1 Complex Formation - (Na^+SCN^-)-C-(Na^+SCN^-)

It is known that in the solid state DB24C8 easily forms 2:1 complexes with sodium o-nitrophenolate[69] and with potassium thiocyanate.[68] In nitromethane solution, the bimolecular exchange passes through a transition state with an intermediate 2:1 complex (see p. 56). We also know that, for the system sodium:18C6, coordinating anions (thiocyanate or iodide) stabilize this 2:1 intermediate and thus promote bimolecular cation interchange (see also Tab. 25).[51]

It is thus probable that the thiocyanate anion stabilizes the analogous sodium:DB24C8 intermediate enough to let it contribute to the observed chemical shifts and relaxation rates. In other words, the 2:1 intermediate present at the transition state reaches measurable concentration and life time. It is formed from the 1:1 complex and an additional sodium thiocyanate ion-pair:

$$(Na^+, SCN^-)_s + (Na^+, C)_s \underset{}{\overset{K_{C2}}{\rightleftharpoons}} (Na^+\text{-}C\text{-}Na^+, SCN^-)_s \qquad (61)$$

Its highest formation probability would be at P equal to 0.5: the product of the concentrations of uncomplexed and complexed sodium has a maximum at this point. Thus this 2:1 model is based on three equilibria:

$$(Na^+)_s + (SCN^-)_s \xrightleftharpoons{K_p} (Na^+, SCN^-)_s \qquad (62)$$

$$(Na^+)_s + (C)_s \xrightleftharpoons{K_c} (Na^+, C)_s \qquad (63)$$

$$(Na^+, C)_s + (Na^+)_s \xrightleftharpoons{K_{c2}} (Na^+\text{-}C\text{-}Na^+, SCN^-)_s \qquad (64)$$

$$\Downarrow + 2\ SCN^-$$

$$SCN^-\text{-}Na^+\text{-}C\text{-}Na^+\text{-}SCN^-$$

The observed shift and relaxation rates have now to be expressed as the sum of four contributions; solvated, ion-paired, 1:1 complexed and 2:1 complexed sodium:

$$\delta_{obsd} = P_f\delta_f + P_p\delta_p + P_c\delta_{1c} + P_{c2}\delta_{c2} \qquad (65a)$$

$$1/T_1 obsd = P_f 1/T_1 f + P_p 1/T_1 p + P_c 1/T_1 1c + P_{c2} 1/T_1 c2 \qquad (65b)$$

Eq. 62 again describes the bimolecular association of the quasi-free ions Na^+ and SCN^- to form the contact ion-pair $(Na^+,SCN^-)_s$. Eq. 63 describes the formation of the 1:1 complex NaC. In fact, Eq. 63 is a combination, as it represents formation of NaC from both the free and the ion-paired sodium:

$$K_c = K_{cf} + K_{cp}K_p[SCN] \qquad (66)$$

$$[NaC] = K_{cf}[Na][C] + K_{cp}K_p[SCN][Na][C] \qquad (67)$$

However, K_c can not be resolved into its components, since only a lower limit for K_c of about $10^5 M^{-1}$ is known.

Eq. 64 needs more consideration. It describes the formation of the 2:1 NaSCN : DB24C8 complex. The general structure of this complex is considered to be analogous to the 2:1 transition state for bimolecular cation exchange with sodium hexafluorophosphate, iodide, and tetraphenylborate. In addition, one or two SCN anions further chelate the sodium cations on their uncomplexed faces. The coordinated anions stabilize the 2:1 complex be reducing the cation-cation repulsion:

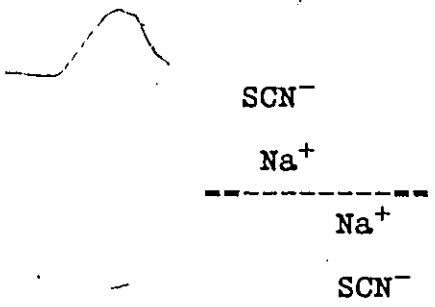

C2

This arrangement leaves each sodium bound to maximally four crown oxygens. The formation of the complex C_2 consists of the opening of the tight 1:1 complex, assisted by the second sodium cation, and the stabilization of the resulting 2:1 species by the thiocyanate counter anions:

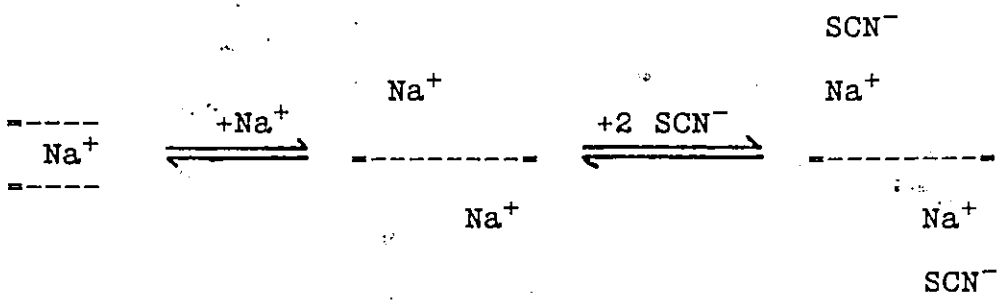

The 2:1 complex will actually be an equilibrium mixture of three species: Na^+-C-Na^+, Na^+SCN^--C-Na^+, and Na^+SCN^--C-Na^+SCN^-. Na^+-C-Na^+ can not be the dominant species, since in that case it would be formed for sodium hexafluorophosphate and sodium tetraphenylborate as

well. It is not possible though to identify either Na^+SCN^--C-Na^+ or Na^+SCN^--C-Na^+SCN^- as dominant species, since the same good fit to the experimental data is obtained assuming either to be predominant.[22]

Table 18 presents the iterated parameter values for simultaneous fitting of concentration (eq. 54, 55) and complexation data (eq. 65a,b). From this table all subcases give equally good fits to the experimental data. So their relative merit is left open to discussion. In the absence of crown, and at a salt concentration of 0.005 M, about 78% of all the sodium cations are ion-paired, as calculated from the ion-pairing constant (Tab. 15). Similarly, the sodium cations of the 2:1 complex will be largely ion-paired: they are less electrophilic due to their coordination to the crown, yet they experience an excess of 'naked' anions. So it is clear that the 2:1 complex is in fact an equilibrium mixture of different ion-paired species. Only for simplicity's sake is only one species considered in the fitting procedure.

The fitted curves presented in Figs. 24 and 26 are based on the assumption of Na^+SCN^--C-Na^+SCN^- as the dominant species. The solid curves in Figs. 24 and 26 are the result of simultaneously fitting eqs. 65a,b to the complexation data (Figs. 24 and 26), and eqs. 54, 55 to the concentration data (Fig. 27 and 28). Figure 30 shows populations of different sodium species, calculated according to the 2:1 model.

The concentration of the 2:1 complex is always very low compared to the concentrations of the other species.

22 Expressing the 2:1 complex C_2 as $[C_2] = K_{c2} \times [C_1] \times [Na] \times [SCN]$ assumes Na^+SCN^--C-Na^+ to be the predominant species;
using $[C_2] = K_{c2} \times [C_1] \times [Na] \times [SCN] \times [SCN]$ assumes Na^+SCN^--C-Na^+SCN^- to be dominant. Both expressions give the same good fit, inspite of their different dependencies upon the free anion concentration.

Table 18: NaSCN Shift - Simultaneous Parameter Fitting

Dominant 2:1-Species	K_p [M^{-1}]	δ_f [ppm]	δ_p [ppm]	K_{c2} [M^{-1}]	δ_{c2} [ppm]	RMS
Na^+ C Na^+	1046 (10)	-14.1 (0.05)	-9.3 (0.1)	108 (10)	-7.4 (0.2)	0.16
Na^+SCN^- C Na^+	1012 (11)	-14.1 (0.05)	-9.2 (0.1)	$3.4 \cdot 10^4$ ($2 \cdot 10^3$)	-7.2 (0.2)	0.16
Na^+SCN^- C Na^+SCN^-	1000 (10)	-14.1 (0.05)	-9.2 (0.1)	$2 \cdot 10^7$ (10^6)	-6.2 (0.2)	0.15

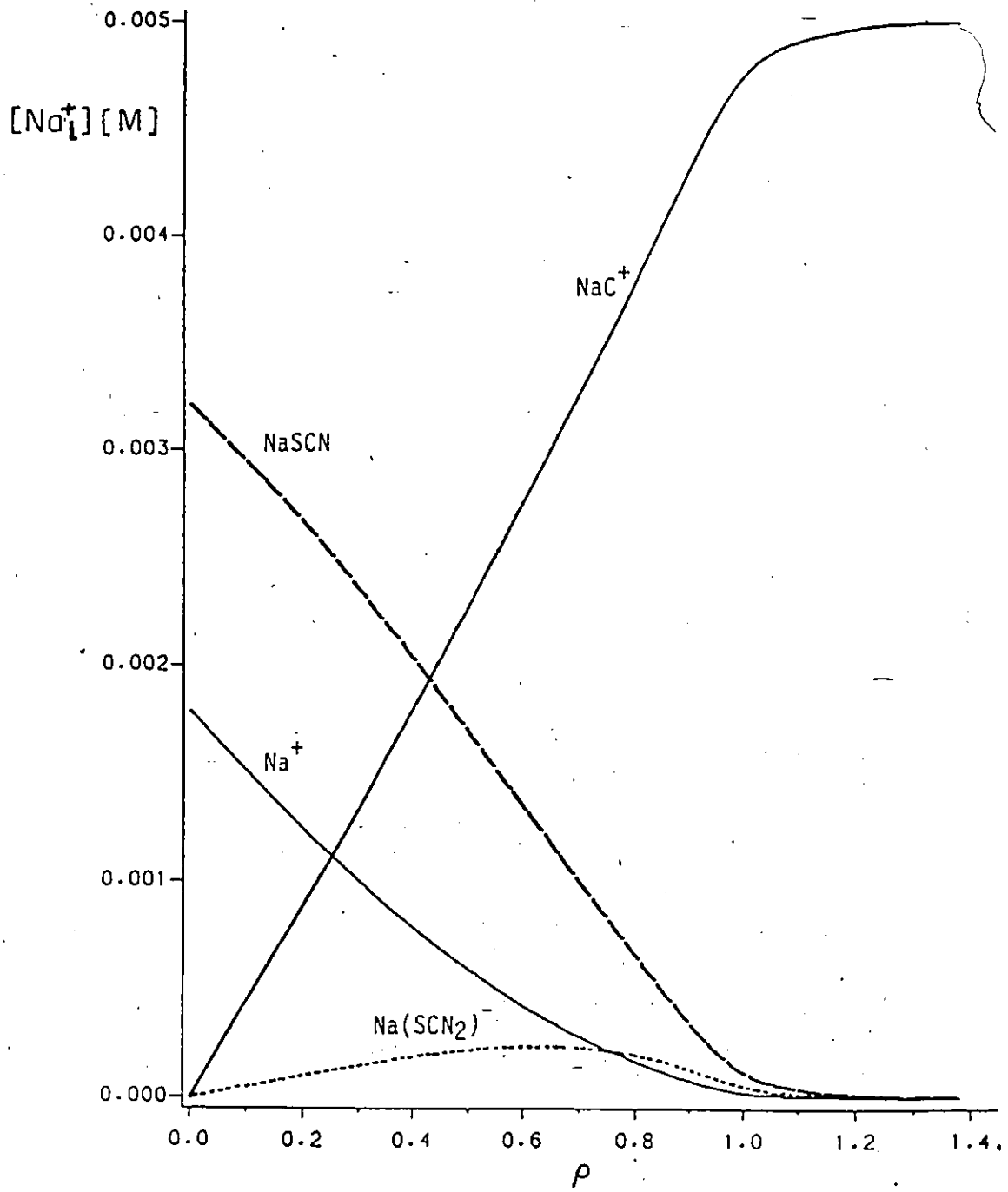

Figure 30: Populations of Different Species - NaSCN:DB24C8. The curves are calculated with the 2:1 Model, using eqs. 65a, b. [NaSCN] is 0.005 M.

1.2.6.3 Alternative Interpretation - Triple Ion Model

Though the 2:1 complex model is the most plausible one, and indeed accounts well for the experimental data, another possible explanation for the excess shift and relaxation rate had to be considered. It is based upon the selective formation of the triple-ion $Na^+(SCN^-)_2$ instead of the 2:1 complex. Chabanel et al.[86][89] have studied the ionic association of sodium thiocyanate in tetrahydrofuran solutions. They detected separate IR and Raman bands for the ion-pair Na^+SCN^-, the dimer of the ion-pair $(Na^+SCN^-)_2$, and the triple-cation $(Na^+)_2SCN^-$. And they suggested the following disproportionation equilibrium:[86]

$$(Na^+)_S + (SCN^-)_S \rightleftharpoons (Na^+, SCN^-)_S \qquad (68)$$

$$2\ (Na^+, SCN^-)_S \rightleftharpoons ((Na^+, SCN^-)_2)_S \qquad (69)$$

$$3\ (Na^+, SCN^-)_S \overset{K}{\rightleftharpoons} ((Na^+)_2, SCN^-)_S + ((Na^+, (SCN^-)_2)_S \qquad (70)$$

$$(K = 0.1\ M^{-1})$$

The ratio of ion-pair over triple-ion was always 30, independent of concentration.[86]

Bacelon et al. detected the triple-ion $Li^+(SCN^-)_2$ after addition of t-butylammonium thiocyanate to a solution of lithium thiocyanate in tetrahydrofuran.[175] Similarly, adding DB24C8 to a solution of sodium thiocyanate in nitromethane would produce an excess of free thiocyanate over uncomplexed sodium cations. These would be excellent conditions for an enhanced formation of the triple-ion $Na^+(SCN^-)_2$.

The maximum concentration of the triple ion would also be around P equal to 0.5, where the product of ion-pair and free anion concentrations has a maximum. Furthermore, its chemical shift and relaxation rate can be extrapolated from the corresponding values for the solvated and ion-paired sodium to be at higher frequency, and higher, respecticely, in comparison with the values of the Na^+SCN^- ion-pair. Thus this species could account for both the excess shift and relaxation rate in Figs. 24 and 26:

Table 19: Estimated Parameters for Triple-Ion $Na^+(SCN^-)_2$

	Na^+ free	Na^+SCN^- ion-pair	$Na^+(SCN^-)_2$ triple-ion (estimated)
Shift[ppm]	-14.1	-9.3	-4.3
$1/T_1[s^{-1}]$	31	400	400 - 800 (600)

The triple-ion equilibrium model considers free sodium, ion-paired sodium, and sodium bound in the triple-ions and the 1:1 complex:

$$(Na^+)_s + (SCN^-)_s \underset{}{\overset{K_p}{\rightleftharpoons}} (Na^+, SCN^-)_s \qquad (71)$$

$$(Na^+)_s + (C)_s \overset{K_c}{\rightleftharpoons} (Na^+, C)_s \qquad (72)$$

$$(Na^+, SCN^-)_s + (SCN^-)_s \overset{K_{tr}}{\rightleftharpoons} (Na^+, (SCN^-)_2)_s \qquad (73)$$

The chemical shift and the relaxation rates can again be expressed as the sum of the contributions from the four sodium species present:

$$Y_{obsd} = P_f Y_f + P_p Y_p + P_c Y_c + P_{tr} Y_{tr} \qquad (74)$$

This triple-ion model gives a fit identical to that of the 2:1 model, so that the solid line in Fig. 24 represents it as well. Table 20 shows the iterated parameters.[23] Only the chemical shifts have been fitted with the triple-ion model.

Table 20: Parameter Values for the Triple-Ion Model

Parameter	Value	RMS
$K_p[M^{-1}]$	1250 (10)	
δ_f[ppm]	-14.1 (0.1)	3.4 (conc. data)
δ_p[ppm]	-9.8 (0.25)	
$K_{tr}[M^{-1}]$	100 (50)	3.2 (comp. data)
δ_{tr}[ppm]	-3.9 (1.2)	

δ_f, δ_p, and δ_{tr} are the chemical shifts for free, paired, and triple sodium; K_p and K_{tr} the formation constant for the ion-pair and the triple-ion. Conc. data and comp. data refer to the concentration study and the complexation study, respectively. K_c was fixed at $10^6 M^{-1}$

23 These results represent the overlapping values obtained in separate fitting procedures for the concentration and the complexation data. Covariance between K_{tr} and δ_{tr} leads to large uncertainties for these two parameters, and a flat minimum of the residual mean square (RMS). Simultaneous fitting to both concentration and complexation data sets should not significantly improve the accuracy of the iterated parameters.

The explicit consideration of $Na^+(SCN^-)_2$ is a reasonable extension to the ion-pairing model, since it is the next higher and stoichiometrically favored ionic aggregate. It also proves sufficient to account for the experimental data. An experiment is thus called for to decide between the triple-ion model and the 2:1 complex model. This would involve adding cryptand to a solution of sodium thiocyanate in nitromethane, to remove cations from the ion-pairing equilibrium. In this case no 2:1 complexes could be formed between the sodium cations and the cryptand. If both the ion-pairing equilibrium (eq. 57, 58) and the ion-pairing parameters from the concentration study (Tab. 15) can account for the resulting changes in chemical shift and the relaxation rates of the uncomplexed sodium, then the triple-ion model is inconsistent. This would leave the 2:1 model as the only plausible model. Conversely, if the triple-ion model (eqs. 71 - 73) with its parameters (Tab. 20) is needed to fit the shift changes, then clearly the triple-ion model is supported by the data.[24,25]

1.2.6.4 Sodium-Anion Interactions

Figure 31 shows the chemical shift variation with concentration of all sodium salts used in nitromethane.

With decreasing concentration, the chemical shifts of all four salts converge towards one chemical shift value. The concentration dependency for the salts of the strongly coordinating anions thiocyanate and iodide can readily be explained with bimolecular contact interaction, leading to paramagnetic shift with increasing concentration. But for the two salts of bulky anions, sodium hexafluorophosphate and sodium tetraphenylborate, we observe a much smaller diamagnetic shift with increasing concentration. This suggests a weak ionic interaction, such as the formation

24 Alternatively, tetraalkylammonium thiocyanate could be added to a solution of sodium thiocyanate in nitromethane, in analogy to the experiment of Bacelon et al.,[175] and the obtained changes in shift and relaxation compared with the 2:1 complex and the triple-ion models.

25 Again either model is only be a simplistic representation of the real system. Certainly both 2:1 complex and triple-ions, as well as other sodium species, will be present at the same time. At this point the goal is to find the (if any) dominating chemical species.

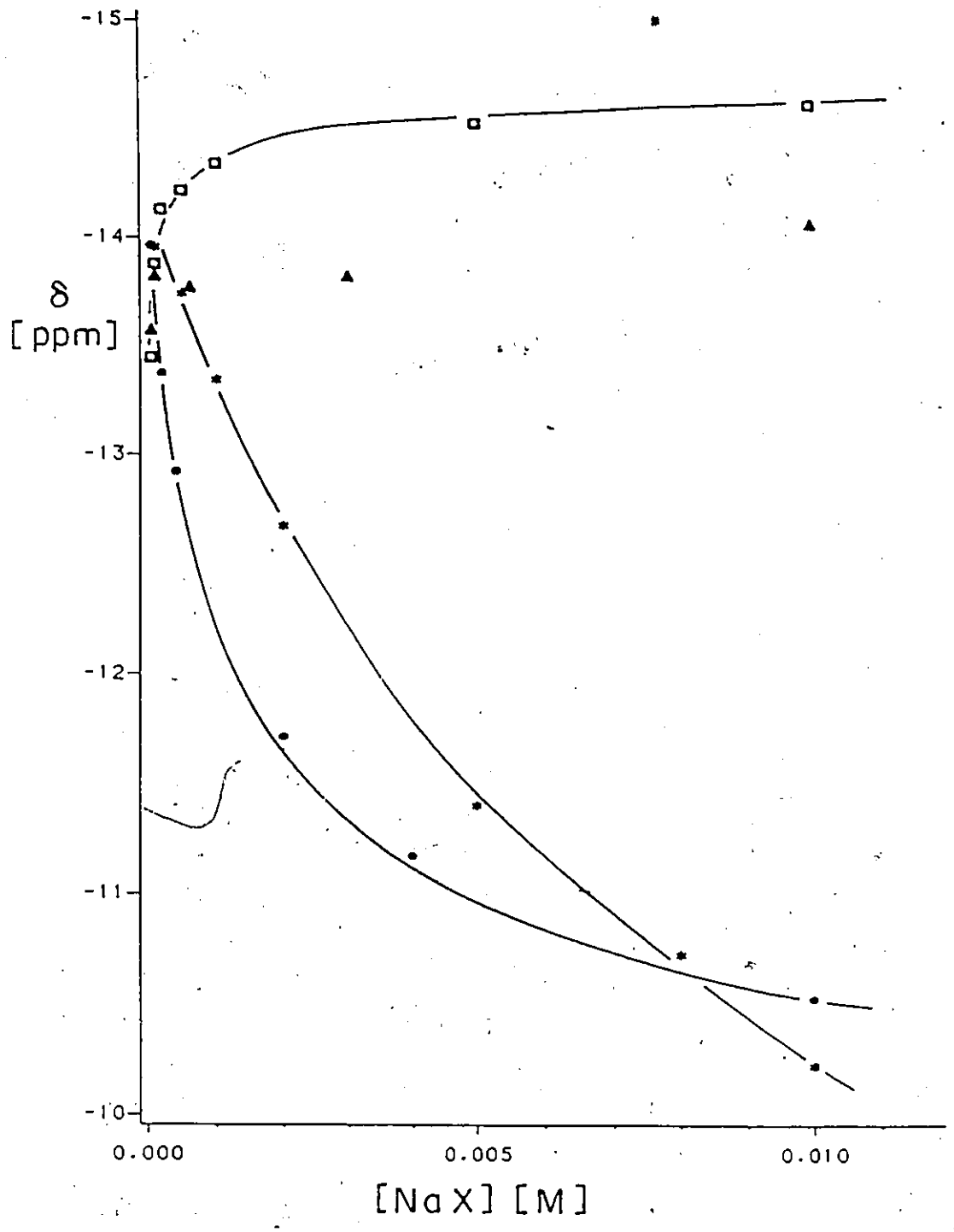

Figure 31: Concentration Dependence of Sodium-23 Chemical Shifts. The points are experimental for $NaBPh_4$ (Δ), $NaPF_6$ (□), NaI (*), and NaSCN (•) at 79.35 MHz in nitromethane in the absence of crown. The curves are calculated according to the ion-pairing model using eqs. 34 and 35.

of solvent separated dimers of ion-pairs. The structure of the ionic coordination shell is still far from being well understood.

The combination of chemical shift and relaxation studies of cations[18][24][64] and other nuclei[90][91] together with the high magnetic fields available, will certainly continue to contribute to our understanding of cation solvation.

1.2.7 Kinetics of Sodium Iodide and Thiocyanate

How does ion-pairing affect the cation exchange between solvated and complexed sites? The transverse relaxation rates for both sodium iodide and sodium thiocyanate are higher than the corresponding longitudinal relaxation rates (Figs. 25 and 26). The differences, less the relaxation due to inhomogeneity, $1/T_2$inh, is the exchange relaxation $1/T_2$ex between the solvated sodium pool (Fpool) and the 1:1 complex. The Fpool consists of free and ion-paired sodium in the case of sodium iodide, and of free, ion-paired and 2:1 complexed sodium in the case of sodium thiocyanate.

The 2:1 model for sodium thiocyanate is really a three-site exchange system, since the sodium cation relaxes in the 1:1 complexed, 2:1 complexed, and uncomplexed states. However the sodium bound in the 2:1 complex exchanges rapidly with the uncomplexed sodium, but not with the 1:1 complex. With this assumption the problem can be treated as exchange between two sites: (A), Fpool, standing for 'uncomplexed' sodium, including free, ion-paired and 2:1 complexed sodium; and (B) standing for the 1:1 complexed sodium. The reason for this is that the rate determining step in cation exchange with DB24C8 is the opening of the tight 1:1 complex, i.e. the rearrangement of the ligand back-bone. According to Truter this step has an activation energy of about 50 kJ/mol.[70][26]

[26] This two-site exchange analysis holds also for the triple-ion model. In that case, solvated,

In analogy to sodium hexafluorophosphate and tetraphenylborate, the exchange rate (k_a+k_b) can be obtained from the exchange contribution $1/T_2ex$ to the observed transverse relaxation rate $1/T_2obsd$, using Woessner's equation (eq. 75 is identical to eq. 8, p.15):

$$k_a+k_b = 4\pi^2 P_a P_b (\upsilon_b-\upsilon_a)^2 T_2ex \qquad (75)$$

where

$$1/T_2ex = 1/T_2obsd - 1/T_1 - 1/T_2inh \qquad (76)$$

Again υ_a and υ_b are the chemical shifts in Hertz, of site (a) (Fpool) and site (b) (1:1 complexed sodium). The shift of the 1:1 complex is 540 Hz, independant of the counter anion (Tab. 2). However, the crucial shift of site (a) depends upon ion-pairing and formation of the 2:1 complex. Its shift could be calculated either from the corresponding equilibrium equations (eqs. 62 - 64); or from the experimental shifts, assuming quantitative complexation, by substracting the chemical shift contribution of the 1:1 complex.

$$\delta_a = 2(\delta_{obsd}-\delta_c) + \delta_c \qquad (77)$$

For $P = 0.5$

Furthermore a concentration study was done for both anions, in order to confirm the bimolecular mechanism of the exchange. Tables 21 and 22 show the results for the sodium iodide case, tabs. 23 and 24 for the sodium thiocyanate case. The bimolecular exchange rates for all four sodium salts are shown in Tab. 25.

Whereas for sodium iodide the exchange rate is only marginally higher than for the two bulky anions tetraphenylborate and hexafluorophosphate, it is about four times higher (see Tab. 25) for the strongly coordinating thiocyanate. This agrees with the solid state findings that coordinating

ion-paired and triple-ion sodium are in fast diffusion controlled equilibrium with each other, and together make up the uncomplexed exchange-site Fpool.

Table 21: NaI Kinetics - Complexation Study

ρ	δ (Fpool) [ppm]	$1/T_2ex$ [s^{-1}]	(k_a+k_b) [s^{-1}]	k_2 ($\times 10^5$) [$M^{-1}s^{-1}$]
0.0	-10.32	-	-	-
0.3	-10.01	30	6000	6.0
0.4	-9.90	45	4100	4.1
0.5	-9.79	43	3900	3.9
0.7	-9.56	36	2900	2.9
0.8	-9.44	27	2500	2.5

δ_{Fpool} is the weighted average of the shifts of the uncomplexed sodium species. (k_a+k_b) are the exchange rates; k_2 the rates of bimolecular cation interchange: $k_2 = (k_a+k_b)/[Na]_t$. $[Na]_t = 0.01$ M.

counter anions promote the formation of 2:1 stoichiometries for sodium[69] and potassium complexes of DB24C8.[68] In nitromethane solution, contact ion-pairing of the sodium will stabilize the intermediate 2:1 complex and so increase the exchange rate. Indeed, this anion-stabilized 2:1 species has now a life time long enough to contribute to the relaxation and chemical shifts of the sodium cations. Thus the exchange analysis supports the 2:1 complex model discussed above.

Table 22: NaI Kinetics - Concentration Study at Rho = 0.5

Conc. [M]	Shift (obs) [ppm]	$1/T_2$ (obs) $[s^{-1}]$	$1/T_1$ $[s^{-1}]$	$1/T_2ex$ $[s^{-1}]$	Shift (Fpool) [ppm]	(k_a+k_b) $[s^{-1}]$	k_2 (x10^{-5}) $[s^{-1}M^{-1}]$
0.01	-8.97	166	113	43	-9.79	3900	3.9
0.005	-9.67	302	111	181	-11.18	3100	6.2
0.004	-9.95	462	109	343	-11.71	2300	5.8
0.002	-8.53 -12.20	(below coalescence)				800	4.0

The spectra above coalescence ($[Na]_t$ >= 0.004 M) were analysed with eq. 75, the spectra below ($[Na]_t$ <= 0.005 M) were analyzed using the full line-shape expression (see appendix 6).[19]

Table 23: NaSCN Kinetics - Complexation Study

ρ	Shift obs [ppm]	Shift Fpool [ppm]	$1/T_{2ex}$ [s^{-1}]	(k_a+k_b) [s^{-1}]	k_2 ($\times 10_6$) [$M^{-1}s^{-1}$]
0.0	-10.84	-10.84	-	-	-
0.1	-10.40	-10.66	22	6600	1.3
0.2	-9.99	-10.47	37	6000	1.2
0.3	-9.72	-10.40	32.5	8400	1.7
0.4	-9.29	-10.07	27.5	8300	1.7
0.5	-9.02	-9.93	27.5	7400	1.4
0.6	-8.78	-9.78	21	7900	1.6
0.7	-8.53	-9.50	11	9100	1.8
0.8	-8.39	-9.52	10	7800	1.6
0.9	-8.24	-6.0	2	(18000)	(3.6)
1.0	-8.12	-	-	-	-
			Average =	7700	1.5

The parameters are defined as in Tab. 21, $[Na]_t$ = 0.005 M.

Table 24: NaSCN Kinetics - Concentration Study at Rho = 0.5

Conc [M]	Shift obsd [ppm]	$1/T_2$ obsd [s^{-1}]	$1/T_1$ obsd [s^{-1}]	Shift Fpool [ppm]	$1/T_1$ Fpool [s^{-1}]	k_a+k_b [s^{-1}]	k_a (10^8) [$s^{-1}M^{-1}$]
0.01	-8.78	377	-	-9.39	-	-	-
0.005	-9.02	324	286	-9.87	383	6300	1.26
0.002	-9.65	459	(236)	-11.10	283	2500	1.25
0.0004	-8.27	324	-			450	1.13
	-12.83	280	-	-12.83	138		
0.0002	-8.86	280	-			200	1.0
	-13.95	201	-	-14.6	94		
					Average =		1.1
0.00004	-8.67	100	No reliable line fitting possible due to low S/N				
	-14.5	40					

All spectra were analysed with the full line shape expression, and the spectra above coalescence were additionally checked with eq. 75, with identical results.

Table-25: Bimolecular Exchange Rates - Overview

Salt	k_2 [$x10_5$ $M^{-1}s^{-1}$]	$dG^{\#}$ [kJ/mol]
$NaBPh_4$	2.8 (0.2)	41.9 (2)
$NaPF_6$	3.5 (0.2)	41.4 (2)
NaI	4.5 (1)	40.7 (5)
NaSCN	13.0 (2)	38.5 (3)

Bimolecular exchange rates for all four sodium salts with DB24C8 in nitromethane.

1.2.7.1 Temperature Study of Sodium Iodide Complexation

The temperature dependence of the bimolecular sodium iodide exchange was measured in order to obtain the activation parameters.[27] The temperature ranged from 4.6°C to 41°C. At the higher temperatures the observable parameter, the exchange broadening $1/T_2ex$ diminishes, and becomes comparable to the error of measurement at 41°C. It was therefor not possible to extract reliable values for the entropy and enthalpy of activation for sodium iodide exchange with DB24C8. The free energy of activation in all measurements is constant within error limits: $dG^{\#}$ = 40kJ/mol.

27 Again Woessner's equation (eq. 75) was used, and the chemical shift of the uncomplexed site obtained by subtracting the shift contribution due to the 1:1 complex from the observed shifts at each temperature (eq. 77).

1.3 Conclusion

Clearly, nuclear magnetic resonance of the cation is a most powerful analytical tool for studying cation complexation. In this study, sodium-23 chemical shifts, longitudinal and transverse relaxation rates together gave a detailed picture of the competition of anions, solvent and crown ether for the coordination shell of the sodium cation. Indeed for the first time the effects of counter anions on the complexation process have been quantitatively accounted for. They include aggregation, ion-pairing and rapid decomplexation.

There are two aspects to the sodium : DB24C8 complexation system:
First, sodium-23 NMR provides a comprehensive picture of the complexation processes. At the same time the diversity of the complexation system provides a showcase for the analytical power of quadrupolar cation NMR.

Second, one can look at the complexation system itself from two perspectives: DB24C8 is a model for natural ionophores such as valinomycin, and mimics much of their behavior: it wraps itself around the cation, and has a balance of binding strength and flexibility that leads to analogous ionophore-properties. Alternatively, one can consider DB24C8 as an array of eight oxygen donor atoms, cooperatively converging on a central cavity. The crown ether brings about a situation with only two sodium environments: one solvated in solution and the other complexed within the ethereal cavity. This perspective forms a useful basis from which to study coordinate bonds between the sodium cation and counter anion, solvent and ligand.

Chapter II

SYNTHESIS OF AMINOACID BEARING CROWN ETHERS

2.1 Introduction

Soon after the initial reports of crown ether synthesis, the basic crown rings were fitted with sidechains to increase their cation selectivity and binding strengths. Cram,[92] Lehn,[93] and others[94][95] achieved chiral recognition of organic ammonium cations via steric or electrostatic interaction with custom-tailored sidechains (binaphtyls,[92] and tartramides.[96][97]) Gokel and others are developing the concept of sidechains bearing neutral donor groups. They coined the name 'Lariat Ether' to suggest the analogy of these sidechains to a lasso, 'roping in' the cation.[98][99][100]

Crown ethers often resemble natural ionophores such as valinomycin and monensin. This resemblance sparked research on crown ethers derived from biomolecules.[101] In 1983, Berthet and Sonveaux synthesized crowned L-dopa.[102] In that same year Haines et al. tested the biological activity of crown ethers incorporating a sugar group.[103] Vögtle and Jansen (1976)[104] and Fenton et al. (1981)[105] synthesized crown ethers based upon the neurotransmitters dopamine and L-adrenaline ((4a), (13), Fig. 32).

These 'Bio-crowns' will probably not be useful in medicine for some time since their biological activity is not specific enough.[101][103][106] However, much research is directed at understanding the relation between crown structure and cation binding properties.

A crown ether's selectivity and efficiency in carrying cations across hydrophobic membranes can tell us much about its complexation behavior. Moreover, functional pendants such as amines are pH sensitive and thus allow pH regulation of the cation transport properties.

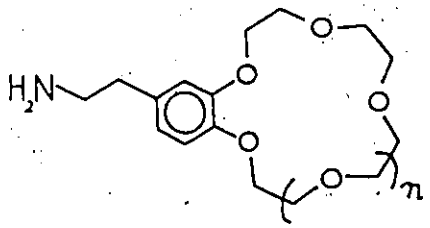

dopamine-15-c-5/18-c-6
(4a) n=1
(4b) n=2

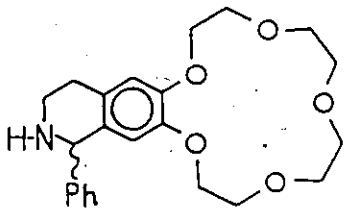

tetrahydroisoquinoline-15-c-5
(10)

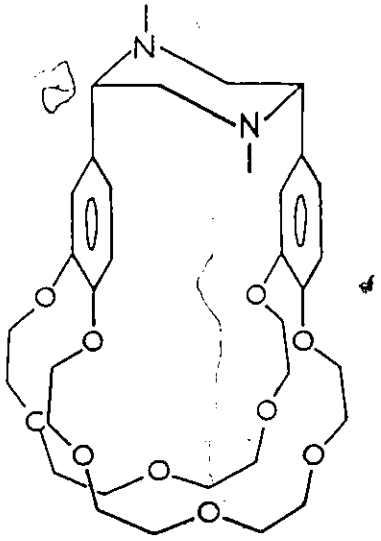

adrenaline-30-crown-10
(14)

Figure 32: Dopamine and Adrenaline derived Crown Ethers

We considered that aminoacid residues would make interesting sidechains because of their ionisability, as well as due to their biochemical nature. For the starting material the catechol function of dopamine was bridged with a tetra- or penta-ethyleneglycol group[104] to obtain the basic dopamine-15-crown-5[107] and dopamine-18-crown-6 structures (Fig. 32, (4a,b)). To their aminoethyl sidechain glycyl, L-alanyl, and L-lysyl groups were then coupled.

On a sideline, benzaldehyde was used to try to protect the dopamine as a Schiff base prior to cyclization. However, the initially formed Schiff-base was not stable under the reaction conditions; it immediately isomerized to a tetrahydroisoquinoline[108], which could easily be cyclized to its corresponding 15-crown-5 derivative (10) (Figs. 32 and 37).

The reaction of L-adrenaline with bis-chloro-tetraethyleneglycol in butanol did not give the expected L-adrenaline-15-crown-5 (12), as found by Vögtle,[104] but rather the dehydrated dimer piperazino-30-crown-10 (14) seen in Fig. 38, p. 140. Sodium-23 NMR played a role in the determination of its structure.

After the description of the synthesis of compounds (3) to (11) in this chapter, some cation transport properties of the compounds (3a), (5b), (5c), (6c) and (10) will be reported in the last chapter.

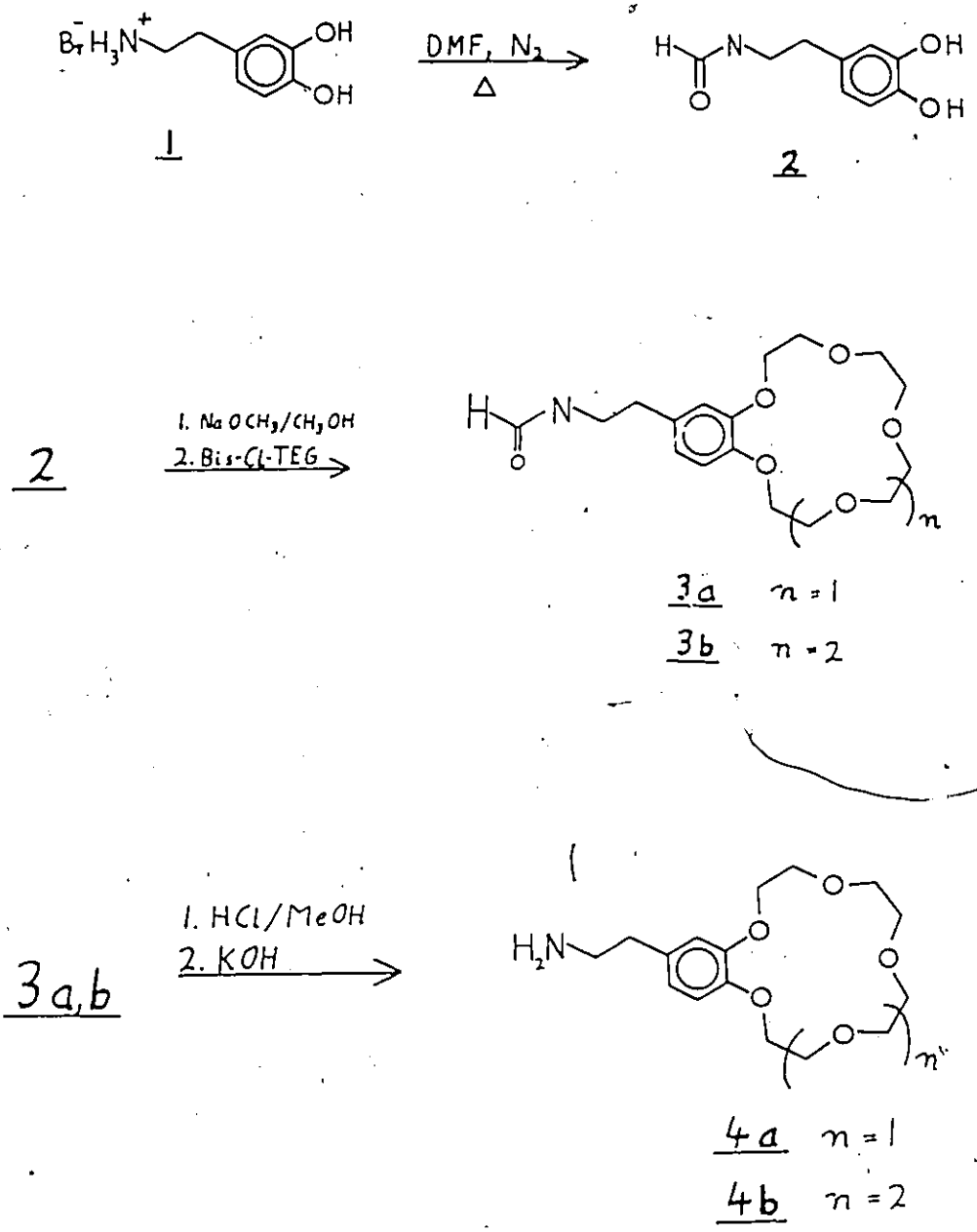

Figure 33: Synthetic Scheme for the Dopamine derived Crown Ethers

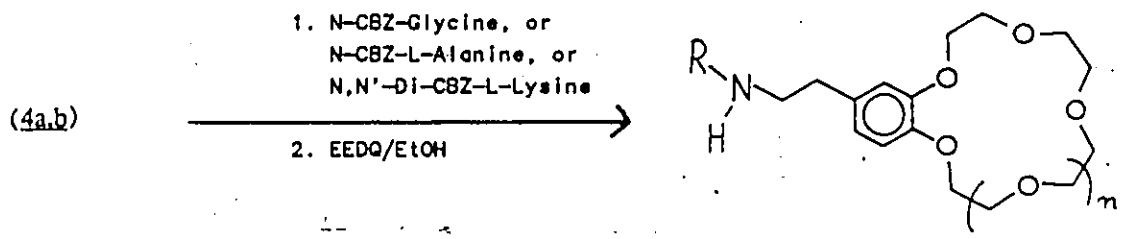

(5a): R = glycine; n = 1
(5b): R = L-alanine; n = 1
(5c): R = L-lysine; n = 1
(5d): R = L-lysine; n = 2

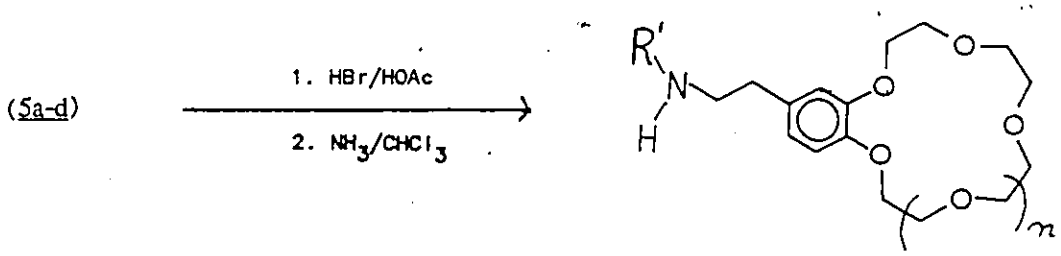

(6a): R' = glycine; n = 1
(6b): R' = L-alanine; n = 1
(6c): R' = L-lysine; n = 1
(6d): R' = L-lysine; n = 2

Figure 34: Synthetic Scheme for Amino Acid Coupling

2.2 Peptide Derivatives of Dopamine-15-crown-5 and Dopamine-18-crown-6

In 1976, Vögtle reported the synthesis of dopamine-15-crown-5 (4a) and adrenaline-15-crown-5 (12) from the corresponding catecholamines and 1,13-bischloro-4,7,10-trioxapentadecane (bis-chloro-pentaethyleneglycol), without however describing the experimental conditions such as solvent, base, and temperature. As well he isolated trace amounts of the dimer bis-adrenaline-30-crown-10 (13) (Fig. 38).[104]

Initial attempts to repeat Vögtle's synthesis of dopamine-15-crown-5 (4a) failed; using n-butanol as a solvent, much C-alkylation and N-alkylation resulted, whereas the dopamine dianion was insoluble in nonpolar solvents such as tetrahydrofuran or dimethoxyethane.

The dipolar aprotic solvent dimethylformamide turned out to be an excellent solvent: besides promoting O-alkylation over C-alkylation it conveniently protects the primary amine of dopamine (1) by transamination.[178] The crown ring can then be cleanly formed via double nucleophilic substitution on bis-chloro-tetraethyleneglycol to give the dopamide-crowns (3a), (3b) in up to 40% yield (Fig. 33).[28] After hydrolyzing to the amines (4a) and (4b), the free amino group was coupled to N-benzyloxycarbonylated glycine, L-alanine and L-lysine, using the coupling reagent N-ethoxy-carbonyl-2-ethoxy-1,2-dihydroquinoline (EEDQ).[110] The free amines (6a-d) were obtained after deprotecting with hydrobromic acid in glacial acetic acid (Fig. 34).[107]

To check the optical purity of the compounds (6b), (6c), and (6d), the L-lysine-15-crown-5 in $CDCl_3$ was treated with up to 0.3 equivalents of the chiral shift reagent $Pr(hfc)_3$. The methyne C-13 peak remained a sharp singlet, which suggests the presence of only one optical isomer, the one corresponding to the L-aminoacid.[111][29]

28 The base sodium methoxide also acts as a template to promote the crown cyclization.[109]

29 In addition, L-ala-15-crown-5 (6b) and L-lysyl-15-crown-5 (6c) were heated with potassium-t-butoxylate in t-butanol to 50°C for 4 hours. The optical rotation of the compounds were unchanged after that time. However, this is hardly surprising, since the most acidic proton in each compound is the amide proton. Its abstraction by the base would effectively inhibit racemization.

Since the synthetic procedure for the L-lysine-18-crown-6 derivative (6d) is the same as for it's 15-crown-5 analogue (6c), (6d) is considered to also be optically pure.

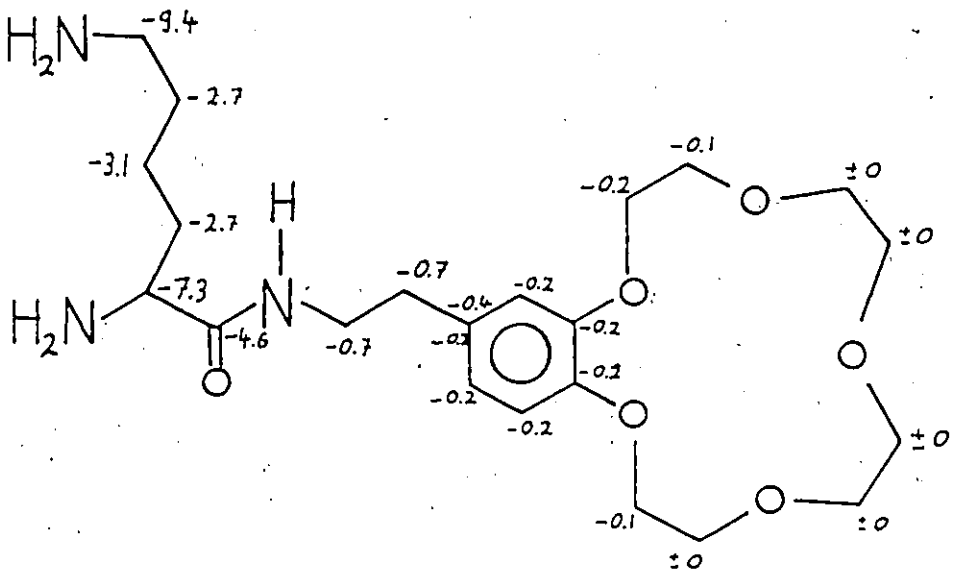

Figure 35: Effect of $Pr(hfc)_3$ on C-13 NMR Shifts of (6c). Change in ppm of the C-13 chemical shifts of (6c) (100 mg/2 ml $CDCl_3$) upon addition of $Pr(hfc)_3$ (160 mg/2 ml; 30 mol%). See Tab. 33 for the chemical shifts in absence of shift reagent.

2.2.1 Self-Association of L-lysine-15-crown-5 and L-lysine-18-crown-6

Consider a peculiarity of L-lysine-15-crown-5 (6c) and L-lysine-18-crown-6 (6d):

Dilute solutions of L-lysine-15-crown-5 in $CDCl_3$ show a sharp Gel-Point, that is they change from liquid state to gel state at a specific temperature (about 27°C for a 5 mmolar solution). This is probably caused by intermolecular complexation of the (protonated) α and especially ε-amines with the crown-ring of another molecule.[112] Thus it is possible to form linear and branched aggregates.

The H-1 NMR of (6c) show a sharp transition from the normal high resolution spectra at a temperature above the gel point, to the spectra below the gel-point, in which all compound signals are severely broadened, and only the TMS reference gives a sharp signal (Fig. 36). One would expect L-lysine-18-crown-6 (6d) to show an even stronger tendency to self-associate, since the 18-crown-6 ring complexes a primary ammonium cation several orders of magnitude stronger than the 15-crown-5 ring.[112][113][114] In fact, the high resolution proton and carbon-13 spectra of (6d) in $CDCl_3$ are already severely broadened at low concentrations. Once again this indicates extensive self-association.

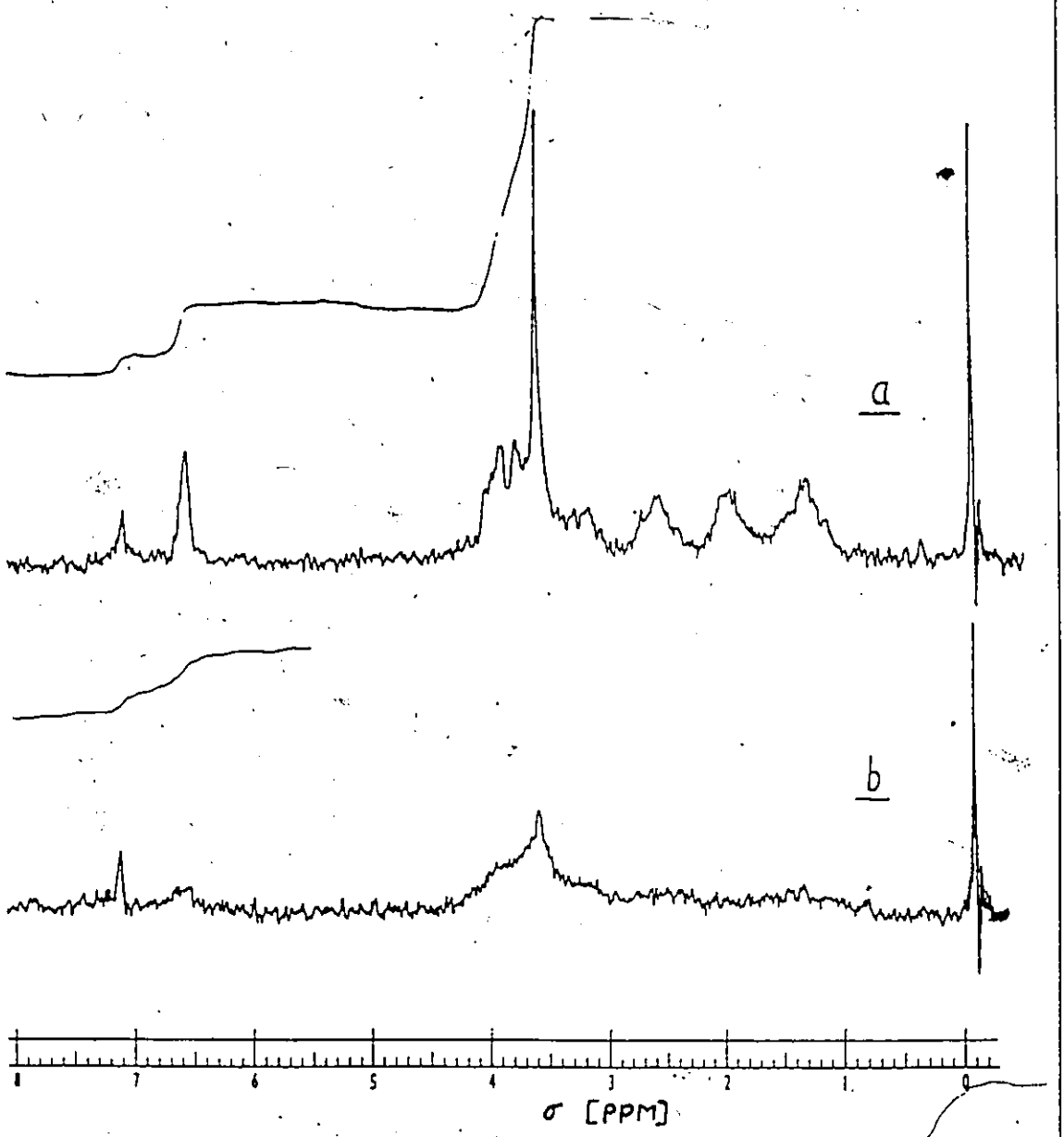

Figure 36: H-1 NMR Spectra of (6c) : Gel-Point. The 60 MHz proton spectra of (6c) are shown at about 35°C (a) and at 20°C (b).

2.3 Tetrahydroisoquinoline Derivatives

We used benzaldehyde in order to protect the dopamine nitrogen as a Schiff base, prior to forming the crown ring (Fig. 37). The Schiff base (8) that formed initially, however, was not stable under the reaction conditions, and immediately cyclized to the tetrahydroisoquinoline (9a). This is known as the Pictet-Spengler reaction.[108][116] Although the solution was neutral or at most slightly acidic, none of the isomer (9b) was formed (Fig. 37).[108][30][115]

The resulting diol (9a) could easily by cyclized with bis-chloro-tetraethyleneglycol and sodium methoxide in dimethylformamide. This gave the crowned tetrahydroisoquinoline (10) in 40% yield (Fig. 37). The secondary amine reacted neither with the dimethylformamide nor with the bis-chloro-glycol.

Tetrahydroisoquinolines have been suggested to be an important intermediate in the metabolism of ethanol by humans.[108] They would be formed by a Pictet-Spengler reaction from catecholamines and acetaldehyde, the primary metabolic product of ethanol.

30 Schiff bases can themselves coordinate to heavy metal cations, or can easily be hydrogenated to the amines. Thus it would be easy to build a second cation binding group onto the side-chain, with preferential binding of a paramagnetic cation.

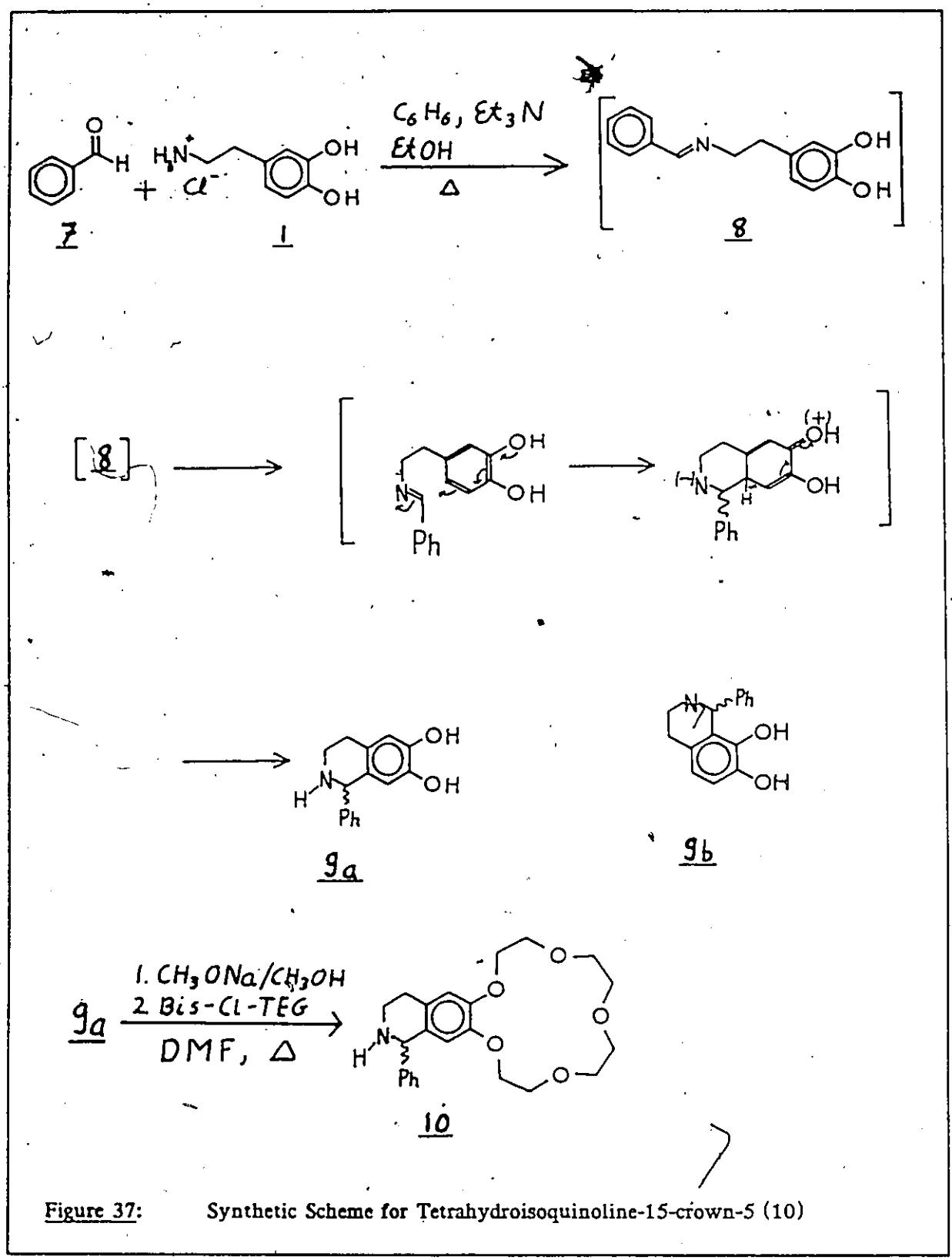

Figure 37: Synthetic Scheme for Tetrahydroisoquinoline-15-crown-5 (10)

Table 26: Crown Ethers derived from Dopamine and L-Adrenaline

Prod. #	Yield [%]	m.p.[°C] (solvent)	Molecular Formula	M.S.(M+) [m/e]	$[\alpha]_D$ (0.1 M/$CHCl_3$)
(3a)	40	130-131 (eth.acet)	$C_{17}H_{25}NO_6$	339	-
(3b)	35	(a) (acetone/dry ice)	$C_{19}H_{29}NO_7$		-
(4a)	38	74-75 (cyclohex.)	$C_{16}H_{25}NO_5$	311	-
(4b)	30	80-82 (cyclohex./hexane)	$C_{18}H_{29}NO_6$		-
(5a)	91	128-129 (eth.acet.)	$C_{26}H_{34}N_2O_8$	502	-
(5b)	86	138-139 (eth.acet.)	$C_{27}H_{36}N_2O_8$	517	-10.4
(5c)	60	164-165 (eth.acet.)	$C_{38}H_{49}N_3O_{10}$	708	-8.2
(5d)	60	119-123 (acetone)	$C_{40}H_{53}N_3O_{11}$		-7.4
(6a)	87	79-81 (diethyl eth.)	$C_{18}H_{28}N_2O_6$	368	-
(6b)	82	99-100 (diethyl eth.)	$C_{19}H_{30}N_2O_6$	382	+3.1
(6c)	56	oil	$C_{22}H_{37}N_3O_6$	439	-5.2
(6d)	90	71-75(a) (cyclohex.)	$C_{24}H_{41}N_3O_7$		-10.3
(9)	80	180-185 (methanol)	$C_{15}H_{15}NO_2$		-
(10)	40	107-108	$C_{23}H_{29}NO_5$		-
(14)	5	184-190 (diethyl eth.)	$C_{34}H_{50}N_2O_{10}$	646	-2.0

a) These compounds show strong intermolecular complexation between their primary amino group and the 18-crown-6 ring, hence their melting points are difficult to measure reliably.

2.4 Adrenaline Derived Piperazine-Crown

In 1976 Vögtle reported the synthesis of two crown ethers derived from adrenaline: the monomer adrenaline-15-crown-5 (12) in unspecified yield; and traces of a white crystalline powder with NMR data similar to those of the monomer (12), and with a molecular mass of 646. Vögtle suggested that the compounds structure was dimeric (13), and that the mass was lower than expected because two water molecules were lost during the mass spectroscopic measurement (Fig. 38). In 1981 Fenton described a seven-step synthesis of adrenaline-15-crown-5 (12) starting from acetovanillone.[105]

In trying to use Vögtle's direct route to L-adrenaline-15-crown-5 (12), I reacted L-adrenaline (11) with sodium methoxide and 1,13-bis-chloro-tetraethyleneglycol in n-butanol and followed the same work-up as for the dopamide-crowns, including separation on a neutral alumina column, but was unable to isolate the monomer (12). Probably this is due to its strong absorption on the polar alumina column, as well as to sidechain and C-alkylation of adrenaline.[31]

Column elution with diethyl ether gave a white crystalline powder.[32] This compound shows a molecular mass of 646 as did the dimer studied by Vögtle. Yet its H-1 and C-13 NMR data are in contrast with those published by Vögtle and Fenton for the adrenaline-15-crown-5 monomer (12) (Tabs. 27 and 28). Thus it cannot be the dimer (13) either.

Using H-1, C-13, and Na-23 NMR, we were able to identify the isolated product as the piperazino-30-crown-10 (14) (Figure 38).

31 Different solvents, such as dimethylformamide, as well as different work-up techniques were of no avail. The monomer (12) should be accessible, however, after protection of the sidechain hydroxyl and amine.

32 Compound (14) can readily be eluted with diethyl ether, so probably the molecular exterior is nonpolar. In contrast, the secondary amino crown (10) and the amidocrowns (3a), (3b) cannot be moved on a neutral alumina column with diethyl ether or ethylacetate; they must be desorbed with methanol.

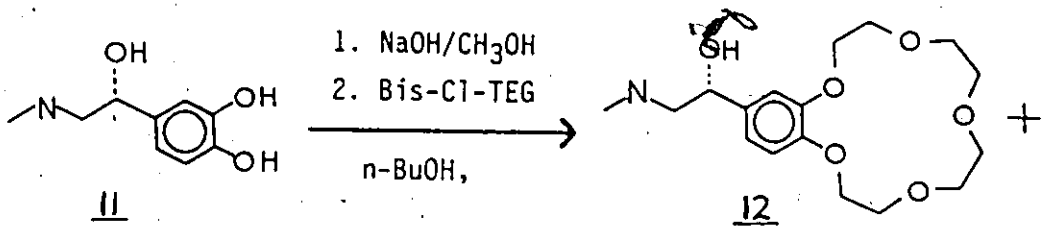

11 12

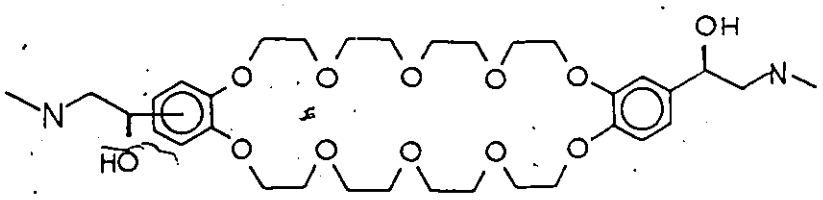

13

13 $\xrightarrow[(-2H_2O)]{Al_2O_3}$

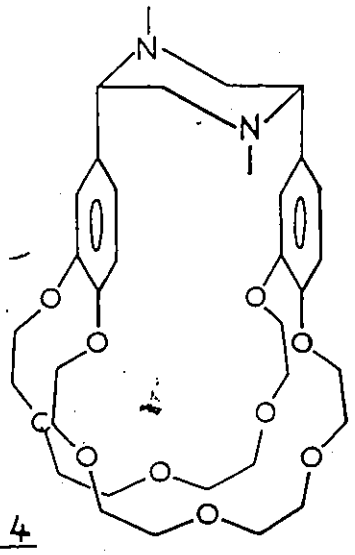

14

Figure 38: Synthetic Scheme for Piperazino-30-crown-10 (14)

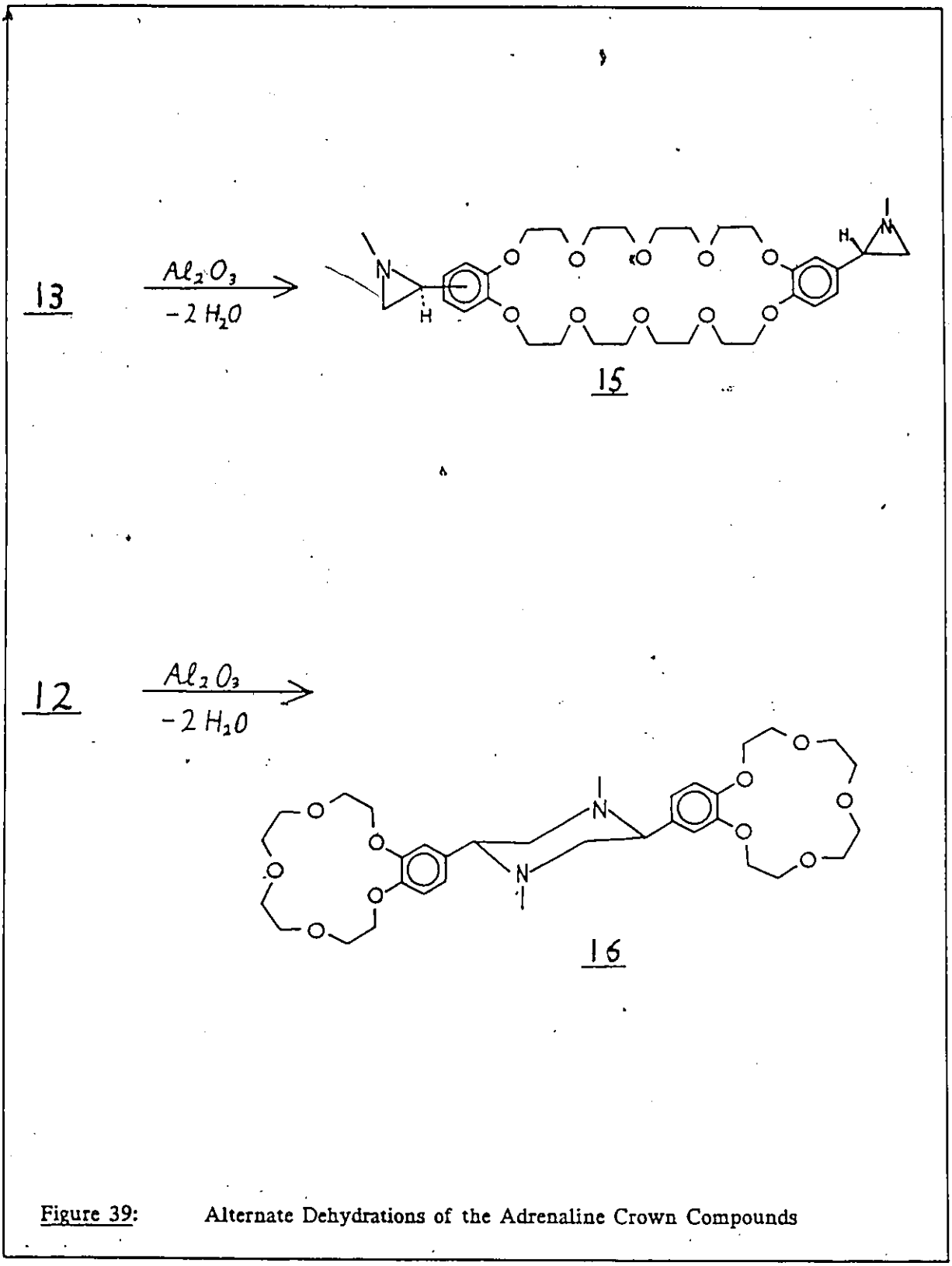

Figure 39: Alternate Dehydrations of the Adrenaline Crown Compounds

Table 27: Proton NMR shifts for Adrenaline Crown Ethers 12, 13, and 14.

#	aromat	CHOH	ether	NCH_2	NCH_3
(12)	6.9 6.82 (m3)	4.68 t1, ^{3}J6	4.1 3.9 3.72 m4 m4 s8	2.67 d2, ^{3}J6	2.38 s3
(Fenton([105])					
(12),(13)	-	4.70 t1, ^{3}J6.5	3.8 (average)	2.70 d2, ^{3}J6.5	2.35 s3
(Vogtle[104])	-				
(14)	6.92 6.82 (m3)	-	4.14 3.9 3.78 m4 m4 m8	3.14 2.92 d1,d1	2.05 s3
(this work)		-			

N-Methyl-styreneimine for comparison:
(Ohtsuru[117])

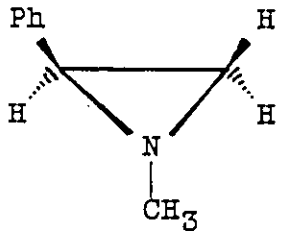

NCH_2	NCH_3	CHPh
1.67 dd1	2.38 s3	2.1 dd1
1.45 dd1		

The alfanumeric codes s, d, dd, t, and m stand for singlet, doublet, doublet of doublet, triplet and multiplet; the associated numbers indicate the number of protons causing the signal.

Table 28: Carbon-13 NMR Shifts of Adrenaline derived Crowns (12) and (14)

(14) ($CDCl_3$, [ppm], 50 MHz):

CH-Ph	CH_2-N	CH_3-N	arom.	ether
-	64.28	43.22	113.1	69.1
			113.9	69.2
			120.8	69.8
			134.5	70.8
			148.6	71.3
			149.4	

(12) (Vögtle [104])
$CDCl_3$, [PPM], 22.5 MHz):

n.r.	59.30	36.02		

The tertiary CH-Ph carbon is masked by the $CDCl_3$ solvent peaks. It could however be measured in C_6D_6 solution.

(14) in C_6D_6
([ppm], 50 MHz):

77.49	64.26	41.84	113.5	69.3
			114.2	69.6
			120.8	70.1
				71.4
			149.4	72.0
			150.3	

2.4.1 Structural Assignment for the Adrenaline Crown (14)

The original sidechain of the L-adrenaline may take on either of the three following structures during the reaction :

1. UNCHANGED ADRENALINE SIDECHAIN (13)

   However, for compound (14), neither the proton NMR data nor the carbon-13 NMR data agree with those reported by Fenton and Vögtle for the intact adrenaline sidechain as in (12) (Tabs. 27 and 28),[104][105] so that this possible structure can be rejected.

2. DOUBLE DEHYDRATION (14), (15), OR (16)

   One ethanolamine group, such as the adrenaline sidechain, can dehydrate to form one aziridine (15) or two such groups can form one piperazine group: (14) or (16). These reactions can be catalyzed either by base (as during the reaction) or by the alumina during the column work-up.[33]

   Considering the proton spectra of (14) (Tab. 27), the aziridine structure (15) can be discounted. But both piperazine structures (14) and (16) agree with the proton NMR data (Tab. 27).[34] Furthermore, the C-13 values for (14) agree well with values calculated for 1,4-dimethyl-2,5-diphenyl-piperazine using two C-13 increment systems:[119]

[33] It is well known that alumina can catalyze nucleophilic substitution reactions. In fact, this feature is finding more and more applications in synthetic chemistry.[118]

[34] The low-field proton triplet around σ = 3.05 ppm corresponds to the two CH_2 protons. They are coupled (^3J=6Hz) to the single proton of CHR_3 (σ = 2.3 ppm) and to each other (^2J=12Hz). At 200 Mhz, these two CH_2 protons appear as two doublets; their roof effect indicates coupling to the right hand triplet (CHR3).[117] At 60 MHz, the two CH_2 doublets have moved closer together and resemble a triplet.

A. Calculation from 1,4-dimethylpiperazine:

	1,4-dimethyl-piperazine [ppm]	increments [ppm]	calculated shifts [ppm]	observed shifts [ppm]
CH	- CH_2 - 55.5	+22.1 (+α-Ph)	77.6	77-78
CH_2	55.5	+9.3 (+β-Ph)	64.8	64.2
CH_3	47.5	-2.6 (+γ-Ph)	44.9	43.1

In the above calculation the proper shift increments for a phenyl group in α,β or γ position have been added to the C-13 shifts of the model compound 1,4-dimethyl-piperazine. The steric shift effects of introducing the phenyl group into a ring rather than a linear aliphatic chain have been neglected.

B. Calculation from 1,2,4-trimethyl-piperazine:

	1,2,4-trimethyl-piperazine [ppm]	increments [ppm]		calculated shifts [ppm]	observed shifts [ppm]
CH	62.5	-9.1 (-α-CH_3)	+22.1 (+α-Ph)	75.5	77-78
CH_2	57.0	-9.4 (-β-CH_3)	+9.3 (+β-Ph)	56.9	64.2
CH_3	43.0	- (-γ-CH_3)	-2.6 (+γ-Ph)	40.4	43.1

In this calculation, the specific chemical shift contributions due to the 2-methyl group has been replaced with those due a phenyl group in the same position. The steric effects of both groups were considered similar.

At this point we have to decide between two possible piperazino structures: one containing two 15-crown-5 groups ((16), Fig. 39, p.165); the other containing one 30-crown-10 ring ((14), Fig. 38, p.164). Can sodium-23 nuclear magnetic resonance distinguish between them?

2.4.2 Sodium Cation Binding of Piperazino-30-crown-10 via Sodium-23 NMR

The sodium-23 NMR spectra of a nitromethane solution containing the crown (0.027 M) and sodium perchlorate (0.0224 M) ($\rho = 1.2$) were taken at 21.39 MHz. Subsequently, lower crown to sodium ratios were obtained by stepwise addition of a stock solution of sodium perchlorate (0.0224 M). Both sodium chemical shifts and transverse relaxation rates vary linearly between crown/sodium equal to 0.0 and 1.0, followed by a plateau for larger values of crown/sodium (Fig. 40).

These data indicate that the compound cannot be the bis-15-crown-5 derivative (16), since the observed formation of a 1:1 complex is characteristic for the large 30-crown-10 group of (14). The linewidth of the sodium:(14) complex (700 Hz) is in close agreement with that of the sodium:dibenzo-30-crown-10 complex; both in nitromethane (Tab. 29).[59]

Were the compound in fact the bis-15-crown-5 derivative (16), then both 15-crown-5 groups should independently complex a sodium.[35] But then chemical shift and linewidth would reach a

[35] Bouquant et al. studied the binding of two sodium cations to a spiro-bis-16-crown-5 in pyridine.[120] Since the two ether groups are joined over the spiro-junction, and are adjacent to each other, the second sodium cation binds by about an order of magnitude weaker than the first cation. For the hypothetical compound (16), the two 15-crown-5 groups would be separated by the phenyl-piperazino-phenyl spacer, and would thus bind cations independently of each other.

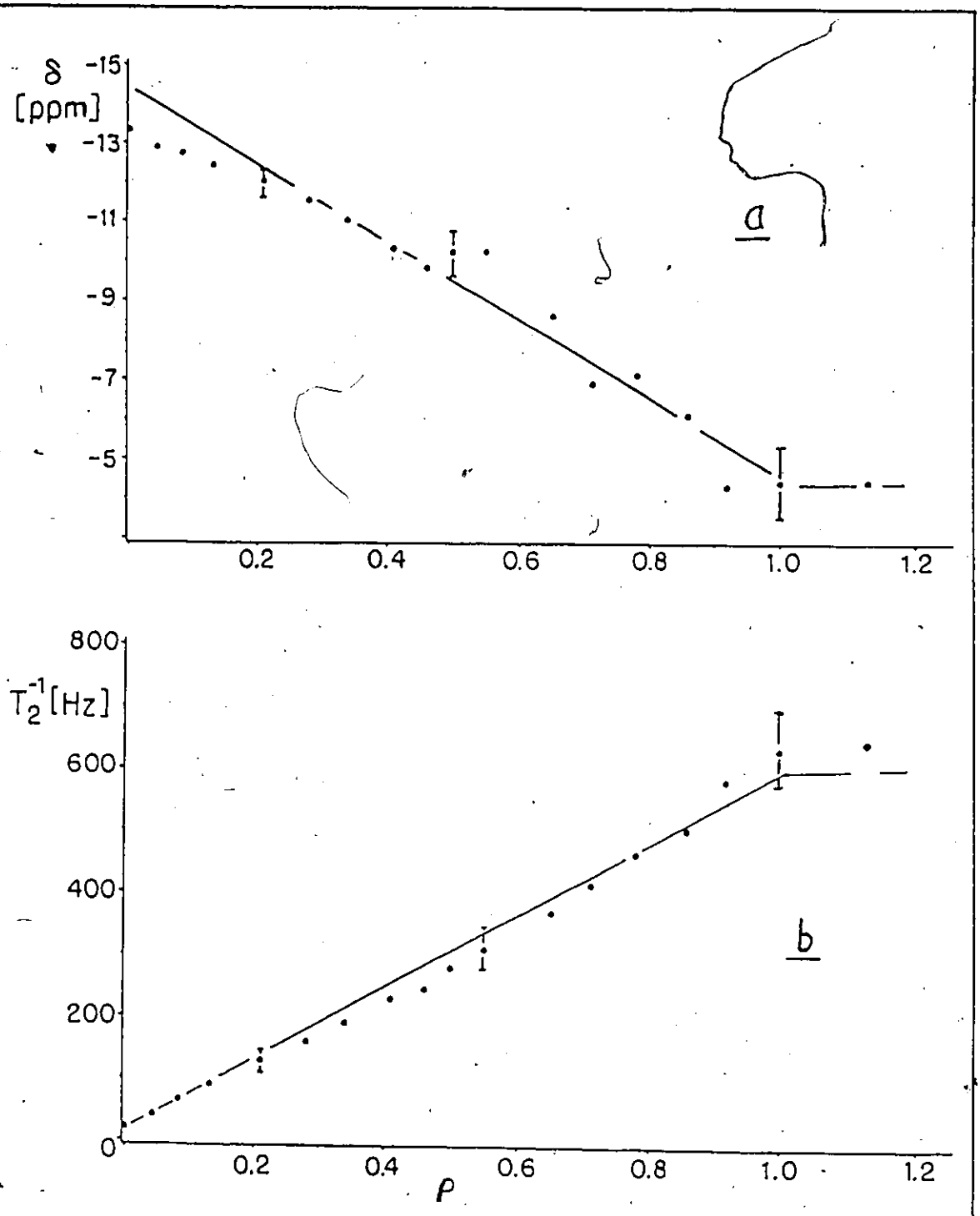

Figure 40: Sodium-23 NMR Data of the Sodium : Piperazino-30-crown-10 Complex. (a) and (b) show the variation of the chemical shift and of the transverse relaxation rate with the ratio ρ.

Table 29: Sodium-23 NMR Data for some Sodium : Crown Complexes

		[Crown]/[Sodium]	Shift[ppm]	$1/T_2$[Hz]
Na		0.0	-14.6	28
Na:(14) (This work)	1:1	>= 1.0	-4.8	2000
Na:DB-30-crown-10 [59]	1:1	>= 1.0	-9.0	2300
Na:MB-15-crown-5 [48]	1:1	= 1.0	-3.8	800
Na:MB-15-crown-5 [48]	1:2	>>= 2.0	-6.0	440

plateau at ρ of 0.5, where the concentration of 'monobenzo-15-crown-5' groups were equal to the total sodium concentration.

A 1:1 sandwich complex of sodium with (16) is similarly unlikely: if the piperazine spacer would allow for an effective sandwich complexation, then the linewidth of this complex should be much smaller than observed due to the high symmetry of the sodium coordination shell in the sandwich complex (see Tab. 29);

conversely, an asymmetric 1:1 sandwich complex would certainly not show the high formation constants evident from the linear variation of both chemical shift and linewidth with ρ (Fig. 40).

Thus via sodium-23 NMR we can eliminate structure (16) and propose the piperazino-30-crown-10 structure (14) for the crown ether obtained from L-adrenaline. It forms through double intramolecular dehydration from the initial dimer 12. Perhaps this condensation takes place during the reaction, catalyzed by base, but more probably it happens during the column work-up, and is catalyzed by the alumina itself.[118]

To the best of our knowledge this is the first time that Sodium-23 NMR has been used as a tool for an organic compound structure determination.

Six bonds are formed during the synthesis of (14). The low yield of 5% for the piperazino-30-crown-10 is understandable, considering it can form only from the dimer 13, which is itself only a minor sideproduct.[104] If the L-adrenaline-15-crown-5 monomer (12) is formed at all in butanol, it is too polar to be recovered from the alumina column.

2.5 Experimental Part - Syntheses

2.5.1 General Experimental

Dopamine hydrochloride and hydrobromide were purchased from Sigma and used directly. Dimethylformamide (Fisher, certified ACS) was refluxed over calcium hydride under nitrogen, and stored over molecular sieves 4Å under nitrogen. Diethyleneglycol, triethyleneglycol and tetraethyleneglycol were purchased from Aldrich and used directly. Trivial names such as dopamine-15-crown-5, are used in text and headings, with the IUPAC names given after each heading. All reactions involving dopamine or L-adrenaline were conducted under a dry nitrogen atmosphere to avoid oxidation of the catechol anions to the deeply red radical anions.

The products were identified and characterized via their mass-spectra;
melting points (Fischer-Johns melting point apparatus, uncorrected);
proton and carbon-13 NMR ($CDCl_3$/TMS; Varian XL-300; Varian XL-200 and Varian FT80 N.M.R. Spectrometer operating at 300 MHz and 200 MHz for proton, and 79 MHz, 53 MHz and 20 MHz for carbon-13 respectively);
infrared spectra (PERKIN ELMER 783 Infrared Spectrophotometer);
micro analysis (Canadian Microanalytical Service Ltd., Vancouver);
and optical rotation where applicable (PERKIN ELMER 241 Polarimeter).

The scheme below shows how the proton NMR data of the crown ether hydrogen are coded (E_e for 18-crown-6 only):

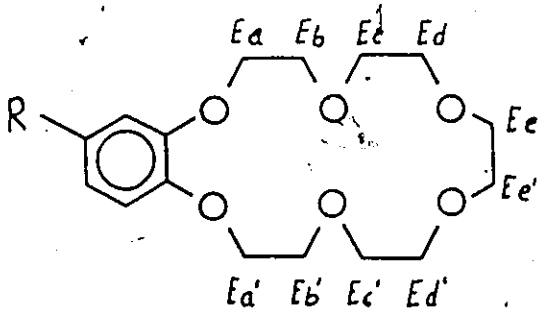

2.5.2 Derivatives of Dopamine-15-crown-5 and Dopamine-18-crown-6

2.5.2.1 Dopamide-15-crown-5 (3a) and Dopamide-18-crown-6 (3b)

2,3-(4'-β-Formamidylethyl)-1,4,7,10,13-pentaoxa-2-cyclopentadecene (3a),

2,3-(4'-β-Formamidylethyl)-1,4,7,10,13,16-hexaoxa-2-cyclooctadecene (3b).

Dopamine hydrochloride (3.8 g, 20 mmol, for dopamide-18-crown-6) or dopamine hydrobromide (2.0 g, 8.5 mmol, for dopamide-15-crown-5) is reacted in dimethylformamide (350 ml) under nitrogen at 100°C for 30 min.

Sodium methoxide in methanol (5.8 ml 25%, 26 mmol for dopamide-15-crown-5 or 13.8 ml, 61 mmol, for dopamide-18-crown-5[36]) is added rapidly. Bis-chloro-tetraethyleneglycol (1.95 ml, 26 mmol) for (3a), or bis-chloro-pentaethylene-glycol (5.3 g, 20 mmol) for (3b), is added dropwise as a solution in dimethylformamide (20 ml, dried and deoxygenated prior to use) over 1-3 hours at 100-110°C.[37]

The reaction is continued for 12 hours at 100°C under nitrogen. After cooling, dimethylformamide is evaporated. The residue is taken up in distilled water (100 ml), and extracted into dichloromethane (3 x 75 ml). The organic phases are dried over molecular sieves 4A, and give, after solvent evaporation, an amber oil consisting to about 70% of the desired product. The pure products are isolated on a column (neutral alumina grade IV, Baker):[38]

Elution with diethylether (for the 15-crown-5) or with first hexane:ethylacetate (3:1), then pure ethylacetate (for the 18-crown-6), removed dimethylformamide and unreacted bis-chloro-oligo-

36 Addition of KBr, or use of potassium-t-butoxide/t-butanol led to substantial amounts of polymeric side products, complicating the isolation of the desired crown product.

37 Addition of the bis-chloro-oligoethyleneglycol turns the solution deep blue-green for a few minutes. Sodium chloride or bromide begins to precipitate after about 30 min. If oxygen has been successfully excluded, the solution will turn only a light yellow.

38 prepared from neutral alumina grade I by addition of 25 ml of distilled water/500g alumina. See also Blackborrow.[121]

ethylene-glycol.[39]

Subsequently, (3a) or (3b) are eluted with methanol as a yellow band to give, after evaporation, a viscous yellow oil. The crude product usually crystallizes spontaneously within 24 hours. (3a) is triturated with diethylether, and recrystallized from ethyl acetate (yield: 1.2 g, 40%), m.p.: 130-131°C.

H-1 NMR (σ, [ppm]): 2.7 (AA'BB', Ph-CH_2); 3.4 (AA'BB', -CH_2-N);
3.70 (s, 8H, E_c,E_d); 3.85, 4.10 (AA'BB', 4H each, E_b and E_a, resp.); 5.7 (br.s, 1H, NH); 6.7 (m, 3H-arom); 8.1 (s, 1H; CHO).

C-13 NMR [ppm]: 35.0, 39.3 (CH_2-CH_2-N); 69.0, 69.2, 69.6, 70.4, 71.0 (ether ring); 114.4, 114.6, 121.3 (tert. C-arom); 131.8, 147.8, 149.2 (quart. C-arom); 161.4 (C=O).

(3b) is recrystallized directly from acetone under cooling in acetone/dry ice, yield: 35%.[40]

H-1 NMR (σ, [ppm]): 2.78 (t, Ph-CH_2); 3.54 (q, CH_2-N); 3.71 (s, 2H, E_e1), 3.72 (s, 2H, E_e2); 3.76 (m, 4H, E_d); 3.78 (m, 4H, E_c); 3.95 (m, 4H, E_b); 4.17 (m, 4H, E_a); 5.92 (m, 1H, N-H); 6.9 (m, 3H, arom.); 8.16 (s, 1H, CHO).

C-13 NMR [ppm]: 35.01, 39.24 (N-CH_2-CH_2-Ph); 69.04, 69.11, 69.66, 70.72 (O-CH_2-CH_2-O); 114.42(t), 114.74(t), 121.36(t), 131.77(q), 147.64(q), 149.04(q) (arom.); 161.31 (CHO).

39 Up to 20% recuperation, IR shows the absence of hydroxyl groups and presence of C-Cl stretching bands at about 1400cm-1.

40 Unlike with the 15-crown-5 derivatives, we could not recrystallize the 18-crown-6 derivatives from ethylacetate or acetone at room temperature. This may be due to complexation of the acidic methyl groups of these solvents with the 18-crown-6 ring.[122]

2.5.2.2 Dopamine-15-crown-5 (4a) and Dopamine-18-crown-6 (4b)

2,3-(4'-β-aminoethylbenzo)-1,4,7,10,13-pentaoxa-2-cyclopentadecene (4a),

2,3-(4'-β-aminoethylbenzo)-1,4,7,10,13,16-hexaoxa-2-cyclooctadecene (4b).

Dopamide-15-crown-5 (3a) (2 g, 5.9 mmol) or dopamide-18-crown-6 (3b) (3g, 8.3 mmol) is hydrolyzed by refluxing in hydrochloric acid (50 ml, 5% HCl, in methanol 1:1) for 2 hours. The acidic solution is brought to pH14 by addition of potassium hydroxide solution (20%) for (4a), and sodium hydroxide solution (20%) for the (4b), and extracted with dichloromethane (4 x 75 ml). The organic phases are dried over molecular sieves 4Å and evaporated to give the corresponding amine as a yellow oil.

The crude dopamine-15-crown-5 (4a) is recrystallized from cyclohexane to give a white crystalline powder; yield: 90%, m.p.: 74-75°C.

H-1 NMR (σ, [ppm]): 1.48 (s, 2H, NH_2); 2.71 (AA'BB', 2H, Ph-CH_2); 2.93 (AA'BB', 2H, CH_2-N);

3.75 (s, 8H, E_c+E_d); 3.90 (m, 4H, E_b); 4.11 (m, 4H, E_a); 6.75 (m, 3H, arom.).

C-13 NMR [ppm]: 39.2, 43.4 (CH_2-CH_2-N); 69,1, 69.3, 69.7, 70.5, 71.0 (ether); 114.5, 114.9, 121.5, 133.0, 147.5, 149.1 (arom.).

Dopamine-18-crown-6 (4b) is recrystallized from 1:1 cyclohexane:hexane under cooling with acetone/dry ice, to give amorphous yellow crystals. Trituration with ethylether gave a pure white powder yield: 1.9 g, 70%; m.p.: 80-82°C.

H-1 NMR (σ, [ppm]): 1.40 (s, NH_2); 2.67 (t, 2H, Ph-CH_2); 2.93 (t, 2H, N-CH_2); 3.70 (s, 4H, E_e); 3.74 (m, 4H, E_d); 3.78 (m,4H, E_c); 3.93 (m, 4H, E_b); 4.14 (m, 4H, E_a); 6.80 (m, 3H; arom.).

C-13 NMR [ppm]: 39.44, 43.53 (N-CH_2-CH_2-Ph); 69.23, 69.40, 69.78, 70.86 (ether); 114.68(t), 115.18(t), 121.51(t); 133.17(q), 147.47(q), 149.07(q) (arom.).

2.5.3 Peptide Derivatives of Dopamine-15-crown-5 and Dopamine-18-crown-6

2.5.3.1 CBZ-Glycyl-, CBZ-L-Alanyl-, Bis-CBZ-L-Lysyl-dopamine-15-crown-5

2,3-(N-(N'-Benzyloxycarbonyl-glycyl)-4'-β-aminoethylbenzo-1,4,7,10,13-pentaoxa-2-cyclopentadecene (5a),

2,3-(N-(N'-Benzyloxycarbonyl-L-alanyl)-4'-β-aminoethylbenzo-1,3,7,10,13-pentaoxa-2-cyclopentadecene (5b), or

2,3-(N-(N',N''-Bis-benzyloxycarbonyl-L-lysyl)-4'-β-aminoethylbenzo)-1,4,7,10,13-pentaoxa-2-cyclopentadecene (5c).

N-Benzyloxycarbonyl-glycine (1.05 g, 5 mmol), N-benzyloxycarbonyl-L-alanine (1.12 g, 5 mmol), or N,N'-bis-benzyloxycarbonyl-L-lysine (2.07 g, 5 mmol) is added to a solution of (3a) (1.55 g, 5 mmol) and N-ethoxycarbonyl-2-ethoxy-1,3-dihydroquinoline (1.31 g, 5.3 mmol) in absolute ethanol (60 ml). The mixture is stirred for 16 h at room temperature, by which time most of the product precipitates. Addition of dry diethyl ether (60 ml) completes the precipitation. The filtrate is washed with cold ethanol/ diethyl ether (5 ml) and then with diethyl ether. Recrystallization from ethyl acetate gives the pure product; yield: 60-91%, see Table 26 on page 137; for NMR data see Tabs. 30 and 32.

2.5.3.2 Bis-CBZ-L-Lysyldopamine-18-crown-6 (5d)

2,3-(N-(N',N''-Bis-benzyloxycarbonyl-L-lysyl)-4'-β-aminoethyl-benzo)-1,3,7,10,13,16-hexaoxa-2-cyclo-octa-decene (5d)

Bis-benzyloxycarbonyl-L-lysine (2.3 g, 5.5 mmol) and (3b) (1.9 g, 5.4 mmol) are dissolved in ethanol (50 ml, dry).

N-ethoxy-carbonyl-2-ethoxy-1,2-dihydroquinoline (1.33 g, 5.6 mmol) in ethanol (15 ml, dry) is added and the mixture stirred at room temperature for 12h. The white precipitate is washed with ethanol (2 ml, dry) and diethylether (20 ml, dry), and recrystallized from acetone under cooling with dry ice / acetone to give the final product; yield: 60%; m.p.: 119-123°C; $[\alpha]_D$: -7.4°, see Table 26 on page 137; for NMR data see Tabs. 30 and 32.

2.5.4 Debenzyloxycarbonylation of (5a), (5b), (5c), and (5d)

2.5.4.1 Glycyl-, L-Alanyl-, L-Lysyl-dopamine-15-crown-5

2,3-(N-Glycyl-4'-β-aminoethylbenzo)-1,4,7,10,13-pentaoxa-2-cyclopentadecene (6a),
2,3-(N-L-Alanyl-4'-β-aminoethylbenzo)-1,4,7,10,13-pentaoxa-2-cyclopentadecene (6b), or
2,3-(N-L-Lysyl-4'-β-aminoethylbenzo)-1,4,7,10,13-pentaoxa-2-cyclopentadecene (6c).

0.4 mmol of the corresponding benzyloxycarbonylated product (5a), (5b), or (5c) is dissolved in 30% hydrobromic acid (8 ml) and stirred at room temperature for 2h. The mixture is poured into dry diethyl ether (50 ml) to give an oily precipitate, which is washed with diethyl ether (2x10 ml) and dissolved in methanol (2 ml). Under ice cooling, a solution of ammonia in chloroform (10%, 10 ml) is added slowly to precipitate ammonium bromide, followed by chloroform (30 ml) to complete the precipitation.[177] The organic filtrate is extracted with distilled water (1x5 ml) to remove complexed ammonium bromide. Recrystallization from diethyl ether after drying over molecular sieves 4Å gives the products; yield: 92-95%, see Table 26 on page 137; for NMR data see Tabs. 31 and 33.

The UV/Vis spectra of L-lysine-15-crown-5 (6c) shows three absorptions:
ω =277nm (ε =2690) and ω =228nm (ε =8070) from the aromatic ring; and ω =200nm (ε =45000) from the amide carbonyl.

2.5.4.2 L-Lysyl-dopamine-18-crown-6 (6d)

2,3-(N-L-Lysyl-4'-β-aminoethylbenzo)-1,4,7,10,13,16-hexaoxa-2-cyclooctadecene (6d)

Bis-CBZ-L-Lysyl-dopamine-18-crown-6 (5d) (2.8 g, 3.7 mmol) is reacted with hydrobromic acid in glacial acetic acid (10 ml, 32%) for 2h at room temperature under stirring. Addition of diethylether (40 ml, dry) precipitates the bis-hydrobromide. This salt is dissolved in distilled water (20

ml) and brought to pH14 by addition of solid sodiumhydroxide. Extraction with dichloromethane (3 x 50 ml), drying over crushed molecular sieves 4Å, and solvent evaporation gave (6d) as a brown oil.

Treatment with hot cyclohexane gave a clear yellow solid glass, possibly an inter/intra-molecular complex: yield: 90%; m.p.: 71-75°C; $[\alpha]_D$: -10.3°; the NMR spectra show only broad bands.

The infrared spectra indicated the amide carbonyl stretching band at 1675cm-1 for compounds (5a), (5b), (5c), and (6b); and for (5a), (5b), and (5c), the urethane carbonyl stretching appeared at 1710cm^{-1} and the two amide N-H stretching bands appeared at 3450(m) and 3340(w).

Table 30: H-1 NMR Data of Amino acid Crowns (5a) - (5d)

Group		Compound (5a)	(5b)	(5c)	(5d)
Ph-CH_2CH_2		2.70	2.70	2.70 (AA'BB')	2.72 (t)
Ph-CH_2-CH_2-N		3.45	3.44	3.12 (AA'BB')	3.48 (m)
3H-arom. (m)		6.67	6.67	6.67	6.77
5H-arom.		7.34 (s,5H)	7.34 (s,5H)	7.32 (s,10H)	7.28 (m,10H)
Ether	E_a	4.09 (m, 4H)	4.10 (m)	4.06 (m)	4.14 (m,4H)
	E_b	3.87 (m, 4H)	3.86 (m)	3.88 (m)	3.92 (m,4H)
	E_c	3.73 (s,8+2H)	3.74 (s,8H)	3.72 (s,8H)	3.76 (m,4H)
	E_d				3.73 (m,4H)
	E_e				3.68 (s,4H)
NHCO		6.22 (br.s)	6.22 (br.s)	6.24 (br.s)	6.12 (d)
NHCO(a)		5.65 (br.s)	5.45 (br.s)	5.62, 5.15	5.53 4.05
Ph-CH_2		5.10 (s,2H)	5.07 (s,2H)	5.06 (s,4H)	5.11 (s,2H, ε) 5.06;5.07 (s,2H, α)
Amino-acid	1	3.73 (m,2H)	4.10 (m,1H)	4.06 (m,1H)	4.06 (m,1H)
	2	-	1.31 (d,3H, ^3J7.1)	1.6;1.8 (m,2H)	1.30
	3	-	-	1.2-1.8 (m,6H)	1.46 (m,2H)
	4	-	-	1.26 (m,2H)	
	5	-	-	3.12 (m,2H)	3.14 (m,2H)

Table 31: H-1 NMR Data of Amino acid Crowns (6a) - (6c)

Group		Compound (6a)	(6b)	(6c)
NH_2		1.31 (s,2H)	1.9 (s,2H)	1.3 - 1.8 (m,4+6H)
Ph-$C\underline{H}_2$-CH_2		2.7 (AA'BB')	2.70 (AA'BB')	2.5-3.0 (m)
Ph-CH_2-$C\underline{H}_2$		3.4 (AA'BB')	3.4 (AA'BB')	2.5-3.0 (m)
3H-arom. (m3)		6.8	6.7	6.8
Ether	E_a	3.8-4.3 (m,8+2H)	3.8-4.3 (m,8+1H)	3.8-4.3 (m,8+1H)
	E_b			
	E_c	3.7 (s,8H)	3.7 (m,8H)	3.7 (m,8H)
	E_d			
	E_e	-	-	-
Amino-acid	1	3.8-4.3 (m,2H)	3.8-4.3 (m,1H)	3.8-4.3 (m,1H)
	2	1.8 (m,2H)	-	1.30 (d,3H, $^3J7$)
	3	-	-	1.3-1.8 (m,6+4H)
	4	-	-	
	5	-	-	2.5-3.0 (m,2+2H)

Table 32: C-13 NMR Data of Amino acid Crowns (5a) - (5c)

Group	Compound (5a)	(5b)	(5c)
$Ph-CH_2-CH_2-N$	35.1	35.1	35.0
	40.1	40.8	40.5
Ether	69.0	69.1	69.0
	69.2	69.3	69.1
	69.6	69.7	69.6
	70.5	70.6	70.5
	71.0	71.7	71.0
CH_2-OCON	67.0	66.9	70.5
			71.0
arom.	114.4	114.5	114.3
	114.7	114.7	114.6
	121.3	121.3	121.3
	128.0	128.0	128.1
	128.3	128.2	128.2
		128.5	128.5
	131.9	131.9	131.8
	136.3	136.2	136.2
			136.6
	147.8	147.8	147.8
	149.2	149.3	149.2
OCON	156.6	155.9	156.3
C=O	169.2	172.3	171.6
CO-CHR-N (1)	44.6	50.7	55.0
(2)	-	18.8	22.2
(3)	-	-	29.4
(4)	-	-	31.9
CH_2-N (5)	-	-	43.7

The numbers (1-5) refer to the aliphatic carbon of the amino acid sidechains, glycine containing only #1.

Table 33: C-13 NMR Data for the Amino acid Crowns (6a) - (6c)

Group	Compound (6a)	(6b)	(6c)	(6d)[a]
$Ph-CH_2-CH_2-N$	35.3 40.1	35.3 40.2	35.3 40.2	
Ether	69.1 69.3 69.7 70.5 71.1	69.0 69.2 69.6 70.5 70.8	69.0 69.1 69.6 70.5 71.0	
arom.	114.4 114.7 121.3 132.2 147.3 149.2	114.4 114.7 121.3 132.2 147.7 149.2	114.3(t) 114.7(t) 121.4(t) 132.3(q) 147.7(q) 149.1(q)	
C=O	172.7	175.6	175.1	
CO-CHR-N (1)	44.8	50.8	55.2	
(2)	-	21.8	" 23.1	
(3)	-	-	33.4 35.0	
(4)	-	-	41.9	
CH_2-N (5)	-	-	"	

a) C-13 signals for (6d) were broadened due to aggregation. The numbers (1-5) refer to the aliphatic carbon of the amino acid sidechains, glycine containing only (1). (t) and (q) indicate tertiary and quarternary carbon atoms, determined via off-resonance decoupling of the attached protons.

2.5.5 Comments to Syntheses:

2.5.5.1 Amino Acid Coupling

Dicyclohexyl-carbodiimide with N-hydroxy-succinimide as moderator were also used for the peptide coupling. The reaction was done in methylene chloride, going from -30°C to room temperature, and gave the glycyl-15-crown-5 (5a) in about 80% yield. However, the product was always accompanied by substantial amounts of dicyclohexylurea, which is often observed as by-product in this reaction.[123][124] Although the crown ether could be separated on silica TLC with ethyl acetate/methanol 5/1, the more convenient and reliable EEDQ coupling method was subsequently preferred.

2.5.5.2 Deprotection

The benzyloxycarbonyl protecting-group can be cleaved by photolysis,[125] catalytic hydrogenolysis,[126] and catalytic transfer hydrogenolysis, using cyclohexene[127] or formic acid as hydrogen donor.[128] All three hydrogenolysis methods transform the benzyloxycarbonyl protecting group into toluene and carbon dioxide.

Catalytic hydrogenolysis: CBZ-glycyl-15-crown-5 was deprotected to 94% after 48 hrs. by catalytic hydrogenolysis. This is in contrast to a reaction time of 5 min for complete debenzyloxycarbonylation of typical protected peptides, as reported by Bergman.[126]

Hydrogen was percolated through a mixture containing CBZ-glycyl-15-crown-5 (5a) (1.56 g, 3.11 mmol) and palladium on charcoal (80 mg, 10% Pd/C). Fig. 41 shows the disappearance of the benzyl and phenyl proton NMR signals of (5a) as a function of hydrogenolysis time. A progressive deactivation of the catalyst is evident.

Catalytic transfer hydrogenolysis: After 12 hrs. of reflux, cyclohexene as hydrogendonor (4% cyclohexene in methanol, 50 ml)[127] gave only partial deprotection of bis-N-benzyloxycarbonyl-L-lysyl-15-crown-5 (5c).

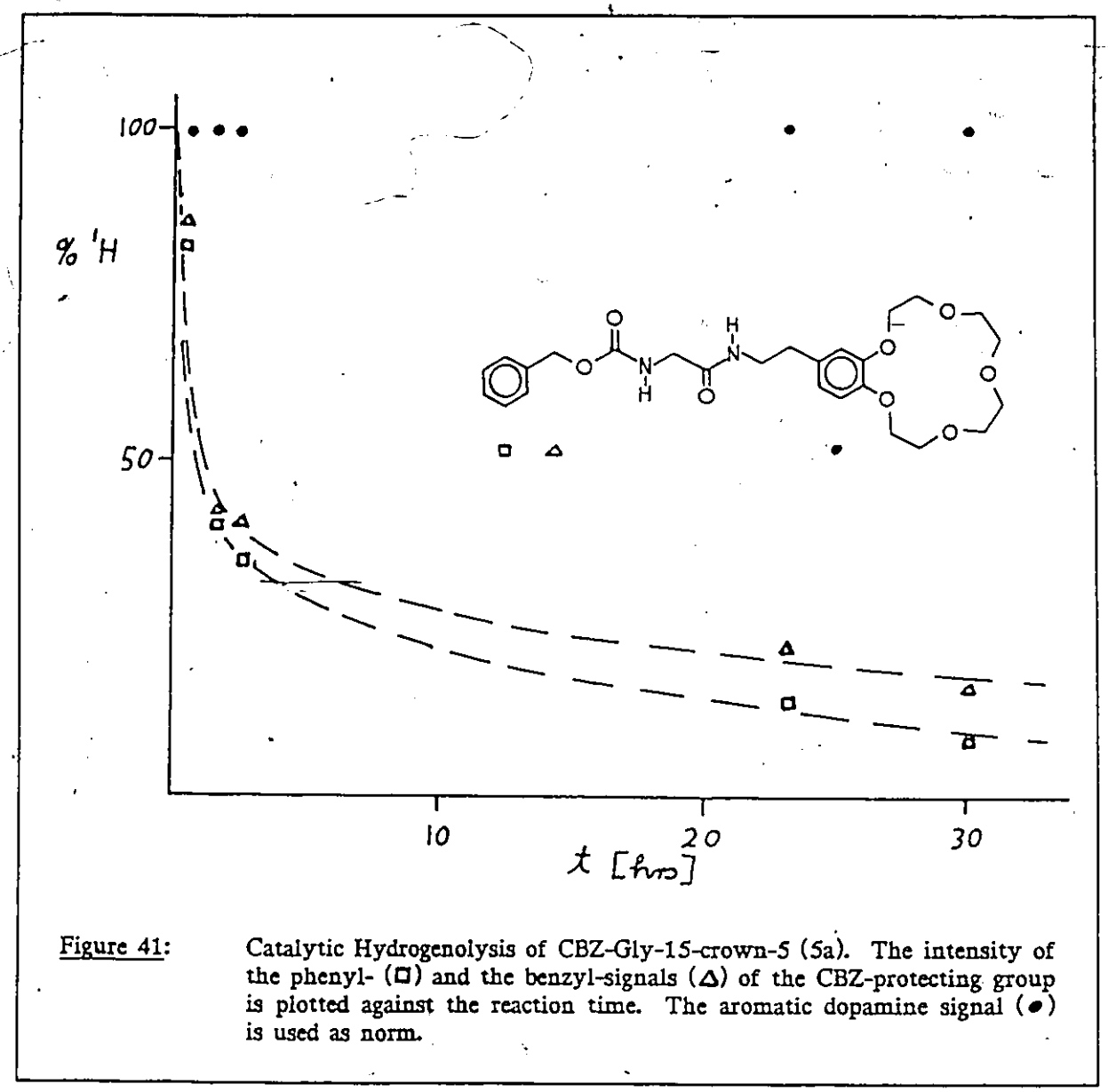

Figure 41: Catalytic Hydrogenolysis of CBZ-Gly-15-crown-5 (5a). The intensity of the phenyl- (□) and the benzyl-signals (△) of the CBZ-protecting group is plotted against the reaction time. The aromatic dopamine signal (●) is used as norm.

On the other hand, N-benzyloxycarbonyl-L-alanyl-15-crown-5(5b) (0.43 g, 0.83 mmol) was completely deprotected by cyclohexene (2% cyclohexene in ethanol, 40 ml) and Palladium on charcoal (150 mg, 10% Pd/C) after reflux for 2h (0.26 g, 81%).

As well, using formic acid as the hydrogen donor (20% formic acid in methanol, 10 ml) and palladium on charcoal as catalyst (200 mg, 10% Pd/C), bis-N-benzyloxycarbonyl-L-lysyl-15-crown-5 (5c) (0.35 g, 0.5 mmol) was completely deprotected after 5min.

2.5.6 Tetrahydroisoquinolines

2.5.6.1 2-Phenyl-4,5-dihydroxy-tetrahydroisoquinoline (9)

Dopamine hydrochloride (10.1 g, 50 mmol), benzaldehyde (6 g, 57 mmol, freshly distilled) and triethylamine (5.6 g, 55 mmol) were added to 75 ml benzene, and the mixture refluxed. Addition of 75 ml dry ethanol caused dissolution of the dopamine hydrochloride, followed by rapid crystallization of the yellow product. It was recrystallized from methanol, and washed with acetone to give pure white crystals, yield: 80%, m.p.: 182-185 (loss of crystal water at 92-95°C).

C-13 NMR data ([ppm], DMSO-d_6, DMSO centerline used as reference at 40.8 ppm, 20.0 MHz): 21.9, 25.2 (CH_2CH_2); 59.3 (CH(Ph)N); 115.4, 116.2, 123.5, 124.0, 129.7, 130.1, 131.0, 138.4, 145.2, 146.4, (arom.).

2.5.6.2 2-Phenyl-4,5-dihydroxy-tetrahydroisoquinoline-15-crown-5 (10)

(9) (6.58 g, 27 mmol) is heated in dimethylformamide (250 ml) to 80°C. Sodiumiodide (0.6g), bis-chloro-tetraethyleneglycol (6.3 g, 27 mmol) and, after ten minutes, sodium methoxide in methanol (12.5 ml, 56 mmol) are added under nitrogen. The color of the clear mixture turned immediately blue, then green and faded after another 10 minutes simultaneous with the first appearance of a pale precipitate of sodium chloride. The work-up is identical to that of the dopamide-15-crown-5 (3a), including absorption on a neutral alumina column (grade IV), elution with diethylether to remove residual dimethylformamide and unreacted bis-chloro-tetraethyleneglycol, followed by elution of the product with methanol. Yield: 40%. The crude product is dissolved in a minimum amount of methylenechloride in a narrow beaker, and the same volume cyclohexane is carefully added on top, without disturbing the bottom layer of methylenechloride. The pure, off-white product crystallizes as a ring just above the cyclohexane layer over a period of several hours. m.p.: 107-108°C.

H-1 NMR data (σ, $CDCl_3$, 200 MHz): 2.12 (br.s, 1H, NH); 2.7-3.2 (m, 4H, CH_2-CH_2); 3.72 (s, 4H, ether); 3.76 (s, 4H, ether); 3.8 (m, 2H, ether); 3.9 (m, 4H, ether); 4.14 (m, 2H, ether); 5.02 (s, 1H, CH(Ph)N); 6.26, 6.64 (s, 1H each, arom.); 7.28 (m, 5H, arom.).

C-13 NMR data ([ppm], $CDCl_3$, 20.0 MHz): 29.3, 40.9 (CH_2-CH_2); 61.5 (C=N); 69.1, 69.6, 69.7, 70.6, 71.1 (ether) 114.0, 114.2, 127.3, 128.4, 128.9, 130.6, 144.9, 147.2, 147.8 (arom.)

2.5.7 Synthesis of Fluorescent Crown Derivative (14)

N-Butanol (150 ml, dry) is purged with nitrogen under reflux for 10 min. Addition of adrenaline (5.0 g, 27.3 mmol) gives a white suspension, which clarifies upon addition of sodium methoxide (12.5 ml sodiummethoxide in methanol 25%, 57 mmol). Bis-chloro-tetraethyleneglycol (6.3 g, 27 mmol) is added and the mixture refluxed for 20h.

The solvent is evaporated and the oily residue taken up in water (100 ml). The resulting emulsion is passed through a water soaked gravity filter to separate the water soluble components. The filtrate is extracted with chloroform (3 x 50 ml), the organic phases dried with magnesium sulfate and the solvent evaporated to give a red oil (6g). This crude product is taken up in chloroform (100 ml, dry), absorbed onto Celite (30g), and packed onto an alumina grade IV column.[121] With ethyl ether the unreacted bis-chloro-tetraethyleneglycol is eluted first[41] followed by butanol and eventually the desired product.[42] The product semicrystallized after solvent evaporation; and trituration with dry diethyl ether gave white crystals; yield: 5%; m.p.: 184-190°C; m/e 646; $[\alpha]_D$: -2.0°

41 IR showed the absence of hydroxyl groups.

42 Further fractions, eluted with tetrahydrofuran and acetone, showed substantial amounts of sidechain alkylated adrenaline compounds.

H-1 NMR (σ, [ppm]): 2.05(s, CH_3); 2.31(t, ^3J5.5, CH); 3.02(dd, ^3J5.5, CH_2); 4.16(m, 8H, A); 3.92(m, 8H, B); 3.78(s, 16H, C); 6.84, 6.92(m, 3H, arom.).

For C-13 NMR data see Tab. 28.

2.5.8 Oligoethyleneglycol Derivatives

2.5.8.1 1,13-Bis-chloro-4,7,10-trioxatridecane

Tetraethyleneglycol (143.1 g, 0.73 mol) and pyridine (130 g, 1.63 mol) are heated in toluene (670 ml) to 90°C, and thionylchloride (195 g, 1.63 mol) is added dropwise over 3 h. The reaction is continued for 12 hours at 90°C, during which a lower phase separated, containing the pyridinium hydrochloride.

After cooling, sulfuric acid (75 ml, 6%) is added. The organic phase is separated[43] and the solvent evaporated. High vacuum distillation of the residual yellow oil gave the pure product (b.p. 108°C at 0.04 Torr, 131 g, 85%).

2.5.8.2 1,10-Bis-chloro-4,7-dioxadecane

Triethyleneglycol (150 g, 1 mol) and pyridine (174 g, 2.2 mol) are heated in toluene (890 ml) to reflux, and thionylchloride (263 g, 2.2 mol) is added dropwise over 3 hours.

The reaction is continued for 4 hours after addition of the thionyl chloride is completed. After cooling, hydrochloric acid (125 ml, 5%) is added and the resulting two phases separated. The toluene phase is washed with hydrochloric acid (2 x 50 ml, 2%), separated and the solvent evaporated. Residual water is automatically removed as the azeotrop with the first fraction. The obtained brown oil is distilled to give the pure, slightly yellow product (0.1 Torr, 95°C, 126 g,

[43] The mixture shows a strong tendency to form emulsions. In this case the phases are separated by passing the emulsion through a gravity filter moistened with toluene. Only the organic phase will pass.

70%).

2.5.8.3 1,4,7,10,13,16-hexaoxahexadecane

(adapted from Newcomb 1975)[129]

Sodium metal (8.12 g, 353 mmol) is dissolved in monoethyleneglycol (110 g, 1.8 mol, Baker, ACS, as received) under nitrogen. Bis-chloro-triethyleneglycol (30 g, 160 mmol) is added slowly over 2 h at 100°C. The reaction is continued for 24h at 100°C under nitrogen. After cooling and filtering, unreacted monoethyleneglycol is evaporated under reduced pressure. Addition of dry acetone (150 ml) precipitates sodium chloride. After filtration and solvent evaporation, final traces of monoethyleneglycol are removed under reduced pressure (0.1 Torr, 50-60°C). The product is distilled at 170-180°C and 0.01 Torr, and identified via IR (3350 cm^{-1} = HO bonded) and H-1 NMR.

2.5.8.4 1,16-Bis-chloro-4,7,10,13-tetraoxahexadecane

Pentaethyleneglycol (26 g, 109 mmol) and pyridine (24.3 ml, 250 mmol) are heated in toluene (150 ml) to 90°C under nitrogen, and thionylchloride (18.1 ml, 250 mmol) is added dropwise over 3h. The reaction is continued overnight at 90°C under nitrogen.

After cooling, the mixture is acidified with hydrochloric acid (20 ml, 5%), dichloromethane (50 ml) is added to facilitate the phase separation, and the organic phase is washed with hydrochloric acid (20 ml, 5%). After solvent evaporation, the obtained crude product is purified by high vacuum distillation to give the pure, light yellow product; yield: 61%; 18.3 g; b.p.: 100-125°C, 0.025 Torr. H-1 NMR (σ, [ppm]): 3.70(s, ether)

C-13 NMR [ppm]: 42.61 (CH_2-Cl); 70.53, 70.60, 71.30 (CH_2-O);

All bis-chloro-oligoethyleneglycols showed the strong C-Cl stretching bands at 680cm^{-1} and 750cm^{-1}, and no hydroxyl absorption at 3500cm^{-1}.

Chapter III

TRANSPORT PROPERTIES OF SOME AMINOACID BEARING CROWN ETHERS

3.1 Introduction

As mentioned in the general introduction, plants and animals depend on efficient chemical communication across cell membranes to sustain their life functions. This communication consists partly of the controlled transfer of messenger chemicals such as cations, amino acids, and protons across the biological membranes. Since these compounds often bear positive or negative charges, they need some screening from the lipophilic membrane during their crossing. The mechanisms and the regulation of this transport is an important biochemical problem.[2]

3.1.1 History of Ionophores

We now know of three complementary pathways that can mediate the selective passage of charged (or neutral) substrates across biological membranes:

Transfer Enzymes, such as the sodium-potassium pump, consist of bulky proteins that extend through the membrane, reaching from one aqueous phase to the other. They bind their substrate on one side of the membrane, and transfer it to the other side by a conformational rearrangement. The energy for this process is often supplied by a coupled ATPase.[130]

Channel Forming Peptides, such as Gramicidin A, 'tunnel' through the membranes, and allow selected cations to pass through their hydrophilic interior, depending upon size and charge density.[131]

Carrier Mediated Transport of charged substrates (such as metal cations, organic ammonium cations, amino acid anions) was confirmed to be possible in 1967, when Pressman demonstrated that valinomycin and nigericin could transport ions across artificial bulk membranes.[132][44]

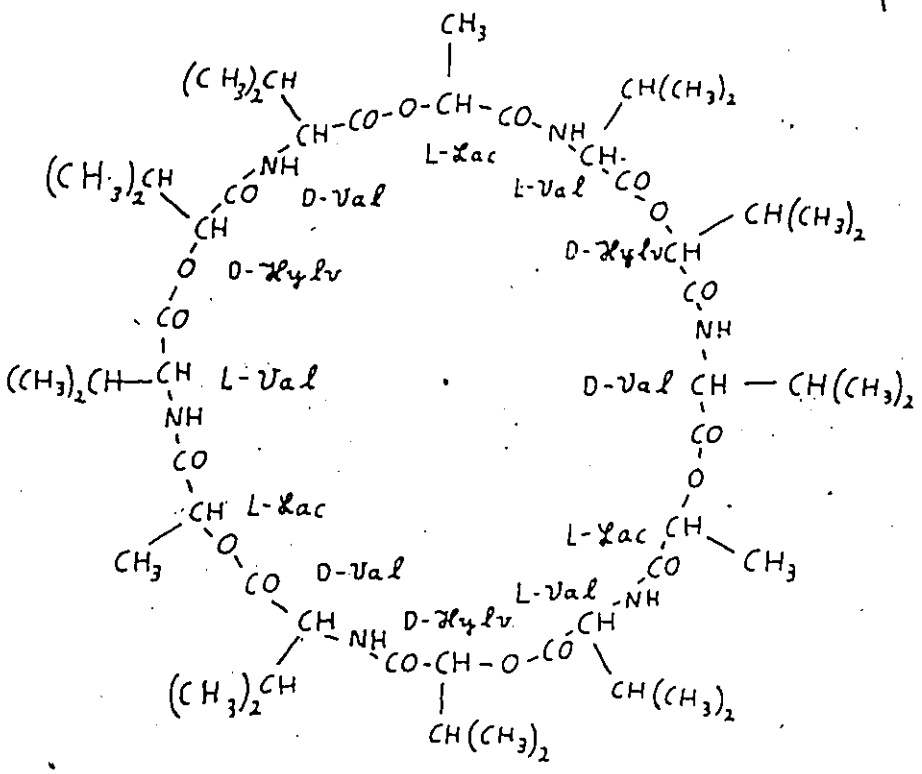

Figure 42: Valinomycin. B.Sakar, p. 279 in [150]

The name ionophore = ion carrier was given to valinomycin and its analogs to emphasize their mobility within the membranes.[133] Hilgenfeld and Saenger defined them concisely as:

> "...receptors [that] form stable lipophilic complexes with charged hydrophilic substrates (such as Na^+, K^+, Ca^{2+} etc.,) and thus are able to transport them into lipophilic phases, for example natural or artificial membranes."[79]

44 This finding superceded two earlier interpretations of valinomycin mediated transport across bilayer membranes: that of a combination of a receptor (valinomycin) with an ion-pump located in the membrane; and the formation of transmembrane channels by valinomycin.

The complex make-up of natural membranes usually makes it difficult to find out how much these three pathways contribute to cross membrane transport. Typically several individual pathways are coupled , making their separation even more difficult.[134]

Valinomycin is a classical example of this problem: In 1967 Pressman suggested that valinomycin would selectively transport potassium across natural membranes by activating a separate enzymatic potassium ion pump.[133] In the same year Mueller used lipid bilayer membranes devoid of any other biological material. He proposed that valinomycin could form a channel through the membrane.[135] Finally, and still in 1967, Pressman used a bulk liquid membrane which can support neither channel formation nor the enzymatic ion pump mechanism. Thus he concluded that valinomycin must be a mobile carrier or ionophore. In fact, Valinomycin forms a hydrogen-bond-stabilized cavity perfectly tailored for the potassium cation. Thus valinomycin can bind potassium thousand times stronger than the smaller sodium cation.[79][132][133][146]

Bulk artificial membrane models are now widely used to study transport mechanisms.[136][137][138][139][140][141] In general, these systems consist of the aqueous source and receiving phases, separated by the organic membrane phase containing the ionophore (See for instance the experimental section). The substrate salts, sodium or potassium picrates in these experiments, are initially contained in the source phase. They form a complex with the ionophore at the interface between source and membrane phases. The bulk membrane phase is stirred mechanically to avoid large concentration gradients within the membrane phase. The rate determining steps of the transport are considered to be the diffusion of the complex and of the ligand through the unstirred Nernst-layers adjacent to the interfaces.[142]

Other artificial transport systems often used to simulate the natural membranes include the lipid bilayer membranes (black membranes),[143][144] and natural and artificial vesicle systems.[143][145]

The simplest driving force for transport is the concentration gradient of the substrate salt between source and receiving phase. Often, we are also interested in the coupling between the salt transport and other energy sources such as pH gradient, redox potential or photochemically induced conformational changes (see below).

3.1.2 Crown-type compounds as Model Ionophores

In 1968 Pedersen discovered that crown ethers have a high capacity for complexing uni- and divalent cations.[3] This finding came just in time to give the ionophore research, at that time still in its infancy, an extensive range of model carrier compounds.[138][148][149] Crown type compounds are relatively easy to synthesize, and can in principle be designed to have specific properties.[97][148][150][45]

Most of the crown type compounds used as model ionophores in transport studies fall into one of the following groups:

3.1.2.1 Neutral, Monocyclic Crown compounds

These compounds are based on a crown ring which consists of usually 4 to 10 oxygen donor atoms, separated by usually two methylene groups.[46] Many studies have dealt with conformations and transport selectivities of these compounds.[47]

A sidechain, bearing additional donor groups, is often attached to the basic crown ring. Gokel coined the name lariat ether for such compounds, refering to the projected capacity of the sidechain to 'rope-in' a cation.[98][99][148][154] These compounds are a middle step between simple

[45] The bicyclic cryptands developed by Lehn[151] as well as acyclic ligands[152] were discovered soon afterwards.

[46] Many analogous cyclic ligands have been synthesized, incorporating into the basic ring one or more of the following donor groups: sulfur, ester, lactone, keto, pyridine, pyrrole, hydroxy, and others.[148][152][153]

[47] See also the chapter on DB-24-crown-8.

crowns and the cryptands. The only driving force for their cation transport is the concentration gradient of the substrate itself; hence the name passive transport or 'primary gradient pumping' (Fig. 43).[134] A (lipophilic) counteranion must always accompany the cation during transport in order to maintain the electroneutrality across the membrane.

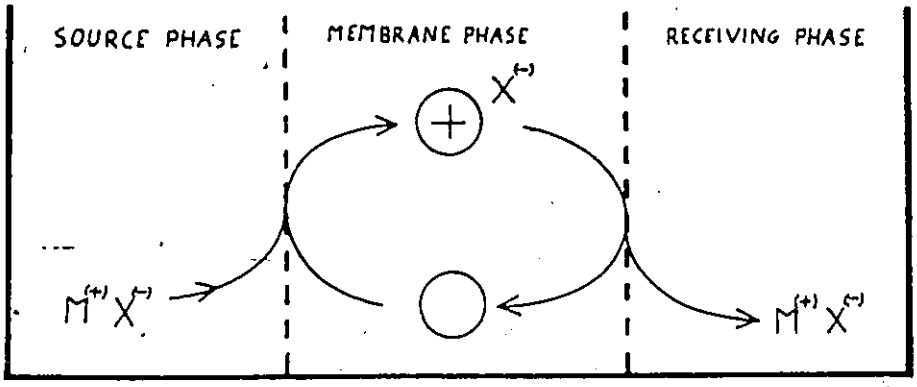

Figure 43: Primary Gradient Pumping. M^+X^- is the salt to be transported from the aqueous source phase through the methylene chloride membrane phase into the receiving phase. There are four steps:
The M^+X^- ionpair diffuses into the interface between source and membrane phase, where it is complexed by the carrier (a). The carrier-salt complex diffuses across the membrane phase (b), and releases the salt into the aqueous receiving phase (c). The transport cycle is closed by the empty carrier diffusing back to the source phase (d).

These passive transport properties remain valuable for characterizing ionophores.[155][156]

3.1.2.2 pH Ionisable Crown Compounds - Carboxylic and Amino Crowns

These crown compounds feature an ionisable group such as carboxyl or amine besides the basic crown ring. Since the protonation state of this group, and thus the carrier properties, depend on the pH, these carrier models allow to study how the pH in the aqueous phases controls the trans-

port. This coupling is of crucial relevance to the biochemical membranes: there it allows for the regulated or active transport of a substrate.[48]

In particular, pH ionisable crowns can transport a monovalent cation in stoichiometric exchange for one proton. If the chemical potential of the proton gradient is larger, and in the opposite direction to that of the substrate salt, the substrate will be pumped uphill against its own concentration gradient.[134][141][157][158][159] Goddard calls this secondary gradient pumping (Fig. 44).[160]

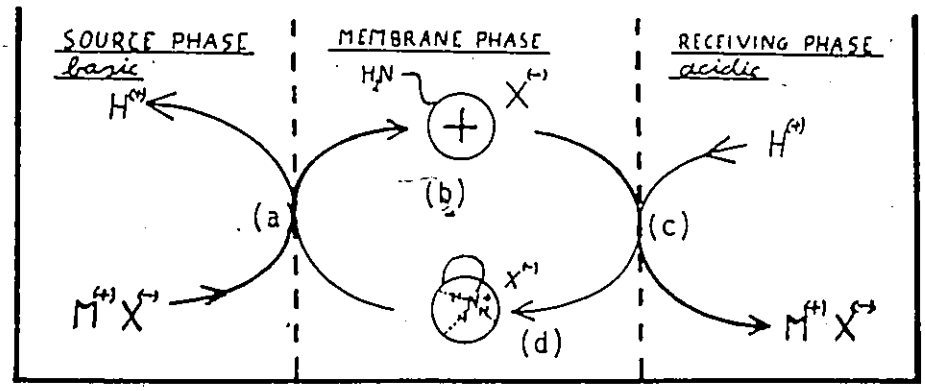

Figure 44: Secondary Gradient Pumping. The sketch shows a proton driven cation transport, using an amino crown as carrier:
The metal cation and the protonated carrier meet at the interface between membrane phase and basic source phase (a). The carrier is deprotonated, and extracts the metal cation into the membrane phase. A lipophilic counteranion is necessary in bulk membranes (b). At the interface to the acidic receiving phase the carrier amine is protonated and extrudes the metal cation into the receiving phase (c). The protonated carrier then diffuses back to the source phase, accompanied by the lipophilic counteranion (d).

48 The term active implies that the transport is driven by a chemical potential other than the concentration gradient of the substrate itself.

Carboxylic acid ionophores of the crown type: these compounds were studied by Fyles[137][140][161][162] and Bartsch.[136][145][163] They do not need a counteranion to accompany the complex in the membrane phase since the cationic charge is compensated for within the complex. Thus they are well suited to selectively remove for instance heavy metal cations from industrial wastes.[136][145][163].

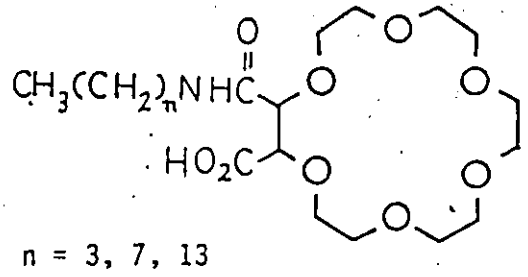

Figure 45: Carboxylic Acid Crown Compounds.[162]

Amine Crowns: they also mediate the active transport of cations from a basic to a neutral (or acidic) phase. Here, the amine can be part of the crown ring,[157] or it can be a pendant (Fig. 46).[141]

Upon arrival at the neutral or acidic receiving phase, the amine is protonated. This enforces the release of the complexed cation, either by charge repulsion between the ammonium and the metal cation, or by intramolecular complexation of the ammonium group with the crown ring.[114][141][164] To return through the membrane to the basic source phase, the protonated carrier needs a lipophilic counter anion. Again, a proton gradient can serve as the driving force to pump a substrate salt uphill against its own concentration gradient.

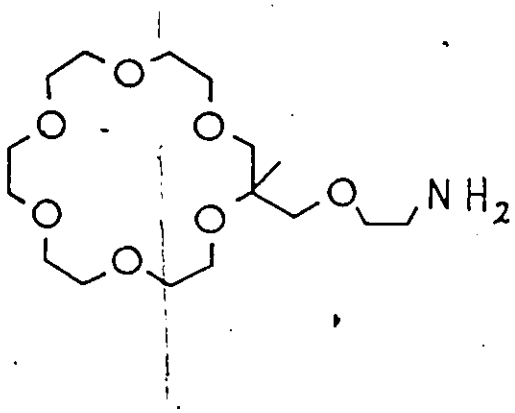

Figure 46: Amine Bearing Crown Compounds.[141]

Among driving forces for membrane transport, the pH gradient is the one most often studied. Yet many other driving forces have been used: redox systems such as the dithiol-disulfide couple of Shinkai[165][166] and the thioether mediated copper transport of Ohki;[167] and the photodriven systems, notably Shinkai's cis-trans interconversion of an aza-bridged bis-crown.[168][169][170]

3.1.3 Methodological Classification

Below is a useful classification of transport studies according to the kind of transport they deal with:

1. PASSIVE TRANSPORT:

Passive downhill transport of metal cations, organic ammonium cations and anions, sometimes with chiral recognition.[92][93]

(Descriptive Studies)

2. ACTIVE TRANSPORT OF ORGANIC AND INORGANIC SUBSTRATES:

Use of various driving forces, such as pH gradients, for coupled co- and counter-transport.

(Mechanistic Studies).

3. REGULATING MECHANISMS IN ACTIVE TRANSPORT:

That which regulates the coupled transport across membranes. Are there FEEDBACK-LOOPS, similar to the well known reflex arcs in organisms?[171]

(Conceptual Studies).

Studies in group 1 and 2 often aim to develop high substrate selectivities, for applications ranging from ion selective electrodes[172] to waste recovery.[136] Group 3 studies clearly receive some impetus from the biological sciences: they help decode the complex couplings of transport across biological membranes.[134][160][164]

3.1.4 Aim of Research

First in this chapter, the passive transport of sodium and potassium picrate by crown ethers bearing aminoacid sidechains will be described. How do these sidechains affect the transport rates and selectivities?

Following this, the ionophoric properties of the amino crown L-lys-15-crown-5 will be detailed in the section on active transport: this crown is characterized by it's two binding sites, the crown ring and the amino group, enabling it to transport picric acid and sodium picrate in parallel , both transports being driven by the concentration gradients of sodium and picrate.

Explaining the complex proton and picrate transport curves by the carrier molecule's chemical properties provides some insight into a tightly coupled and self-regulated proton-sodium-picrate transport system.

3.2 Passive Transport - Results and Discussion

The ability of the compounds listed in Tab. 34 to facilitate the 'downhill' diffusion of sodium and potassium picrate across a bulk methylene chloride membrane was measured. The synthesis of all compounds except MB-15-crown-5 and DB-18-crown-6 is described in chapter 2. The experiments were performed in a Pressman type transport cell as described in the experimental part. The transport of the picrate salt was followed by measuring the strong picrate absorption at 356nm in the receiving phase. The measured transport rates were reproducible within 10%. Figure 47 shows the passive transport of potassium picrate with Di-CBZ-L-lys-15-crown-5 as carrier, in order to illustrate a typical passive transport curve.

For monobenzo-15-crown-5, di-CBZ-L-lysine-15-crown-5 and L-lysine-15-crown-5, sodium picrate transport rates increase linearly with the sodium picrate concentration in the source phase, for two concentrations. In contrast, Lamb et al. found the transport rate to increase linearly with the square of the substrate activity.[138] This discrepancy is comes from the fact that the substrate concentration in the present experiments is close to the solubility limit (ca. 0.25 M for sodium picrate). In this situation, the substrate's activity coefficient is does not follow the concentration linearly.

The transport rate of the unprotected lysine crown ether is about six times lower than that of other 15-crown-5 derivatives. This is primarily due to this crown ether's high hydrophilicity, as shown by its K_d of 5.8.[49] The properties of the lysine-15-crown-5 will be discussed in detail in the next chapter.

[49] See experimental part.

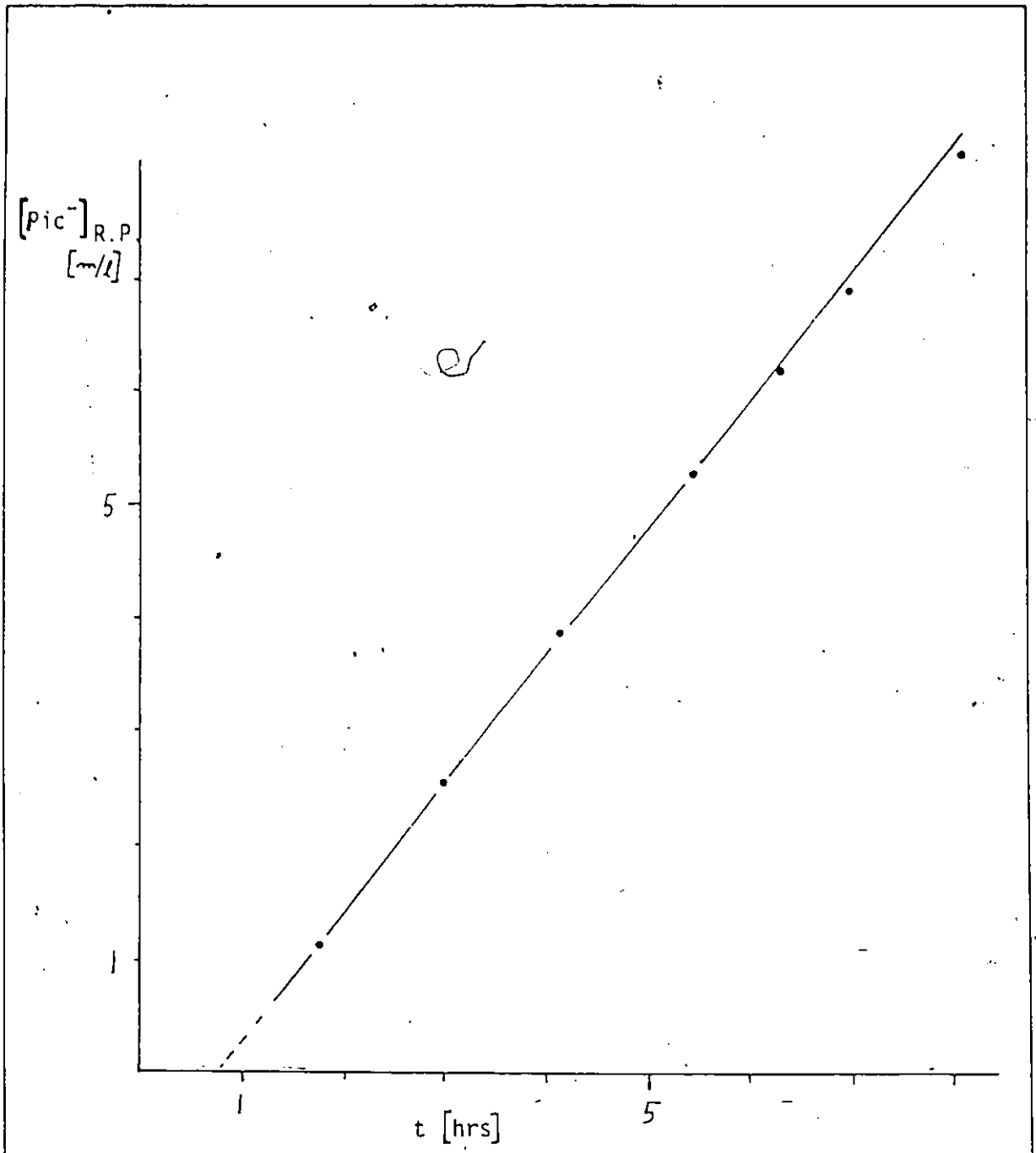

Figure 47: Passive Transport of KPic by Di-CBZ-L-lys-15-crown-5. Picrate concentration in the receiving phase as a function of time. The initial concentrations are potassium picrate in the source phase (0.01 M), and carrier in the membrane phase (0.001 M).

Table 34: Rates of Alkali Cation Transport

	Sodium-picrate (0.024 M)	Sodium-picrate (0.01 M)	Potassium-picrate (0.01 M)
MB-15-crown-5	3.1	1.44	1.36
Di-CBZ-L-lys-15-crown-5	3.6	1.32	1.14
L-lys-15-crown-5	0.58	0.22	-
DB-18-crown-6	0.056	-	3.0
dopamide-15-crown-5	2.8	—	—
Quinoline-15-crown-5	2.4	—	—
CBZ-L-Alanine-15-crown-5	1.9	—	—

The carrier concentration was 0.001 M, the transport rates are given in 10^{-4} mol/hour x liter.

3.2.1 Selectivity

Monobenzo-15-crown-5 and dibenzo-18-crown-6 served as reference compounds. Monobenzo-15-crown-5 shows only a slight preference in transport of sodium over potassium picrate, while dibenzo-18-crown-6 differentiates strongly between these two salts (Tab. 34). These results agree well with the literature data.[138]

Most of the 15-crown-5 derivatives studied show transport rates comparable to the reference compound monobenzo-15-crown-5 (Tab. 34). This indicates that for dopamide-15-crown-5, dopamine-15-crown-5, quinoline-15-crown-5 and di-CBZ-L-lys-15-crown-5 complexes, the crown ring is the only chelating moiety, and that the sidechains do not participate noticably in the binding.

In the 15-crown-5 derivatives studied here, the sidechains are attached to the remote side of the planar benzene ring. Stereo-electronic strain of the sidechain and the entropically unfavourable loss of mobility combine to prevent its intramolecular complexation with a crowned cation.[50] Gokel strongly developed the concept of crown ethers bearing a side chain with additional, neutral, donor groups.[148] He found that interaction with this sidechain can in fact strengthen the cation binding by a factor of about 10. However, this happens only if the sidechain is directly attached to a nitrogen pivot in the crown back-bone; and if the donor atom is in, or close to, the 3' position of the side chain as well.[100]

The following chapter describes the indirect effect of an amine sidechain on sodium picrate transport.

50 This lack of interaction between the ring and the side chain suggests an interesting possibility: bridging the gap between these two binding sites with a zwitterionic molecule. This could well be done with a (chiral) amino acid such as lysine or glutamine. At a pH of about 7, their ε-amine group would be protonated and complexed to the 15-crown-5 or 18-crown-6 crown moiety,[112][169] while the carboxyl group would ion pair with the ammonium group of the side chain.

3.3 Active Transport - Results and Discussion

3.3.1 Introduction

Recent research has concentrated on how ionisable sidechains participate in complexation and cation transport across membranes. They allow for instance to externally drive the cation transport via a pH gradient set up between source and receiving phases. Yet this is only one special case of proton-cation coupling in transport, are there any general rules?

The unprotected L-lysine-15-crown-5 crown ether is an interesting carrier as it combines two potential binding sites: the crown-moiety and the two pendant amino groups of the L-lysine rest. In this study we focused on the internal coupling between the proton, picrate and sodium transport by the ionophore L-lysine-15-crown-5.

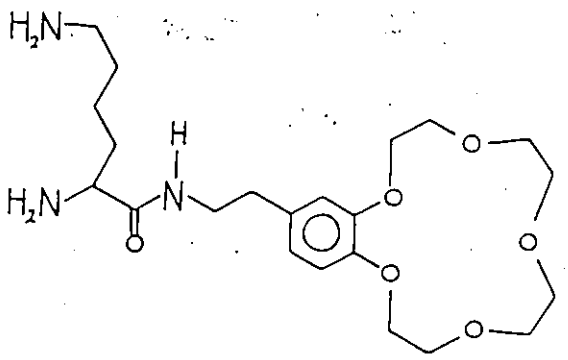

L-Lysine-15-crown-5

3.3.2 Proton and Picrate Transport Profiles

The source phase was initially 0.01 M in NaPic, the membrane phase 0.001 M in L-lysine-15-crown-5. The picrate appearance in the receiving phase (Fig. 48) and the pH in both source and receiving phases (Fig. 49) were measured as functions of time.

Four distinct periods can be identified in the picrate transport curve (Fig. 48):

1. The first 20 min. are an induction period that is observed in all such transport experiments. It's length is determined by the rate of stirring, volume and shape of the three phases, and the diffusional mobility of all species.

2. After this induction period, and during the next six hours, picrate is transported at the constant rate of 4.4×10^{-5} M/hr, which is about two times slower than with the simple 15-crown-5 derivatives (Tab. 34).

3. At t = 6 hrs. the picrate transport rate drops rapidly to about 0.7×10^{-5} M/hr. The picrate concentration in the receiving phase, [Pic]rph, is only 20×10^{-5}M at this point.

4. This rate now remains constant for 25 hrs: it then slowly reduces to 0.4×10^{-5}M/hr. At t = 144 hrs., the concentration of picrate in the receiving phase is only 78×10^{-5}M, while that of the source phase is still 350×10^{-5}M. Thus the picrate concentration gradient is still far from exhaustion.[51]

51 In comparison, Di-CBZ-L-lysine-15-crown-5 maintains a linear transport rate of 13×10^{-5} M/hr beyond a receiving phase concentration of 50×10^{-5}M ([NaPic]init. = 0.01 M). At higher initial NaPic concentration ([NaPic]init. = 0.024 M), linear transport occurs until close to the equilibration of source and receiving phase concentrations in NaPic. This suggests that the rate limiting step occurs at the interface between membrane and receiving phase.[137][142]

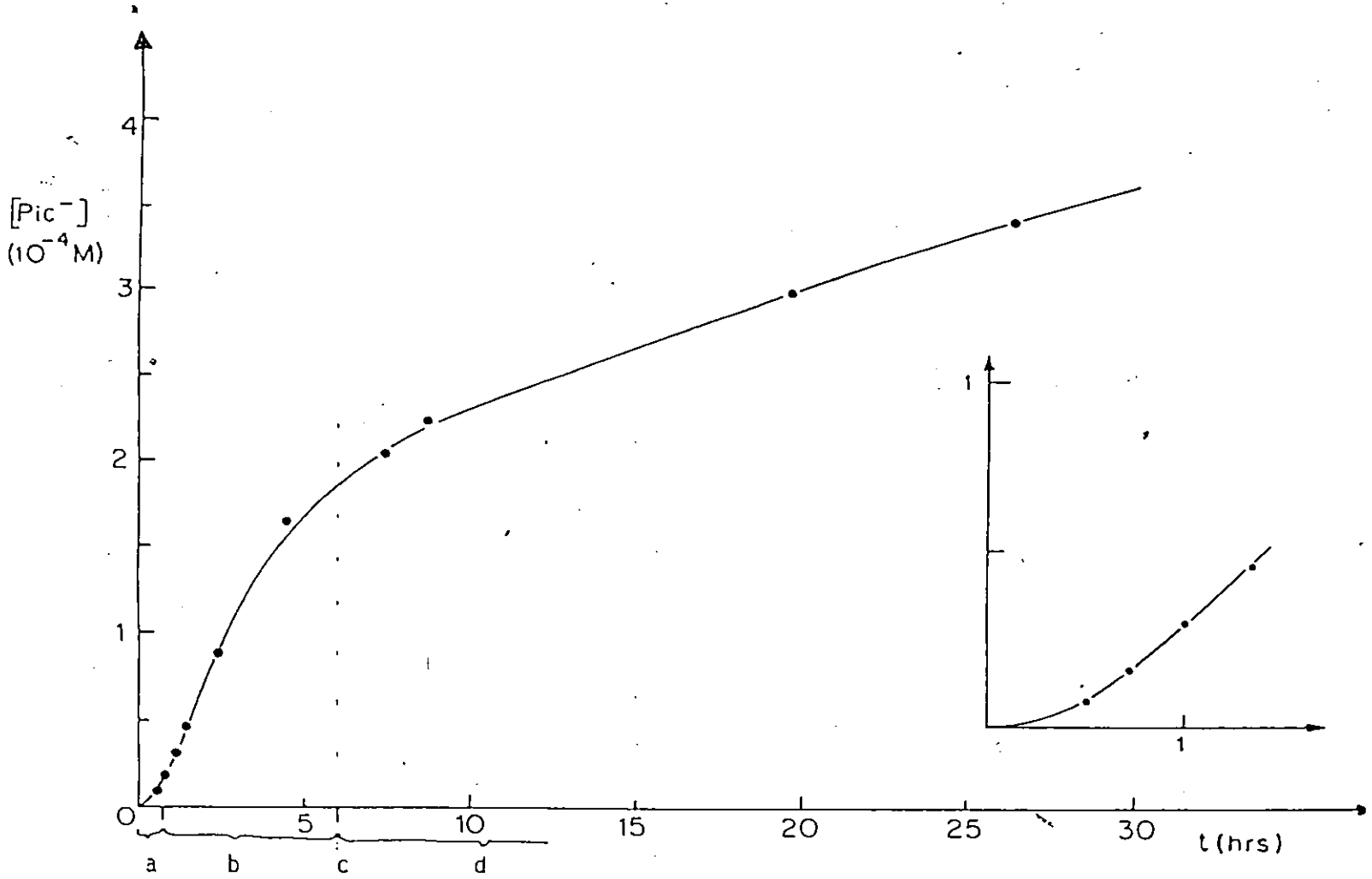

Figure 48: Picrate Transport by l-lys-15-crown-5. The picrate concentration in the receiving phase is measured by UV-Vis. The transport regimes are:
a) Induction; b) Transport; c) Equilibrium Point;
d) Post-equilibrium Transport

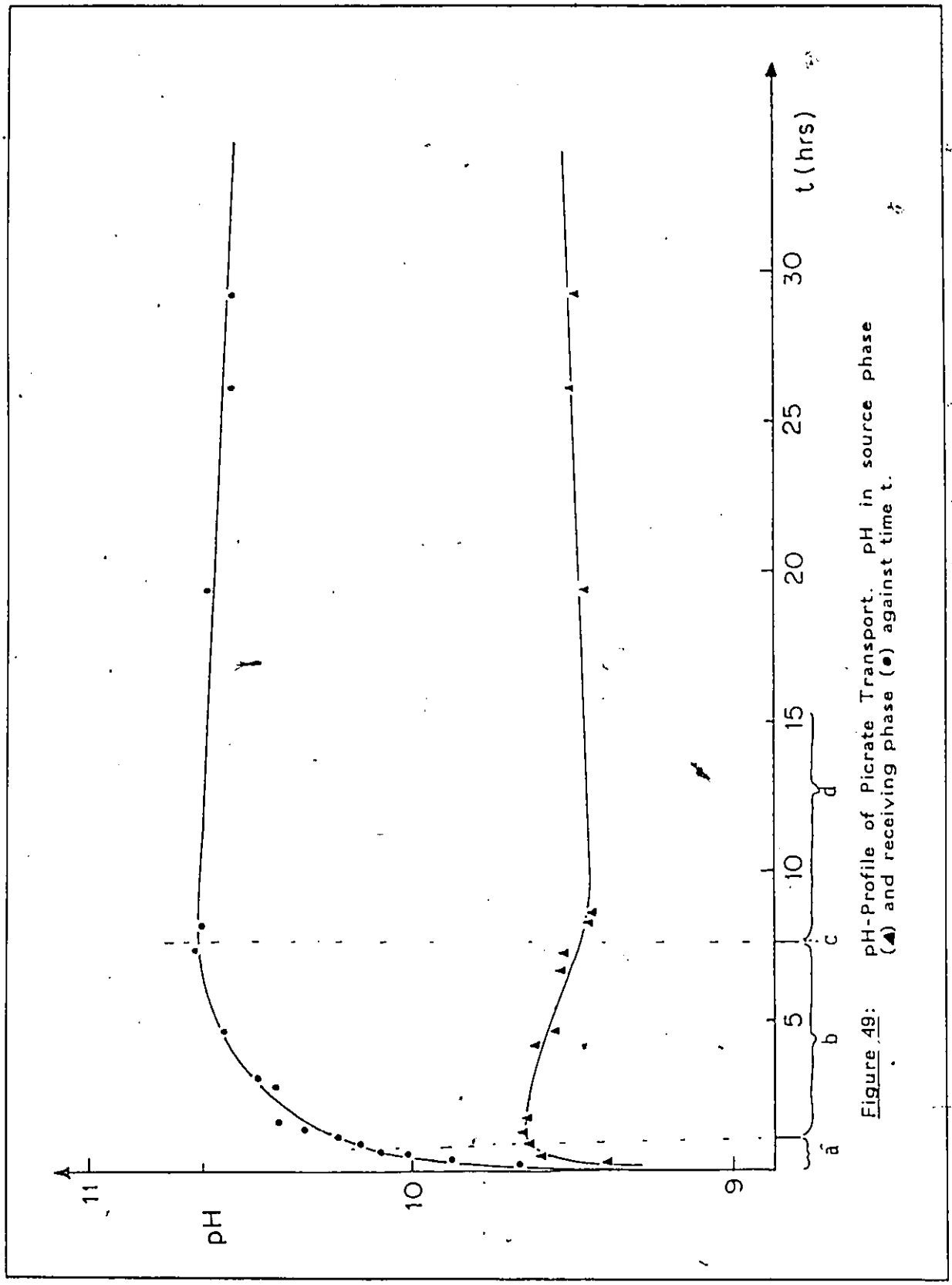

Figure 49: pH-Profile of Picrate Transport. pH in source phase (▲) and receiving phase (●) against time t.

Thus the transport of picrate by L-lys-15-crown-5 slows down long before the picrate concentration reaches equilibrium. The key to this system lies in the pH diagrams (Fig. 49). Here we can again distinguish four regions:

1. The induction period of again about 20 min shows a rapid increase in pH: from 7.0 to 9.65 in the receiving phase and from 7.0 to 10.3 in the source phase, respectively.

2. For the next seven hours the pH of the source phase continues to increase much more slowly: from 10.3 to 10.7. But more important is the reversal of the pH variation in the receiving phase, that is an acidification from pH 9.65 to pH 9.40 during the same time.

3. At t = 7 hours, the pH gap between source phase and receiving phase has reached its maximum: Both pH curves level off.

4. After t > 7 hours, the pH gap begins to close again very slowly.

3.3.3 Discussion and Interpretation

The drastic and simultaneous changes in both proton and picrate transport rates suggests a close coupling between these two. The interpretation of these observations is based on the chemical properties of the carrier, L-lysine-15-crown-5. Figure 50 shows all possible states that the carrier can attain in this transport system. The initial neutral carrier will partially protonate at the interfaces between the membrane and the aqueous phases; further both protonated and unprotonated carrier will enter into a complexation equilibrium with the sodium picrate of the source

52 The protonated complex (HCC in Fig. 50) will probably exist only in low concentration.

phase.[52]

At t = 0, all of the carrier resides in the membrane in its neutral form C. The move of this non-equilibrium system moves along its osmotic gradients can be described by four phases that can be correlated with the four distinct transport phases observed in Figs. 48 and 49:

1. During the induction period, the neutral amine C is partly extracted into the two aqueous phases. There, by complexation and protonation, it reaches equilibrium with the species CC, HC and HCC.[53] As a result both aqueous phases turn alkaline during the induction period.[54]

2. The cationic species CC,HC and HCC, accompanied by picrate counteranions, can now diffuse back into the membrane phase. Both the high concentration of sodium picrate and the lipophilicity of the counter anion picrate promote this process.[138] Eventually CC, HC and HCC will reach the receiving phase. Here they become trapped: The relative lack of lipophilic counter anion in the receiving phase prevents these three cationic species from escaping back into the membrane phase. Only in its neutral form, as C, can the carrier diffuse back to the source phase. Thus there are three possible transport cycles (see Fig. 51): CC carries sodium picrate (NaPic), HC carries picric acid (HPic), and HCC can carry both together. The resulting net transport of picric acid explains the widening of the pH gap between the two aqueous phases during the transport period.

53 This equilibrium is thermodynamically controlled by the complexation constant and the two amine pK_a values ($pK_a(\alpha) = 7.2$; $pK_a(\varepsilon) = 10.5$; see chpt. 3.4.3.); and kinetically controlled by the diffusion of carrier and complex molecules across the quiescent Nernst layer close to the phase boundaries.

54 A blank experiment in the absence of salt was done to test the pH development with time due to environmental effects, especially carbondioxide from the air. After the simultaneous addition of distilled water to the membrane phase containing (being 1mM in L-lysine-15-crown-5), the pH in both source and receiving phases rose within 20 min to 9.65, and stayed constant at this level for over 40 hrs.

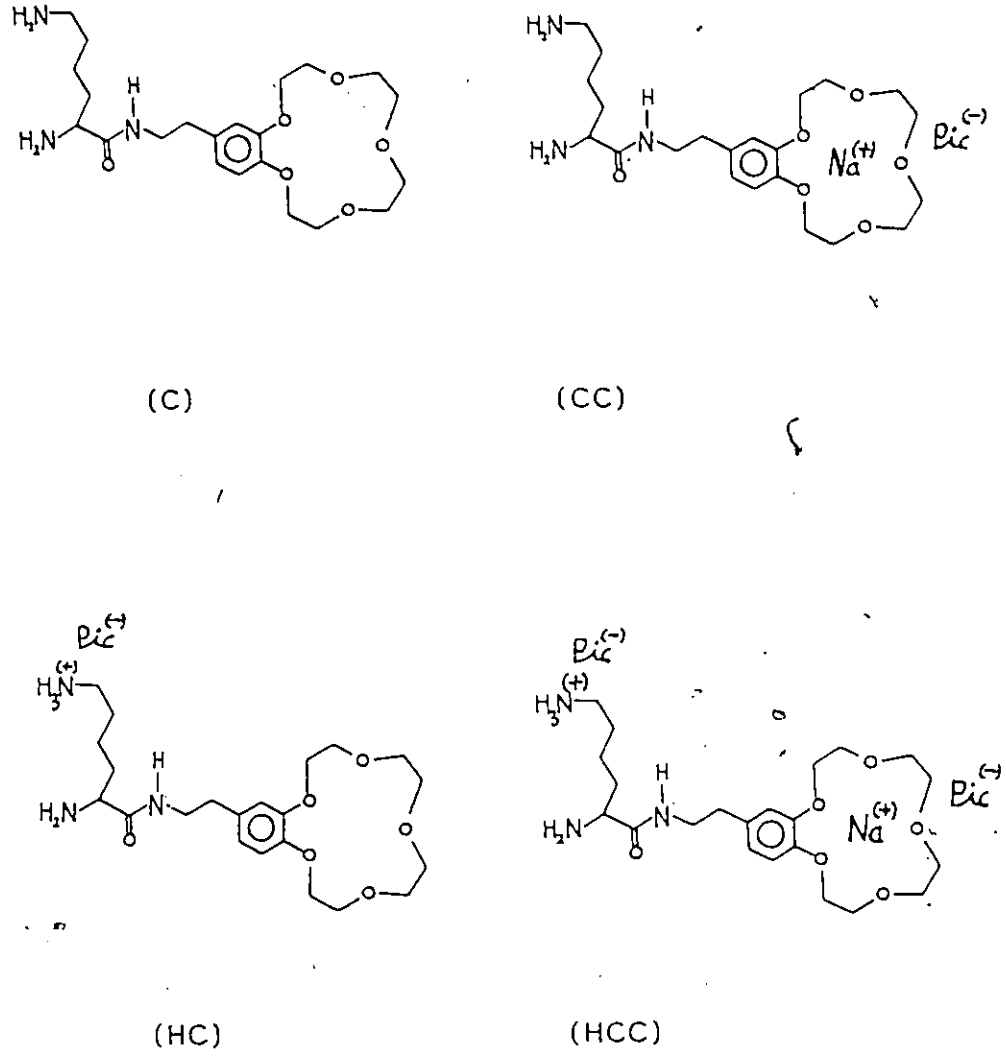

Figure 50: Different States of the Carrier L-lys-15-crown-5. Neutral carrier L-lys-15-crown-5 (C); sodium picrate complex (CC); ε-protonated carrier (HC); ε-protonated sodium complex (HCC). The α-amine, with its pK_a of ~~7.2~~, will not be significantly protonated above pH 9.5.

This NaPic-HPic co-transport during period B. depletes the source phase of the protonated carrier species HC and HCC as well as of NaPic. Meanwhile in the receiving phase, the concentrations of both the protonated carrier species HC and HCC, and of picrate, increase due to the continuous influx from the source phase. This increases the chemical potential of species HC and HCC in the receiving phase. Eventually, the forward transport by HC is stopped by the induced proton gradient. HCC continues to transport, driven by it's stronger dependence on the picrate gradient, and induces a HC back transport.

3. At t = 7 hours, the remaining forward chemical potential of HCC is counterbalanced exactly by the induced reverse chemical potential of HC (Fig. 51). As a result, the transport of picric acid across the membrane stops. as can be diagnosed from the plateaux in the pH curves at this time (Fig. 49).

4. Were they stoichiometrically coupled, as is the case with many carboxylic acid ionophores, both sodium picrate and picric acid transport should end here.[146][162] But in this system the carrier pairs CC-C and HCC-HC continue to transport sodium picrate, independantly of the proton gradient. This gives us a residual 'picrate leak' from source to receiving phase.[162][55] However, it is exactly this picrate gradient that supported the induced proton gradient via the carrier couple HC-C and HCC-CC. The slow collapse of this picrate gradient will therefore cause the concomitant collapse of the induced proton gradient. We can see this process (Fig. 51 D.) in the slow narrowing of the pH gap starting at t = 7 hours (Fig. 49).

55 The picrate transport rate of 0.7 - 0.4 x 10^{-5} M/hr measured at this time - compared with the transport rates of 13 x 10^{-5} M/hr for lipophilic 15-crown-5 derivatives - indicates that only a small part of the total carrier is available for the carrier couple CC-C, even when we consider the preference of the carrier for an aqueous environment.

Figure 51 shows schematically the four proposed transport periods.

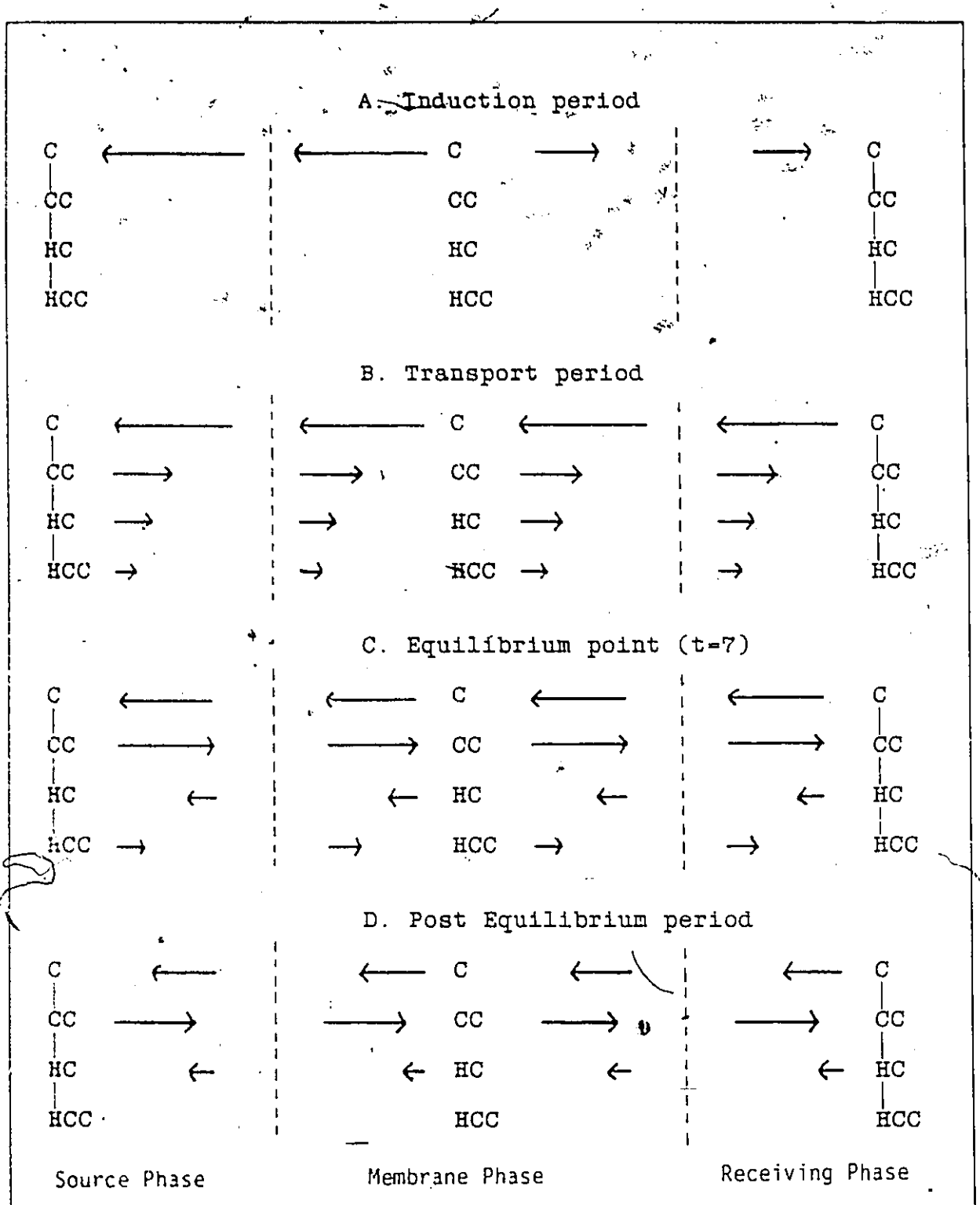

Figure 51: Transport Phases for L-lys-15-crown-5. C, CC, HC and HCC stand for the carrier species as described in Fig. 50.

3.3.4 Condensed Interpretation of the Active Transport

1. INDUCTION PERIOD A.

The initial alkalinization of the source and receiving phases is caused by extraction of the carrier compound (in base form) into the aqueous phases and equilibration with its conjugate acid form. Alkalinization is stronger in the source phase (pH=10.3) than in the receiving phase (pH=9.64), probably due to the picrate-driven redistribution of $\mathcal{E}$-monoprotonated carriers HC and HCC back into the membrane phase.

2. TRANSPORT PERIOD B.

The sodium picrate complex CC carries sodium picrate; the $\mathcal{E}$-monoprotonated species HC carries picric acid; and the $\mathcal{E}$-monoprotonated carrier complex HCC can carry both. These transports are driven by the initial sodium and picrate concentration gradients. (molecular transport, ionophoric transport)

3. EQUILIBRIUM POINT C.

At t = 6-7 hrs, the induced reverse proton gradient counterbalances the residual sodium picrate gradient such that the net picric acid transport by HC and HCC is nil. CC and HCC continue to transport sodium picrate.

4. POST-EQUILIBRIUM PERIOD D.

The residual NaPic transport via the carrier couples HCC-HC and CC-C allows for the slow collapse of the induced proton gradient via the couple HC-HCC.

3.3.5 Discussion of Transport Model

The model has somewhat speculative character, since the individual carrier species are only deduced from the chemical nature of the system, not actually identified.

However, the model is in good agreement with the chemical properties of the system: Both organic ammonium picrate salts (HC) and crowned sodium picrate are well known to diffuse across methylene chloride membranes. The enhanced alkalinization of the source phase can be attributed to a salting-in effect, an increased pK_a in the presence of salt, and to the redistribution of acid forms of the carrier (HC and HCC) into the membrane.

The protonated complex HCC will exist only in low concentrations, so that it's role in the transport processes will probably not be evident, considering the experimental uncertainties. Further, in a mathematical model, it's transport functions could probably be filfilled by a combination of HC and CC, so that HCC would not be nessecary to fit the model to the experimental data. Nevertheless, HCC has been included in the theoretical analysis presented here, partly because it's role should not be disregarded perhaps prematurely at this early stage of investigation, and partly to aid in an appreciation of the complexity of the system.

3.3.6 Conclusion

This study explains how an induced (proton) concentration gradient can:

1. counterbalance the original concentration gradient of the substrate picrate and stop its transport long before it reaches its chemical concentration equilibrium;

2. regulate the transport rate of a third substrate (here Na^+) by changing its transport path via the carrier species HCC. Further we can see how the relaxation of a simple initial

concentration gradient produces a complex co- and counter-transport profile, involving three substrates: protons, sodium, and picrate.

Effect 1 constitutes an auto feedback loop, whereas effect 2 exemplifies how the transport of three or possibly more substrates may be regulated in biochemical transport systems.

3.4 Experimental Part - Transport

3.4.1 Passive Transport

The experiments were performed in a Pressman type transport cell similar to that described by Lamb et al.,[139] at 25.0 (0.5) °C.

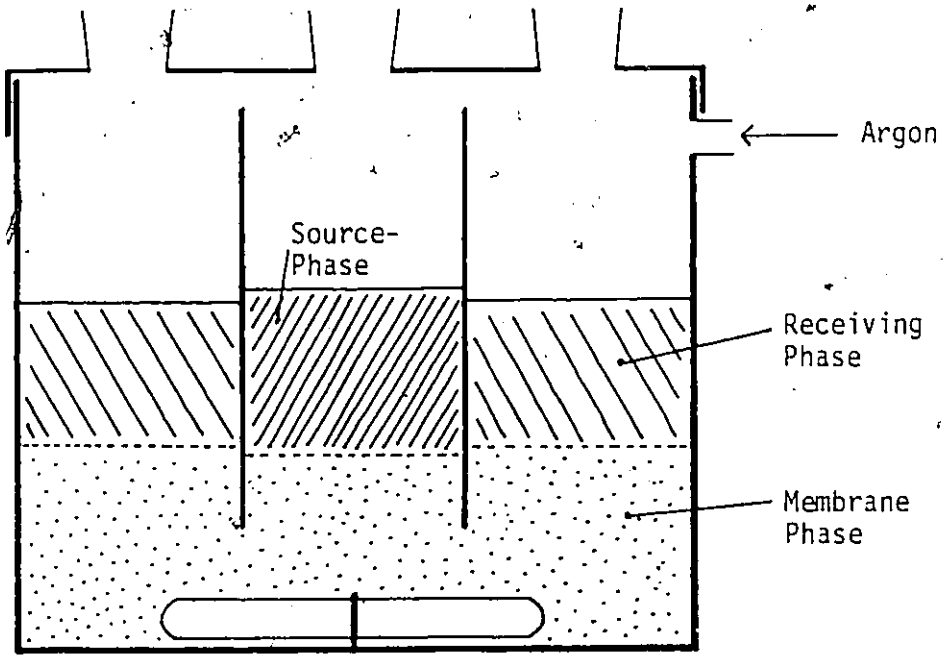

Figure 52: Transport Cell utilized in this Study. For description see text.

Two aqueous phases were separated by a methylene-chloride phase representing the membrane. The aqueous source phase consisted of 25 ml 10 mmolar sodium or potassium picrate (2.5×10^{-4} moles picrate salt) at pH 7.0. The stock solutions were obtained by neutralizing a stock solution of the proper hydroxide with picric acid. The concentrations were checked via the visible light

absorption of picrate at 356nm (ε = 17280).[56]

The aqueous receiving phase consisted of 100 ml dist. water, which was decarbonated by boiling and adjusted to pH 7.0 with NaOH. The organic membrane phase consisted of 175 ml distilled and washed methylene chloride. It was 1 mmolar in the corresponding carrier (1.75×10^{-4} moles carrier). The membrane phase was stirred with a magnetic stirring bar, driven by a constant speed motor at 85 r.p.m.. The interfaces between the aqueous source and receiving phases, and the organic membrane phase were 9.1 and 37.6 cm^2, respectively. The picrate transport was followed by measuring the appearance in the receiving phase of the strong picrate absorption at 356 nm, with ε = 17280, on a Varian DMS 90 UV VISIBLE spectrophotometer.

The procedure for a passive transport experiment was as follows: 175 ml membrane stock solution was placed in the transport cell first. Then simultaneously 25 ml source phase and 100 ml receiving phase stock solution were added into their respective compartments at time t=0. A close-fitting cell cover reduced methylene chloride loss to a negligible amount. 5 ml of the receiving phase were sampled at varying time intervals to measure the picrate concentration. They were replaced by 5 ml dist. water, and the resulting dilution corrected for in the data analysis.

During the induction period of 20 min, the membrane phase would slowly turn yellow. At the end of this period, picrate would begin to be visible in the receiving phase. Following this induction period, the transport of picrate occurred linearly with time for 8 to 10 hours. Then exhaustion of the concentration gradient would slowly begin to decrease the transport rate. The given values for the transport rates were taken from this initial linear period of the transport.

Upon addition of the source phase into the central compartment of the transport cell, the methylenechloride membrane phase would often turn opaque or milky. This apparent microemulsion was caused by the substantial amounts of water dissolved in the methylenechloride, and

56 Kimura reports the adsorption coefficient ε for picrate salts in aqueous solutions at 356nm as 13200.[156] Haines states it is 15000;[103] Shinkai 17280.[168]

would persist from twenty minutes to several hours. It was unrelated to the presence or absence of the different carriers, and did not affect the measured transport rates.

3.4.2 Active Transport

The experimental set-up was identical to that used in the passive transport experiments, except that a special cell cover featuring three ports was used. These ports allowed for sampling the receiving phase and insertion of the pH electrode. At the same time an argon atmosphere was maintained to successfully protect the basic aqueous phases from carbon dioxide of the air. The pH-development in both source phase and receiving phase were followed with a Canlab H4360-50 glass pH electrode in combination with a Corning 155 pH/ion meter, to an accuracy of better than 0.005 pH units.

Both source and receiving phase were initially adjusted to pH 7.00 with sodium hydroxide.[57] The methylenechloride used for the membrane phase was distilled and washed with water of pH 7.00. A blank experiment in the absence of carrier showed a picrate leakage rate of less then 0.1 percent of the carrier facilitated rate.[137][162]

3.4.3 Determination of pK_a values for L-lysine-15-crown-5

The pK_a values of L-lysine-15-crown-5 (6c) were determined by a pH titration of 100 mg (6c) in 50 ml potassium hydroxide solution (pH=12.1) against 0.01 M HCl. Fig. 53 shows the variation of pH with volume HCl (0.01 M) added. The $pK_a(\alpha)$ at 7.2 was taken as the minimum in the first derivative of the pH versus vol(HCl) curve. The volume of HCl corresponding to the difference between the titration steps 1 and 2 (7 ml) was taken as equivalent to one amine. The

57 The traces of sodium introduced here to the receiving phase, as well as the minute leakages of potassium chloride into the source phase through the liquid junction of the glass electrode, are negligible compared to the total concentrations of sodium picrate.

$pK_a(\varepsilon)$ was then obtained by substracting 7 ml HCl from the volume corresponding to $pK_a(\alpha)$, and graphically measuring the related pH value (pH = $pK_a(\varepsilon)$ = 10.5. This value is in good agreement with the value reported for the ε-amine of free L-iysine: 10.55.

The distribution coefficient K_d between H_2O (initial pH=7) and CH_2Cl_2 is 5.8.[58]

58 5 ml methylene chloride (1 mmolar in L-lysine-15-crown-5) and 5 ml dist. water (pH 7.00) were intensively emulsified for 15 min.. Then 2 ml of each phase were UV-spectranalyzed for the aromatic absorption at 280 nm. ε (280) was 3019 in methylenechloride; the final pH in the aqueous phase was 9.64.

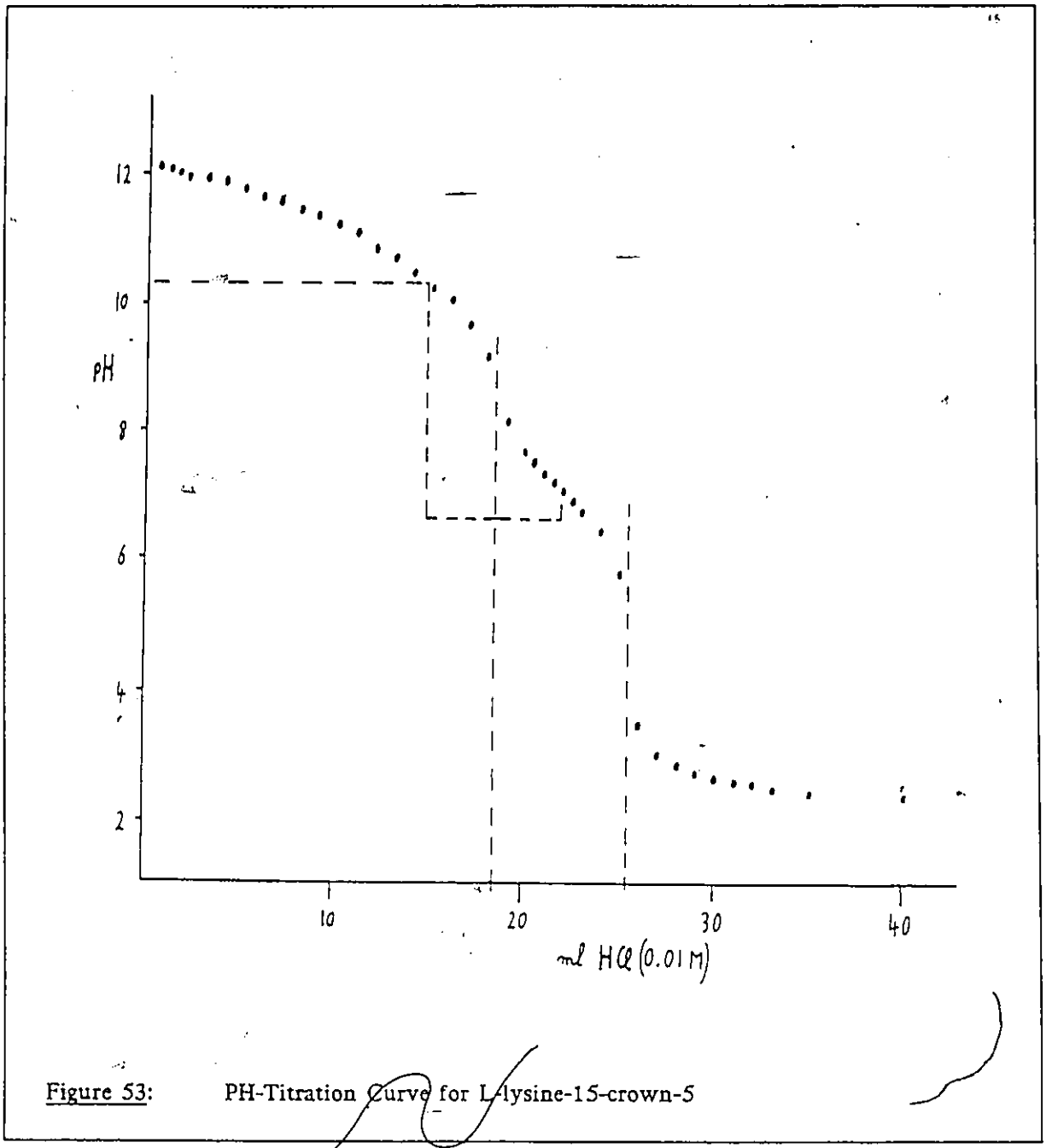

Figure 53: PH-Titration Curve for L-lysine-15-crown-5

3.5 Appendix 1 - Complexation Constant in Pyridine

The calculation of the complexation constant of sodium with dibenzo-24-crown-8 in pyridine uses the following expression:

$$(Na^+)_s + (C)_s \underset{}{\overset{K_c}{\rightleftharpoons}} (Na^+;C)_s$$

$$K_c = \frac{[NaC]}{[Na][C]} = \frac{[Na]_T - [Na]}{[Na]([C]_T - [Na]_T + [Na])}$$

$$[Na] = -\frac{[C]_T - [Na]_T + K_C^{-1}}{2} + \left(\frac{[Na]_T}{K_C} + \frac{([C]_T - [Na]_T + K_C^{-1})^2}{4}\right)^{0.5}$$

$$[NaC] = [Na]_T - [Na]$$

3.6 Appendix 2 - Concentration Analysis

The chemical system is:

$$(Na^+)_s + (X^-)_s \quad \underset{\rightleftharpoons}{\overset{K_P}{\rightleftharpoons}} \quad (Na^+, X^-)_s$$

$$K_P = \frac{[NaX]}{[Na][X]} = \frac{[Na]_T - [Na]}{[Na]^2}$$

$$[Na]^2 + \frac{[Na]}{K_P} = \frac{[Na]_T}{K_P}$$

$$[Na] = -\frac{1}{2K_P} + \left(\frac{[Na]_T}{K_P} + \frac{1}{4K_P^2}\right)^{0.5}$$

$$[NaX] = [Na]_T - [Na]$$

3.7 Appendix 3 - Complexation Analysis

Expression for the observed chemical shift as a function of ion-pairing and complexation:

$$(Na^+)_f + (X^-)_f \underset{}{\overset{K_P}{\rightleftharpoons}} (Na^+, X^-)_f$$

$$(Na^+)_f + (C)_f \underset{}{\overset{K_C}{\rightleftharpoons}} (Na^+, C)_f$$

$$K_P = \frac{[NaX]}{[Na][X]} = \frac{[Na]_T - [Na] - [C]_T^*}{[Na]^2 + [Na][C]_T}$$

* This contains the assumption $[NaC] = [C]$.

$$[Na]^2 + [Na]\left(\frac{[C]_T K_P + 1}{K_P}\right) = \frac{[Na]_T - [C]_T}{K_P}$$

$$[Na] = -\frac{K_P[C]_T + 1}{2K_P} + \left(\frac{[Na]_T - [C]_T}{K_P} + \frac{(K_P[C]_T + 1)^2}{2K_P^2}\right)^{0.5}$$

$$[NaX] = K_P[Na][X] = \frac{K_P[Na][Na]_T}{1 + K_P[Na]_T}$$

3.8 Appendix 4 - Aggregation Model

$$(Na^+)_s + (C)_s \rightleftharpoons (Na^+, C)_s$$

$$(Na^+, C)_s + (Na^+)_s \rightleftharpoons (Na_2^+, C)_s$$

$$(Na_2^+, C)_s + (Na^+, C)_s \rightleftharpoons (Na_3^+, C_2)_s$$

$$(Na_i^+, C_{i-1})_s + (Na^+, C)_s \rightleftharpoons (Na_{i-1}^+, C_i)_s$$

$$[NaC] = K_c [C][Na]$$

$$[Na_2C] = K_C [C][Na] K_2 [Na]$$

$$[Na_3C_2] = (K_C [C][Na])^2 K_2 [Na] K$$

$$[Na_{n+1}C_n] = K_C [C][Na]^n K_2 [Na] K^{n-1}$$

Set $K_1 [C][Na] K = X = [NaC] K$

Then:

$$[NaC] = \frac{X}{K}$$

$$C_1 = [Na_2C] = X \frac{K_2}{K} [Na]$$

$$C_2 = [Na_{n+1}C_n] = X_n \frac{K_2}{K} [Na]$$

The observed longitudinal relaxation rate is the sum of contributions from all sodium species:

$$\frac{1}{T_{1,obsd}} = \frac{P_f}{T_{1,f}} + \frac{P_C}{T_{1,C}} + \sum_{n=1}^{\infty} P_n/T_{1,n}$$

$$\text{where:} \qquad P_n = \frac{[Na_{n+1}C_n]}{[Na]_T}$$

$$\text{and:} \qquad \frac{1}{T_{1,n}} = \left(\frac{2}{T_{1,out}} + \frac{n-1}{T_{1,in}}\right) n$$

$1/T_{1,n}$ is the relaxation rate of $(Na^+_{n+1}, C_n)_s$, assuming 2 'out' binding units and (n-1) internal binding units for sodium cations. The factor n accounts for the increase of r_c with aggregate size.

$1/T_{1,agg}$ is the contribution of all aggregate species to $1/T_{1,obsd}$:

$$\frac{1}{T_{1,agg}} = \frac{\sum_{n=1}^{\infty} [Na] \frac{K_2}{K} X^n (T_{1,n})^{-1}}{[Na]_T}$$

$$= P_f \frac{K_2}{K} \sum_{n=1}^{\infty} X^n (T_{1,n})^{-1}$$

$$= P_f \frac{K_2}{K} \sum_{n=1}^{\infty} nX^n \left(\frac{2}{T_{1,out}} + \frac{n-1}{T_{1,in}}\right)$$

$$= P_f \frac{K_2}{K} \sum_{n=1}^{\infty} nX^n \left(\frac{2}{T_{1,out}} - \frac{2}{T_{1,in}} + \frac{n+1}{T_{1,in}}\right)$$

$$= P_f \frac{K_2}{K} \left(\frac{X}{(1-X)^2}\left(\frac{2}{T_{1,out}} - \frac{2}{T_{1,in}}\right) + X \sum_{n=1}^{\infty} (n+1)\, nX^{n-1} (T_{1,in})^{-1}\right)$$

$$= P_f \frac{K_2}{K} \left(\frac{X}{(1-X)^2}\left(\frac{2}{T_{1,out}} - \frac{2}{T_{1,in}}\right) + \frac{2X}{(1-X)^3} \frac{1}{T_{1,in}}\right)$$

$$= 2P_f \frac{K_2}{K} \frac{X}{(1-X)^2}\left((T_{1,out})^{-1} - (T_{1,in})^{-1} + ((1-X)T_{1,in})^{-1}\right)$$

Finally:

$$\frac{1}{T_{1,obsd}} = \frac{P_f}{T_{1,f}} + \frac{P_C}{T_{1,C}} + \frac{1}{T_{1,agg}}$$

The sums could be solved by two series expansions:

$$\sum_{n=1}^{\infty} nX^n = \frac{X}{(1-X)^2}$$

$$\sum_{n=1}^{\infty} X^n = \frac{1}{1-X}$$

$$\sum_{n=1}^{\infty} nX^n = \frac{1}{(1-X)^2}$$

$$\sum_{n=1}^{\infty} n(n-1)X^{n-2} = \sum_{n=1}^{\infty} n(n+1)X^{n-1} = \frac{2}{(1-X)^3}$$

Now $1/T_{1,obsd}$ is a function of K_c, K_2, K, $T_{1,out}$, $T_{1,in}$, $[Na]$ and $[C]$. $[Na]$ and $[C]$ are themselves functions of K_c, K_2, K, $[Na]_T$ and $[C]_T$:

$$[Na]_T = [Na] + [NaC] + \sum_{n=1}^{\infty} (n+1)\, C_n$$

$$[C]_T = [C] + [NaC] + \sum_{n=1}^{\infty} (n+1)\, C_n$$

$$\text{where:} \qquad C_n = K_2[Na]X^n/K$$
$$\text{and:} \qquad X = K_c K [Na][C]$$

Then:

$$[Na]_T = [Na] + [NaC] + \frac{K_2[Na]}{K} \sum_{n=1}^{\infty} (n+1)\, X^n$$

$$[C]_T = [C] + [NaC] + \frac{K_2[Na]}{K} \sum_{n=1}^{\infty} n\, X^n$$

and after series expansion:

$$[Na]_T = [Na] + [NaC] + \frac{K_2[Na]}{K} \left(\frac{1}{(1-X)^2} - 1 \right)$$

$$[C]_T = [C] + [NaC] + \frac{K_2[Na]}{K} \frac{1}{(1-X)^2}$$

Or:

$$[Na]_T = [Na] + K_c[Na][C] + \frac{K_2[Na]}{K} \left(\frac{1}{(1 - K_c K[Na][C])^2} - 1 \right)$$

$$[C]_T = [C] + K_c[NaC] + \frac{K_2[Na]}{K} \frac{K_2 K[Na][C]}{(1 - K_c K[Na][C])^2}$$

The last two equations contain $[Na]$ and $[C]$ as functions of each other, as well as of K_c, K, K_2, $[C]^T$ and $[Na]_T$. I can numerically solve the two expressions for $[Na]$ and $[C]$, a simultaneous Newton-gauss procedure.

3.9 Appendix 5 - Shift and Relaxation Data for NaPF6

The full tables of shift and relaxation data at three fields for $NaPF_6$ in nitromethane. $[NaPF_6]$ = 0.037M. $1/T_2obsd = \pi \upsilon 1/2$; $1/T_2ex = 1/T_2obsd - 1/T_1 - 1/T_2inh$. The estimated measurement errors are given in percent under the table heading. The errors for (k_a+k_b) are absolute cummulative errors. The experimental inhomogeneities to the transverse relaxation, $1/T_2inh$, are 10 Hz, 30 Hz and 0 Hz at 79.35 MHz, 53.2 MHz and 21.04 MHz.

Table 35: $NaPF_6$ Data - 79.35 MHz

ρ	$1/T_2obsd$ [s^{-1}] (1%)	$1/T_2ex$ [s^{-1}] (5%)	δ [ppm] (0.5%)	k_a+k_b [$10^4 s^{-1}$]
0.0	36	-	-14.81	-
0.1	113	55	-14.18	1.7 (0.2)
0.2	174	102	-13.54	1.6 (0.1)
0.3	226	137	-12.93	1.6 (0.1)
0.4	267	158	-12.19	1.61 (0.07)
0.5	286	165	-11.57	1.61 (0.07)
0.6	295	157	-10.76	1.62 (0.08)
0.7	292	142	-10.16	1.58 (0.08)
0.8	263	99	-9.45	1.7 (0.1)
0.9	226	45	-8.71	2.00 (0.3)
0.95	206	20	-8.37	2.1 (0.5)
1.00	-	-	-8.20	-
1.05	195	5	-8.22	-
1.15	195	2	-8.21	-
1.5	192	0	-8.20	-

Table 36: $NaPF_6$ Data - 53.2 MHz

ρ	$1/T_2$obsd [s^{-1}]	$1/T_1$ [s^{-1}]	$1/T_2'$ex [s^{-1}]	δ [ppm]	k_a+k_b [$10^4 s^{-1}$]
(2%)	(1%)	(2%)	(5%)	(0.5%)	
0.0	40	30	-	-14.83	-
0.1	98	48	20	-14.20	2.2 (0.5)
0.2	134	63	41	-13.55	1.9 (0.2)
0.3	170	79	61	-12.95	1.6 (0.2)
0.4	197	99	68	-12.19	1.7 (0.1)
0.5	217	111	76	-11.61	1.6 (0.1)
0.6	226	128	68	-10.78	1.7 (0.1)
0.7	233	140	63	-10.18	1.6 (0.1)
0.8	230	154	46	-9.49	1.7 (0.2)
0.9	224	172	22	-8.73	2.0 (0.4)
0.95	214	176	7	-8.38	3.2 (2)
1.00	210	181	-	-8.25	-
1.05	210	180	-	-8.24	-
1.15	-	183	-	-	-
1.5	212	181	-	-	-

Table 37: $NaPF_6$ Data - 21.04 MHz

P	$1/T_2$obsd [s^{-1}]	$1/T_2$ex [s^{-1}]	δ [ppm]	k_a+k_b [$10^4 s^{-1}$]
(2%)	(4%)	(50%)	(2%)	
0.0	30	-	-14.2	-
0.1	53	5	-13.5	1.4 (1)
0.2	70	8	-12.9	1.6 (1)
0.3	90	10	-12.3	1.7 (0.8)
0.4	110	11	-11.5	1.7 (0.7)
0.5	126	15	-10.9	1.4 (0.5)
0.6	144	16	-10.1	1.2 (0.5)
0.7	152	13	-9.5	1.4 (0.5)
0.8	164	10	-8.8	1.3 (0.8)
0.9	180	8	-8.0	0.9 (1)
0.95	177	1	-7.6	5 (20)
1.00	178	-	-7.4	-
1.05	181	-	-7.4	-
1.15	-	-	-	-
1.5	180	-	-7.4	-

3.10 Appendix 6 - Full Line-Shape Analysis of Exchange Broadened Lines

Below the line shape expression used in the kinetic analysis is given, as taken from the literature.[19] It is derived from the Bloch equations modified to account for exchange between two uncoupled spins. The amplitude C_0, the life time , and the chemical shift of the free sodium were used as parameters to fit the expression to 20 - 60 data-points that were manually taken from the spectrum. A SIMPLEX routine was used for the fitting procedure.

$$v = -C_0 \frac{\left\{P\left[1 + \tau\left(\frac{p_B}{T_{2A}} + \frac{p_A}{T_{2B}}\right)\right] + QR\right\}}{P^2 + R^2}$$

$$\delta\nu = \nu_A - \nu_B, \Delta\nu = 0{\cdot}5\,(\nu_A + \nu_B) - \nu$$

$$P = \tau\left[\frac{1}{T_{2A} \cdot T_{2B}} - 4\pi^2\Delta\nu^2 + \pi^2(\delta\nu)^2\right] + \frac{p_A}{T_{2A}} + \frac{p_B}{T_{2B}}$$

$$Q = \tau[2\pi\Delta\nu - \pi\delta\nu(p_A - p_B)]$$

$$R = 2\pi\Delta\nu\left[1 + \tau\left(\frac{1}{T_{2A}} + \frac{1}{T_{2B}}\right)\right] + \pi\delta\nu\tau\left(\frac{1}{T_{2B}} - \frac{1}{T_{2A}}\right) + \pi\delta\nu(p_A - p_B)$$

$$\tau = \frac{p_A}{k_B} = \frac{p_B}{k_A}$$

Chapter IV

CLAIMS TO ORIGINAL RESEARCH

For the exchange of sodium between solvated state and the dibenzo-24-crown-8 complex in nitromethane, the exchange contribution to the sodium-23 transverse nuclear magnetic relaxation rates has been obtained directly, by substracting the longitudinal relaxation rates and the inhomogeneity relaxation rates from the observed transverse relaxation rates.

Using this exchange relaxation as an analytical tool, both the classical unimolecular decomplexation, as well as the bimolecular cation interchange have been determined for several sodium salts and dibenzo-24-crown-8 in nitromethane. This is one of the first times that the bimolecular cation interchange has been clearly described.[59]

Both exchange mechanisms were shown to dominate at different concentrations; the unimolecular mechanism near the low concentration limit, and the bimolecular mechanism at concentrations above 0.001 M.

The longitudinal relaxation rates of sodium tetraphenylborate in the presence of dibenzo-24-crown-8 in nitromethane revealed stacking of planar 1:1 complexes to larger aggregates. The stronger coordinating anions hexafluorophosphate, iodide and thiocyanate inhibit this aggregation; in fact they enter into solvent-separated (PF_6^-) and contact (I^-, SCN^-) ion-pairing equilibria with the sodium cation. At the low concentrations used (between 0.01 M and 0.000012 M), the secondary ion-solvent interactions are concentration independent, so that the observed concentration dependencies of chemical shifts and relaxation rates could be quantitatively interpreted as direct bimolecular interactions. The ion-pairing parameters have been determined from sodium-23

[59] Popov independently described the bimolecular exchange around the same time.[51][52]

chemical shifts and relaxation rates, and their effects on complexation and exchange quantitatively accounted for. The combined use of all three sodium-23 NMR parameter proved necessary to separate and analyze, within one system, ionic interactions, 1:1 and 2:1 complexation as well as exchange rates and mechanisms.

Further, four novel aminoacid-derivatized 15-crown-5 and a novel adrenaline-derived 30-crown-10 ligand have been synthesised. For the first time, sodium-23 NMR was used for the structure determination of an organic compound.

Finally, several of the synthesised crown ethers were studied regarding their passive transport of sodium and potassium picrate through a bulk methylene chloride membrane. One of the compounds, L-lysine-15-crown-5, demonstrated a marked capacity for the coupled co-transport of sodium picrate and picric acid. A transport model was proposed on the basis of the chemical properties of the carrier molecule, that can account for the observed transport rates.

[1] P.Laszlo; Angew.Chem.,Int.Ed.Engl. (1978), 17, 254

[2] M.Hofer, 'Transport across Biological Membranes', Pitmann, London, 1981

[3] C.J.Pedersen; J.Am.Chem.Soc. (1967), 89, 7018

[4] M.Dobler; 'Ionophores and their Structures'; Wiley-Interscience, New York 1981

[5] G.A.Melson (Ed.); 'Coordination Chemistry of Macrocyclic Compounds', Plenum Press, New York 1979

[6] B.Lindman, S.Forsén; 'The Alkali Metals', p129 cont. in: 'NMR and the Periodic Table'; Eds.: R.K.Harris, B.E.Mann, Academic Press: New York, 1978

[7] C.Detellier; in 'NMR of Newly Accessible Nuclei', P.Laszlo, Ed.; Academic Press: New York, 1983; chapter 5, p. 105-151.

[8] R.H.Erlich, A.I.Popov; J.Am.Chem.Soc. (1971), 93, 5620

[9] A.Delville, C.Detellier, A.Gertsmans, P.Laszlo; J.Magn.Reson. (1981), 42, 14

[10] V.Gutmann, E.Wychera; Inorg.Nucl.Chem.Lett. (1966), 2, 257

[11] V.Gutmann; 'Coordination Chemistry in Non-Aqueous Solvents', Springer-Verlag, Vienna 1968

[12] H.Kistenmacher, H.Popkie, E.Clementi; J.Chem.Phys. (1974), 61; 799

[13] D.E.Woessner; J.Chem.Phys. (1961), 35, 41

[14] P.S.Hubbard; J.Chem.Phys. (1970), 53, 985

[15] T.E.Bull; J.Magn.Reson. (1972), 8, 344

[16] C.P.Slichter; 'Principles of Magnetic Resonance' 2nd Ed., Springer Verlag Berlin 1978, p163

[17] M.Bisnaire, C.Detellier, D.Nadon; Can J.Chem. (1982), 60, 3071

[18] A.I.Popov; Pure Appl. Chem. (1975), 41, 275

[19] J.Sandström; 'Dynamic NMR Spectroscopy', Academic Press Inc. (London) 1982

[20] M.Eisenstadt, H.L.Friedman; J.Chem.Phys. (1967), 46, 2182

[21] H.G.Hertz, M.Holz, G.Keller, H.Versmold, C.Yoon; Ber.Bunsenges.Phys.Chem., (1974), 78, 493

[22] C.Deverell, R.E.Richards; Mol.Phys. (1966), 10, 551

[23] G.J.Templeman, A.L.van Geet; J.Am.Chem.Soc. (1972), 94, 5578

[24] C.A.Melendres, H.G.Hertz; J.Chem.Phys. (1974), 61, 4156

[25] E.G.Bloor, R.G.Kidd; Can.J.Chem. (1968), 46, 3425

[26] M.S.Greenberg, R.L.Bodner, A.I.Popov; J.Phys.Chem. (1973), 77, 2449

[27] A.I.Popov; In 'Stereodynamics of Molecular Systems'; R.H.Sarma, Ed.; Pergamon Press, New York, pp.197-207, 1981

[28] C.Detellier, P.Laszlo; Bull.Soc.Chim.Belg. (1975), 84, 1081

[29] C.Hall, R.E.Richards, R.R.Sharp; Proc.Roy.Soc.Lond.A. (1974), 337, 297

[30] M.Shporer, H.Zemel, Z.Luz; FEBS Lett. (1974), 40, 357

[31] D.H.Haynes, B.C.Pressman, A.Kowalsky; Biochemistry (1971), 10, 852

[32] A.Hourdakis, A.I.Popov; J.Solution Chem. (1977), 6, 299

[33] R.M.Izatt, J.S.Bradshaw, S.A.Nielsen, J.D.Lamb, J.J.Christensen; Chem.Rev. (1985), 85, 271

[34] J.Dale; Isr.J.Chem. (1980), 20, 3

[35] M.Shamsipur, G.Rounaghi, A.I.Popov; J.Solution Chem. (1980), 9, 701

[36] J.M.Lehn, J.P.Sauvage, B.Dietrich; J.Am.Chem.Soc. (1970), 92, 2916

[37] A.Paris, P.Laszlo; ACS Sympos. Ser. (1976), 34, 418

[38] W.H.Braunlin, H.J.Vogel, S.Forsén; Eur.J.Biochem. (1984), 142, 139

[39] A.Cornélis, P.Laszlo; Biochem. (1979), 2004

[40] C.M.Venkatachalam, D.W.Urry; J.Magn.Reson. (1980), 41, 313

[41] K.H.Wong, G.Konizer, J.Smid; J.Am.Chem.Soc. (1970), 92, 666

[42] D.H.Haynes; FEBS Lett. (1972), 20, 221

[43] E.Shchori, J.Jagur-Grodzinski, Z.Luz; J.Am.Chem.Soc. (1971), 93, 7133

[44] H.Diebler, M.Eigen, G.Ilgenfritz, G.Maas, R.Winkler; Pure Appl.Chem. (1969), 20, 93

[45] E.Shchori, J.Jagur-Grodzinski, M.Shporer; J.Am.Chem.Soc. (1973), 95, 3842

[46] M.Shporer, Z.Luz; J.Am.Chem.Soc. (1975), 93, 665

[47] E.Schmidt, A.I.Popov; J.Am.Chem.Soc. (1983), 105, 1873

[48] J.D.Lin, A.I.Popov; J.Am.Chem.Soc. (1984), 103, 3773

[49] C.Chen, W.Wallace, E.Eyring, S.Petrucci; J.Phys.Chem. (1984), 88, 2541

[50] K.J.Maynard, D.E.Irish, E.M.Eyring, S.Petrucci; ibid. 729

[51] B.O.Strasser, K.Hallenga, A.I.Popov; J.Am.Chem.Soc. (1985), 107, 789

[52] B.O.Strasser, A.I.Popov; J.Am.Chem.Soc. (1985), 107, 7921

[53] R.C.Phillips, S.Khazaeli, J.L.Dye; J.Phys.Chem. (1985), 89, 600

[54] R.C.Phillips, S.Khazaeli, J.L.Dye; ibid. 606

[55] A.Delville, H.D.H.Stöver, C.Detellier; J.Am.Chem.Soc. (1985), 107, 4172

[56] H.D.H.Stöver, A.Delville, C.Detellier; J.Am.Chem.Soc. (1985), 107, 4167

[57] P.B.Chock; Proc.Natl.Acad.Sci., USA, (1972), 69, 1939

[58] M.Shamsipur, A.I.Popov; J.Am.Chem.Soc. (1979), 101, 4051

[59] H.D.H.Stöver, L.J.Maurice, A.Delville, C.Detellier; Polyhedron (1985), 4, 1091

[60] T.Funck, F.Eggers, E.Grell; Chimia (1972), 12, 637

[61] M.Shamsipur, G.Rounaghi, A.I.Popov; J.Solution Chem. (1980), 9, 701

[62] J.Homer; J.Magn.Reson. (1984), 57, 171

[63] H.K.Frensdorff; J.Am.Chem.Soc. (1971), 93, 600

[64] A.Sacco, M.Holz, H.G.Hertz; J.Magn.Reson. (1985), 65, 82

[65] D.Live, S.I.Chan; J.Am.Chem.Soc. (1976), 98, 3769

[66] D.G.Parsons, M.R.Truter, J.N.Wingfield; Inorg.Chim.Acta (1975), 14, 45

[67] J.D.Owen, M.R.Truter; J.Chem.Soc., Dalton Trans. (1979), 1831

[68] M.Mercer, M.R.Truter; J.Chem.Soc., Dalton Trans. (1973), 2469

[69] D.L.Hughes; J.Chem.Soc., Dalton Trans. (1975), 2374

[70] M.Truter; cited as private communication in reference 45

[71] D.E.Fenton, M.Mercer, N.S.Poonia, M.R.Truter; J.Chem.Soc.,Chem.Commun. (1972), 66

[72] D.Poland; 'Cooperative Equilibria in Physical Biochemistry'; Claredon Press: Oxford, 1978; pp 35-55.

[73] S.N.Deming, S.S.Morgan; Anal.Chem. (1973), 45A, 278

[74] I thank Dr.E.Enwall, University of Oklahoma, for the use of his generalized Newton-Gauss

fitting program.

[75] R.Rymden, P.Stilbs; Biophys.Chem. (1985), 21, 145

[76] I.Stokkeland, P.Stilbs; Biophys.Chem. (1985), 22, 65

[77] P.Debye; Polar Molecules, Dover Press, New York, 1972

[78] A.Gierer, K.Wirtz; Z.Naturforsch. (1953), A8, 532

[79] R.Hilgenfeld, W.Saenger; Top.Curr.Chem. (1982), 101, 1

[80] J.M.Lehn; Pure Appl. Chem. (1980), 52, 2441

[81] A.C.Coxon, D.A.Laidler, R.B.Pettman, J.F.Stoddart; J.Am.Chem.Soc. (1978), 100, 8261

[82] H.G.Hertz; Ber.Bunsenges.Phys.Chem. (1973), 77, 688

[83] T.L.Buxton, J.A.Caruso; J.Am.Chem.Soc. (1974), 96, 6033

[84] C.Detellier, A.Gerstmans; Inorg.Chim.Acta (1982), 65, L157

[85] C.Hall, R.E.Richards, R.R.Sharp; Proc.Roy.Soc.Lond.A. (1974), 337, 297

[86] M.Chabanel, Z.Wang; J.Phys.Chem. (1984), 88, 1441

[87] C.Deverell; Mol Phys. (1969), 16, 491

[88] C.Deverell; Prog.Nucl.Magn.Reson.Spectrosc. (1969), 4, 235, 278

[89] M.Chabanel, Z.Wang; Can.J.Chem. (1984), 62, 2320

[90] H.Weingärtner, H.G.Hertz; J.Chem.Soc., Faraday Trans. I (1979), 75, 2700

[91] H.Weingärtner, C.Muller, H.G.Hertz; ibid., p.2712

[92] M.Newcomb, J.L.Toner, R.C.Helgeson, D.J.Cram; J.Am.Chem.Soc. (1979), 101, 4941

[93] J.P.Behr, J.M.Lehn, P.Vierling; Helv.Chim.Acta (1982), 65, 1853

[94] K.Yamamoto, H.Fukushima, Y.Okamoto, K.Hatada, M.Nakazaki; J.Chem.Soc., Chem.Commun. (1984), 1111

[95] J.S.Bradshaw, P.K.Thompson, R.M.Izatt; J.Heterocyclic Chem. (1984), 21, 897

[96] J.P.Behr, J.M.Lehn, D.Moras, J.C.Thierry; J.Am.Chem.Soc. (1981), 103, 701

[97] J.M.Lehn; Proc.Int.Meet.Soc.Chim.Phys. (1983) (36th), 181

[98] G.W.Gokel et al.; J.Am.Chem.Soc. (1982), 104, 626

[99] F.R.Fronczek, V.J.Gatto, C.Minganti, R.A.Schultz, R.D.Gandour, G.W.Gokel; J.Am.Chem.Soc.

(1984), 106, 7244

[100] R.B.Davidson, R.M.Izatt, J.J.Christensen, R.A.Schultz, D.M.Dishong, G.W.Gokel; J.Org.Chem. (1984), 49, 5080

[101] U.Elben, H.B.Fuchs, K.Frensch, F.Vogtle; L.Ann.Chem. (1979), 1102

[102] M.Berthet, E.Sonveaux; J.Chem.Soc., Chem. Comm. (1983), 10

[103] A.H.Haines, I.Hodgkinsson, C.Smith; J.Chem.Soc., Perkin Trans. I (1983) 311

[104] B.Jansen, F.Vögtle; Tetrahedron Lett. (1976), 52, 4895

[105] D.E.Fenton, D.Parkin, R.F.Newton; J.Chem.Soc.,Perkin Trans. I (1981), 449

[106] W.H.Müller; Naturwissenschaften (1977), 22, 177

[107] C.Detellier, H.D.H.Stöver; Synthesis (1983), 990

[108] H.A.Bates; J.Org.Chem. (1983), 48, 1932

[109] L.Mandolini, B.Masci; J.Am.Chem.Soc. (1984), 106, 168

[110] B.Belleau, G.Macek; J.Am.Chem.Soc. (1968), 90, 1651

[111] S.Eberhart, R.Rothchild; Appl.Spec. (1983), 293

[112] M.Meot-Ner; J.Am.Chem.Soc. (1983), 105, 4912

[113] R.M.Izatt, B.L.Nielsen, J.J.Christensen, J.D.Lamb; J.Membrane Sci. (1981), 9, 263

[114] H.Tsukube; J.Membrane Sci. (1983), 14, 155

[115] D.E.Fenton; Inorg.Chim.Acta (1981), 51(2), 195

[116] D.B.MacLean, W.A.Szarek, I.Kvarnstrom; J.Chem.Soc., Chem.Commun. (1983), 601

[117] M.Ohtsuru, K.Tori; J.Mol.Spectroscopy (1968), 27, 296

[118] G.H.Posner; Angew.Chem., Int.Ed.Engl., (1978), 17, 487

[119] M.Hesse, H.Meier, B.Zeeh; 'Spektroskopische Methoden in der organischen Chemie', pp. 230-232, Georg Thieme Verlag, Stuttgart 1979;

[120] J.Bouquant, A.Delville, J.Grandjean, P.Laszlo; J.Am.Chem.Soc. (1982), 104, 686

[121] J.R.Blackborrow, J.C.Lockhart, D.E.Minnikin, A.C.Robson, M.E.Thompson; J.Chromatography (1975), 107, 380

[122] A.Van Zon, F.De Jong, D.N.Reinhoudt, G.J.Torny, Y.Onwezen; Recl.: J.R.Neth.Chem.Soc.

(1981), 100, 453

[123] D.I.Marlborough, H.N.Rydon; J.Chem.Soc., Perkin Trans. I (1972), 1

[124] V.Bruckner, M.Kajtar, J.Kovacs, H.Nagy, J.Wein; Tetrahedron (1958), 2, 211

[125] J.A.Barltrop, P.Schofield; Tet.Lett. (1962), 697

[126] M.Bergman, L.Zervas; Ber.Dtsch.Chem.Ges. (1932), B65, 1192 and 1201

[127] A.E.Jackson, R.A.W.Johnstone; Synthesis (1976), 685

[128] B.ElAmin, G.M.Anantharamaiah, G.P.Royer, G.E.Means; J.Org.Chem. (1979), 44, 3442

[129] M.Newcomb, S.S.Moore, D.J.Cram; J.Am.Chem.Soc. (1975), 99, 6405

[130] D.E. Fenton; Chem.Soc.Rev. (1977), 6, 325

[131] R.Nagaraj, P.Balaram; Acc.Chem.Res. (1981), 14, 356

[132] B.C.Pressman; Proc.Natl.Acad.Sci.U.S. (1965), 53, 1076

[133] B.C.Pressman; Proc.Natl.Acad.Sci.U.S. (1967), 58, 1949

[134] T.A.Krulwich; Biochim. Biophys. Acta (1983), 726, 245

[135] R.Mueller, D.O.Rudin, H.Ti Tien, W.C.Wescott; Nature (1962), 194, 979

[136] W.A.Charewicz, G.H.Heo, R.A.Bartsch; Anal.Chem. (1982), 54, 2094

[137] T.M.Fyles, V.A.Malik-Diemer, D.M.Whitfield; Can.J.Chem. (1981), 59, 1734

[138] J.D.Lamb, J.J.Christensen, S.R.Izatt, K.Bedke, M.S.Astin, R.M.Izatt; J.Am.Chem.Soc. (1980), 102, 3399

[139] J.D.Lamb, R.M.Izatt, D.G.Garrick, J.S.Bradshaw, J.J.Christensen; J.Membrane Sci.,1981,

[140] T.M.Fyles; J.Chem.Soc., Faraday Trans. I (1986), 82, 617

[141] Y.Nakatsuji, H.Kobayashi, M.Okahara; J.Chem.Soc.,Chem.Commun. (1983), 800

[142] J.-P. Behr, M.Kirch, J.-M.Lehn; J.Am.Chem.Soc. (1985), 107, 241

[143] J.H.Fendler; 'Membrane Mimetic Chemistry' Wiley-Interscience, New York 1982

[144] P.Mueller, D.O.Rudin; Biochem.Biophys.Res.Commun. (1967), 26, 398

[145] W.A.Charevicz, R.A.Bartsch; Anal.Chem. (1982), 54, 2300

[146] G.R.Painter, B.C.Pressman: 'Dynamics Aspects of Ionophore Mediated Membrane Transport.' in: Top.Curr.Chem., 101, Ed.: F.L.Boschke, Springer-Verlag 1982

[147] M.M.Shemyakin,et al.; Biochem.Biophys.Res.Commun. (1967), 29, 834

[148] G.W.Gokel, S.H.Korzeniowski; 'Macrocyclic Polyether Syntheses', Springer-Verlag, Berlin 1982

[149] J.D.Lamb, R.M.Izatt, J.J.Christensen, D.J.Eatough; in 'Coordination Chemistry of Macrocyclic Compounds' Ed.: G.A.Melson, Plenum Press, New York, 1979

[150] R.M.Izatt (Ed.), 'Progress in Macrocyclic Chemistry', Wiley, New York, 1981

[151] M.Kirch, J.M.Lehn; Angew.Chem.,Int.Ed.Engl. (1975), 14, 555

[152] F.Vögtle, T.Kleiner, R.Leppkes, M.W.Laubli, D.Ammann, W.Simon; Chem.Ber. (1983), 116, 2028

[153] E.Weber, F.Vögtle; 'Crown-Type Compounds - An Introductory Overview', in: Top.Curr.Chem. (1981), 98, 1

[154] E.R.Fronczek, V.J.Gatto, R.A.Schultz, S.J.Jungk, W.J.Colucci, R.D.Gandour, G.W.Gokel; J.Am.Chem.Soc. (1983), 105, 6717

[155] J.P.Degelaen, P.Pham, E.R.Blout; J.Am.Chem.Soc. (1984), 106, 4882

[156] S.Kimura, Y.Imanishi; Biopolymers (1984), 23, 563

[157] K.Matsushima, H.Kobayashi, Y.Nakatsuji, M.Okahara; Chem.Lett. (1983), 701

[158] H.Tsukube; J.Chem.Soc., Perkin Trans.I (1982), 2359

[159] Y.N.Antonenko, L.S.Yaguzhinsky; FEBS Lett., 0915 (1983), 163, 4245

[160] J.D.Goddard; J.Phys.Chem. (1985), 89, 1825

[161] L.A.Frederick, T.M.Fyles, N.P.Gurprasad, D.M.Whitfield; Can.J.Chem. (1981), 59, 1724

[162] T.M.Fyles, V.A.Malik-Diemer, C.A.McGavin, D.M.Whitfield; ibid. (1982), 60, 2259

[163] J.Strzelbicki, R.A.Bartsch; J.Membrane Sci. (1982), 10, 3547

[164] R.Maron, Y.Stern, B.I.Kanner, S.Schuldiner; J.Biol.Chem. (1983), 258, 11476

[165] S.Shinkai, K.Inuzuka, O.Miyazaki, O.Manabe; J.Am.Chem.Soc. (1985), 107, 3950

[166] S.Shinkai, T.Minami, Y.Araragi, O.Manabe; J.Chem.Soc., Perkin Trans. II, (1985) 503

[167] A.Ohki; J.Membrane Sci. (1983), 15, 231

[168] S.Shinkai, K.Shigematsu, M.Sato, O.Manabe; J.Chem.Soc., Perkin Trans.1 (1982), 2735

[169] S.Shinkai, O.Manabe; 'Photocontrol of Ion Extraction and Ion Transport by Photofunctional Crown ethers', Top.Curr.Chem. (1984), 67 Ed.: F.L.Boschke, Springer Verlag, Berlin 1984

[170] S.Shinkai, M.Ishihara, K.Ueda, O.Manabe; J.Chem.Soc., Perkin Trans. II (1985), 511

[171] A.M.Creighton, S.Turner; 'The Chemical Regulation of Biological Mechanisms', Proc. 11th Medicinal Chemistry Symposium, Royal Soc.Chem., Cambridge, 1981

[172] W.E.Morf; 'The Principles of Ion-Selective Electrodes and of Membrane Transport', Elsevier, New York 1981

[173] J.M.Ceraso, J.L.Dye; J.Am.Chem.Soc. (1973), 95, 4432

[174] J.P.Kintzinger, J.M.Lehn, E.Kauffmann, J.L.Dye, A.I.Popov; J.Am.Chem.Soc. (1983), 105, 7549

[175] P.Bacelon, J.Corset, C.de Loze; J.Solution Chem. (1980), 9, 129

[176] U.Olsher, G.A.Elgavish, J.Jagur-Grodzinski; J.Am.Chem.Soc. (1980), 102, 3338

[177] G.Hillmann; Z.Naturforsch. (1946), 1, 682

[178] M.A.Kraus; Synthesis (1973), 361

[179] V.J.Gatto, K.A.Arnold, A.M.Viscariello, S.R.Miller, G.W.Gokel; Tet.Lett. (1986), 27, 327

[180] P.L.Kuo, I.Ikeda, M.Okahara; Bull.Chem.Soc.Jpn. (1982), 55, 3356

I hereby declare that I am the sole author of this thesis. I authorize the University of Ottawa to lend this thesis to other institutions or individuals for the purpose of scholarly research.

Harald Stöve

Harald D.H. STÖVER

I further authorize the University of Ottawa to reproduce this thesis by photocopying or by other means, in total or in part, at the request of other institutions or individuals for the purpose of scholarly research.

Harald Stöve

Harald D.H. STÖVER